

Copyright

by

Matthew R. Huizinga

2007

**Strength and Serviceability Performance of Large-Scale Deep Beams:
Effect of Transverse Reinforcement**

by

Matthew R. Huizinga, B.S.C.E.

Thesis

Presented to the Faculty of the Graduate School of

The University of Texas at Austin

in Partial Fulfillment

of the Requirements

for the Degree of

Master of Science in Engineering

The University of Texas at Austin

August 2007

**Strength and Serviceability Performance of Large-Scale Deep Beams:
Effect of Transverse Reinforcement**

**Approved by
Supervising Committee:**

Oguzhan Bayrak, Supervisor

James O. Jirsa

Acknowledgements

There are a number of individuals I would like to thank for their contributions to this research project.

Foremost, I would like to thank my family not only for their unwavering support in my academic endeavors, but also for their immeasurable influence in my development as a person. To Mom, Dad, Ken, Erin, Rob, Sara, and Mary, you have made me the person I am today.

This research study was conducted with funds generously provided by the Texas Department of Transportation. I would like to acknowledge Dean Van Landuyt, the TxDOT Project Director, for his steady involvement in the current study. In addition, I would like to acknowledge David Hohmann, the TxDOT Program Coordinator, and John Vogel, TxDOT Project Advisor, for their contributions to the project.

To my supervising professor, Dr. Oguzhan Bayrak, your tireless work, guidance, and dedication to maintaining high standards have made the successful completion of the current project possible. Also, to Dr. Jim Jirsa and Dr. Sharon Wood, your advice on the current research project has been most helpful.

I would like to specifically acknowledge fellow graduate student Robin Tuchscherer for his hard work, practical knowledge, and useful advice that made the successful completion of the project possible.

In addition, I would like to thank Thomas Stablon, Carlos Jordan, and Brian Schnittker for the vast number of hours they have contributed to the project. I would also like to thank current and past staff members at FSEL for their contributions, including Blake Stassney, Dennis Phillip, Eric Schell, Mike Wason, Barbara Howard, Ella Schwartz, and Cari Billingsley.

Strength and Serviceability Performance of Large-Scale Deep Beams: Effect of Transverse Reinforcement

Matthew R. Huizinga, B.S.C.E.

The University of Texas at Austin, 2007

SUPERVISOR: Oguzhan Bayrak

Past research programs investigating the shear strength of reinforced concrete deep beams lack a consensus on the effect of transverse reinforcement on the ultimate shear strength of reinforced concrete deep beams. Pertinent data regarding the serviceability performance of deep beams is also largely absent from past research studies. In addition, the overwhelming majority of test specimens in historical research studies are significantly smaller than the large-scale deep beams often utilized in practice.

To investigate the shear strength and serviceability performance of large-scale deep beams, a research study funded by the Texas Department of Transportation was conducted at the University of Texas at Austin. The objective of the study was to study the effect of the amount and detailing of transverse reinforcement and bearing area on the strength and serviceability performance of large-scale deep beam specimens. In addition, strut-and-tie modeling was evaluated in terms of its ability to provide both a conservative estimate of ultimate strength and address issues of serviceability in the specimens.

The experimental program consisted of nine tests on three large-scale deep beam specimens. The specimens are the largest specimens with shear reinforcement reported in shear research literature. It was found that the amount and detailing of transverse reinforcement and bearing area had only a marginal effect on the strength and serviceability performance of deep beams. In addition, the amount of transverse reinforcement had no effect on the first diagonal cracking load, but a large amount of transverse reinforcement was effective at reducing crack widths. It was also found that AASHTO LRFD, TxDOT 4371, and ACI 318 Appendix A strut-and-tie modeling provisions each provided conservative estimates of strength in the specimens. However,

the strut-and-tie modeling provisions of ACI 318 Appendix A were not adequate from a standpoint of serviceability, if the formation of diagonal cracks under service loads is not desired.

Table of Contents

CHAPTER 1 INTRODUCTION.....	1
1.1 Overview	1
1.2 Objectives of Research	2
1.3 Scope of Research.....	2
1.4 Chapter Outline.....	3
CHAPTER 2 BACKGROUND.....	5
2.1 Introduction To Discontinuity Regions and Deep Beams	5
2.1.1 Strut-and-Tie Modeling	7
2.2 Design of Deep Beams.....	12
2.2.1 Strut-and-Tie Modeling Provisions	14
2.2.2 TXDOT Research Project 4371	23
2.2.3 ACI 318-05	25
2.3 TxDOT Bent Cap Field Evaluation	31
2.3.1 Greens Road Bent Cap.....	31
2.3.2 I-345 Pier Cap.....	33
2.4 State of Knowledge: Shear Strength of Deep Beams	35
2.5 Literature Review.....	38
2.5.1 DePaiva and Siess (1965)	38
2.5.2 Leonhardt and Walther (1966).....	39
2.5.3 Kong, Robins, and Cole (1970)	39
2.5.4 Smith and Vantsiotis (1982)	41
2.5.5 Hsiung and Frantz (1985)	41
2.5.6 Rogowski, MacGregor, and Ong (1986).....	43
2.5.7 Anderson and Ramirez (1989)	43
2.5.8 Tan, Kong, Teng, and Weng (1997)	45
2.5.9 Shin, Lee, Moon, Gosh (1999).....	46

2.5.10 Oh and Shin (2001).....	46
2.5.11 Young, Bracci, Keating, Hueste (2002).....	47
2.5.12 Powanusorn and Bracci (2006).....	49
2.5.13 Brown, Sankovich, Bayrak, Jirsa, Breen, Wood (2006).....	50
2.5.14 Summary and Discussion.....	54
2.6 Remarks	56
CHAPTER 3 EXPERIMENTAL PROGRAM.....	58
3.1 Introduction.....	58
3.2 Test Setup.....	58
3.3 Test Program.....	65
3.4 Specimen Design	69
3.4.1 Shear Criticality of Specimen	74
3.5 Specimen Details	75
3.6 Materials	83
3.6.1 Concrete	83
3.6.2 Reinforcing Bars	84
3.7 Instrumentation	85
3.7.1 Load Measurement and Verification	86
3.7.2 Displacements.....	88
3.7.3 Strain measurements	89
3.8 Summary	92
CHAPTER 4 EXPERIMENTAL RESULTS AND ANALYSIS.....	94
4.1 Overview	94
4.2 Summary of Tests Performed	94
4.3 Experimental Results and Analysis	100
4.3.1 Ultimate Strength.....	100

4.3.2 Serviceability	116
4.3.3 Capacity Estimated by Strut-and-Tie Models.....	138
4.4 Minimum Horizontal and Vertical Transverse Reinforcement Ratios	163
4.5 Summary	168
4.5.1 Transverse Reinforcement Ratio.....	169
4.5.2 Quantity of Stirrup Legs at a Section.....	170
4.5.3 Bearing Area	171
4.5.4 Strut-and-Tie Modeling	172
CHAPTER 5 SUMMARY, CONCLUSIONS, AND RECOMMENDATIONS	174
5.1 Summary of Research Study.....	174
5.2 Conclusions.....	175
5.2.1 Transverse Reinforcement Ratio.....	176
5.2.2 Quantity of Stirrup Legs	177
5.2.3 Bearing Area	178
5.2.4 Strut-and-Tie Modeling	178
5.3 Recommendations for Future Research.....	180
APPENDIX A	183
APPENDIX B	208
APPENDIX C	212
BIBLIOGRAPHY	216
VITA.....	219

List of Tables

Table 2-1: Strut and node efficiency factors.....	17
Table 2-2: Greens road bent reinforcement details.....	32
Table 2-3: I-345 cap reinforcement details.....	34
Table 2-4: Hsuing and Frantz specimen experimental capacities.....	42
Table 2-5: Anderson and Ramirez Wide Specimen Experimental Results	45
Table 3-1: Test program.....	66
Table 3-2: Typical bent cap details.....	71
Table 3-3: Specimen details.....	76
Table 3-4: Concrete specifications.....	83
Table 3-5: Concrete mix proportions.....	83
Table 3-6: Concrete compressive strengths	84
Table 3-7: Reinforcing bar properties.....	85
Table 4-1: Summary of testing	95
Table 4-2: Detailed summary of testing.....	97
Table 4-3: Experimental strut efficiencies.....	103
Table 4-4: Comparison of tests with 4-legged stirrups.....	112
Table 4-5: Comparison of tests with 2-legged stirrups.....	112
Table 4-6: Comparison of tests with varying quantity of stirrup legs	114
Table 4-7: Comparison of tests with varying bearing area.....	115
Table 4-8: Diagonal cracking loads	122
Table 4-9: Propagation of parallel shear diagonal cracks into CCT node	123
Table 4-10: STM capacities and maximum applied loads.....	142
Table 4-11: STM capacities and maximum applied loads.....	152
Table 4-12: Diagonal cracking loads and STM capacities	159
Table 4-13: Load and resistance factors	160
Table 4-14: Cracking load fraction of STM capacity	161

List of Figures

Figure 2-1: Typical discontinuity regions (ACI 318-05, Appendix A)	6
Figure 2-2: D-Regions in an asymmetrically loaded deep beam	7
Figure 2-3: Strut types in a deep beam (Brown et al., 2006)	9
Figure 2-4: Impractical use of hydrostatic nodes in a beam (Brown et al., 2006)	10
Figure 2-5: Stresses on hydrostatic and non-hydrostatic nodes (Brown et al., 2006)	11
Figure 2-6: Deep beam strut-and-tie models	12
Figure 2-7: Calculation of ρ_h in a current project specimen	20
Figure 2-8: AASHTO limited strut width provision (AASHTO LRFD Figure 5.6.3.3.2-1, Brown et al., 2006)	22
Figure 2-9: Dispersion of compression in a bottle-shaped strut; view is perpendicular to the plane of the dispersion of compression (Brown et al. 2006, Schlaich and Weischede 1982)	24
Figure 2-10: Nomenclature for Equation 2-18 (Brown et al., 2006)	28
Figure 2-11: Strut-and-tie model for a bottle-shaped strut (Brown et al., 2006)	29
Figure 2-12: Greens road bent cross-section	32
Figure 2-13: a) Typical cracking pattern; b) Highlighted diagonal shear cracks; c) Completed structural retrofit	33
Figure 2-14: a) Interstate 345 pier cap in Dallas, TX; b) Highlighted diagonal shear cracks	34
Figure 2-15: I-345 bent	35
Figure 2-16: History of shear tests	36
Figure 2-17: History of shear tests (continued)	37
Figure 2-18: Transverse reinforcement configurations (Kong et al., 1970)	40
Figure 2-19: Hsuing and Frantz specimens	42
Figure 2-20: Anderson and Ramirez narrow beam stirrup detailing schemes	44
Figure 2-21: Anderson and Ramirez wide specimens	44
Figure 2-22: Typical bent cap specimen (Young et al., 2002)	47
Figure 2-23: Bent cap cross-sections (Young et al., 2002)	48
Figure 2-24: Comparison of crack patterns (Young et al., 2002)	49
Figure 2-25: Bent cap cross-sections (Powanusorn and Bracci, 2006)	50
Figure 2-26: Typical series one specimen (Brown et al., 2006)	51
Figure 2-27: Series two specimens (Brown et al., 2006)	53
Figure 3-1: a) Platen; b) Excavation; c) Excavated pit; d) Foundation construction; e) Platen lift; f) Platen in position	59
Figure 3-2: Test setup	61
Figure 3-3: Test setup, elevation view	62
Figure 3-4: Test setup, elevation view	63
Figure 3-5: Test setup, plan view	64
Figure 3-6: a) Loading configuration A; b) Loading configuration B	67
Figure 3-7: Strengthening of a beam after strut failure: external PT clamp	68
Figure 3-8: Bent caps and test specimen	70

Figure 3-9: Specimen cross section with aluminum ducts.....	72
Figure 3-10: Effect of support conditions on bent cap moments.....	73
Figure 3-11: Test specimens in context of TxDOT project 4371 shear database.....	74
Figure 3-12: Shear span 1A a) Cross-section; b) Elevation.....	77
Figure 3-13: Shear span 1B a) Cross-section; b) Elevation.....	78
Figure 3-14: Shear span 2A a) Cross-section; b) Elevation.....	79
Figure 3-15: Shear span 2B a) Cross-section; b) Elevation.....	80
Figure 3-16: Shear span 3A a) Cross-section; b) Elevation.....	81
Figure 3-17: Shear span 3B a) Cross-section; b) Elevation.....	82
Figure 3-18: Stress vs. strain relationship, specimen 1, #5 bars.....	85
Figure 3-19: 500 kip load cells.....	87
Figure 3-20: Linear potentiometer locations.....	88
Figure 3-21: 6-inch linear potentiometer.....	89
Figure 3-22: Strain gauge locations adjacent to reaction point.....	90
Figure 3-23: Stirrup strain gauge locations.....	91
Figure 3-24: Surface strain gauge locations.....	92
Figure 4-1: Typical specimen shear force diagram at maximum applied load.....	99
Figure 4-2: Test #1 Bearing Geometry.....	100
Figure 4-3: Typical node geometry.....	102
Figure 4-4: Test #1 shear failure.....	105
Figure 4-5: Test #1 applied load vs. deflection.....	105
Figure 4-6: Test #1 stirrup strain along shear span at maximum applied load.....	106
Figure 4-7: Test #1 applied load vs. longitudinal reinforcement strain.....	107
Figure 4-8: Longitudinal strain gauge location.....	107
Figure 4-9: Test #2 load vs. deflection.....	108
Figure 4-10: Illustration of compression failure.....	109
Figure 4-11: Photograph of compression block crushing.....	109
Figure 4-12: Test #3 applied load vs. longitudinal reinforcement strain.....	110
Figure 4-13: Test #5 applied load vs. longitudinal reinforcement strain.....	111
Figure 4-14: Comparison of cracking patterns at maximum applied load.....	118
Figure 4-15: Typical progression of cracking.....	119
Figure 4-16: Stirrup strain at diagonal cracking load.....	121
Figure 4-17: Location of parallel diagonal cracks.....	124
Figure 4-18: Percent of maximum applied load vs. maximum shear crack width.....	126
Figure 4-19: Maximum stirrup strain vs. maximum shear crack width.....	126
Figure 4-20: Percent of maximum applied load vs. maximum shear crack width.....	128
Figure 4-21: Percent of ultimate capacity vs. maximum shear crack width.....	130
Figure 4-22: Stirrup leg strains at 50% of the maximum applied load.....	131
Figure 4-23: Longitudinal reinforcement gauge location.....	132
Figure 4-24: Test #1 longitudinal reinforcement strains.....	133
Figure 4-25: Test #2 longitudinal reinforcement strains.....	133
Figure 4-26: Test #3 longitudinal reinforcement strains.....	134
Figure 4-27: Test #5 longitudinal reinforcement strains.....	134
Figure 4-28: Percent of ultimate capacity vs. maximum shear crack width.....	136
Figure 4-29: Longitudinal rebar strain profile near reaction point.....	137

Figure 4-30: Strut-and-tie model of a test specimen.....	138
Figure 4-31: Typical strut-and-tie geometry.....	140
Figure 4-32: STM capacities and maximum applied loads	141
Figure 4-33: STM element naming scheme.....	143
Figure 4-34: $\frac{P_{MAX}}{P_{STM}}$ vs. applied load bearing area	146
Figure 4-35: Illustration of node confinement	146
Figure 4-36: Two-panel strut-and-tie model.....	147
Figure 4-37: Stirrups engaged in tie BC	148
Figure 4-38: Two-panel strut-and-tie model: CTT node	149
Figure 4-39: Limited strut width for shear span 2B.....	150
Figure 4-40: Strut-and-tie model of a sectional member	151
Figure 4-41: CCC node geometry.....	152
Figure 4-42: Two-panel STM capacities and maximum applied loads	153
Figure 4-43: Surface strain gauge locations.....	155
Figure 4-44: Concrete strain and stress vs. distance from strut centerline	156
Figure 4-45: Estimation of bottle-shaped strut using concrete strain profile.....	157
Figure 4-46: Strut-and-tie model comparison to cracking behavior.....	158
Figure 4-47: Diagonal cracking loads and STM capacities	159
Figure 4-48: Effect of strut inclination on effectiveness of reinforcement.....	165
Figure 4-49: Suggested minimum transverse reinforcement ratio.....	168

CHAPTER 1

Introduction

1.1 OVERVIEW

The geometry or loading configuration of a reinforced concrete member may cause it to contain regions of discontinuity where complex states of stress and nonlinear distributions of strain exist. In such regions it cannot be assumed that plane sections remain plane after loading, and therefore traditional design assumptions do not apply. In particular, the assumption of a linear strain distribution is invalid.

The design of members with regions of discontinuity, such as deep beams, requires a unique set of considerations. In the past, regions of discontinuity were designed using rules of thumb and reinforcement was placed using empirical equations. More recently, strut-and-tie modeling (STM) has been adopted as a design tool in major structural design codes in the United States. In STM, the complex flows of stress in a discontinuity region are represented by a series of simple axially-loaded elements. The design of each element using structural mechanics dictates the amount and location of reinforcement, i.e. detailing of reinforcement.

Strut-and-tie modeling is governed by the lower bound theory of plasticity, and is therefore inherently conservative. On the other hand, STM does not permit design by serviceability limit states. Therefore, empirical code provisions are used in conjunction with STM to successfully design deep beams.

The amount of transverse reinforcement required within a deep beam designed using strut-and-tie modeling is typically dictated by the amount of reinforcement required to restrain tensile dispersion forces in bottle-shaped strut

elements. The two major U.S. design codes stipulate different requirements for the minimum amount of transverse reinforcement in a deep beam. The minimum transverse reinforcement requirements of the AASHTO LRFD Bridge Design Specifications result in approximately 40% additional transverse reinforcement in comparison to the specifications of ACI 318-05 Appendix A.

From past research programs, there is no consensus on the effect of transverse reinforcement on the ultimate shear strength of deep beams. In addition, pertinent data regarding the serviceability performance of deep beams is largely absent from past research studies. The overwhelming majority of test specimens in historical research studies are significantly smaller than the large-scale deep beams often utilized in practice.

1.2 OBJECTIVES OF RESEARCH

A research project, funded by the Texas Department of Transportation, was initiated at the Ferguson Structural Engineering Laboratory at the University of Texas at Austin. The objective of the research project was to evaluate the effect of the amount and detailing of transverse reinforcement, and the applied load bearing area, on the strength and serviceability performance of large-scale reinforced concrete deep beams. In addition, strut-and-tie modeling was evaluated in terms of its ability to provide both a conservative estimate of ultimate strength and address issues of serviceability in the specimens. The project is described in this thesis.

1.3 SCOPE OF RESEARCH

Within the current project an extensive literature review was completed, along with experimental research on the strength and serviceability performance of reinforced concrete deep beams. The literature review encompasses over a half-century of research studies that were performed to investigate the effect of

transverse reinforcement in deep beams. The experimental program consisted of a series of nine tests on three deep beam specimens. Multiple tests were performed on each specimen. The specimens contained varying amounts of transverse reinforcement and were similar in scale to existing large-scale bent caps designed by the Texas Department of Transportation.

1.4 CHAPTER OUTLINE

The contents of this document are spread over five chapters. Chapter 2 provides a brief introduction to discontinuity regions in reinforced concrete members and to the basic concepts of strut-and-tie modeling. In addition, the chapter contains a summary of strut-and-tie modeling provisions for various design codes, with an emphasis on provisions regarding the design of transverse reinforcement. An extensive literature review of the effect of transverse reinforcement on the shear strength and serviceability performance of deep beams is included.

The experimental program is described in Chapter 3, including information on the test setup, testing procedure, test specimens and instrumentation used to collect experimental data. The chapter also contains a discussion of objectives considered in the design of test specimens. The test specimens are compared with structural members utilized by TxDOT.

The results of the experimental program are presented in Chapter 4. The effect of each of the test variables on the strength and serviceability performance is discussed. The chapter also contains analysis of the experimental results, including an evaluation of the ability of strut-and-tie modeling to provide both a conservative estimate of ultimate strength and address issues of serviceability in the specimens. In addition, a provision stipulating a minimum transverse reinforcement ratio is presented.

Finally, Chapter 5 contains a summary of conclusions from the current study. Recommendations for future work are also provided.

CHAPTER 2

Background

2.1 INTRODUCTION TO DISCONTINUITY REGIONS AND DEEP BEAMS

Reinforced concrete structural members are typically separated into regions referred to as either beam regions, also called B-regions, or as discontinuity regions, or D-regions (MacGregor and Wight, 2005). The former definition is reserved for regions with simple states of stress and linear distributions of strain. The behavior of B-regions is well understood, and with the assumption that plane sections remain plane a great majority of beam designs are handled with relative ease. Conversely, D-regions contain nonlinear distributions of strain and complex states of stress; historically the design of such regions has proven to be somewhat more difficult, due to the lack of simple and practical design methods and clear understanding of the behavior.

Discontinuity regions are subdivided into two types. Geometric discontinuities are a result of abrupt geometric changes within a structural member, whereas statical discontinuities occur as a result of concentrated loads or reaction points. Examples of geometric discontinuities, such as dapped beams or members that contain openings, and statical discontinuities, such as deep beams, are shown in Figure 2-1.

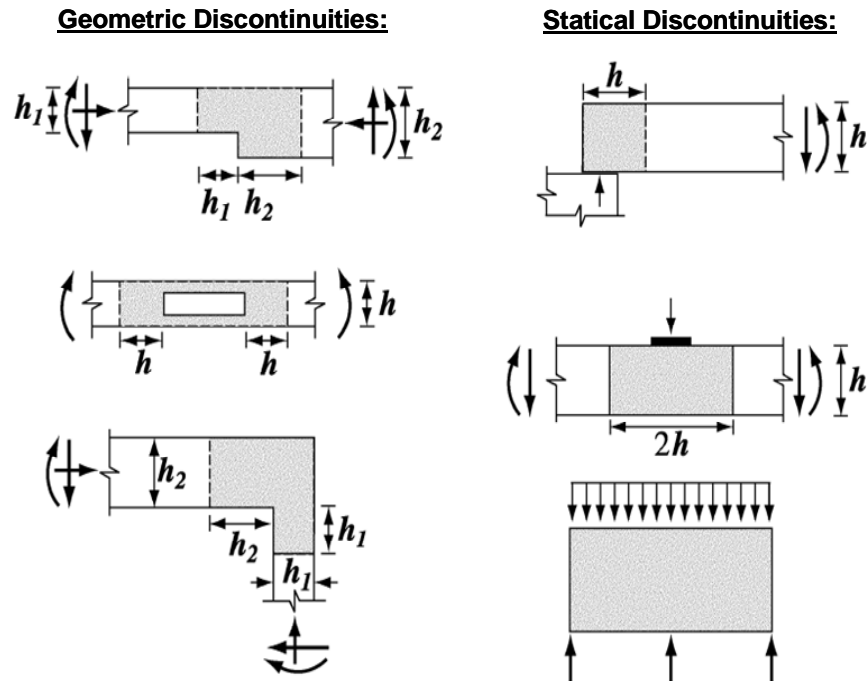


Figure 2-1: Typical discontinuity regions (ACI 318-05, Appendix A)

The serviceability and strength of D-regions is the main focus of this research project. Figure 2-2 shows the D-regions for a deep beam supporting an asymmetrically applied concentrated load, similar to the test specimens in the current research project. ACI 318-05 defines a deep beam as one with a clear span equal to or less than four times the overall member depth, or as one that supports a concentrated load applied within twice the member effective depth of the support (that is, $a/d \leq 2.0$). For clarity, ACI 318-05 provisions indicate that the above definition applies when a member is loaded on one face and supported on the opposite face. Similarly, AASHTO LRFD Bridge Design Specifications (4th Edition) defines a deep beam as one where the distance between the centers of applied load and supporting reactions is less than about twice the member thickness.

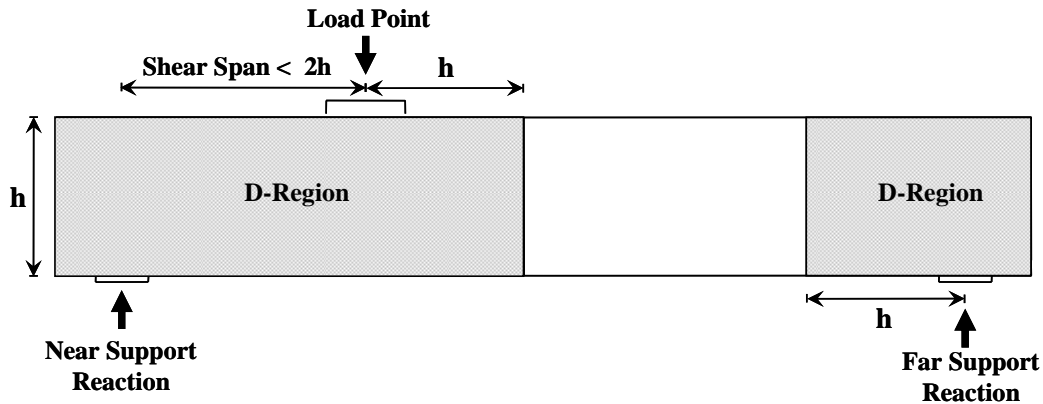


Figure 2-2: D-Regions in an asymmetrically loaded deep beam

2.1.1 Strut-and-Tie Modeling

It is well-established that the traditional beam theory does not apply to D-regions. Until recently, ACI-318 and AASHTO LRFD design provisions for D-regions consisted of little more than a series of empirical rules of thumb. This was true of code equations for deep beam shear design, in which the shear strength due to reinforcement was an empirical combination of horizontal and vertical shear steel.

More recently strut-and-tie modeling (STM) has been incorporated into American structural design codes. The origins of strut-and-tie models (STM) can be traced back to Ritter (1899) and Mörsch (1903), but codification of STM in the U.S. did not occur until 1989 with provisions included in the AASHTO Guide Specifications for Design and Construction of Segmental Concrete Bridges. STM design provisions were adopted by the AASHTO LRFD Bridge Design Specifications in 1998, and ACI-318 in 2002.

The complex flows of stress in a discontinuity region are represented by a series of simple axially-loaded members in a typical STM, creating a straightforward design method. Aside from its relative ease of use, STM is also inherently conservative. The method conforms to the lower bound theory of plasticity, which ensures that the collapse load of a member will be equal to or greater than the capacity estimated by STM.

The three fundamental elements of a strut-and-tie model are struts, ties, and nodes. Struts are model members that carry compressive stress; strut forces are generally carried by concrete that is restrained by reinforcing bars. Ties transfer tensile forces, which are generally carried by reinforcing bars. Nodes are regions of intersection between struts and ties, and are typically named according to STM elements that frame into the nodes. For example, a node that is situated at the intersection of a strut with two ties is referred to as a CTT node, where each ‘C’ or ‘T’ refers to the compressive or tensile nature of the elements that connect to the node.

Struts are generally designated as being one of three types: a prismatic strut of uniform cross-section, a compression fan characterized by stresses flowing radially outward from a single point, or a bottle-shape strut (Brown et al., 2006). A bottle-shaped strut can develop when compressive stresses disperse through the depth of a structural member.

The different types of struts are used to model different parts of a deep beam. When a strut is used to model the compression block of a flexural member, it is often considered prismatic. Conversely, diagonal struts are nearly always considered bottle-shaped. In addition, a fan-shaped strut can occur due the application of a distributed load. Figure 2-3 illustrates the different types of struts in a deep beam.

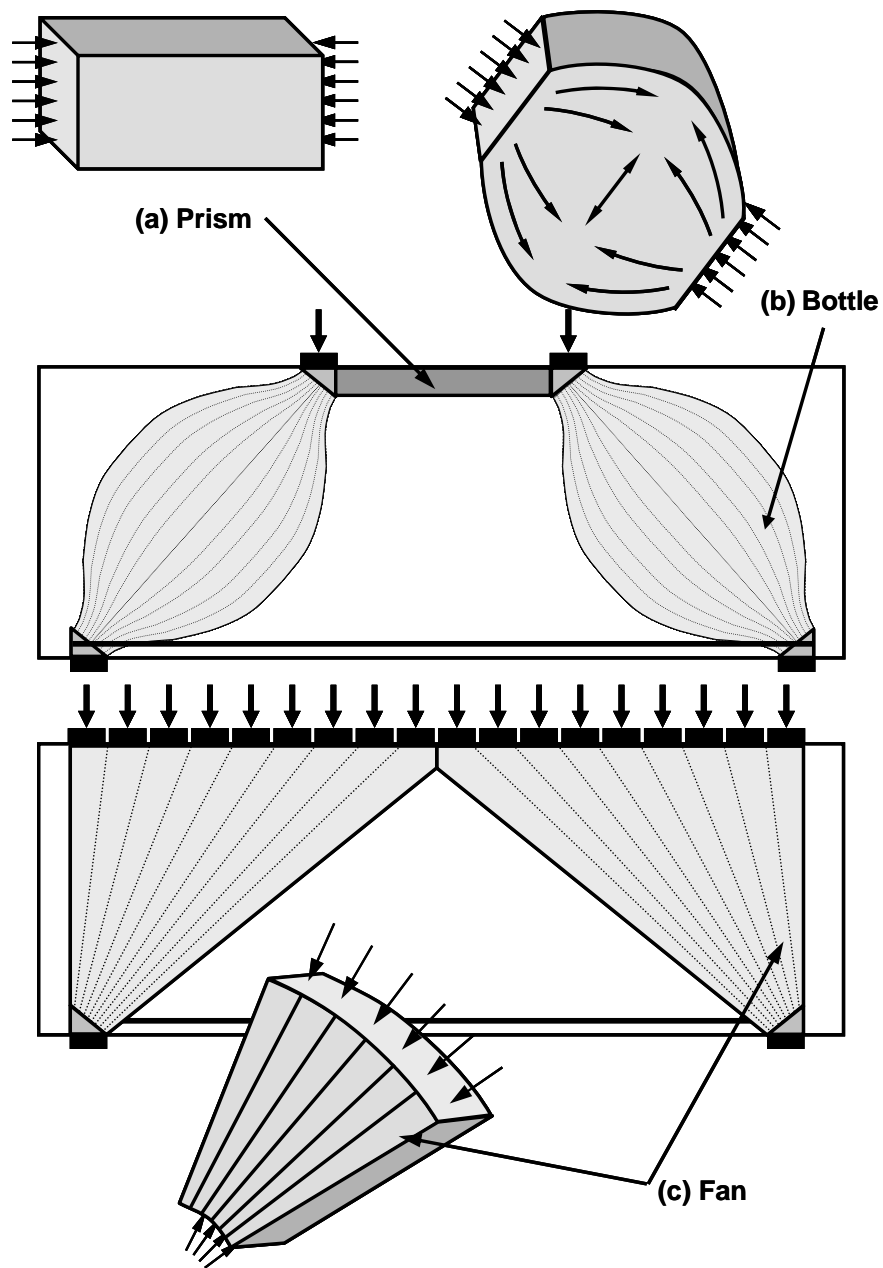


Figure 2-3: Strut types in a deep beam (Brown et al., 2006)

Typically nodes are assumed to be hydrostatic. Hydrostatic nodes have equal stresses on all faces, and strut or tie forces that act perpendicular to each face. However,

the geometry of a deep beam can often times make use of hydrostatic nodes difficult. An example is shown in Figure 2-4.

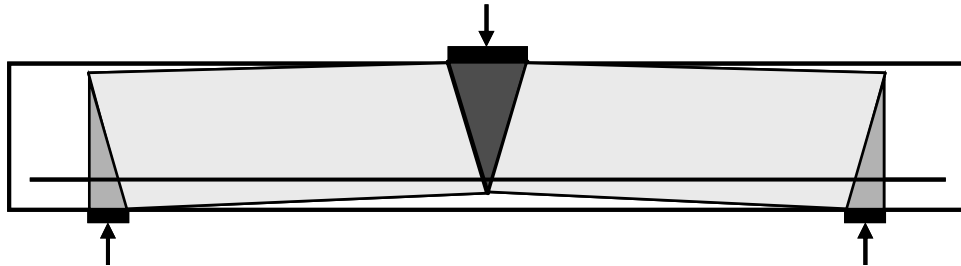


Figure 2-4: Impractical use of hydrostatic nodes in a beam (Brown et al., 2006)

In such a case, non-hydrostatic nodes can be used. Faces of non-hydrostatic nodes are not perpendicular to incoming strut and tie forces. The result is the formation of shear stresses along the node faces. While the code does not limit the use of non-hydrostatic nodes, it is suggested by Schlaich, Schäfer, and Jennewein (1987) that the stress on any face of a given non-hydrostatic node should not be more than double the stress on any other face. In this way, shear stresses and distortions within a node can be limited.

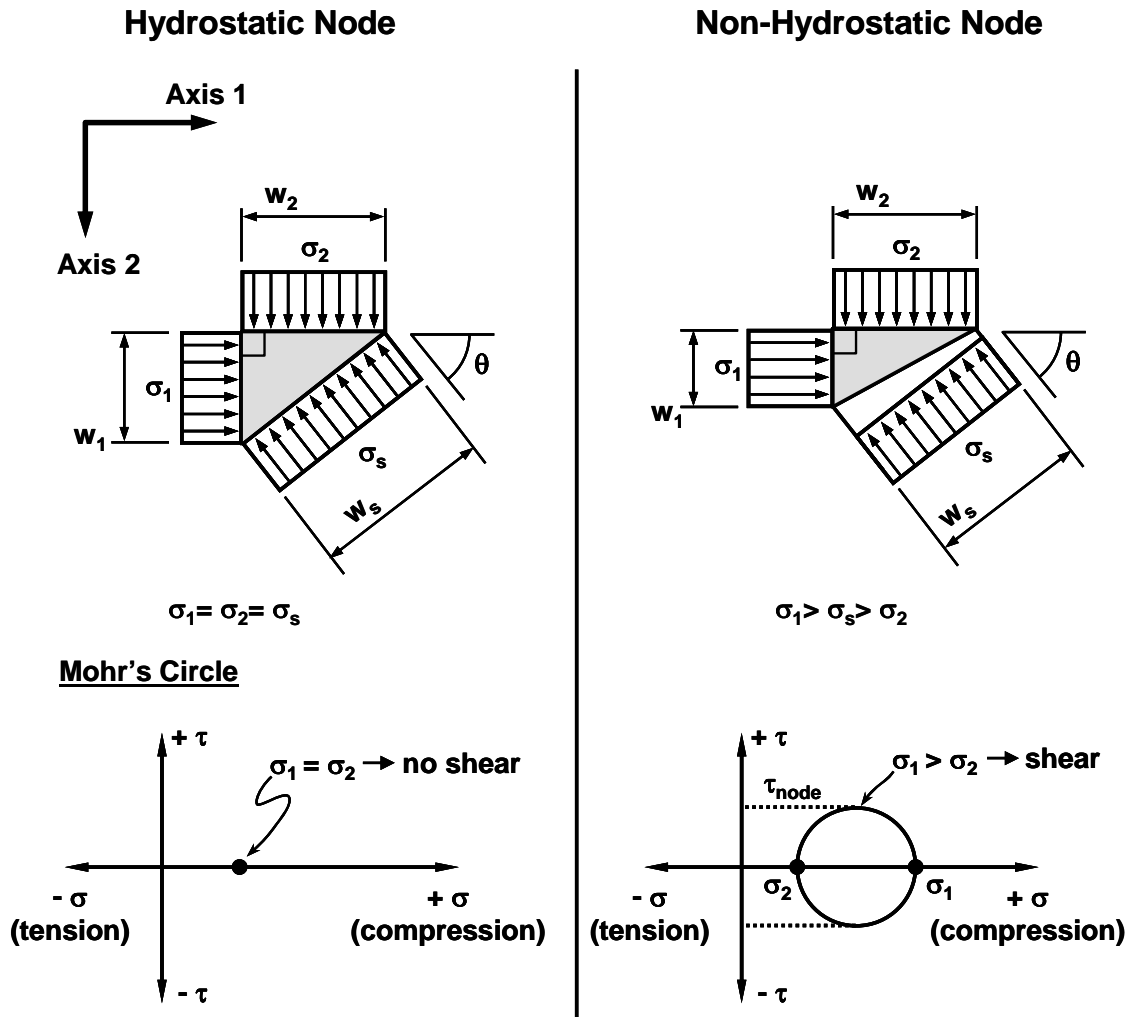


Figure 2-5: Stresses on hydrostatic and non-hydrostatic nodes (Brown et al., 2006)

Deep beams designed using STM can be modeled in a number of different ways. Four typical deep beam strut-and-tie models are shown in Figure 2-6. The one-panel model neglects the contribution of vertical shear reinforcement. The two-panel model accounts for vertical shear reinforcement and assumes a single vertical tie at the mid-length of the shear span. The superimposed model assumes a combination of the one and two-panel models. Finally, the fanned strut model assumes a vertical tie at the location of each stirrup in the shear span. Although the latter two models closely represent the flow

of forces within a deep beam, they are also difficult to successfully model; in particular, the geometry of the interior nodes is ambiguous.

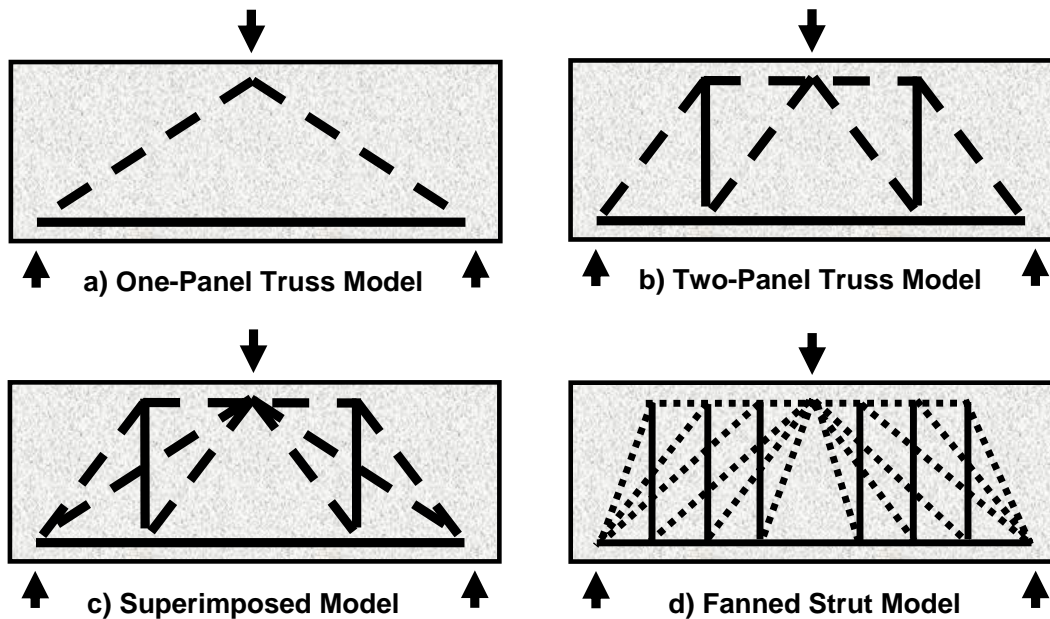


Figure 2-6: Deep beam strut-and-tie models

The test specimens of the current research project were modeled using both one and two-panel models. The applicability and conservatism of each of these models for the test specimens is discussed in Chapter 4.

2.2 DESIGN OF DEEP BEAMS

As outlined above, discontinuity regions and beam regions within a member exhibit very different structural behavior. As a result, the design of each requires a unique set of considerations and design equations.

The shear design of a beam loaded such that the shear span to depth ratio, a/d , is greater than 2.0 must meet code stipulations for sectional shear design. Sectional design equations can be quite straightforward. ACI 318-05 separates the contribution of

concrete and reinforcement to shear strength; the equation for each is listed as Equations 2-1 and 2-2, below. The AASHTO LRFD Bridge Design Specifications, on the other hand, stipulate sectional shear design through the more complex Modified Compression Field Theory (MCFT).

$$V_c = 2\sqrt{f'_c} b_w d \quad \text{Equation 2-1}$$

where:

V_c = nominal shear strength provided by concrete (lb)

f'_c = specified concrete strength (psi)

b_w = web width (in)

d = member effective depth (in)

f_y = yield strength of reinforcement (psi)

$$V_s = \frac{A_v f_y d}{s} \quad \text{Equation 2-2}$$

where:

V_s = nominal shear strength provided by shear reinforcement (lb)

A_v = Area of shear reinforcement within a distance s (in²)

f_y = yield strength of reinforcement (psi)

d = member effective depth (in)

s = spacing of shear reinforcement, measured in a direction parallel to shear reinforcement (in)

Conversely, a member loaded such that $a/d \leq 2.0$ is considered a deep beam, and must be designed with a different set of code provisions. As outlined above, strut-and-tie modeling is the method most commonly used in deep beam design. Regardless of the strut-and-tie model or design method selected to design a given deep beam, transverse

reinforcement is necessary to restrain diagonal cracks due to dispersion forces in diagonal bottle-shape struts, and to provide adequate shear strength of the member.

ACI 318-05 and AASHTO LRFD each provide provisions for strut-and-tie modeling that stipulate a minimum amount of transverse reinforcement. In addition, TxDOT Research Project 4371 provides suggested modifications to the AASHTO STM provisions. The STM design provisions and minimum transverse reinforcement requirements for deep beams included in these structural design codes are outlined in this section.

2.2.1 Strut-and-Tie Modeling Provisions

2.2.1.1 AASHTO LRFD Bridge Design Specifications

The AASHTO LRFD Bridge Design Specifications (4th Edition) STM provisions limit the allowable stress on the faces of the struts and nodes. The factored resistance of a strut or tie element is given by:

$$P_r = \phi P_n \qquad \text{Equation 2-3}$$

where:

P_r = factored axial force in a strut or tie (kip)

P_n = nominal force of a compressive strut (kip)

ϕ = resistance factor (Table 2-1)

The nominal capacity of a strut element is given by the equation:

$$P_n = f_{cu} A_{cs} \qquad \text{Equation 2-4}$$

where:

P_n = nominal resistance of a compressive strut (kip)

f_{cu} = limiting (usable) compressive stress (ksi)

A_{cs} = effective cross-sectional area of strut (in²)

The minimum cross-sectional area of a strut will occur at its interface with an adjoining node, and can be limited to by the AASHTO limited strut width provision, discussed in section 2.2.1.1.2. The limiting compressive strength of a strut is based on the Modified Compression Field Theory (MCFT):

$$f_{cu} = \frac{f'_c}{0.8 + 170\varepsilon_1} \leq 0.85f'_c \quad \text{Equation 2-5}$$

$$\varepsilon_1 = \varepsilon_s + (\varepsilon_s + 0.002) \cot^2 \alpha_s \quad \text{Equation 2-6}$$

where:

α_s = the smallest angle between the compressive strut and the adjoining tie (rad)

ε_s = the tensile strain in the concrete in the direction of the tension tie (in/in)

f'_c = specified concrete strength (ksi)

f_{cu} = limiting (usable) compressive strength (ksi)

The usable compressive strength is a function of the angle between the strut and adjoining tie. As a result, a strut that adjoins to a tie with a shallow angle will have a low strut efficiency. The limiting compressive strength is also based the anticipated tensile strain the concrete, ε_s . This term can be measured in a laboratory setting, but is difficult for designers to correctly anticipate.

The nominal capacity of a node is:

$$P_n = f_{cu} A_{node}$$

where:

P_n = nominal capacity of a node (kip)

f_{cu} = limiting (usable) compressive stress (ksi)

A_{node} = area of node face (in²)

The limiting compressive stress is simply equal to the product of the node efficiency factor and the nominal concrete compression strength. The value of the node efficiency factor depends on the type of node (Table 2-1).

The capacity of a tie is given by:

$$P_n = f_y A_{st}$$

Equation 2-7

where:

P_n = nominal resistance of a tie (kips)

f_y = yield strength of reinforcement in the tie (ksi)

A_{st} = area of reinforcement in the tie (in²)

Table 2-1: Strut and node efficiency factors

Strut or Node Efficiency	ACI 318-05		AASHTO LRFD	
	β_s	ϕ	ν	ϕ
Strut with uniform cross-section	1.0	0.75	Equation 2-5	0.70
Bottle-shaped strut with reinforcement satisfying A.3.3	0.75	0.75	Equation 2-5	0.70
Bottle-shaped strut without reinforcement satisfying A.3.3	0.60	0.75	Equation 2-5	0.70
Struts in tension members	0.40	0.75	Equation 2-5	0.70
All other cases	0.60	0.75	Equation 2-5	0.70
CCC Node	1.0	0.75	0.85	0.70
CCT Node	0.80	0.75	0.75	0.70
CTT or TTT Node	0.60	0.75	0.65	0.70

2.2.1.1.1 Minimum Transverse Reinforcement

Four separate provisions for minimum transverse shear reinforcement in deep beams are specified in the AASHTO LRFD Bridge Design Specifications. Two of the four are designated specifically for deep beam design, and all but one are based on serviceability requirements rather than strength requirements.

The only requirement based on strength considerations is given in AASHTO 5.8.2.5, as part of the reinforcement requirements for shear and torsion:

$$A_v \geq 0.0316 \sqrt{f'_c} \frac{b_v s}{f_y} \quad \text{Equation 2-8}$$

where:

A_v = area of shear reinforcement (in²)

f'_c = specified concrete strength (ksi)

b_v = beam width (in)

s = stirrup spacing (in)

f_y = yield strength of the reinforcement (ksi)

A serviceability provision is provided in AASHTO 5.7, the section of the code that provides design requirements for flexural and axial effects. AASHTO 5.7.3.4 specifies that for members exceeding 36 inches in depth, longitudinal skin reinforcement must be uniformly distributed along both faces of the member for a distance $d_e/2$ nearest the flexural reinforcement. The area of this skin reinforcement must satisfy:

$$A_{sk} \geq 0.012(d_e - 30) \leq \frac{A_s + A_{ps}}{4} \quad \text{Equation 2-9}$$

where:

A_{sk} = area of skin reinforcement (in²/ft)

d_e = effective beam depth (in)

A_s = area of tensile reinforcement (in²)

A_{ps} = area of prestressing steel (in²)

In addition, the spacing of the longitudinal reinforcement may not exceed $d_e/6$ or 12 inches.

Another provision based on serviceability requirements is included in AASHTO 5.13.2.3, and is specified exclusively for deep beams:

$$N_R = \phi f_y A_s \geq 0.12 b_v s \quad \text{Equation 2-10}$$

where:

f_y = yield strength of the reinforcement (ksi)

A_s = area of tensile reinforcement (in²)

b_v = beam width (in)

s = stirrup spacing (in)

A grid of reinforcement must be provided along each vertical face of a member; The amount of reinforcement in each orthogonal direction must satisfy Equation 2-10. The spacing of the reinforcing bars in the grid may not exceed $d_c/3$ or 12 inches. For beams that are less than 10 inches wide, the code specifies that a single grid of reinforcement may be used in lieu of a grid at each face.

A final serviceability provision specifies a minimum amount of crack control reinforcement. AASHTO 5.6.3.6 specifies that structures designed using STM “*shall contain an orthogonal grid of reinforcing bars near each face. The spacing of the bars in these grids shall not exceed 12.0 in. The ratio of reinforcement area to gross concrete area shall not be less than 0.003 in each direction.*” This provision is more conservative than deep beam transverse reinforcement requirements in other structural design codes, such as ACI 318-05.

The code commentary suggests that for thinner members, the crack control reinforcement should consist of two orthogonal grids, one at each face. For very wide members, the commentary suggests that multiple grids throughout the width of the member may be necessary. Notably, the code specifies that this crack control reinforcement may also be utilized as tie reinforcement in the strut-and-tie model.

As specified above, both the horizontal shear reinforcement ratio (ρ_h) and the vertical shear reinforcement ratio (ρ_v) of a deep beam must be equal to or greater than 0.003. However, the code does not specify whether flexural longitudinal reinforcement placed near side faces may also be counted as horizontal skin reinforcement.

It is reasonable to assume that flexural reinforcement will restrain cracks in areas adjacent to the reinforcement. Using this assumption, the gross area used in the calculation of ρ_h omitted the concrete area that is adjacent to longitudinal reinforcement. Thus, in the example of the beam shown in Figure 2-7, ρ_h is calculated as the area of horizontal shear reinforcement divided by the area shaded in gray. The depth of each

unshaded area is roughly equal to twice the distance from the centroid of the longitudinal reinforcement to the nearest face. This interpretation was suggested by the TxDOT project director of the current study, Mr. Dean Van Landuyt, and was utilized for the calculation of ρ_h for test specimens in the current experimental program.

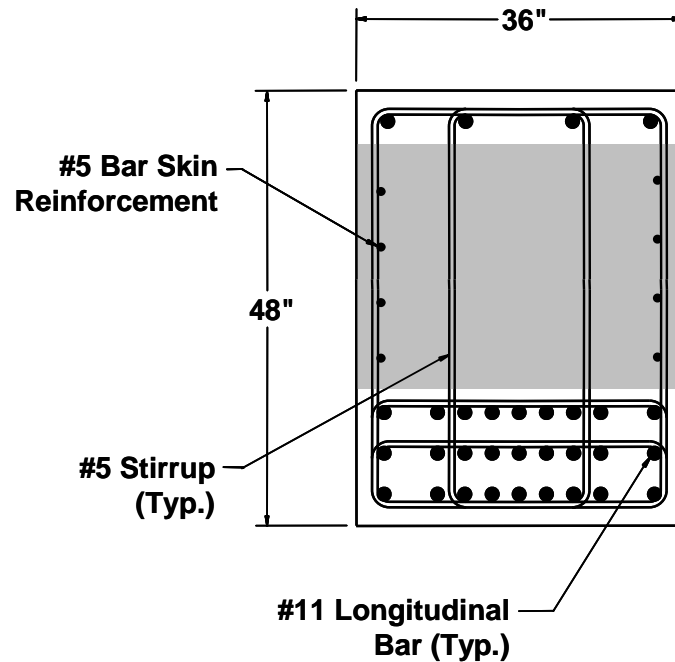
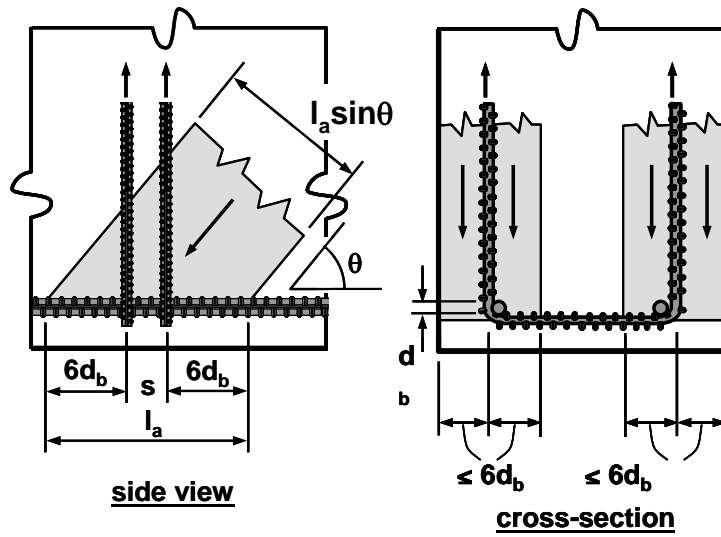


Figure 2-7: Calculation of ρ_h in a current project specimen

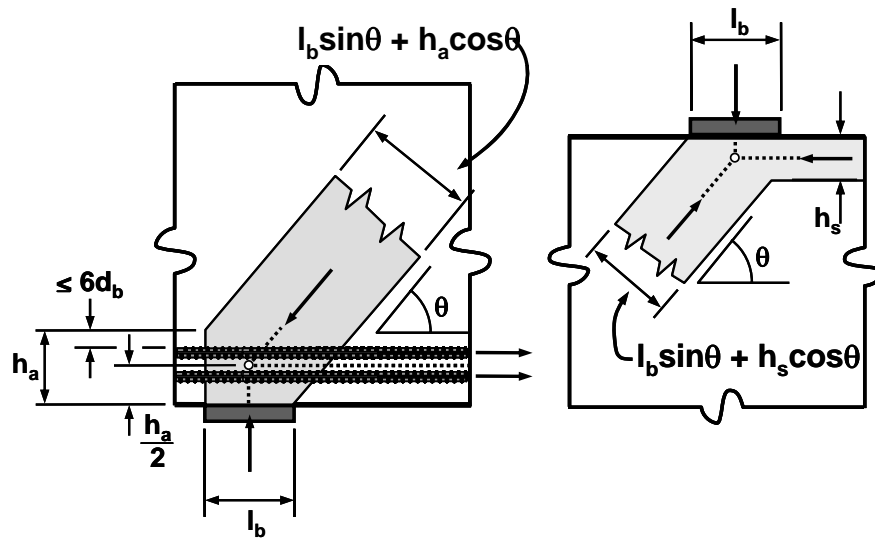
2.2.1.1.2 Limited Strut Width Provision

AASHTO LRFD Bridge Design Specifications strongly encourage the use of multiple stirrup legs for wide members. The code stipulates that when struts are anchored by reinforcement (such as stirrups anchoring a CTT node in a deep beam), only areas near the plane of the stirrup legs may be utilized as part of the strut. Thus, the width of strut may be limited if stirrup legs are not adequately distributed throughout the width of a member, as shown in Figure 2-8a. In addition, the vertical height of a node is limited by the placement of adjoining longitudinal reinforcement, as shown in Figure 2-8b.

The limited strut width provision is intended for use in D-regions, and is based on research by Collins and Mitchell in 1986 on members subjected to torsion (Brown et al., 2006). However, there has been very little research on its applicability to strut-and-tie modeling. An examination of this code provision's applicability to large-scale deep beams designed using STM is an objective of the current research program.



(a) Strut anchored by reinforcement (CTT node)



(b) Strut anchored by bearing and reinforcement (CCT node)

(c) Strut anchored by bearing and strut (CCC node)

Figure 2-8: AASHTO limited strut width provision (AASHTO LRFD Figure 5.6.3.3.2-1, Brown et al., 2006)

2.2.2 TxDOT Research Project 4371

University of Texas researchers developed new STM design expressions as part of TxDOT research project 4371. The expressions were presented in the form of modifications to the current AASHTO code, and can require less transverse steel than the current AASHTO provisions.

Two modifications were suggested to the transverse reinforcement requirements of AASHTO. The first is a modification of the crack control reinforcement provision in AASHTO 5.6.3.6. The modified expressions stipulate that the amount of reinforcement within a strut shall be calculated as:

$$\rho_{\perp} = \sqrt{\left(\frac{A_{sH}}{bs_H}\right)^2 + \left(\frac{A_{sV}}{bs_V}\right)^2} \quad \text{Equation 2-11}$$

where:

ρ_{\perp} = equivalent reinforcement perpendicular to the strut axis

A_{sH} = total area of horizontal reinforcement in a strut within spacing s_H (in²)

b = width of the member (in)

s_H = spacing of horizontal reinforcement (in)

A_{sV} = total area of vertical reinforcement in a strut within a spacing s_V (in²)

s_V = spacing of vertical reinforcement (in)

This method of quantifying the amount transverse reinforcement crossing a strut is practically identical to the ACI minimum transverse reinforcement provision (Equation 2-18) that will be introduced in the following section.

The TxDOT 4371 modifications specify that that the minimum amount of reinforcement within a strut shall be taken as:

$$\rho_{\perp, \min} = \frac{P_u}{f_y b \ell m} \geq 0.003 \quad \text{Equation 2-12}$$

where:

P_u = factored load in a strut (kip)

f_y = yield strength of the reinforcement within a strut (ksi)

b = width of the member transverse to the plane of the strut-and-tie model (in)

ℓ = length of the strut (in)

m = slope of the angle of compression dispersion (see Figure 2-9)

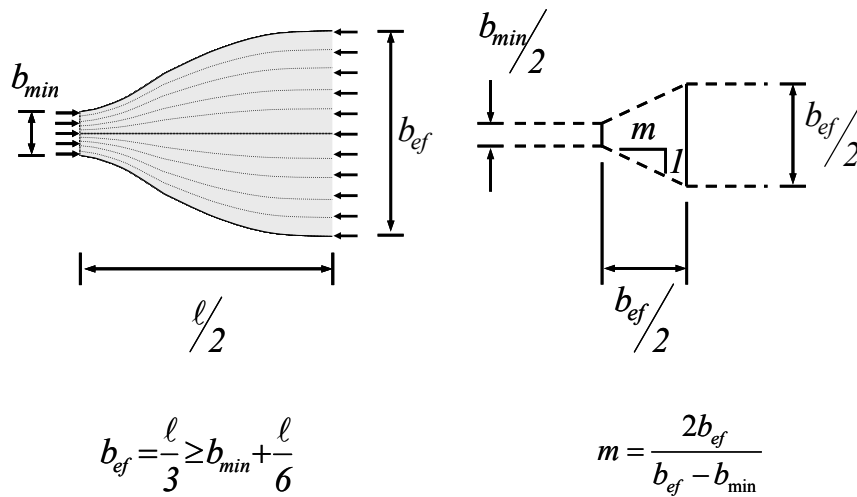


Figure 2-9: Dispersion of compression in a bottle-shaped strut; view is perpendicular to the plane of the dispersion of compression (Brown et al. 2006, Schlaich and Weischede 1982)

The efficiency factor for a strut that is reinforced with this minimum amount of transverse reinforcement is given by:

$$\nu = \frac{0.85 \tan \theta}{\sqrt{f'_c}} \frac{l_n}{w_s \sin \theta} \quad \text{Equation 2-13}$$

But not greater than the minimum of $0.85 \frac{l_n}{w_s \sin \theta}$ and 0.85.

Conversely, if a given strut does not have sufficient reinforcement as defined by Equations 2-11 and 2-12, its strut efficiency is given by:

$$v = \frac{0.85 \tan \theta}{3\sqrt{f'_c}} \frac{l_n}{w_s \sin \theta} \quad \text{Equation 2-14}$$

But not greater than the minimum of $0.85 \frac{l_n}{w_s \sin \theta}$ and 0.85.

where:

P_n = nominal capacity of a strut (kips)

v = efficiency factor

f'_c = specified compressive strength (ksi)

A_c = cross-sectional area of the strut at the face of the node (in²)

θ = angle between the compressive strut and the adjoining tie.

(degrees)

ℓ = length of the node adjoining the strut. For CCC and CCT nodes $\ell_n = \ell_b$. For CTT nodes and $\ell_n = \ell_a$ (see Figure 2-8)

w_s = width of the strut at the face of the node (see Figure 2-8)

2.2.3 ACI 318-05

ACI 318-05 allows two different methods for the design of deep beams. ACI 10.7 stipulates it is permissible to design a deep beam by either taking into account its nonlinear strain distribution, or by using the strut-and-tie provisions outlined in Appendix A of ACI 318-05.

The strut-and-tie provisions of Appendix A specify the nominal strength of a strut, tie, or node is based on:

$$\phi F_n \geq F_u \quad \text{Equation 2-15}$$

where:

F_n = nominal strength of strut, tie, or node (lbs)

F_u = force in a strut or tie, or force acting on one face of a nodal zone (lbs)

ϕ = strength reduction factor (Table 2-1)

The nominal capacity of a strut is given as:

$$F_{ns} = f_{cu} A_c \quad \text{Equation 2-16}$$

$$f_{cu} = 0.85 \beta_s f'_c \quad \text{Equation 2-17}$$

where:

F_{ns} = nominal strut capacity (lbs)

f_{cu} = effective concrete compressive strength (psi)

A_c = cross-sectional area at one end of the strut (in²)

β_s = strut efficiency factor (see Table 2-1)

f'_c = concrete compressive strength (psi)

The effective concrete compressive strength is taken as the lesser of f_{cu} in the strut or f_{cu} in the adjacent nodal zone. The strut efficiency factor β_s depends on the strut type; ACI 318-05 stipulates a different efficiency factor for each of five different strut types (Table 2-1).

If a bottle-shaped strut is utilized, the strut efficiency depends on the amount of transverse reinforcement provided. A less stringent strut efficiency factor is required if transverse reinforcement is provided as per ACI A.3.3, which stipulates that reinforcement across the strut must be placed in one of two ways. The first method for assigning reinforcement stipulates layers of transverse reinforcement must cross the bottle-shaped strut in order to satisfy:

$$\sum \frac{A_{si}}{bs_i} \sin \alpha_i \geq 0.003 \qquad \text{Equation 2-18}$$

where:

A_{si} = area of surface reinforcement in the i^{th} layer crossing a strut (in²)

s_i = spacing of reinforcement in the i^{th} layer adjacent to the surface of the member (in)

b = width of strut perpendicular to the plane of reinforcing bars (in)

α_i = angle between the axis of a strut and the bars in the i^{th} layer of reinforcement crossing that strut (deg)

Nomenclature for this provision is illustrated in Figure 2-10.

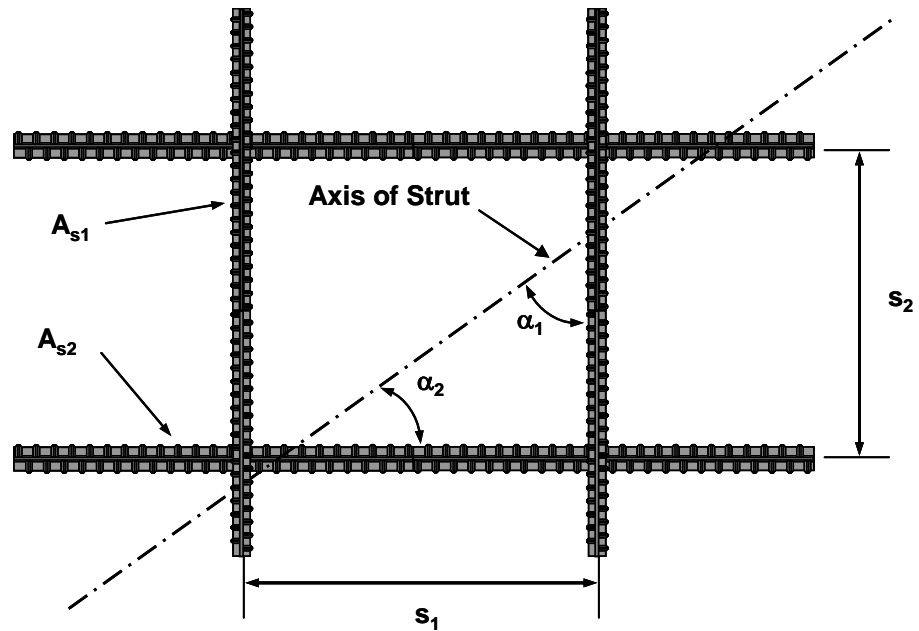


Figure 2-10: Nomenclature for Equation 2-18 (Brown et al., 2006)

As an alternate method, a strut-and-tie model may be used to represent the dispersion of forces within a bottle shape strut (Figure 2-11). Transverse reinforcement is placed to meet the requirements of the ties within that model. It is permitted to assume the compressive force in the strut spreads at a slope of 2 longitudinal to 1 transverse (Figure 2-11).

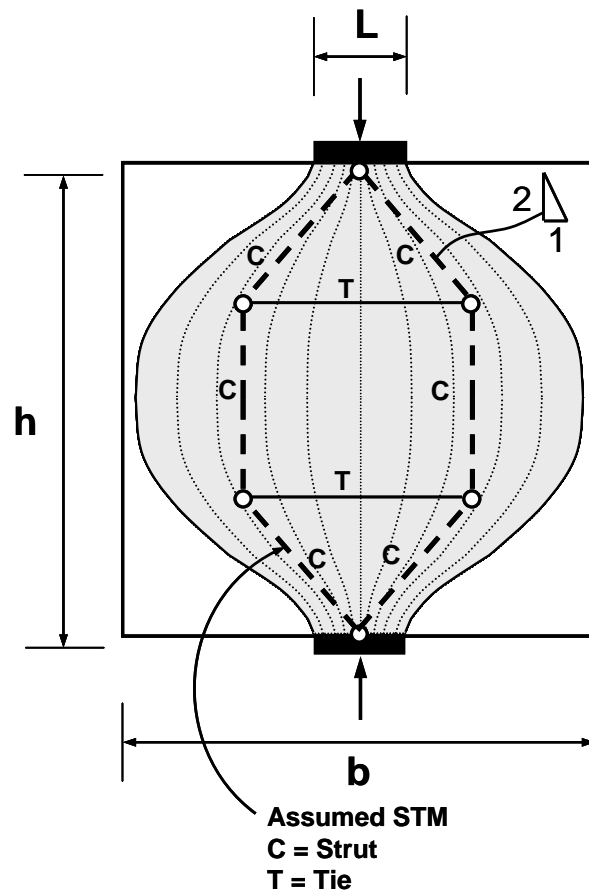


Figure 2-11: Strut-and-tie model for a bottle-shaped strut (Brown et al., 2006)

The nominal strength of a node in ACI 318-05 Appendix-A provisions is given as:

$$F_{nn} = f_{cu} A_n \quad \text{Equation 2-19}$$

$$f_{cu} = 0.85 \beta_n f'_c \quad \text{Equation 2-20}$$

where:

F_{nn} = nominal strength of nodal zone face (lbs)

f_{cu} = effective concrete compressive strength (psi)

A_n = cross-sectional area of a node face (in²)

β_n = node efficiency factor (see Table 2-1)

f'_c = concrete compression strength (psi)

The capacity of a tie element is given by:

$$F_{nt} = A_{st}f_y$$

Equation 2-21

where:

F_{nt} = nominal capacity of a tie (lbs)

f_y = yield strength of reinforcement in the tie (psi)

A_{st} = area of reinforcement in the tie (in²)

In lieu of using strut-and-tie modeling, it is permissible to use a design method that accounts for the nonlinear strain distribution of deep beams. However, the code does not offer guidance on completing design using this method, other than to stipulate minimum transverse reinforcement requirements. If this method is used, the designer may either satisfy the above requirements of ACI 318-05 Appendix A, or two other requirements, listed in ACI 11.8.4 and 11.8.5, respectively:

$$A_v \geq 0.0025b_w s$$

Equation 2-22

$$A_{vh} \geq 0.0015b_w s_2$$

Equation 2-23

where:

A_v = area of shear reinforcement perpendicular to the span (in²)

A_{vh} = area of shear reinforcement parallel to the span (in²)

s = spacing of shear reinforcement measured in a direction parallel to longitudinal reinforcement (in)

s_2 = spacing of shear reinforcement measured in a direction perpendicular to longitudinal reinforcement (in)
 b_w = web width (in)

Additionally, both s and s_2 must not exceed $d/5$, or 12 inches. It is of note that the vector sum of the coefficients in Equations 2-22 and 2-23 (that is, 0.0025 and 0.0015) were used as the basis for the coefficient in Equation 2-18. Notably, ACI 11.8.3 stipulates that the nominal shear capacity of member shall not exceed $10\sqrt{f'_c}b_wd$.

Given the lack of simple and reliable design methods that incorporate a nonlinear strain distribution, the current research program will focus on the design methods of ACI 318-05 Appendix A.

2.3 TXDOT BENT CAP FIELD EVALUATION

A number of TxDOT structural deep beams have recently exhibited poor serviceability performance. The questionable performance of these members partially spurred the funding of the current research project. This section highlights the performance of two such deep beams. The design details of these and other TxDOT bent caps are further discussed in section 3.4.

2.3.1 Greens Road Bent Cap

Recently a number of bent caps in the Houston area have developed significant diagonal shear cracks. These bent caps are part of the superstructure of I-45 over Greens Road, and were designed in 1993 using the AASHTO Standard Specifications. The bents typically consist of multiple spans, and therefore contain longitudinal reinforcement near both the top and bottom faces of the beam to provide adequate capacity for both positive and negative moments. A typical cross-section is shown in Figure 2-12, and reinforcement details are listed in Table 2-2.

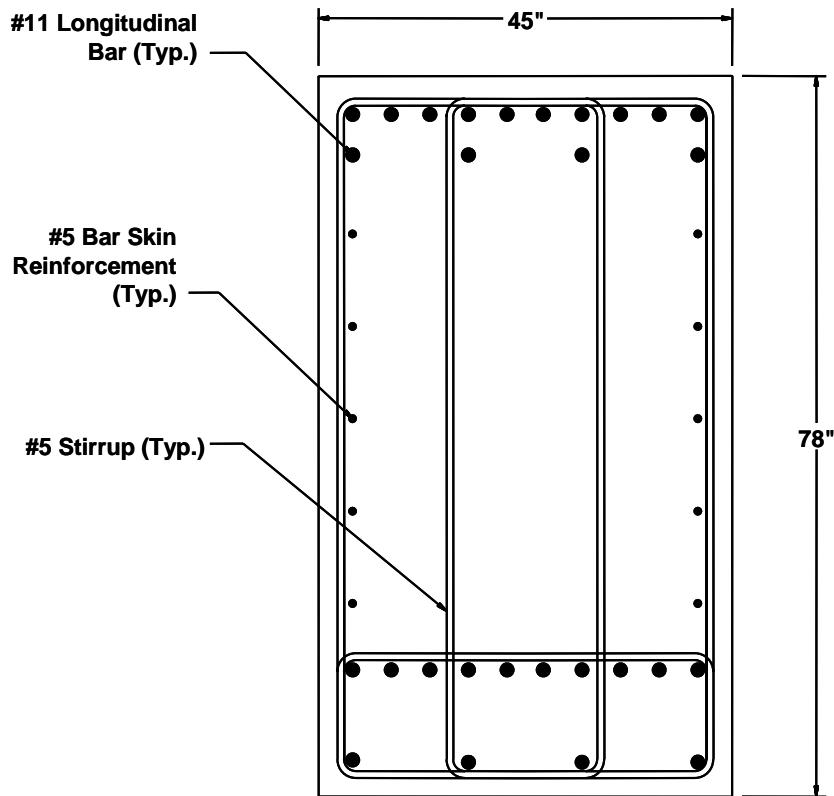


Figure 2-12: Greens road bent cross-section

Table 2-2: Greens road bent reinforcement details

Vertical Shear Reinforcement	Four-legged #5 stirrups @ 6"
ρ_v	0.0065
Horizontal Shear Reinforcement	(8) #5 bars
ρ_H^*	0.0020
$\sum \frac{A_{si}}{bs_i} \sin \alpha_i$	0.0068
Tensile Longitudinal Reinforcement	(28) #11 bars
ρ_L	0.0124

*As defined in section 2.2.1.1.1

Inspections performed in 2005 revealed significant shear cracking in the bents, with diagonal cracks as wide as 0.030 inches. Due in part to the lack of applicable research on large scale deep beams, the bent caps underwent a structural retrofit in 2005

to ensure their structural integrity. Photographs of the bent caps and shear cracks are exhibited in Figure 2-13.

The bent caps performed poorly even though the design adhered to the AASHTO Standard Specifications. The Greens Road bent caps contained quantities of vertical shear reinforcement well in excess of both current AASHTO LRFD standards and TxDOT Project 4371 recommendations.

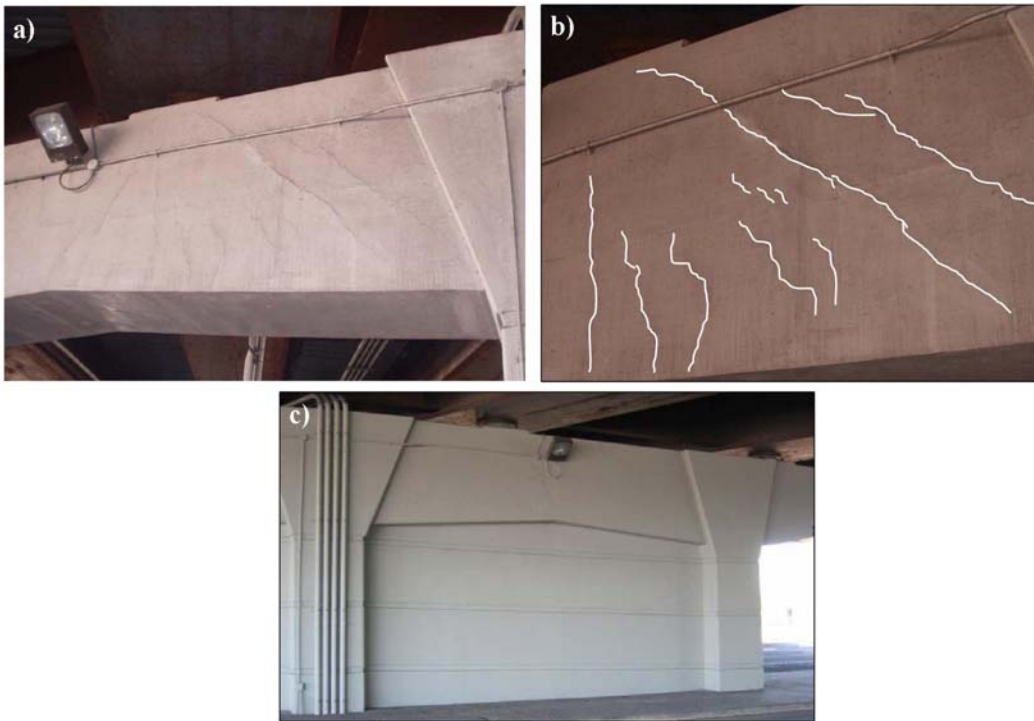


Figure 2-13: a) Typical cracking pattern; b) Highlighted diagonal shear cracks; c) Completed structural retrofit

2.3.2 I-345 Pier Cap

A large pier cap supporting the northbound lanes of Interstate 345 in downtown Dallas, Texas recently exhibited significant shear cracking. A typical cross-section is shown in Figure 2-15, and pertinent member details listed in Table 2-3. The shear span

pictured in Figure 2-14b), which has an a/d ratio of approximately 1.78, exhibited maximum shear crack widths of approximately 0.060 inches.

The cap was designed in 1968 using the AASHTO Standard Specifications, and contains a significant amount of vertical shear reinforcement. However, the shear span pictured in Figure 2-14b was re-evaluated using TxDOT 4371 design provisions (section 2.2.2) and found to have inadequate capacity.

Table 2-3: I-345 cap reinforcement details

Vertical Shear Reinforcement	Four-legged #6 stirrups @ 5 1/2"
ρ_v	0.0049
Horizontal Shear Reinforcement	(10) #5 bars
ρ_H^*	0.00049
$\sum \frac{A_{s_i}}{b s_i} \sin \alpha_i$	0.0049
Tensile Longitudinal Reinforcement	(24) #11 bars top (45) #14 bars bottom
ρ_L	0.0175

*As defined in section 2.2.1.1.1



Figure 2-14: a) Interstate 345 pier cap in Dallas, TX; b) Highlighted diagonal shear cracks

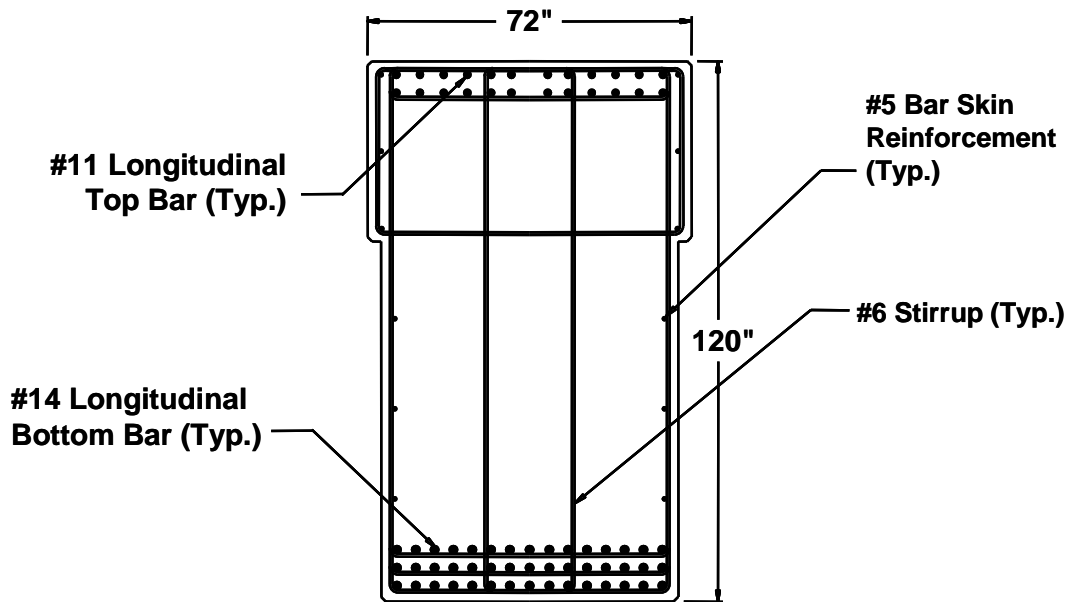


Figure 2-15: I-345 bent

2.4 STATE OF KNOWLEDGE: SHEAR STRENGTH OF DEEP BEAMS

As part of Research Project 4371 recently completed at the University of Texas, a database of shear tests was compiled from nearly 50 years of technical literature. The database contains over 1,200 shear tests, of which nearly 500 are tests performed on deep beams.

Analysis of the test specimens contained in the shear database sheds light on trends in modern shear testing. The overwhelming majority of shear tests performed in the last 50 years have been conducted on test specimens that are much smaller than bents recently designed by TxDOT, as indicated in Figure 2-16 and Figure 2-17. The figures simultaneously highlight the lack of testing on large-scale specimens and the unique nature of the specimens tested in the current research program.

The specimens in the current research program are among the largest ever tested. In fact, the specimens in current research program may be the largest ever tested (in terms of gross area) when considering only specimens that contained transverse reinforcement.

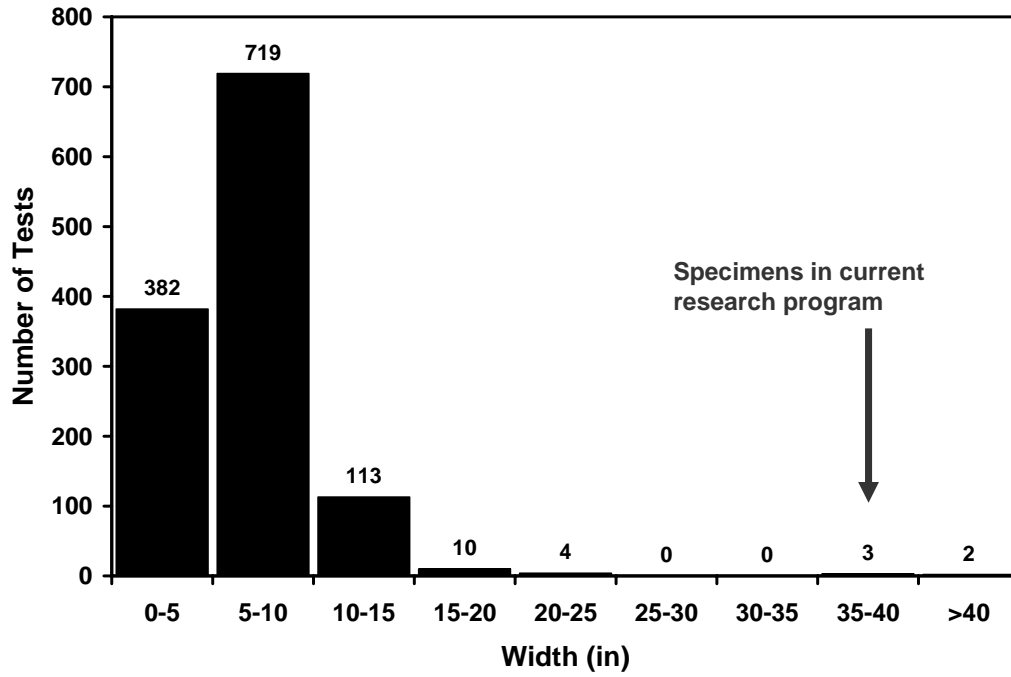
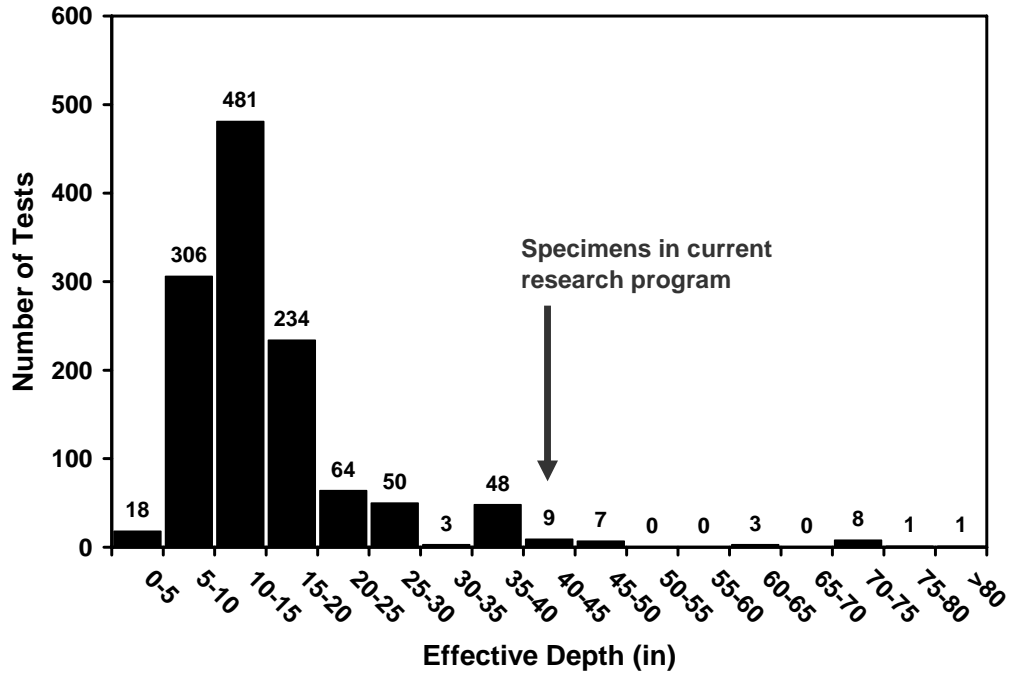


Figure 2-16: History of shear tests

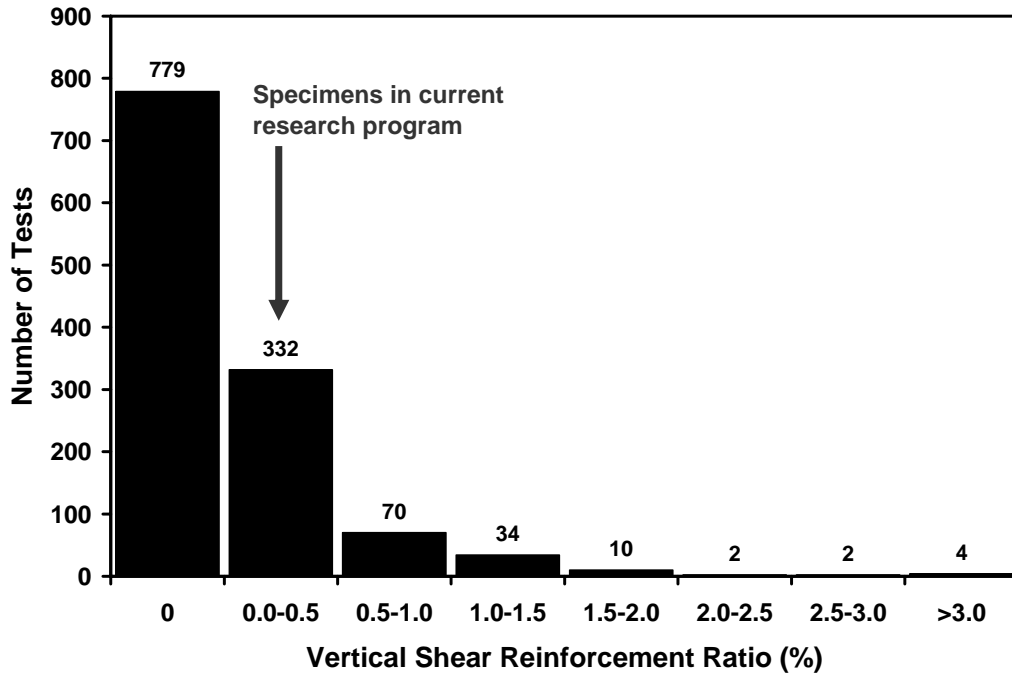
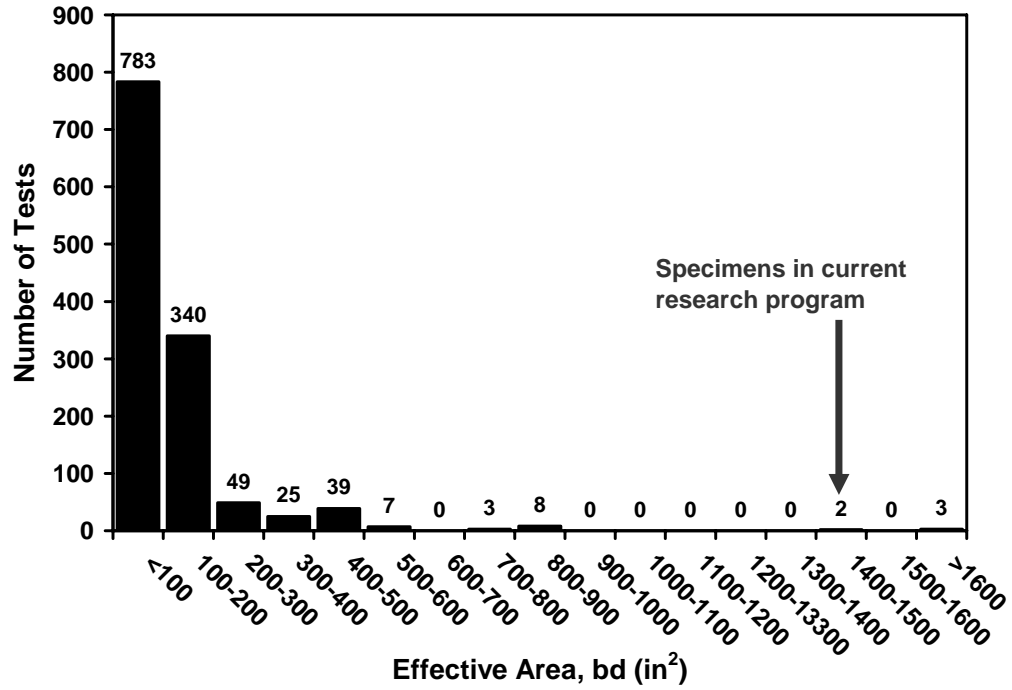


Figure 2-17: History of shear tests (continued)

2.5 LITERATURE REVIEW

Many research projects investigating the effect of transverse steel in the shear strength of deep beams have been completed in recent history. A large number of these studies are summarized and discussed in the following sections. These research studies are outlined and discussed individually in chronological order. The conclusions of the studies are summarized at the conclusion of the review.

The three main variables discussed are the vertical shear reinforcement ratio, horizontal shear reinforcement ratio, and the quantity and transverse spacing of stirrup legs. These variables are discussed in terms of their effect on both ultimate shear strength and serviceability performance on deep beams. A number of studies that contain specimens loaded such that a/d is just above 2.0 are also included in the review.

2.5.1 DePaiva and Siess (1965)

DePaiva and Siess tested 19 simply supported deep beams with varying amount of longitudinal tensile reinforcement, the concrete strength, the a/d ratio, and the amount and location of vertical shear reinforcement. Some specimens included inclined shear reinforcement in lieu of orthogonal shear reinforcement. The beams were tested at third points with L/d ratios of 2, 3 or 4, corresponding to a/d ratios of 0.67, 1.0, and 1.33. The compressive strength ranged from 2890 to 5360 psi. The specimens had effective depths ranging from six to 12 inches, and widths ranging from two to four inches. They were heavily reinforced, with vertical shear reinforcement ratios ranging from 0.0070 to 0.0142.

The researchers found that vertical or inclined shear reinforcement had very little effect on the ultimate strength of the beams. However, they noted that that increased shear reinforcement made the beams less likely to fail in shear. In addition it was found that the shear reinforcement had no effect on the formation of inclined cracks, but did have an effect on deflection.

2.5.2 Leonhardt and Walther (1966)

Leonhardt and Walther led a series of studies in the 1960s to investigate the shear strength of reinforced concrete deep beams. One series tested 11 large-scale deep beams; nine of the tests were conducted on single-span beams, while two others were completed on double-span deep beams.

The researchers found the ultimate shear strength of deep beams is independent of web reinforcement (Kong, Robins, and Cole, 1970). It was noted that beams demonstrated “arch” behavior; that is, forces flowed directly from the point of the loading to the support. Their work formed the basis of the 1978 European CEB-FIP Model Code design provisions for deep beams (Rigotti, 2002).

2.5.3 Kong, Robins, and Cole (1970)

Thirty-five simply supported deep beams were tested in an effort study of the effect of orthogonally placed shear reinforcement on the failure mode, ultimate load in shear, crack widths, and crack patterns in deep beams. The beams had depths ranging from 10 to 30 inches, a three inch width, concrete strengths of approximately 3000 psi, and a/d ratios ranging from 0.23 to 0.70.

The transverse reinforcement configurations of the specimens are shown in Figure 2-18. A wide range of transverse reinforcement ratios were tested; the vertical shear reinforcement ratio ranged from 0.0061 to 0.0245, while the horizontal shear reinforcement ratio ranged from 0.0017 to 0.0245.

The researchers found that the effectiveness of shear reinforcement depended on the a/d ratio. Whereas vertical reinforcement was effective in reducing cracks widths at higher a/d ratios (such as 0.7), horizontal reinforcement was most effective at low a/d ratios (such as 0.35), particularly when spaced closely and near the bottom of the beam. In addition, all the specimens had similar modes of shear failure, regardless of reinforcement amount or arrangement; nearly all the specimens failed by diagonal splitting and crushing of concrete under the bearing area.

The researchers also made observations regarding the serviceability performance of the specimens. It was found that transverse reinforcement had no effect on the cracking pattern. The researchers noted that while crack widths were generally inversely proportional to shear reinforcement ratio, the widths also depended heavily on the arrangement of reinforcement within the beam. The formation of parallel shear cracks occurred at about 70 to 90% of the ultimate applied load, and was therefore a strong indication of impending failure.

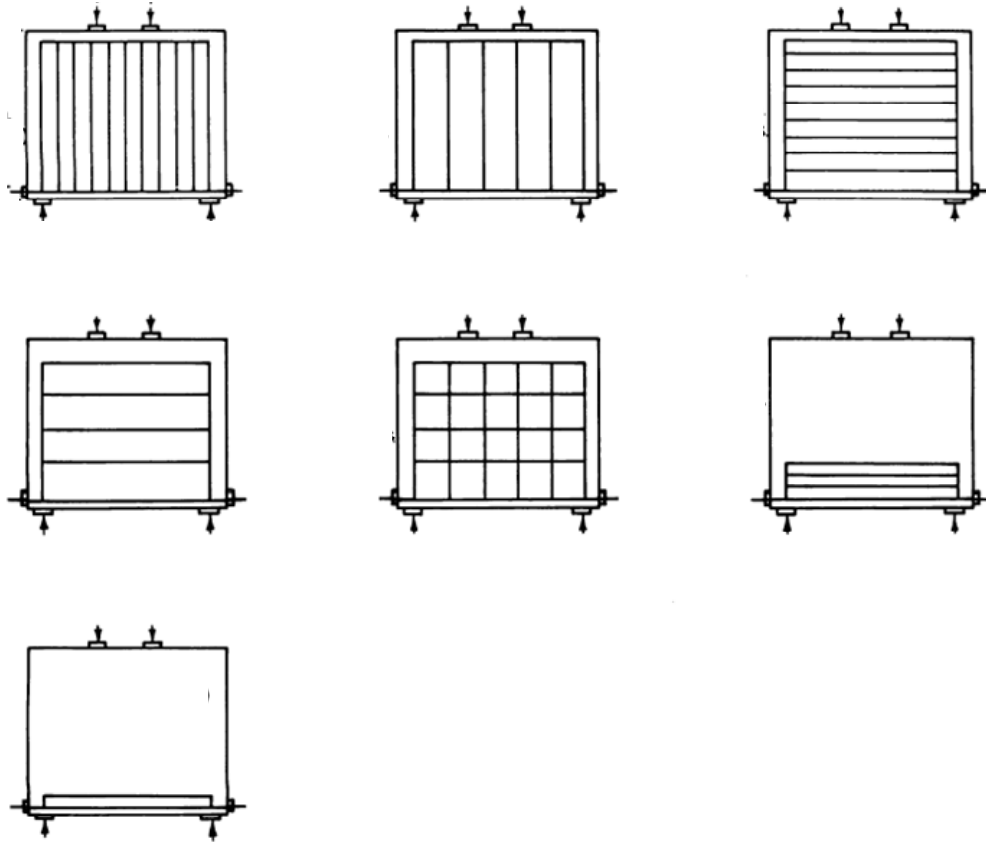


Figure 2-18: Transverse reinforcement configurations (Kong et al., 1970)

2.5.4 Smith and Vantsiotis (1982)

Smith and Vantsiotis tested 52 deep beams in an effort to determine the effect of shear reinforcement and shear span-to-effective depth ratio on first shear cracking, crack width, and ultimate strength. The beams had a concrete strength of approximately 2800 psi and an effective depth of 14 inches. The vertical shear reinforcement ratio (ρ_v) was varied from 0.0018 to 0.0125, horizontal shear reinforcement ratio (ρ_h) was varied from 0.0023 to 0.0091, and a/d was varied from 0.77 to 2.01.

The researchers observed that ρ_v had a moderate effect on the ultimate shear strength, and that vertical shear steel was most effective for a/d ratios greater than one. Conversely it was observed that ρ_h had little or no influence on the ultimate shear strength, and that the minimal positive effect of horizontal shear steel was only effective for beams with small a/d ratios. In addition, it was noted that web reinforcement had no effect on the mode of failure, but that less damage was observed in reinforced beams than unreinforced beams.

The researchers found that transverse reinforcement had no effect on the formation of the first inclined crack; inclined cracks first occurred at 40 to 50 percent of ultimate loads. Also, beams with shear reinforcement had considerably smaller crack widths than those without, especially at $a/d < 1.0$.

2.5.5 Hsiung and Frantz (1985)

Hsiung and Frantz tested five one-third scale models of large reinforced concrete beams, with the intent of studying the effect of stirrup leg spacing in wide beams. The transverse reinforcement ratio was identical for each of the five specimens, while the stirrup spacing and quantity of stirrup legs was varied. Four of the beams had two stirrup legs, one near each edge of the cross-section, while another had six stirrup legs distributed evenly throughout the width of the beam. As shown in Figure 2-19, the beams were 18" deep with an effective depth of 16.5", and with varying widths. The average concrete strength was 6,235 psi and the a/d ratio was equal to 3.0.

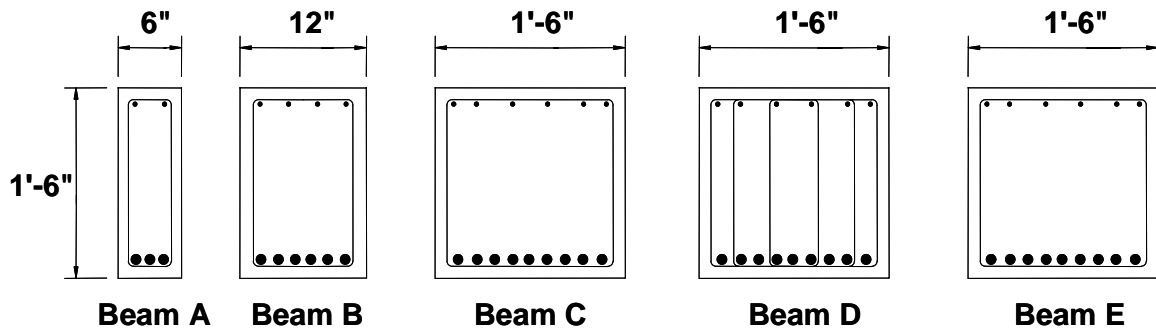


Figure 2-19: Hsuing and Frantz specimens

The researchers found that the ultimate shear capacity of a given beam was simply proportional to its width; stirrup spacing, stirrup leg quantity, and transverse distribution of stirrup legs across the web width had no effect on the shear strength. However, it was noted that the specimen containing multiple stirrup legs exhibited greater stresses in interior stirrup legs than exterior stirrup legs.

In addition, several serviceability conclusions were reported. It was found that surface inclined crack widths were the same for all beams at failure. Previous to the yield of the shear reinforcement, surface crack widths were smaller for beams with more shear reinforcement located near the surface.

Table 2-4: Hsuing and Frantz specimen experimental capacities

Beam	Width (in)	Effective Depth (in)	3/16" Diameter Stirrup Configuration	Ultimate Shear Capacity (kips)
A	6	16.5	1 @ 4.2 in	24.8
B	12	16.5	2 @ 4.5 in	45.0
C	18	16.5	3 @ 4.2 in	76.2
D	18	16.5	3 @ 4.2 in	78.2
E	18	16.5	3 @ 4.5 in	-

Beams A through D were tested to failure, while Beam E was only loaded to about 80% of its expected shear capacity. At that point, the load was held constant while epoxy was injected into the shear cracks. After epoxy curing, the load was removed and cores located along the main shear crack were removed from the beam. It was found that there was no significant variation in crack width through the width of the beam. In other words, a lack of interior stirrup legs did not adversely affect interior crack widths; interior cracking was no more severe than the exterior cracking.

The relatively constant crack widths throughout the width of the beam refute the concept that interior stirrup legs are superior from a serviceability standpoint. In fact, the research suggests that interior stirrup legs are not advantageous from either a strength or serviceability standpoint. Given the complexity and cost of constructing beams with interior stirrup legs, this research would suggest it advisable to avoid interior stirrup legs altogether.

2.5.6 Rogowski, MacGregor, and Ong (1986)

Seven simply supported and 17 two-span reinforced concrete deep beams were tested. The goal of the study was to study the effect of continuity on deep beams. The specimens had effective depths ranging from 20 to 40 inches, concrete strengths ranging from 3,800 to 6,300 psi, and a/d ratios ranging from 1.0 to 2.5.

It was found that horizontal shear reinforcement had no effect on the shear strength of the deep beams. Beams with light or no reinforcement failed suddenly in shear, whereas beams with heavy shear reinforcement tended to fail in a ductile manner. In tests of continuous multi-span beams, it was found that shear reinforcement had no effect on ultimate shear strength.

2.5.7 Anderson and Ramirez (1989)

Anderson and Ramirez performed a study to determine proper stirrup detailing in reinforced concrete members with high shear stresses. The researchers tested 12 “narrow” beams that were 8 inches wide and 20 inches deep; the main variable in these

was the stirrup detailing scheme (Figure 2-20). In addition, four 16 inch by 16 inch “wide” beams were tested, shown in Figure 2-21. The main variable in the wide beam tests was the number of stirrup legs and stirrup spacing.

The amount of longitudinal reinforcement was identical for each of the four wide beam specimens (five #9 bars in the base of the beam and five #5 bars near the top face). The a/d ratio was approximately equal to 2.0 for all experimental tests. The concrete strength of the specimens ranged from 4,000 to 6,000 psi.

The researchers reached two major conclusions as a result of the narrow beam tests. First, it was found that single-legged stirrups (Figure 2-20, scheme 5) had inferior performance and should not be used. In addition, it was concluded that if U-shaped stirrups were used, the ends should be anchored by hooks that are bent into the concrete core.

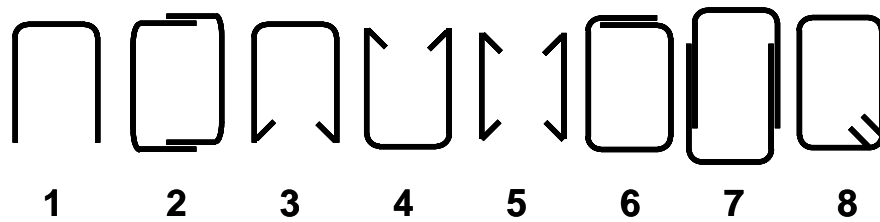


Figure 2-20: Anderson and Ramirez narrow beam stirrup detailing schemes

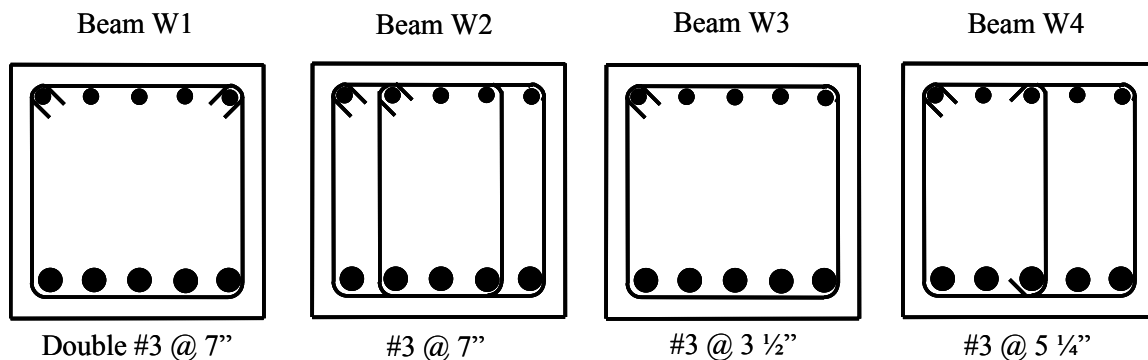


Figure 2-21: Anderson and Ramirez wide specimens

Table 2-5: Anderson and Ramirez Wide Specimen Experimental Results

Beam	f'_c (psi)	V_{test} (kips)	Failure Mode
W1	4230	103.4	Shear-Compression
W2	4670	123.4	Shear-Compression
W3	4690	113.4	Shear-Compression
W4	4900	131.4	Flexure

As a result of the wide beam tests, the researchers concluded that it is preferable for wide beams to contain multiple stirrup legs spaced uniformly across the width of the cross-section. The researchers found that specimens with only two stirrup legs had higher strains in the corner longitudinal bars than in interior longitudinal bars. It was noted the beams with small stirrup spacing lessened the effect of stress concentrations at the beam corners. Most importantly, it was found that beams with interior stirrup legs had higher ultimate load capacities (Table 2-5).

2.5.8 Tan, Kong, Teng, and Weng (1997)

Tan et al. tested 18 high strength reinforced concrete deep beam specimens with compressive concrete strengths ranging from 8,000 to 12,500 psi. Each specimen was 4.29 inches in width, 19.5 inches in depth, and 17.4 inches in effective depth. The main variables were the a/d ratio, ρ_v , and ρ_h .

The researchers concluded that the most effective layout of shear reinforcement is an orthogonal grid consisting of shear reinforcement in both the vertical and horizontal directions. In addition, it was noted that the vertical shear reinforcement ratio was most effective at reducing crack widths and increasing the ultimate shear capacity in specimens loaded such $a/d > 1.13$.

It was also found that the amount and configuration of transverse reinforcement steel had virtually no effect on the diagonal cracking load. As established by many

previous researchers, it was found that the effect of horizontal shear reinforcement diminishes at span-to-depth ratios greater than 1.0.

2.5.9 Shin, Lee, Moon, Gosh (1999)

Shin et al. tested 30 deep beams in an effort to investigate the effect of the vertical transverse reinforcement ratio on the first diagonal cracking load and the nominal shear capacity. Specimens had a concrete strength of 7600 or 10,600 psi, an effective depth of 8.5 in, and a width of 4.9 in; a/d was varied from 1.5 to 2.5. The beams had no horizontal shear reinforcement and the vertical shear reinforcement ratio (ρ_v) was varied from zero to 0.0181.

It was found that for a given a/d ratio, an increase in vertical shear reinforcement increased the ultimate shear capacity. However, the mode of failure was not dependent on ρ_v , but rather the a/d ratio. In addition, it was found that ρ_v had no effect on the first diagonal cracking load.

2.5.10 Oh and Shin (2001)

Fifty-three deep beams were tested in an effort to determine both their ultimate shear strength and diagonal cracking strength. The beams had concrete strengths ranging from 3,335 to 10,730 psi, an effective depth of 19.7 inches, and a width of 5.12 inches. The shear span-to-effective depth ratio (a/d) ranged from 0.5 to 2.0. Specimens had vertical shear reinforcement ratios were ranging from zero to 0.0034, and horizontal shear reinforcement ratios ranging from zero to 0.0094.

It was found while ρ_v had a marginal effect on ultimate shear strength, the effect diminishes for small a/d ratios; ρ_h had virtually no effect ultimate shear strength. Instead, the a/d ratio was reported to have the greatest effect on ultimate shear strength. The amount of vertical reinforcement did not greatly affect the first diagonal cracking load.

2.5.11 Young, Bracci, Keating, Hueste (2002)

Sixteen full scale bent caps specimens were tested in an effort to investigate cracking in Texas Department of Transportation (TxDOT) bent caps. The beams were tested at an a/h ratio of approximately 1.5 (corresponding a/d of approximately 1.6), as shown in Figure 2-22. The three sets of cross-sections that were tested are shown in Figure 2-23. Among the variables tested were transverse reinforcement detailing and side face (horizontal shear) reinforcement. The horizontal shear reinforcement ratio was equal to 0.0010 for all beams, while vertical shear reinforcement ratio was 0.003 for group #1 and #2 specimens, and 0.006 for group #3 specimens.

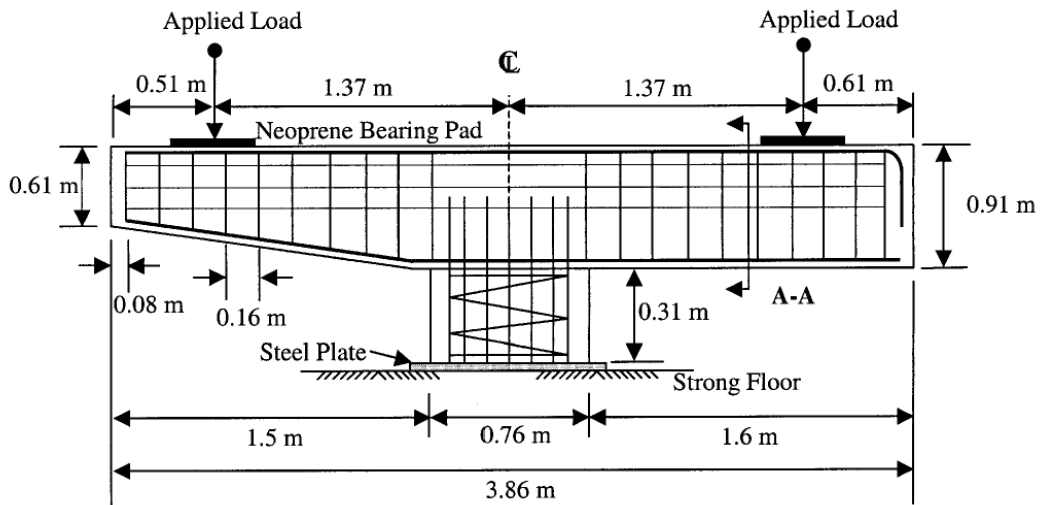


Figure 2-22: Typical bent cap specimen (Young et al., 2002)

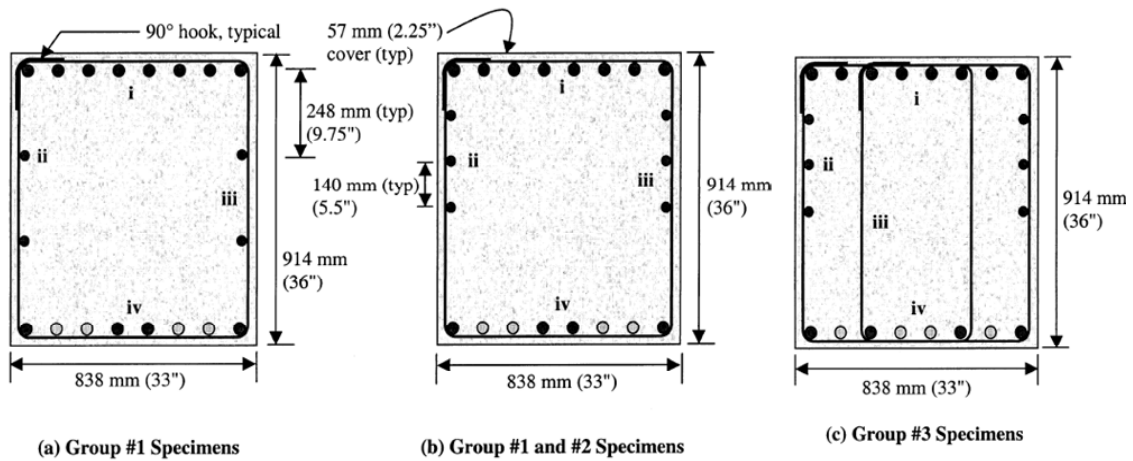
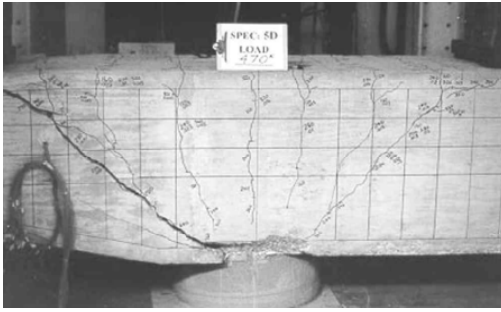


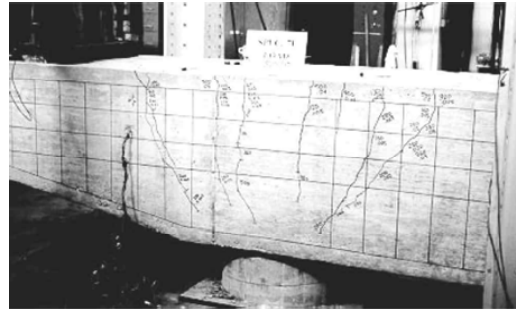
Figure 2-23: Bent cap cross-sections (Young et al., 2002)

Only a small portion of the experimental program was set up to examine transverse shear reinforcement and its effect on strength and serviceability. It was noted that horizontal skin reinforcement controlled cracking most effectively when lumped within the web-tension region. This horizontal reinforcement was effective at controlling flexural cracks at service loads, but its effectiveness at restraining the cracks diminished at higher loads.

It was found that the group #3 specimens, which contained four stirrup legs and twice the vertical shear reinforcement as the previous specimens, had superior performance. They not only had significantly narrower crack widths than the specimens with half the vertical shear reinforcement, but were also effective in restraining flexure-shear cracks at high loads. Figure 2-24 shows a comparison of cracking patterns between a two-legged stirrup specimen and four-legged stirrup specimen at similar applied loads.



Two-Leg Stirrup Specimen



Four-Leg Stirrup Specimen

Figure 2-24: Comparison of crack patterns (Young et al., 2002)

The researchers did not hypothesize whether the superior performance of the specimens with four-legged stirrups was due to the quantity of stirrup legs, area of vertical reinforcement, or both. This issue, along with the effect of horizontal and vertical shear reinforcement on shear strength, is discussed further in Powanusorn and Bracci (2006).

2.5.12 Powanusorn and Bracci (2006)

Powanusorn and Bracci evaluated the effects of confinement on shear-dominated reinforced concrete members, using the experimental program by Young et al. in 2002. The experimental program by Young et al. was comprised of testing 16 bent caps to failure. As part of their research the authors developed a new analytical model to incorporate the beneficial effect of confinement from transverse reinforcement.

The authors compared the performance of the two sets of specimens in Figure 2-25. One set contains two-legged stirrups, while the other contains four-legged stirrups. The two-legged specimens had a ρ_v of 0.003, while the four-legged stirrups had a ρ_v of 0.006. Both specimens had a ρ_h of 0.001, concrete strengths ranging from 5323 to 7716 psi, and shear span-to-depth ratio of approximately 1.5 (corresponding a/d of approximately 1.6).

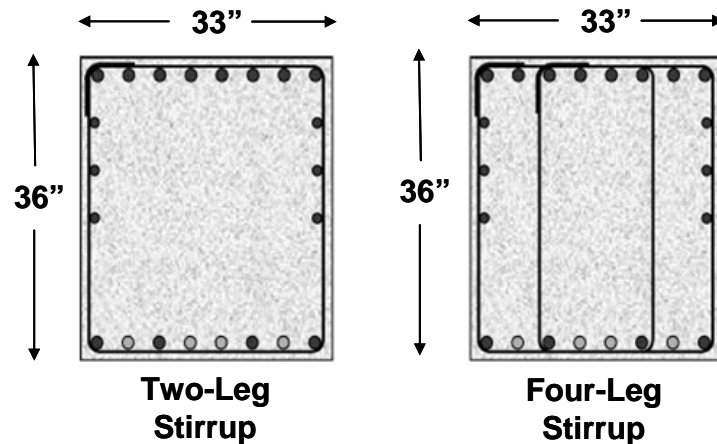


Figure 2-25: Bent cap cross-sections (Powanusorn and Bracci, 2006)

It was noted that while both sets of specimens failed in shear, the four-legged specimens had superior deformability and an increased ultimate failure load. The researchers argued that this increase in performance was not due to the direct effect of additional stirrup area; they suggested that data from strain gauges installed on the four-legged stirrups indicated that the stirrups themselves did not directly add to the strength of the deep beam. Instead, it was hypothesized that the increased performance of the four-legged stirrup specimen was due to the effect on confinement due to the transverse reinforcement. In a separate issue, researchers noted that (based on strain gauge data) only one or two stirrups along the length of beam actually participated in resisting the vertical load.

It is notable that two variables—both the number of stirrups legs and the area of the vertical shear reinforcement—varied between the two beams. A comparison of specimens with equal area of vertical shear reinforcement but unequal number of stirrup legs could have more explicitly supported the conclusion of the researchers.

2.5.13 Brown, Sankovich, Bayrak, Jirsa, Breen, Wood (2006)

Brown et al. performed two series of deep beam tests as part of a larger test program investigating the shear strength of reinforced concrete members designed using

strut-and-tie modeling. The first series consisted of 10 specimens with various shear reinforcement configurations; the researchers sought to examine the effects of vertical and horizontal reinforcing bars on shear strength.

A typical series one specimen is shown in Figure 2-26. The beam had concrete strengths ranging from 2370 to 3230 psi. The amount of transverse reinforcement, reported in terms of $\sum \frac{A_{s_i}}{bs_i} \sin \alpha_i$, ranged from zero to 0.003 in the 10 specimens tested.

The beams were loaded using one of three loading configurations: a single point load at $a/d = 1.11$, a pair of equal point loads at a/d ratios of 0.56 and 1.67, or a series of concentrated loads representing a distributed load, with a/d ratios ranging from zero to 2.22. Notably, each of the loading configurations had an “average” a/d ratio of 1.11.

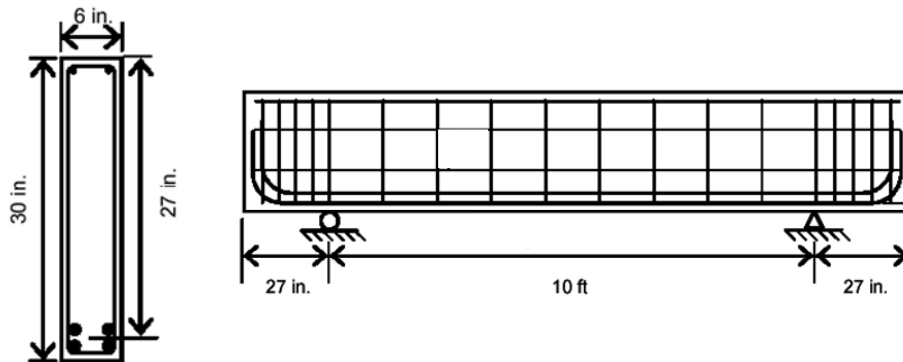


Figure 2-26: Typical series one specimen (Brown et al., 2006)

The researchers found that the amount of transverse reinforcement did not appreciably affect ultimate shear strength. Specimens with no shear reinforcement typically failed in diagonal shear. Specimens with a small amount of shear reinforcement ($\sum \frac{A_{s_i}}{bs_i} \sin \alpha_i = 0.0015$) failed by concrete crushing adjacent to the node under the

applied load. Specimens with additional shear reinforcement ($\sum \frac{A_{si}}{bs_i} \sin \alpha_i = 0.0030$) did not demonstrate increased shear strength.

There was no discernable trend between shear reinforcement ratio and the diagonal cracking load. In addition, it was noted that parallel diagonal shear cracks formed at 70 to 80% of the ultimate load, and were a strong indicator of impending failure.

A second series of tests was conducted to determine the effect of beam width on shear strength. The specimens were sufficiently wide to examine the AASHTO limited strut width provisions outlined in Section 2.2.1.2. The cross-sections of the two specimens tested, and corresponding bearing plate configurations, are shown in Figure 2-27. The beams were load asymmetrically with a single point load, as is also shown in Figure 2-27; the a/d ratio to the near support was 1.68.

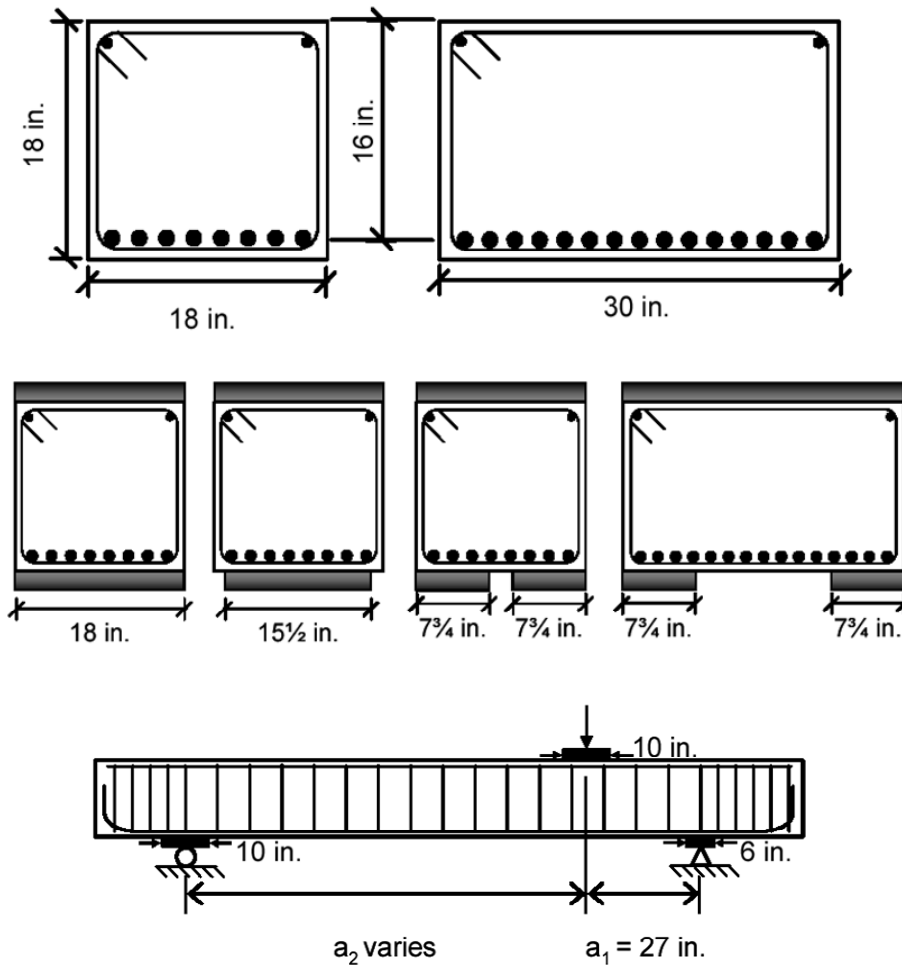


Figure 2-27: Series two specimens (Brown et al., 2006)

It was found that the shear strength of each specimen was at least proportional its width. Therefore, the absence of interior stirrup legs in the widest specimen was not detrimental to its ultimate shear strength. In addition, the bearing plate configuration had no effect on shear strength. In terms of serviceability, parallel diagonal shear cracks were observed at 65-80% of the ultimate load, and were therefore an indicator of impending shear failure.

2.5.14 Summary and Discussion

2.5.14.1 *Ultimate Shear Capacity and Type of Failure*

The experimental studies lack a consensus on the effect of transverse reinforcement on ultimate shear strength of reinforced concrete deep beams. Several researchers (DePaiva and Siess 1965, Rogowski et al. 1986, and Brown et al. 2006) found that the amount vertical shear reinforcement does not appreciably increase the shear strength of reinforced concrete deep beams. Conversely, others (Kong et al. 1970, Smith and Vantsiotis 1982, Tan et al. 1997, Shin et al. 1999, Oh and Shin 2001) noted that the amount of vertical shear reinforcement did have an effect on the shear strength. However, each of these researchers noted that the vertical transverse reinforcement ratio had a greater effect on shear strength with high a/d ratios, especially at a/d ratios nearing 2.0.

On the other hand, researchers noted that the effectiveness of horizontal shear reinforcement only increased shear capacity for very small a/d ratios. Kong et al. (1970) and Powanusorn and Bracci (2006) et al. both noted that horizontal reinforcement is best utilized in the bottom of the beam, or in the web tension region. Perhaps as a result of such research, the AASHTO provision associated with Equation 2-9 codifies the inclusion of horizontal reinforcement near tensile longitudinal reinforcement for beams of sufficient depth.

DePaiva and Siess (1965) and Rogowski et al. (1986) found that large amounts of transverse steel can decrease the chance of a shear mode of failure, while Smith and Vantsiotis (1982), Shin et al. (1999), and Brown et al. (2006) observed similar shear failures irrelevant of the amount of transverse steel.

2.5.14.2 *Serviceability Performance*

Very few of the experimental programs above were undertaken specifically to study the serviceability performance of deep beams. Even so, many of the research

studies contain valuable information on first diagonal cracking loads, crack widths, and other serviceability observations.

DePaiva and Siess (1965) noted that the amount of transverse reinforcement did not affect the formation of inclined cracks. Similarly, Smith and Vantsiotis (1982) noted that the amount of transverse reinforcement did not affect the formation of the first inclined crack. This conclusion was also verified in experimental testing by Tan et al. (1997), Shin et al. (1999), and Oh and Shin (2001) on specimens with much higher concrete strengths. More recently, Brown et al. (2006) noted the same conclusion for specimens with much lower concrete strengths.

A handful of research publications such as Kong et al. (1970), Smith and Vantsiotis (1982), and Tan et al. (1997) made note of crack width information, and each reported that crack widths were inversely proportional to amount of transverse reinforcement.

Kong et al. noted that parallel diagonal shear cracks opened up anywhere from 70 to 90% of the ultimate load, and were a strong indicator of impending failure. Similarly Brown et al. noted that parallel shear cracks opened up at 65 to 80% of the ultimate load.

2.5.14.3 Effect of Quantity of Stirrup Legs and Beam Width

Two experimental programs (Hsiung and Frantz 1985, Anderson and Ramirez 1989) were conducted specifically to investigate the effect of multiple stirrup legs on ultimate shear capacity. The studies reported opposite conclusions. In addition, Powanusorn and Bracci (2006) included the number of stirrup legs as a variable, and Brown et al. (2006) studied the effect of beam width on ultimate shear strength.

Hsiung and Frantz found no benefit to six stirrup legs as opposed to two, both in terms of ultimate shear strength and in terms of interior or exterior crack widths. In contrast, Anderson and Ramirez tested specimens with two, three, and four stirrup legs and found that specimens with three or more legs had superior ultimate shear strength. It should be noted that the maximum difference in ultimate strength between specimens with two legs and specimens with multiple legs that failed in shear was less than 10%,

when capacities are normalized relative to concrete strength. In both studies the quantity of specimens tested was very small.

Powansuorn and Bracci assert the benefit of four stirrup legs as opposed to two. However, the specimens with four-legged stirrups also contained double the vertical shear reinforcement area as compared to the two-legged stirrup specimen. The number of stirrup legs was not isolated as a variable.

Brown et al. tested width as a variable while holding constant the vertical reinforcement ratio and number of stirrup legs (two). It was found that the shear strength of wide specimens was simply proportional to width (despite the fact that all specimens had two stirrup legs).

2.6 REMARKS

The main objective of the current study is to examine the effect of transverse reinforcement on the ultimate shear strength and serviceability performance of reinforced concrete deep beams, and to examine current design code requirements for transverse reinforcement.

The primary value of the current experimental program lies in the large size of the specimens tested. The specimens may be the largest ever tested (in terms of gross cross-sectional area) when considering only specimens that contain transverse reinforcement. A considerable quantity of research has been performed on the effect of transverse reinforcement on the shear strength of deep beams, but very few specimens have been tested at a scale representative of large TxDOT bent caps.

The large specimen size is of particular importance in examining effect of the quantity of stirrup legs on shear strength, and the AASHTO limited strut width provision. Specifically, a beam of significant width was necessary to successfully examine this variable. In addition, the large scale is beneficial in the examination the shear performance of deep beams; the large specimen size eliminates the potentially questionable practice of extrapolating trends for large-scale beams based on small-scale tests.

The use of strut-and-tie modeling to address serviceability of structures is also examined. While serviceability and strength are generally considered equally important in structural design, adequate serviceability design in deep beams is difficult given current code provisions. In particular, strut-and-tie modeling is based on the lower bound theory of plasticity and therefore does not take into account issues of serviceability.

The majority of past research on deep beams has not focused on issues of serviceability as a primary variable, or foregone the collection of such data altogether. The size of the test specimens will allow a realistic examination of serviceability issues. For example, relationships between shear crack widths and the remaining capacity of specimens can be of immediate use in similarly sized field bent caps.

From a broader perspective, the value of large scale deep beam research is underscored by the fact that many deep beams used in practice, such as transfer beams in a building or bent caps in bridges, are indeed very large. Deep beams of this size are difficult and time consuming to design and costly to construct. Minor design adjustments can result in significant design time and cost economies.

CHAPTER 3

Experimental Program

3.1 INTRODUCTION

The experimental program for the current research project consisted of nine tests conducted on three large-scale reinforced concrete deep beams. The primary variables were the amount and detailing of transverse reinforcement and the applied load bearing area. The main objective of the experimental program was to examine the effect of these variables on the shear strength and serviceability performance of large-scale deep beams.

The testing procedure and test setup had a significant influence on the specimen design, and are therefore introduced first, followed by the specimen design, materials, and instrumentation. In short, all relevant details of the experimental program are described in this chapter.

3.2 TEST SETUP

In order to accommodate the high loads required to fail large-scale deep beams, a new test setup was designed and constructed in Ferguson Structural Engineering Laboratory (FSEL).

The new high-capacity test setup required considerable time and effort to construct. The centerpiece of the apparatus was a 96,000 lb. cast-steel platen that was commissioned as part of a 6-million-pound test frame in the late 1940s by the U.S. Navy; much later, the universal test machine was decommissioned and donated to FSEL. A 600 yd³ pit was excavated within the lab to house the platen, and a reinforced concrete foundation was designed and cast within the excavated area. Moving the platen from its location outdoors to its below-grade placement within the lab was a significant operation that required the use of a high-capacity truck-mounted crane. Various stages of the strong floor construction are pictured in Figure 3-1.



Figure 3-1: a) Platen; b) Excavation; c) Excavated pit; d) Foundation construction; e) Platen lift; f) Platen in position

The completed test setup is pictured in Figure 3-2, and detailed plans for the test setup are shown in Figure 3-3 through Figure 3-5. As seen in Figure 3-3, the specimens

59

are simply supported at their ends. A double-acting hydraulic ram with six-million-pound load capacity exerted an upward force and two 7,000 pound steel plate-girders at the reaction points were tied-down through the use of twelve 3 inch diameter high-strength rods. As a result, the applied load and the self-weight of the specimen were oriented in opposite directions; this was accounted for in all data analysis and will be discussed in Chapter 4.

Transfer beams and high-strength threaded rods were designed to safely resist an asymmetrically applied load of 2,500 kips as depicted in Figures 3-2 and 3-3. If the load is applied at mid-span and six tie-down rods are used at each support, the capacity of the setup is slightly over 4000 kips. If a greater number of tie-down rods are used, the full 6,000 kip capacity of the double-acting centerhole hydraulic ram can be utilized; the 96,000-lb cast-steel strong floor has the flexural and shear capacity to withstand a concentrated force of nearly 6,000 kips.

A roller assembly was utilized at the load point and reaction points to create a well-defined simply-supported condition for the specimen. Hydrostone was placed in between the bearing plates and specimen surface to ensure that load was evenly distributed on the bearing plates utilized at load and reaction points.

As shown in Figure 3-4, the test setup requires that four threaded rods, two on each end of the setup, pass directly through the specimen itself. As a result, any specimen wider than 21" requires threaded rods to pass directly through its cross section. Since the test specimens were 36" wide, four rods (two at each end) were passed through the specimen and longitudinal bars were designed such that their placement accommodated the rods passing through the section.

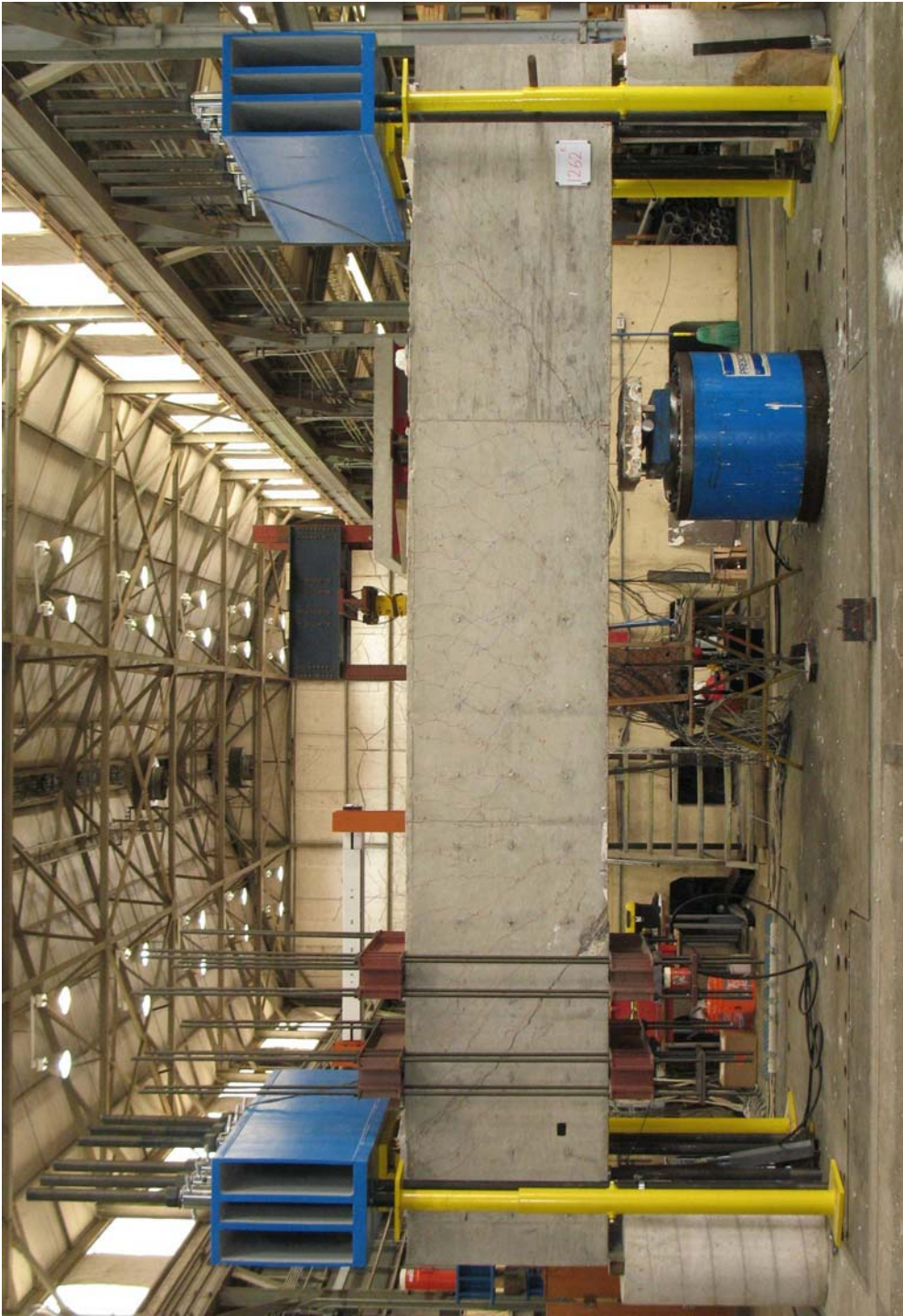


Figure 3-2: Test setup

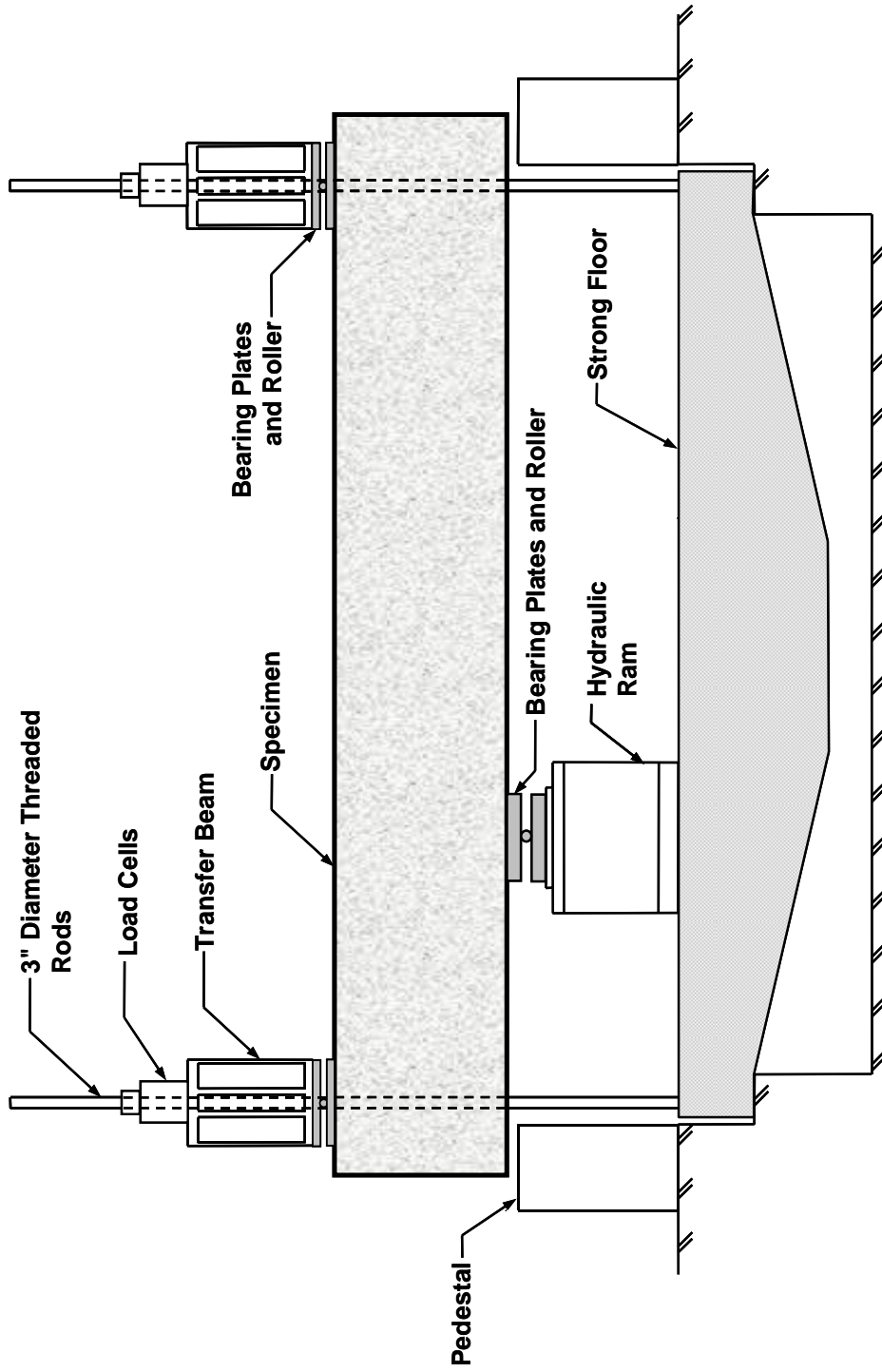


Figure 3-3: Test setup, elevation view

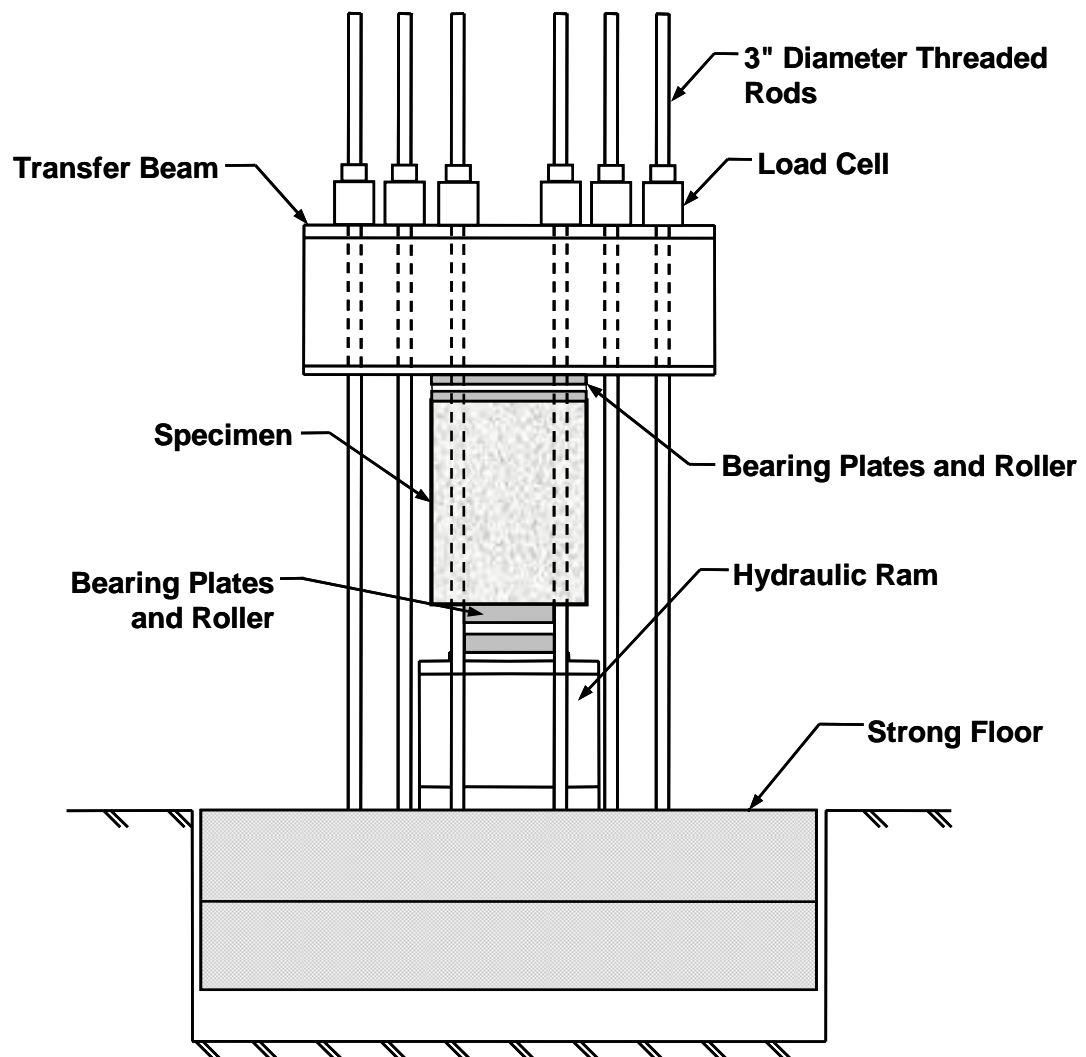


Figure 3-4: Test setup, elevation view

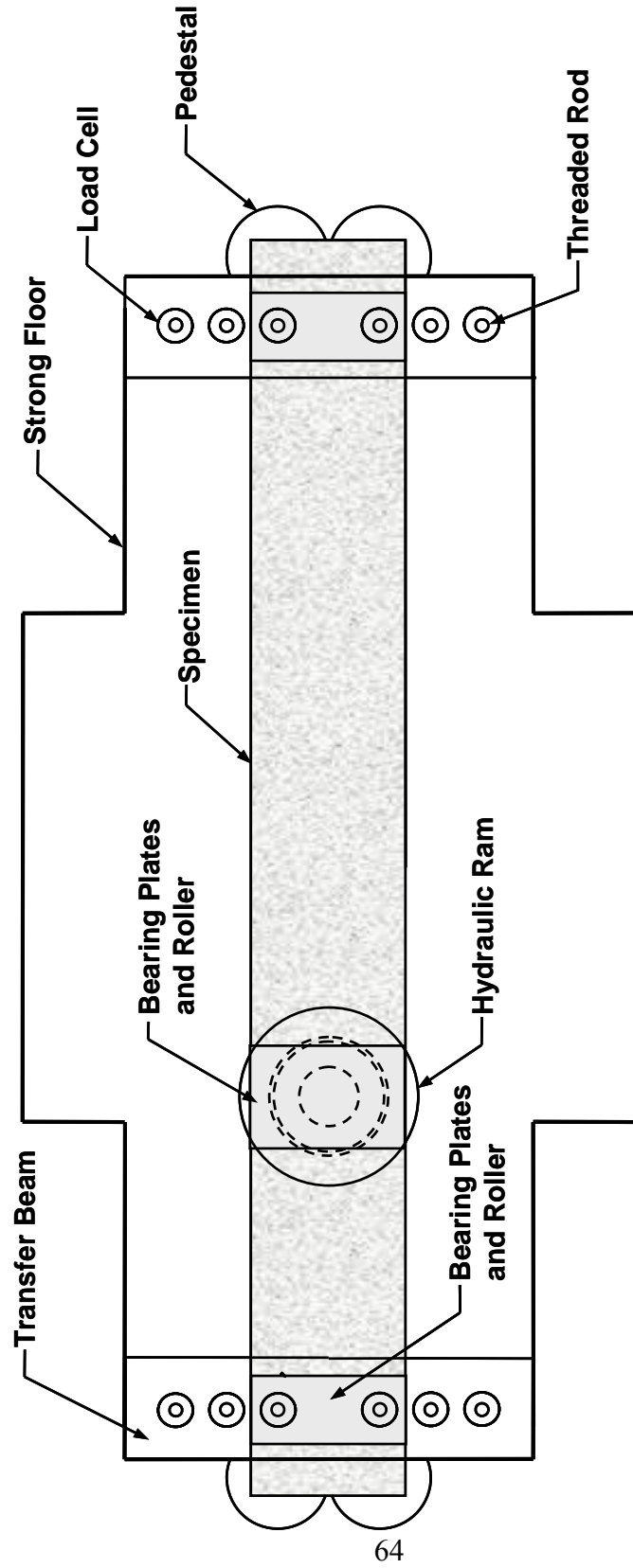


Figure 3-5: Test setup, plan view

3.3 TEST PROGRAM

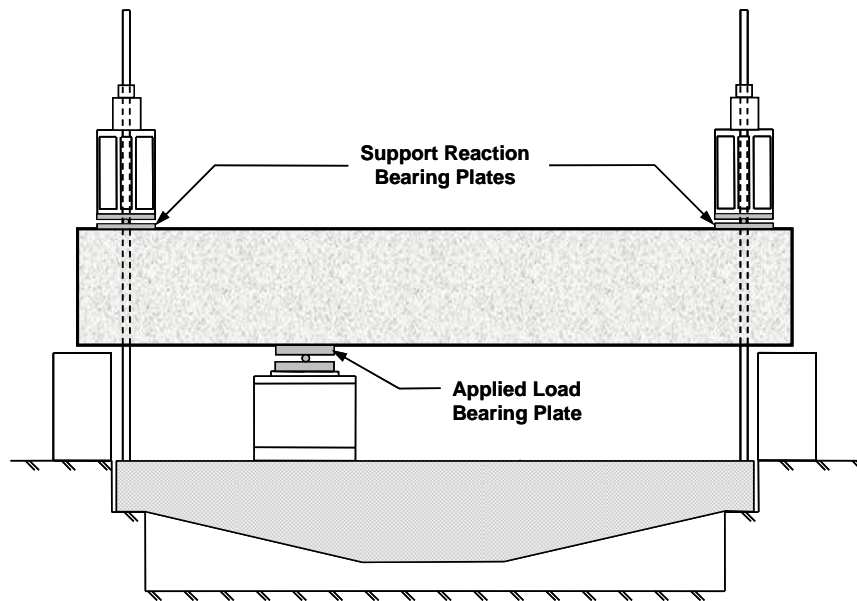
Nine tests were conducted on three large-scale test specimens (Table 3-1). It was possible to perform several tests on each test specimen. The beams had sufficient length (L/d ratio of 6.4) to test two independent shear spans, one on each end of the specimen. A given specimen was first tested with an asymmetrically placed concentrated load near one end of the beam in order to create a shear span-to-effective depth (a/d) ratio of 1.85. After testing the first side of the specimen, the hydraulic ram (i.e. the concentrated load) was then moved to opposite side of the beam for another test with an identical a/d ratio. Since shear strength increases with a decreasing shear span-to-effective ratio, an a/d ratio of 1.85 was selected to give a conservative estimate of the shear strength of the specimen, yet still be well within the code definitions of a deep beam described in section 2.1.

The two loading points and shear spans are referred as to A and B, respectively, as shown in Figure 3-6. After the shear failure in shear span A, the span was clamped together as shown in Figure 3-6 and Figure 3-7, to allow testing of the second shear span of the specimen without compromising overall specimen stability.

The primary objective of the test program was to study the shear strength and serviceability behavior of deep beams. As part of this primary objective, inducing a shear failure in each shear span was of interest. A test early in the program (Test #2) resulted in the flexural failure of a shear span. As a result, subsequent tests were stopped if yielding of flexural reinforcement initiated in the test region. The test was then repeated with a reduced applied load bearing area. The intent of this process was to select a bearing size that would induce a shear failure in each shear span rather than a flexural failure. Pertinent details for each test are given in Table 3-1. Further details of each specimen are given in section 3.5.

Table 3-1: Test program

Test #	Shear Span Tested	Qty. Stirrup Legs	ρ_v	ρ_H	Applied Load Bearing Size*	Support Reaction Bearing Size*	Serviceability Data Collected?	Comment
1	1A	4 legs	0.0031	0.0030	24" x 36"	16" x 36"	Yes	Shear Failure
2	1B	4 legs	0.0086	0.0030	24" x 36"		Yes	Flexural Failure
3	2A	2 legs	0.0031	0.0030	24" x 36"		Yes	Initiation of Flexural Yielding
4	2A	2 legs	0.0031	0.0030	8" x 36"		No	Shear Failure
5	2B	2 legs	0.0061	0.0030	24" x 36"		Yes	Initiation of Flexural Yielding
6	2B	2 legs	0.0061	0.0030	24" x 18"		No	Initiation of Flexural Yielding
7	2B	2 legs	0.0061	0.0030	8" x 36"		No	Shear Failure
8	3A	4 legs	0.0022	0.0022	24" x 36"		Yes	Shear Failure
9	3B	4 legs	0.0031	0.0030	8" x 12"		Yes	Shear Failure



*bearing areas are reported as [dimension in direction of span] x [dimension in transverse direction]

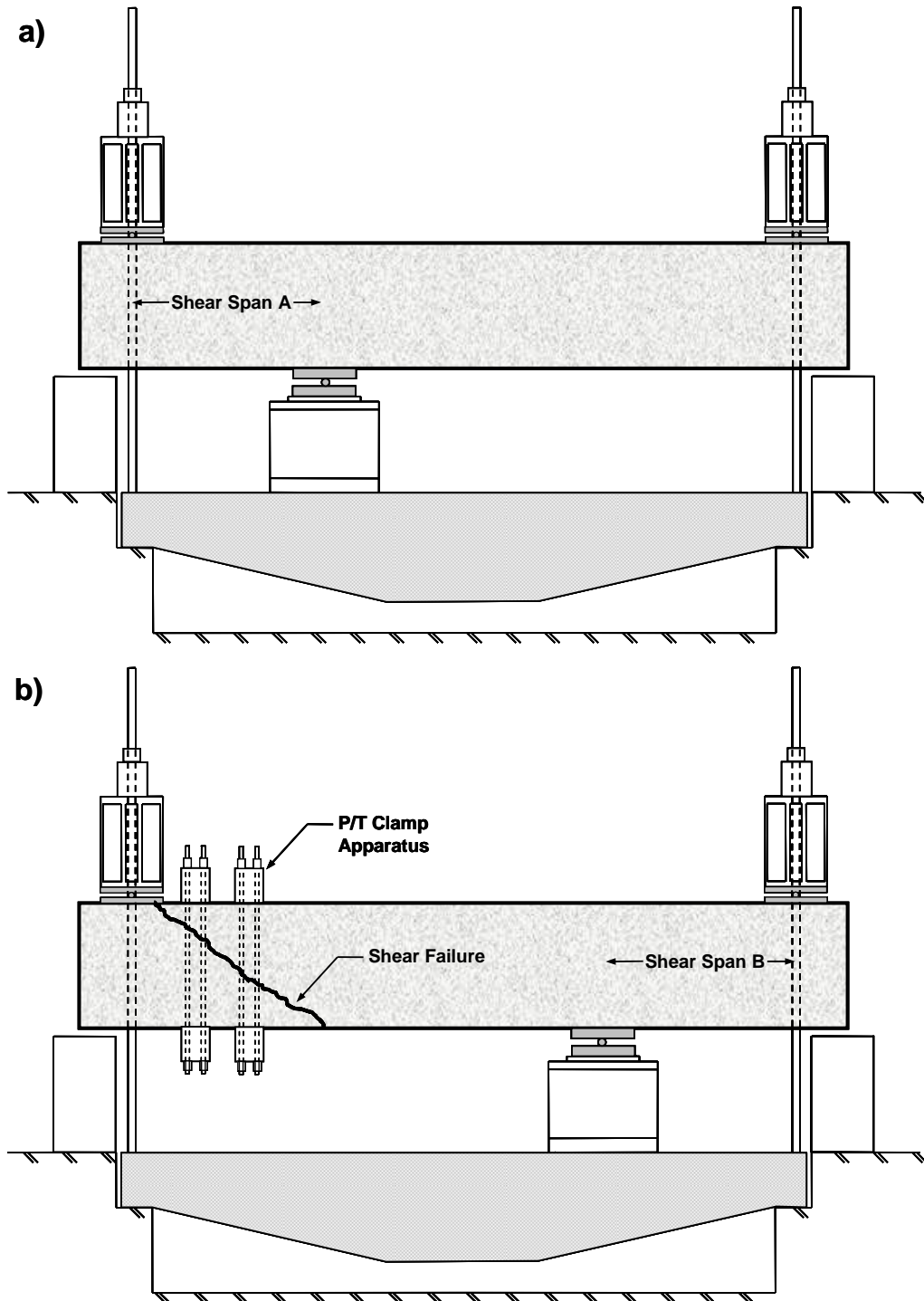


Figure 3-6: a) Loading configuration A; b) Loading configuration B



Figure 3-7: Strengthening of a beam after strut failure: external PT clamp

Each test was carried out in 100 kip loading increments, with the exception of Test #1, which was carried out in 50 kip increments. At the conclusion of each loading increment cracks were marked and crack widths were measured.

Of the nine independent tests conducted on three specimens, both strength and serviceability data was collected for six of the tests; these tests represent the initial test on each of the six independently tested shear spans. The remaining three tests are those in which a reduced bearing area was utilized to induce a shear failure in a given shear span. As noted in the previous paragraphs, these latter three tests were completed on shear spans where flexural yielding had already initiated. Thus, upon unloading shear cracks did not close, and hence reliable serviceability data could no longer be obtained. However, an ultimate strength value could still be obtained while knowing a pristine shear span would have at least the capacity of the damaged shear span.

3.4 SPECIMEN DESIGN

The specimens were designed to meet a number of objectives. These factors are discussed in this section.

The main variables in the experimental program were the amount and detailing of transverse reinforcement, and the bearing area under the applied load. As a result, the specimens were designed to represent a wide range of vertical shear reinforcement ratios. With the exception of shear span 3A (Test #8), the horizontal shear reinforcement ratio was held constant. As outlined in section 2.5.14.1, researchers such as Kong et al. (1970) reported that for deep beams with a/d ratios near 2.0 (such as the specimens in the current experimental program) horizontal web reinforcement has little effect on shear strength.

As indicated in section 2.3, the poor performance of a number of TxDOT bent caps served as a primary motivation for the current research project. As a result, a main objective of the experimental program was to test specimens that possessed a general size and aspect ratio as near as possible to existing full-size TxDOT bent caps. The amount and configuration of reinforcement in the specimen was also designed to mimic that of typical TxDOT bent caps. In this way, the data could be examined without extrapolation for large-scale beams based on small-scale tests.

Figure 3-8 shows the cross-sections of four bent caps currently in use by TxDOT, and a cross section of the current project specimen. Details for each of the five bent caps are shown in Table 3-2. The I-345 cap and I-45 bent cap over Greens Road are unusually large bent caps designed for a specific application. Conversely, the caps for Type C and Type IV girders are standard designs used frequently by TxDOT. Specimens in the current project are smaller than the largest TxDOT bent caps, but still larger than the majority of bents currently in use.

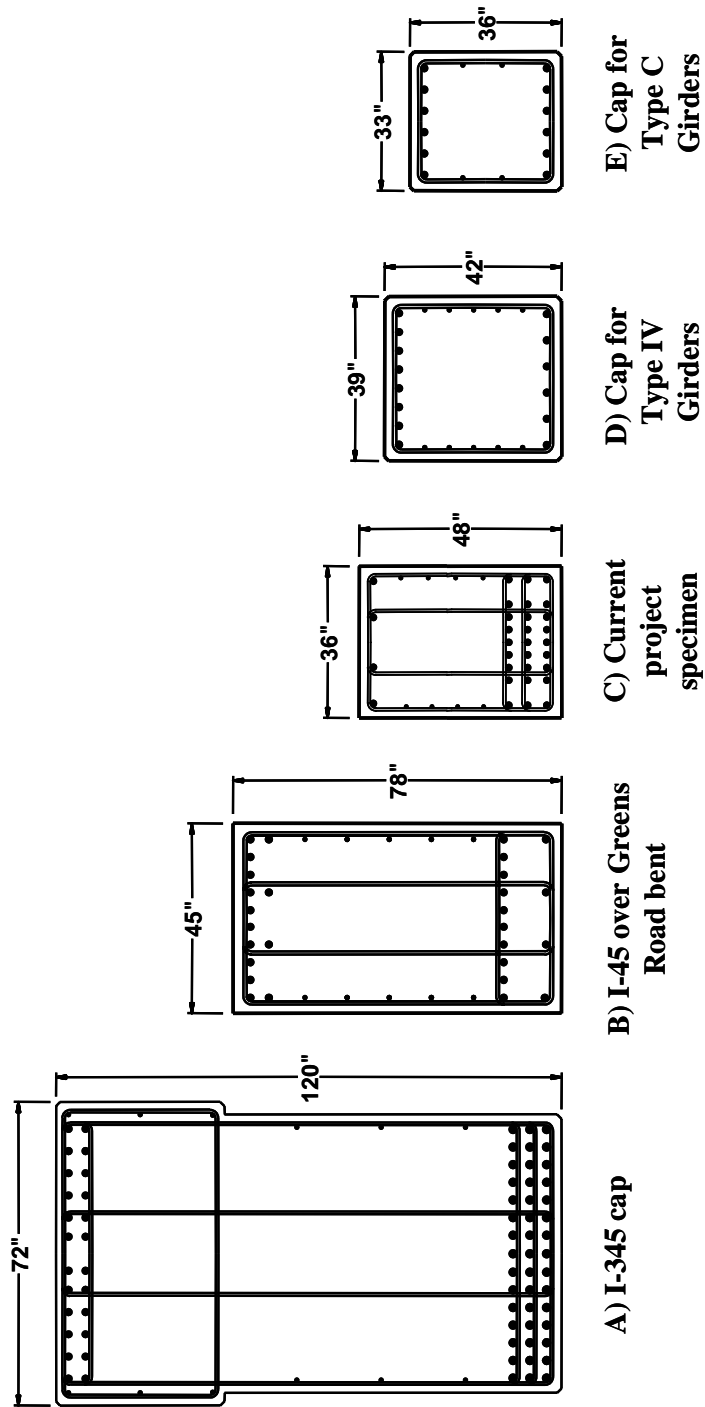


Figure 3-8: Bent caps and test specimen

Table 3-2: Typical bent cap details

	I-345 Cap	Greens Road Bent	Current Project Specimen	Cap for Type IV Girders	Cap for Type C Girders
Gross Area (in²)	8160	3510	1728	1638	1188
Typical Vertical Shear Reinforcement	4 legs #6 @ 5½"	4 legs #5 @ 6"	Varies	2 legs #5 @ 6¼"	2 legs #5 @ 6¼"
ρ_v	0.0049	0.0065	0.0022 – 0.0086	0.0014	0.003
Horizontal Shear Reinforcement	10 #5 bars	8 #5 bars	Varies	10 #5 bars	4 #5 bars
ρ_H^*	0.00049	0.0020	0.0022 – 0.0030	0.003	0.003
Tensile Longitudinal Reinforcement	24 #11 bars top; 45 #14 bars bottom	28 #11 bars	27 #11 bars	14 #11 bars	12 #11 bars
ρ_L^\dagger	0.0175	0.0142	0.0244	0.0133	0.0158

*As defined in section 2.2.1.1.1

†Corresponds to tensile longitudinal reinforcement ratio

Given the stated goal of constructing and testing specimens that were near full-scale, the governing factor in the specimen design was the limited capacity of the 25-ton (50-kip) overhead crane in FSEL that was used to lift and transport a specimen from the casting area to the test setup. The specimens were designed to be as large as possible without exceeding this weight limit; consequently, each test specimen weighed approximately 48,000 lbs.

The high-capacity test setup also influenced the specimen design. As noted in section 3.2, the test setup required a pair of high strength threaded rods to pass through the specimen itself in the end regions of the beam. As a result, a pair of 3¾" diameter aluminum ducts were cast directly into the specimen at the reaction points of the beam, allowing the rods to pass through. Consequently, the placement of the longitudinal reinforcing bars had to be adjusted. As depicted in Figure 3-9, longitudinal bars could not be placed with a uniform spacing.

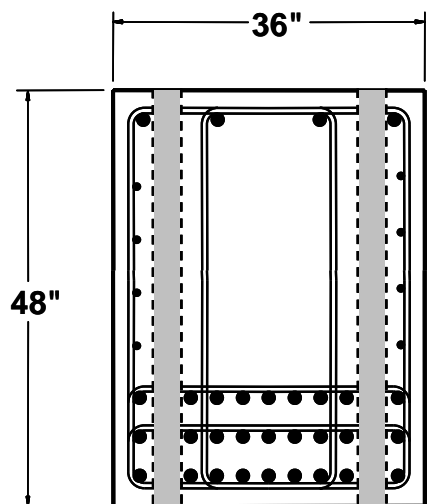


Figure 3-9: Specimen cross section with aluminum ducts

As seen in Figure 3-8, typical TxDOT caps contain longitudinal reinforcement near both the top and bottom faces, whereas the test specimens have nearly all the longitudinal reinforcement near the bottom face. As noted in the test setup overview, the testing apparatus was designed to test specimens with simply supported end conditions. Conversely, multi-column TxDOT bents have different boundary conditions. Figure 3-10 shows the moment diagrams as a result of point load for both fixed end (approximately equivalent to an interior span of a multi-column bent) and simply supported beams. While both conditions will require approximately the same amount of longitudinal reinforcement, correct placement of that reinforcement will differ; chiefly, simply supported caps like those in the current test program require longitudinal reinforcement to be lumped near one face.

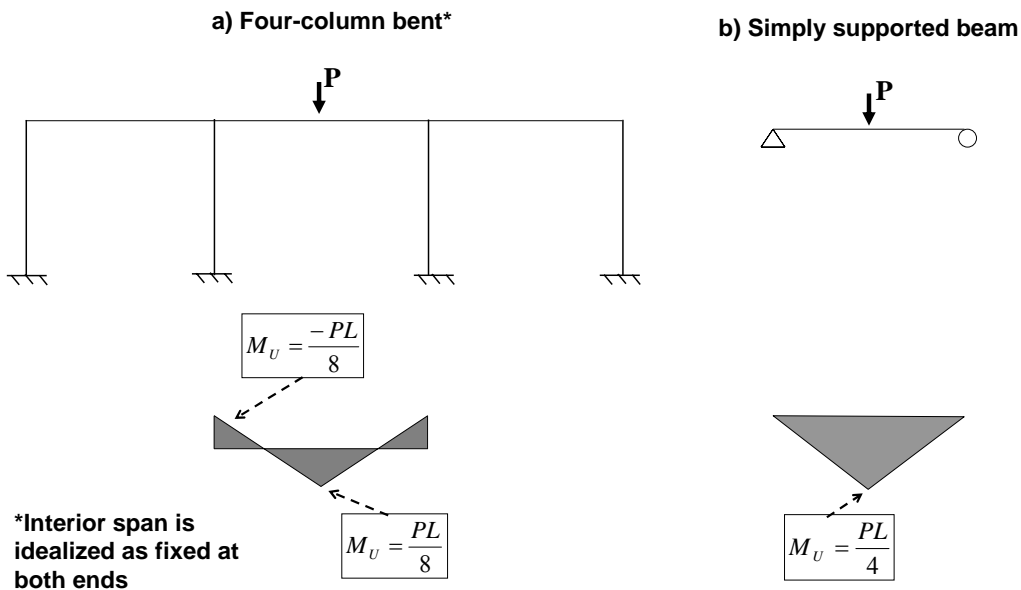


Figure 3-10: Effect of support conditions on bent cap moments

Beyond having the longitudinal reinforcement placed near one face, the current specimen also contained a higher longitudinal reinforcement ratio than typical TxDOT bent caps. Given the stated goal of studying shear in deep beams, the specimens were designed with sufficient longitudinal reinforcement to make a shear failure more likely. The shear criticality of the specimens is discussed further in section 3.4.1.

After many design iterations, a specimen size of 48" (height) by 36" (width) by 23'-8" (length) was selected to meet all the aforementioned design considerations. The specimen length was effectively fixed by the requirement that it both fit within the strong floor geometry and provide adequate development for the longitudinal reinforcing bars. The width was governed by the placement of longitudinal steel. As illustrated in Figure 3-9, a width less than 36" would cause interference of the outer longitudinal bars with the ducts. A width greater than 36" results in section aspect ratios different from large scale TxDOT bent caps. With the width set at 36", the height of 48" was selected as the maximum height that would still allow the beam to meet the aforementioned weight requirements.

In order to maximize the cross-sectional area of the specimens, the length of the specimens was kept as small as possible. The required development length of the longitudinal bars was kept to a minimum by providing additional reinforcement within the anchorage zone. Details of anchorage reinforcement are given in Appendix B.

3.4.1 Shear Criticality of Specimen

The shear database from TxDOT project 4371 (introduced in section 2.4) was utilized to help estimate the performance of the test specimens. Figure 3-11 is a plot of the strut efficiency versus $\frac{a}{d}\sqrt{f'_c}$ for 261 specimens from the shear database. The data includes only deep beams that are “sufficiently reinforced” as per Equation 2-12 (Chapter 2). A “sufficiently reinforced” strut was defined as one that has an adequate amount of transverse reinforcement to maintain equilibrium in a bottle-shaped strut (TxDOT project 4371); these specimens are pertinent to the current discussion because all specimens in the current research program also meet Equation 2-12 for being “sufficiently reinforced.”

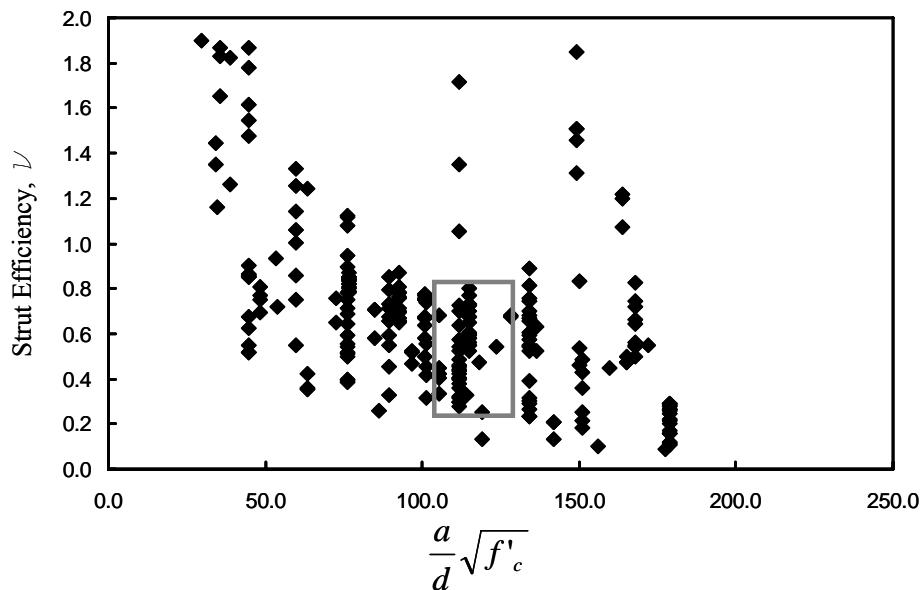


Figure 3-11: Test specimens in context of TxDOT project 4371 shear database

The data points enclosed in the grey rectangle highlight the majority of the shear tests that have a similar $\frac{a}{d}\sqrt{f'_c}$ ratio to the current test specimens. The strut efficiencies range from approximately 0.2 to 0.8; assuming a direct strut forms between the load point and the nearest support reaction in the current project specimens, the failure loads predicted through the use of these strut efficiencies range from 600 to 2,500 kips. The applied load corresponding to flexural failure of the test specimens is roughly equal to 1,500 kips, but depends on the concrete strength. Designing the specimens for the very highest strut efficiencies encountered in past shear testing is not practical. However, analysis of the historical shear data suggests that the test specimens in the current program will likely fail in shear.

3.5 SPECIMEN DETAILS

As outlined in section 3.3, nine tests were conducted three specimens. Pertinent details for the test specimens are listed in Table 3-3. Detailed drawings of the test specimens are shown in Figure 3-12 through Figure 3-17.

Table 3-3: Specimen details

Shear Span I.D.	Specimen I.D.					
	Specimen 1		Specimen 2		Specimen 3	
	1A	1B	2A	2B	3A	3B
Tests Performed on Shear Span	Test #1	Test #2	Tests #3, #4	Tests #5, #6, #7	Test #8	Test #9
Vertical Shear Reinforcement	4 legs #5 @ 11"	4 legs #5 @ 4"	2 legs #7 @ 11"	2 legs #7 @ 5½"	4 legs #4 @ 10"	4 legs #5 @ 11"
ρ_v	0.0031	0.0086	0.0031	0.0061	0.0022	0.0031
Horizontal Shear Reinforcement	8 #5 bars	8 #5 bars	8 #5 bars	8 #5 bars	6 #5 bars	8 #5 bars
ρ_H^*	0.003	0.003	0.003	0.003	0.0022	0.003
$\sum \frac{A_{s_i}}{b s_i} \sin \alpha_i$	0.0043	0.0091	0.0043	0.0068	0.0031	0.0043
Comment on Shear Reinforcement	AASHTO minimum	Aprox. 3x AASHTO vertical minimum	AASHTO minimum	Aprox. 2x AASHTO vertical minimum	ACI minimum	AASHTO minimum
Tensile Longitudinal Reinforcement	27 #11 bars	27 #11 bars	27 #11 bars	27 #11 bars	27 #11 bars	27 #11 bars
ρ_L	0.0244	0.0244	0.0244	0.0244	0.0244	0.0244
f'c (psi) †	4100	4100	4900	4900	2800	3000

*As defined in section 2.2.1.1

† At time of testing

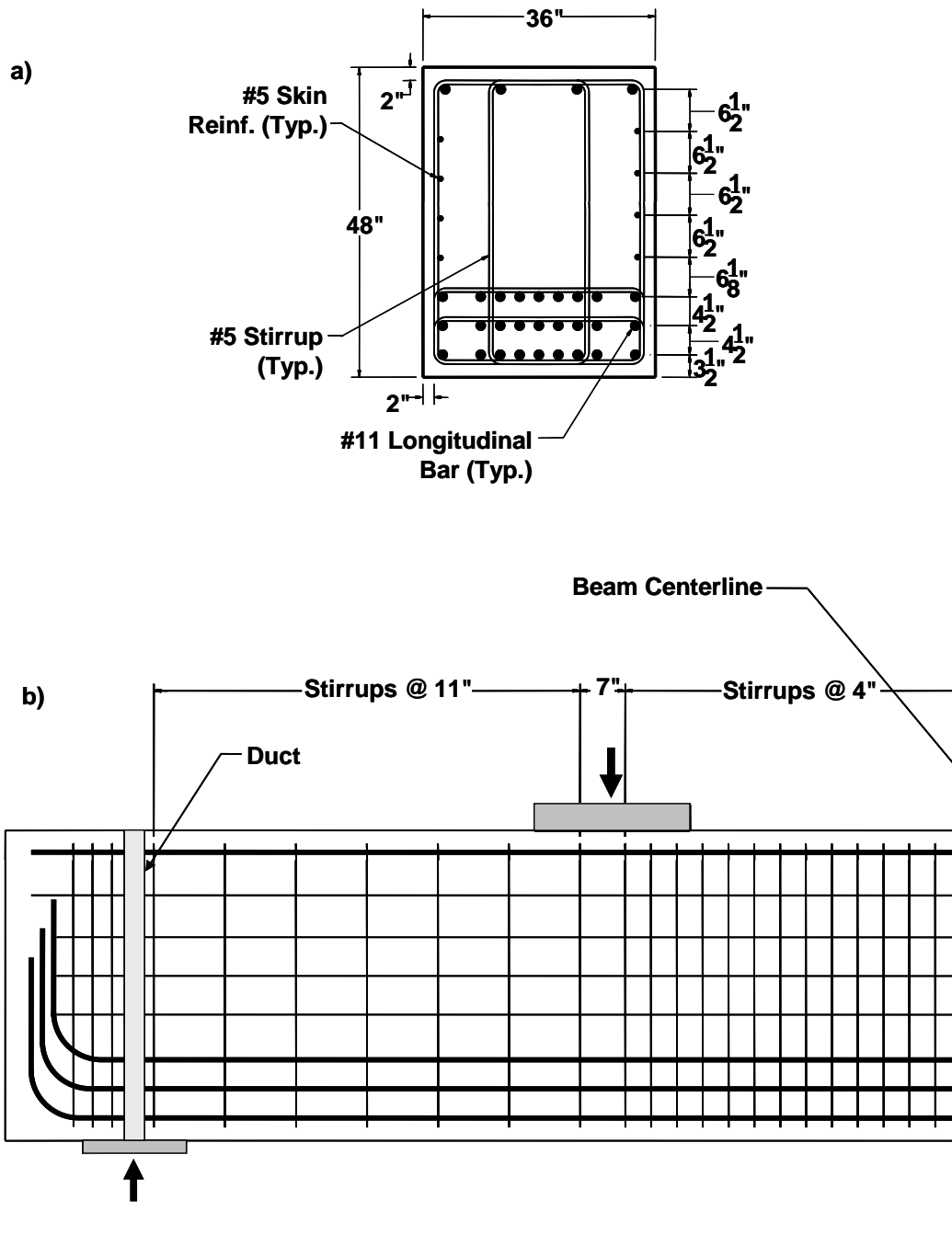


Figure 3-12: Shear span 1A a) Cross-section; b) Elevation

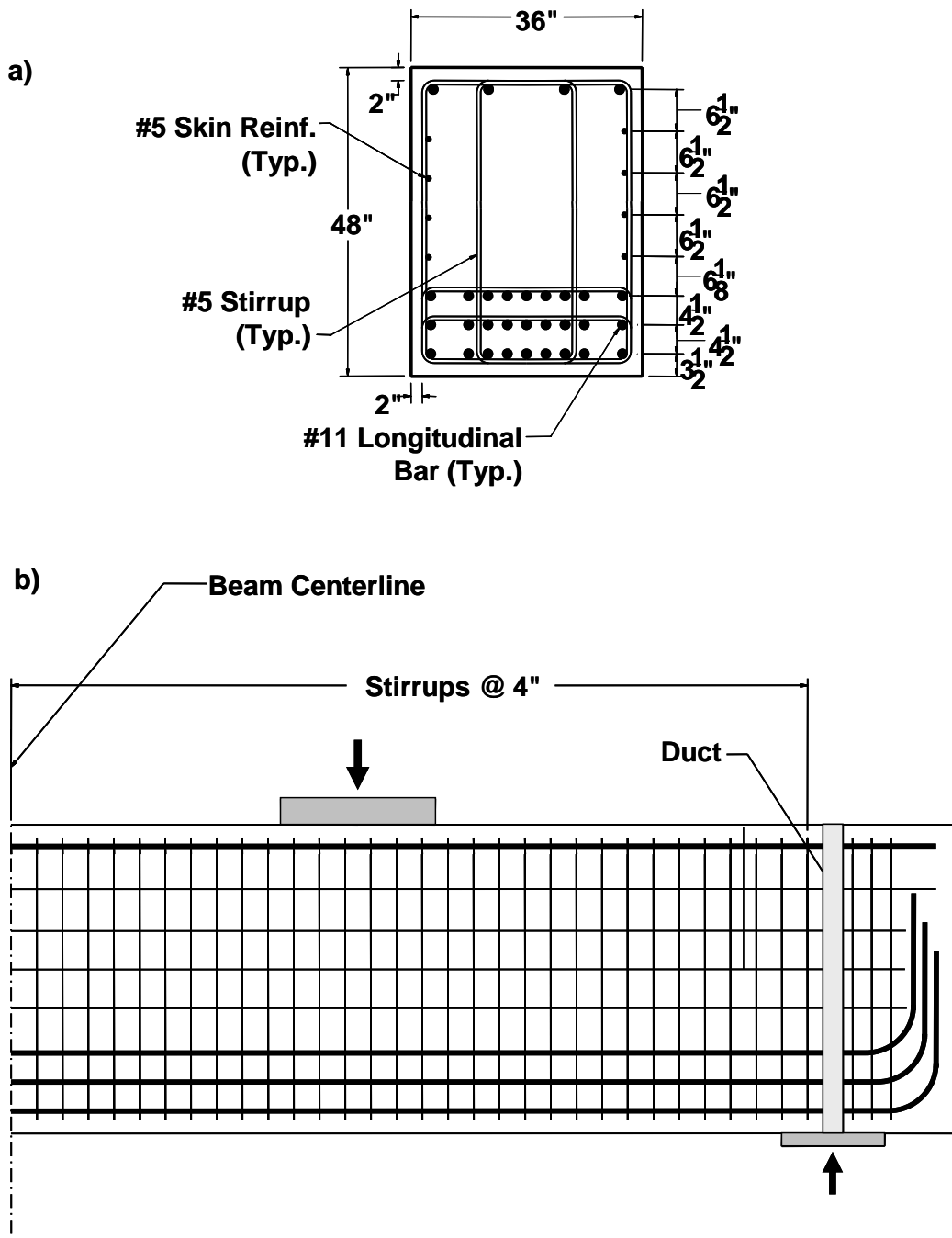


Figure 3-13: Shear span 1B a) Cross-section; b) Elevation

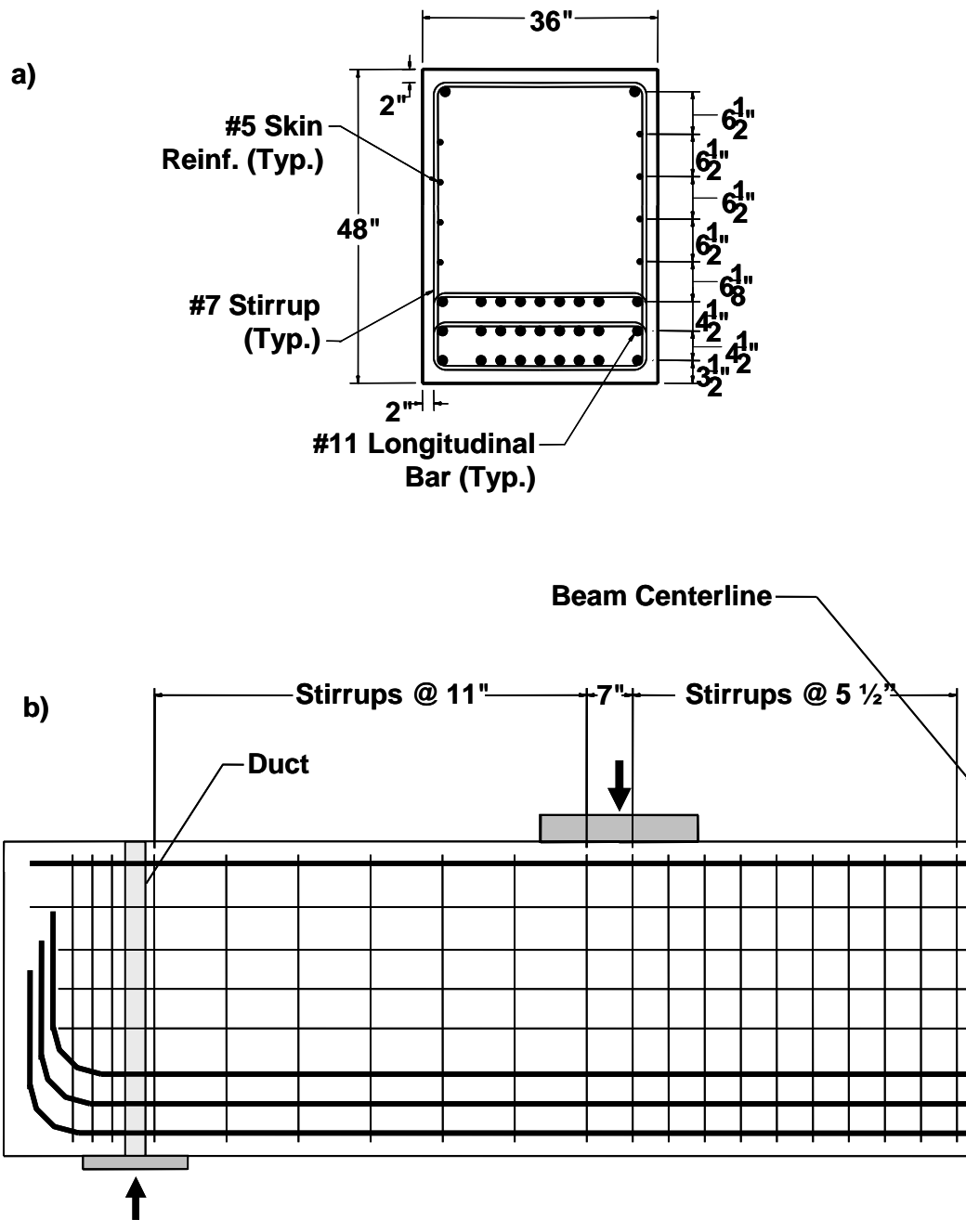


Figure 3-14: Shear span 2A a) Cross-section; b) Elevation

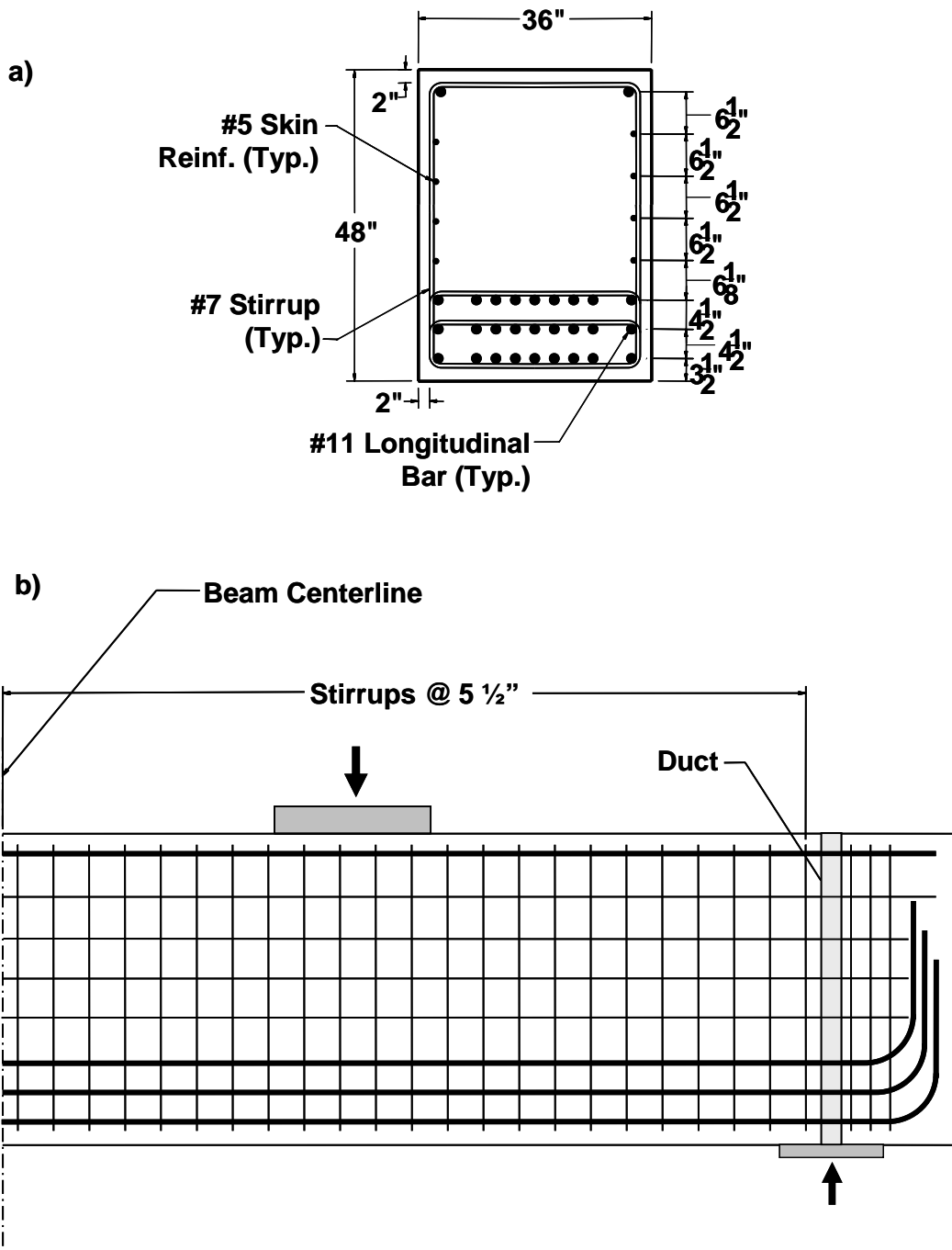


Figure 3-15: Shear span 2B a) Cross-section; b) Elevation

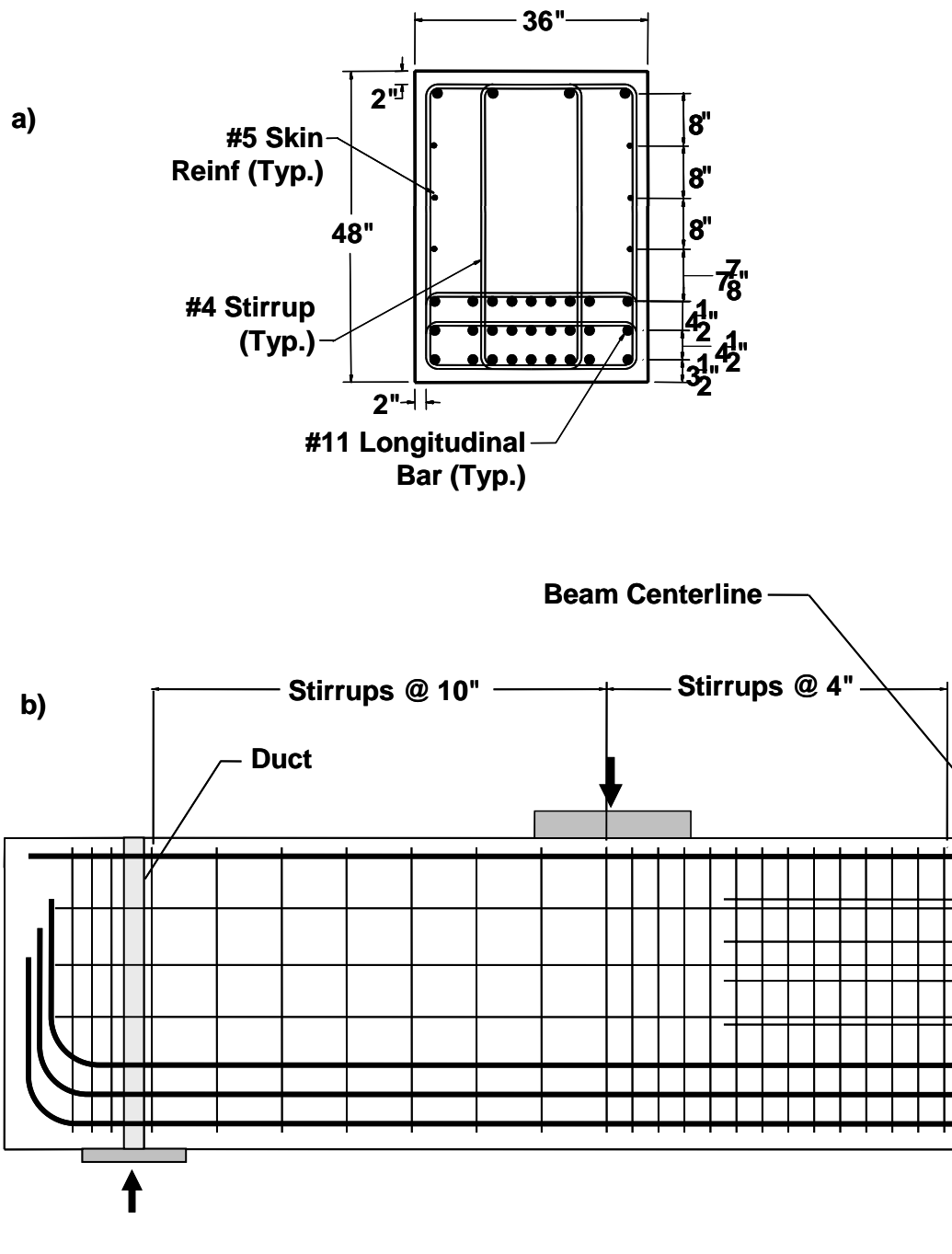


Figure 3-16: Shear span 3A a) Cross-section; b) Elevation

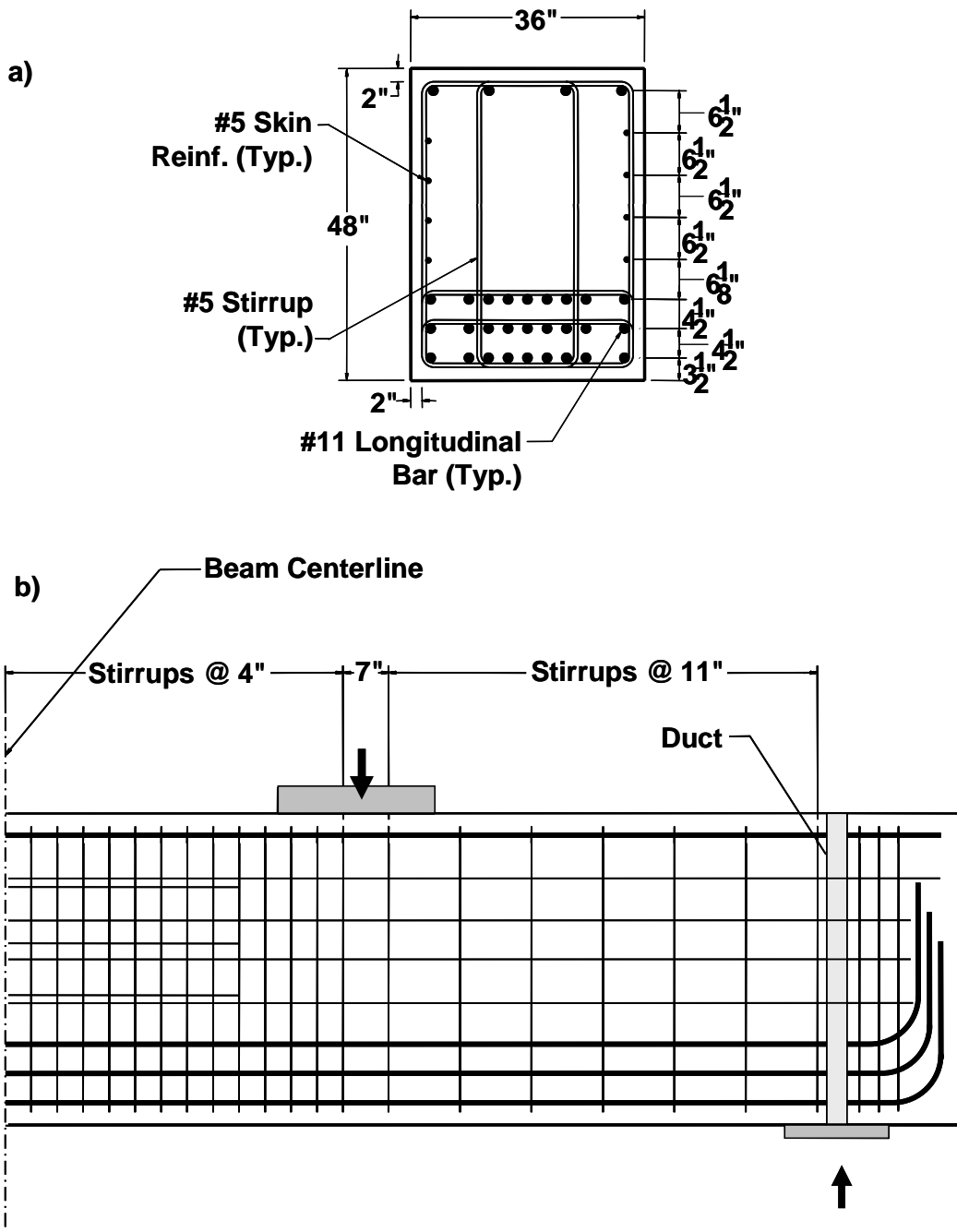


Figure 3-17: Shear span 3B a) Cross-section; b) Elevation

3.6 MATERIALS

3.6.1 Concrete

Concrete with 28-day compressive strengths ranging from 2800 to 4900 psi were utilized in the experimental program. The specifications and mix proportions for the concrete are shown in Table 3-4 and Table 3-5, respectively.

Table 3-4: Concrete specifications

f_c (psi)	Slump (in)	Total Air Content (%)	Unit Weight (pcf)	Water / Cement Ratio
3000	4 to 6	3 to 6	145	0.57

Table 3-5: Concrete mix proportions

Component	Quantity	Description (Source)
Type 1 Cement	338 lbs/yd.*	Capitol ASTM C-150 (San Antonio)
Class F Fly Ash	85 lbs/yd.	Boral Materials (Rockdale, TX)
Coarse Gravel	1874 lbs/yd.	Capitol ASTM #67 (Austin, TX)
Concrete Sand	1362 lbs/yd.	Capitol ASTM C-33 (Austin, TX)
Water	242 lbs/yd.	TxDOT 421 / AASHTO T-26
Polyheed 997	16.9 oz./yd.	Master Builders Type A
MB AE-90	2.1 oz/yd.	Master Builders ASTM C-260

*Concrete for specimen 3 had 20% less cement

Test specimens required delivery of concrete from two ready-mix concrete trucks. Cylinders were cast for each concrete truck batch. Immediately following each test, three cylinders from each truck batch were tested. The reported concrete strength is the weighted average of the cylinder breaks for each truck batch. Table 3-6 lists the concrete strength for each truck batch in each specimen. All experiments on the first two specimens were carried out after well after casting, and therefore concrete strengths did not vary between tests. Tests on the third specimen were carried out shortly after 28 days

and so the concrete strength was slightly different for each shear span. Cylinder testing was carried out as per ASTM Standard C39.

Table 3-6: Concrete compressive strengths

Specimen I.D.	Shear Spans Tested	Truck One f'_c (psi)	Truck Two f'_c (psi)	Reported f'_c (psi)
1	1A, 1B	4215	3730	4100
2	2A, 2B	4970	4690	4900
3	3A	2775	2835	2800
3	3B	2930	3230	3000

3.6.2 Reinforcing Bars

The reinforcing bars used in the specimens had a nominal yield strength of 60ksi and conformed to ASTM A615. In order to obtain a stress vs. strain curve for each bar size in each specimen, two sample lengths of each bar were tested in tension using a 600 kip universal testing machine in FSEL. Two tests were used to verify the data by ensuring the test data from each length was nearly identical. During the test, load was measured using load cells within the machine and displacements (and therefore strains) were measured using an extensometer.

The general shape of the stress vs. strain relationship for each rebar test was virtually identical. As an example, the stress and strain relationship for the #5 stirrup bars in the first specimen is given in Figure 3-18. The yield stress and corresponding strain for each bar size of each specimen is listed in Table 3-7. The yield strains were used in conjunction with experimental strain data to determine the point at which reinforcing bars within the specimens yielded.

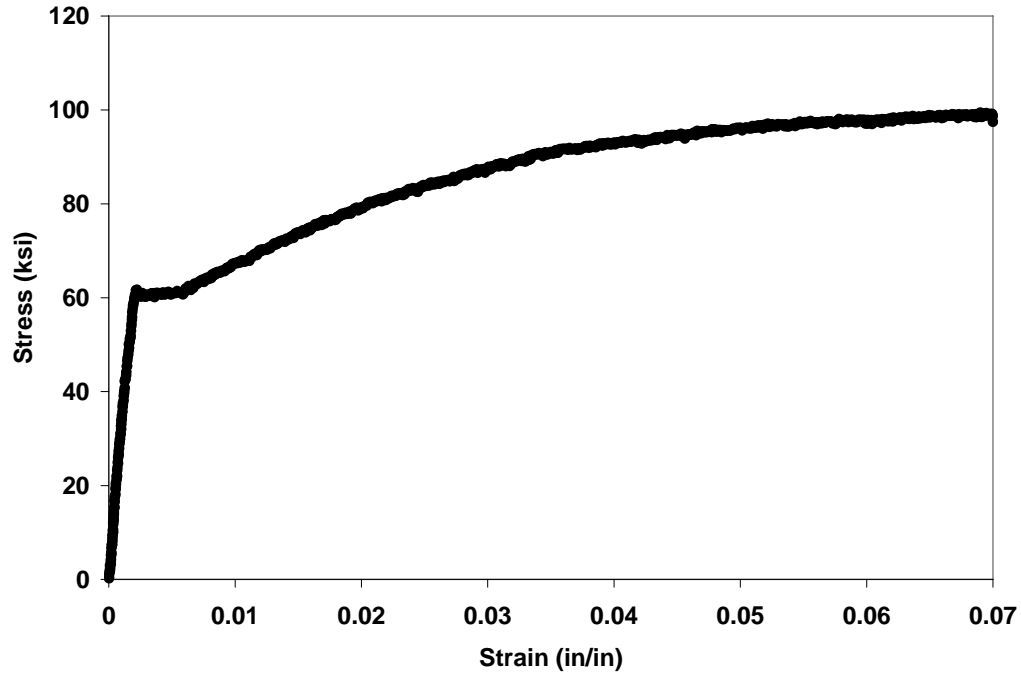


Figure 3-18: Stress vs. strain relationship, specimen 1, #5 bars

Table 3-7: Reinforcing bar properties

Specimen Number	Bar Size	Yield Stress (ksi)	Yield Strain (in/in)
1	#5	61.0	0.0021
1	#11	67.0	0.0023
2	#7	62.0	0.0021
2	#11	68.0	0.0023
3	#4	62.5	0.0022
3	#5	62.5	0.0022
3	#11	65.0	0.0022

3.7 INSTRUMENTATION

A computer with data acquisition software together with a 120-channel scanner and bridge-completion boxes were used to measure reinforcing bar and concrete strains, displacements, and loads. Changes in measured voltage were scanned, recorded, and consequently converted into proper engineering quantities through the use of calibration

equations. The specific devices and methods used to obtain information are outlined in the sections below.

3.7.1 Load Measurement and Verification

Tests on the first specimen utilized a pressure transducer to measure the applied load. In order to ensure to accuracy of the pressure transducer, a 1000 kip load cell was utilized for the first 800 kips of loading for the tests performed on the first test specimen. The load as recorded by the pressure transducer was compared to the true load reported by the load cell. Applied loads well in excess of 1000 kips were required to complete testing; therefore, the 1000 kip capacity load cell was removed before exceeding 800 kips of applied load. The pressure transducers were calibrated prior to the test and the calibration was confirmed within the first 800 kips of applied load through the use of a 1000 kip load cell. The pressure transducer-based load readings were accurate for the first 800 kips and were assumed to be as accurate for the remainder of the loading regime.

In order to simplify testing and further confirm the load readings deduced from the pressure transducers used for the first test, the vertical rods were instrumented by center-hole load cells with 500-kip capacity for the remaining two specimens. For the second specimen, six load cells were available and utilized for all six rods on one end of the test setup; the third specimen utilized 12 load cells, one for each of the 12 rods used in the test setup.

The load cells as used in the test setup are pictured in Figure 3-19, and can also be seen in Figure 3-2 and Figure 3-3. The load cells measured the support reactions next to the test region, and the applied load was calculated using static equilibrium and confirmed with pressure transducer readings.

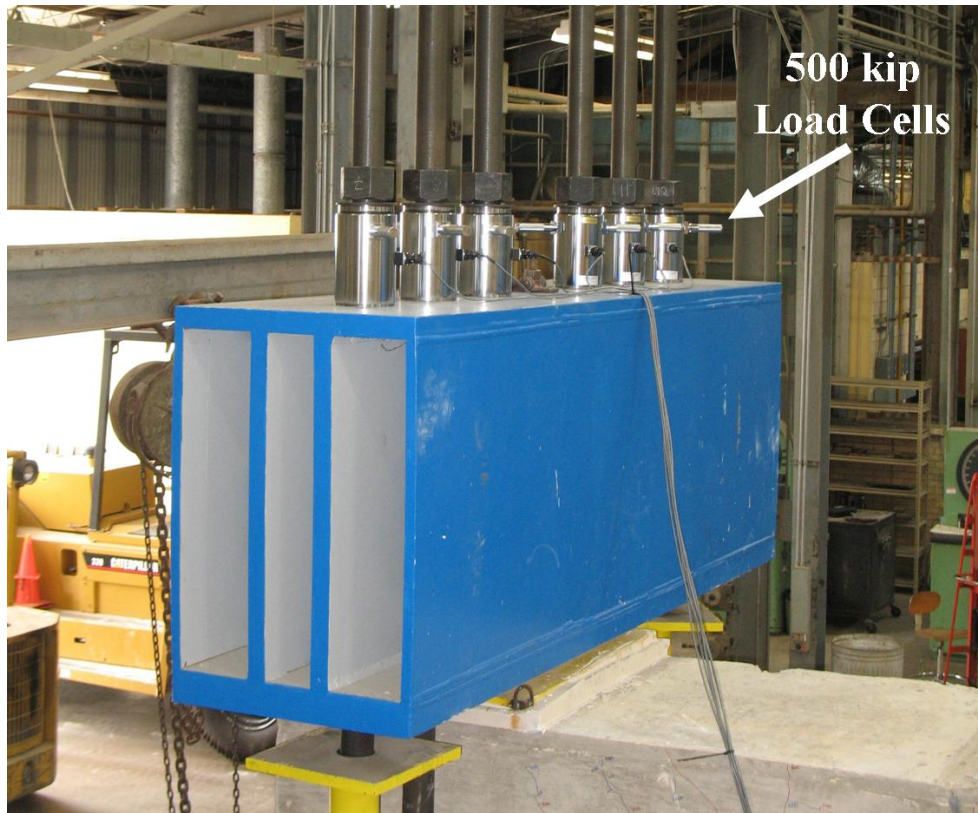


Figure 3-19: 500 kip load cells

Once again, the 1000 kip load cell was used to verify the accuracy of this method. The specimens were loaded up to 800 kips with the 1000 kip load cell installed at the load point. The applied load was calculated using the 500 kip centerhole load cells, and then compared to the true value reported by the 1000 kip load cell and the pressure transducer. Once verified, the 1000 kip load cell was removed and the remainder of the test was completed.

From the verification exercise, the accuracy of loads reported for the first test specimen is expected to be better than 0.5% and that reported for the subsequent test specimens better than 0.05%.

3.7.2 Displacements

Displacement data was gathered using a set of four 6-inch linear potentiometers. The displacement of the specimens was measured on the bottom face of the specimen at four points: the load point, mid-span, and at the supports (see Figure 3-20). A linear potentiometer, as used in the test setup, is pictured in Figure 3-21.

As the applied load was increased during a test, the threaded rods that restrain the specimen at its ends elongated in tension and allow small deflections at the end points of the specimen. These deflections are greater at one end of the specimen than the other due to the asymmetrical location of the applied load. Thus, in addition to the deflection of the center of the beam relative to its ends, the beam as a whole undergoes rigid body motion.

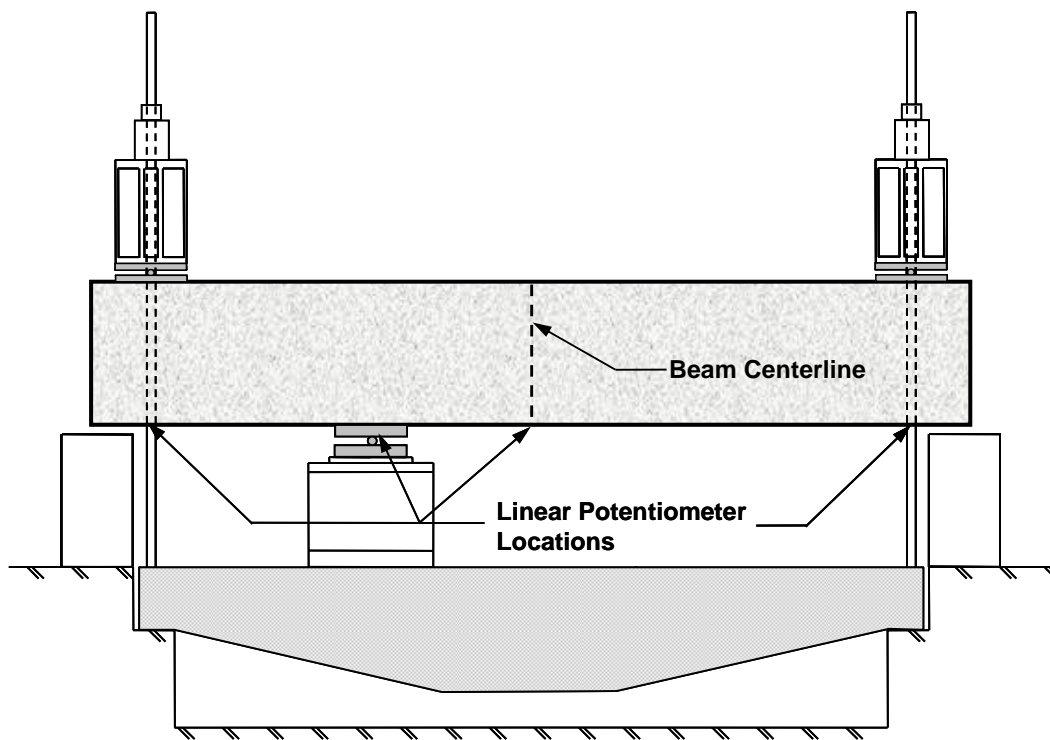


Figure 3-20: Linear potentiometer locations

Deflections reported in the experimental results section of this report account for rigid body motion. The deflection at the load point was calculated as follows

(approximately 71% of the applied load was resisted by the near support at loads near ultimate—thus the coefficient 0.71):

$$\Delta = \Delta_{LP} - [\Delta_{FAR} + 0.71(\Delta_{NEAR} - \Delta_{FAR})] \quad \text{Equation 3-1}$$

where:

Δ = Deflection at load point (in)

Δ_{LP} = Recorded deflection at load point (in)

Δ_{NEAR} = Recorded deflection at near reaction point

Δ_{FAR} = Recorded deflection at far reaction point



Figure 3-21: 6-inch linear potentiometer

3.7.3 Strain measurements

Strain gauges were used to measure both rebar and concrete strains at select locations for in the specimen. All strain gauges were obtained from Tokyo Sokki Kenkyujo Co., Ltd.

3.7.3.1 Reinforcing Bar Strains

Strain gauges were utilized to measure strains in the reinforcing bars at various locations. Strains were measured on several tensile longitudinal bars at each of the two load points. In addition, in the first specimen strains were measured along a corner longitudinal bar at various locations adjacent to the reaction bearing plate (Figure 3-22). Gauges were placed in this manner to allow the examination of strains adjacent to the specimen's anchorage detail (given in Appendix B). Gauges were also equally spaced on each leg of five stirrups in each shear span. The stirrup strain gauges were placed at the mid-height of the stirrup legs for the first specimen. For the remaining two specimens, gauges were placed along the centerline of the theoretical location of the strut that forms between the load point and support reaction; the strut centerline coincided with the anticipated location of the widest inclined shear crack. Since rebar strains are largely proportional to their proximity to a crack, this latter arrangement was used to ensure that all rebar strain gauges were located near the major inclined shear crack. The shear span for a typical specimen is shown in Figure 3-23, along with locations of stirrup strain gauges.

Depending on the number of stirrup legs for a particular specimen, the total number of reinforcing bar strain gauges used for each specimen ranged from 30 to 46.

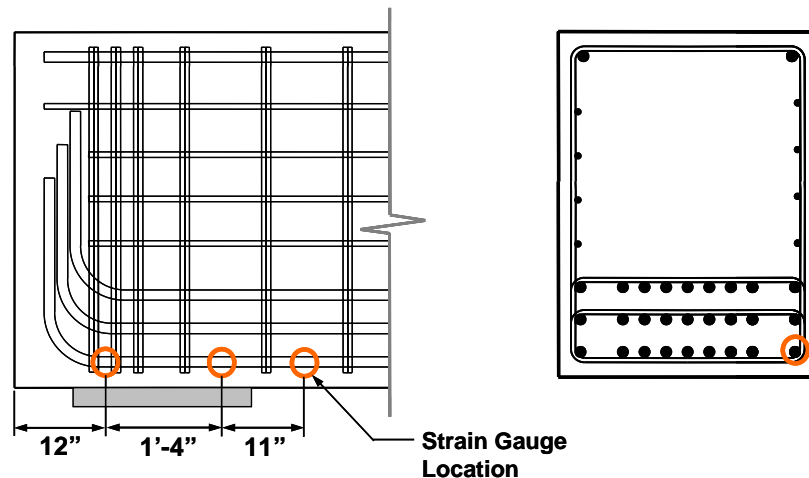


Figure 3-22: Strain gauge locations adjacent to reaction point

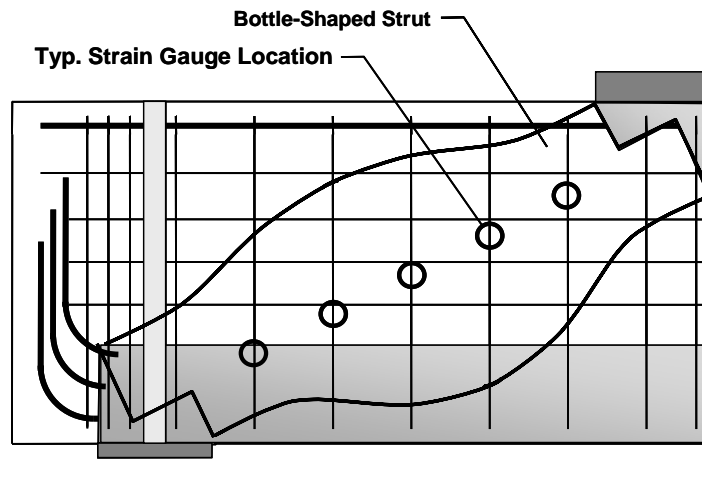


Figure 3-23: Stirrup strain gauge locations

3.7.3.2 Concrete Strains

Concrete surface strain gauges were utilized to better understand the flow of forces from the load point to the near support in Test #1. Five equally spaced gages were placed at mid-length of the direct strut, along a line perpendicular to the centerline of the strut. In this orientation, the dispersion of the compression across a bottle-shaped strut was measured. The strain gauge locations, concrete strut, and photo of the surface strain gages are shown in Figure 3-24.

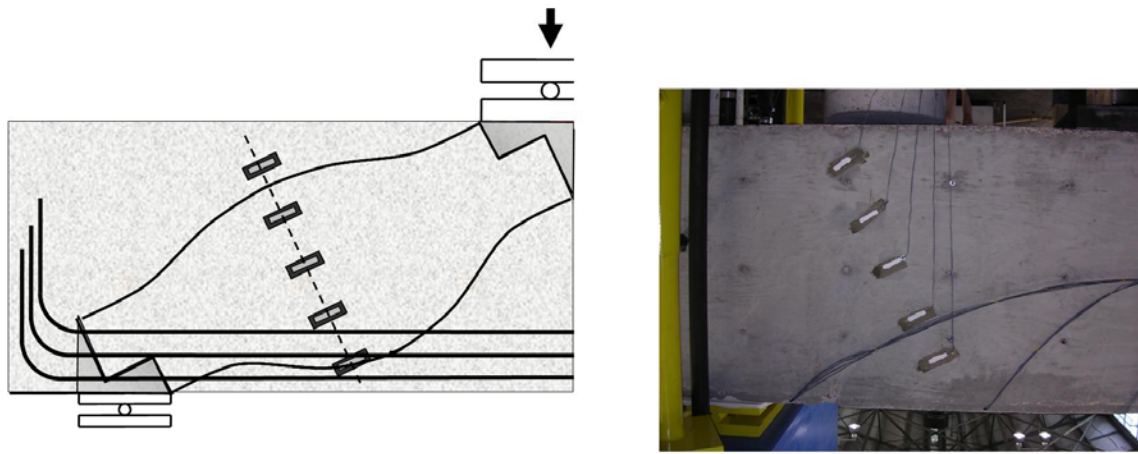


Figure 3-24: Surface strain gauge locations

3.8 SUMMARY

The test setup, specimen design and details, and information on the instrumentation used to gather data are described in this chapter. Testing of the large-scale specimens required the construction of a new testing apparatus in the Ferguson Structural Engineering Laboratory; pertinent details of the design and construction process are described in this chapter.

The experimental program consisted of nine tests performed on three specimens. It was possible to perform multiple tests on each test specimen. The beams had sufficient length (L/d ratio of 6.4) to obtain two independent shear tests, one on each end of the specimen. A given specimen was first tested with an asymmetrically placed concentrated load near one end of the beam; after testing the first side of the specimen, the hydraulic ram (i.e. the concentrated load) was then moved to opposite side of the beam for a second test with an identical a/d ratio. If the flexural reinforcement in a shear span yielded during the course of a test with a given bearing plate size, the test was stopped prior to flexural failure and additional tests with different bearing plate sizes were conducted. The intent of this process was to select a bearing size that would induce a shear failure in each shear span rather than a flexural failure. Strength and serviceability data were

collected for the initial test on each shear span, whereas subsequent tests on a given span were conducted only for the purpose of obtaining the ultimate applied load with a reduced bearing area.

The test setup and data acquisition system together allowed the successful testing of large scale reinforced concrete members while monitoring a variety of pertinent data.

CHAPTER 4

Experimental Results and Analysis

4.1 OVERVIEW

The results of nine tests performed on three specimens are described in this chapter. The sequence of tests is outlined first, along with the rationale for each test. The performance of the specimens is discussed from both a strength and serviceability perspective. The results are reported with a focus on the main test variables: the horizontal and vertical shear reinforcement ratio, the quantity of stirrups legs, and the applied load bearing area. In addition, experimental or measured capacities are compared to the design capacities estimated by using strut-and-tie models.

4.2 SUMMARY OF TESTS PERFORMED

This section outlines the sequence of the nine tests performed; detailed results and analyses are presented in the latter sections of this chapter. Table 4-1 displays a summary of primary details and results for the tests completed. The rationale for each test was affected by the tests preceding it, and the table outlines the motivation for undertaking each test. Several of the points in the table are expanded upon in the pages that follow. An expanded summary of test results is given Table 4-2.

Table 4-1: Summary of testing

Test Number	Shear Span Tested	ρ_v	Qty. Stirrup Legs	ρ_H	Applied Load Bearing Size*	Rationale for Test	Result
1	1A	0.0031	4	0.0030	24" x 36"	<ul style="list-style-type: none"> Shear span contained AASHTO minimum vertical shear reinforcement Utilized 4 stirrups legs, as is most common in TxDOT bent caps 	<ul style="list-style-type: none"> Shear Span 1A failed in shear at applied load of 1,626 kips Shear span 1A was clamped to allow testing of shear span 1B†
2	1B	0.0086	4	0.0030	24" x 36"	<ul style="list-style-type: none"> Shear span contained nearly triple AASHTO minimum vertical shear reinforcement Stirrup spacing of 4" considered minimum practical (constructible) 	<ul style="list-style-type: none"> In Shear Span 1B, flexural yielding initiated at 1,650 kips Test was continued, flexural failure occurred at 2,050 kips‡
3	2A	0.0031	2	0.0030	24" x 36"	<ul style="list-style-type: none"> Matches Test 1, except stirrups had two legs instead of four Served as direct comparison to Test 1 	<ul style="list-style-type: none"> In Shear Span 2A, flexural yielding initiated at 1,573 kips Test was halted, bearing area changed for the following test
4	2A	0.0031	2	0.0030	8" x 36"	<ul style="list-style-type: none"> Same as previous test, except bearing area was 1/3 as large The thin, full width bearing size was used to ensure the specimen was shear critical 	<ul style="list-style-type: none"> Shear Span 2A failed in shear at 1,510 kips Shear span 2A was clamped to allow testing of shear span 2B†
5	2B	0.0061	2	0.0030	24" x 36"	<ul style="list-style-type: none"> Contained approx. double AASHTO minimum vertical reinforcement ρ_v halfway in between the amount contained in shear spans 1A and 2A 	<ul style="list-style-type: none"> In Shear Span 2B, flexural yielding initiated at 1,628 kips Test was halted, bearing area changed for the following test

Table 4-1 (continued): Summary of testing

Test Number	Shear Span Tested	ρ_v	Qty. Stirrup Legs	ρ_H	Applied Load Bearing Size*	Rationale for Test	Result
6	2B	0.0061	2	0.0030	24" x 18"	<ul style="list-style-type: none"> Same as Test 5, but the bearing width was halved to test effect of limited bearing width 	<ul style="list-style-type: none"> Applied load was again raised to 1,628 kips, at which point flexural reinforcement underwent further yielding Test was halted, bearing area changed for the following test
7	2B	0.0061	2	0.0030	8" x 36"	<ul style="list-style-type: none"> Same as Test 5, except bearing area was 1/3 as large The thin, full width bearing size was used ensure the specimen was shear critical 	<ul style="list-style-type: none"> Shear Span 2B failed in shear at 1,853 kips
8	3A	0.0022	4	0.0022	24" x 36"	<ul style="list-style-type: none"> Contained ACI minimum amount of shear reinforcement, which is considerably less than the AASHTO minimum 	<ul style="list-style-type: none"> Shear Span 3A failed in shear at 1,510 kips Shear span 3A was clamped to allow testing of shear span 3B†
9	3B	0.0030	4	0.0030	8" x 12"	<ul style="list-style-type: none"> Same as Test 1, except that bearing area was significantly smaller Bearing size selected to have both similar aspect ratio to TxDOT Greens Road bent bearings, and be exactly 1/3 the area of the 8" x 36" bearing used in previous tests. 	<ul style="list-style-type: none"> Shear Span 3B failed in shear at 1,262 kips

*Bearing plate sizes are reported as [dimension in direction of span] x [dimension in transverse direction]

†As outlined in section 3.3

‡See following pages for discussion of flexural failure

Table 4-2: Detailed summary of testing

Test #	Shear Span Tested	f'_c (psi)	Qty. Stirrup Legs	Vertical Shear Reinforcement	ρ_v	Horizontal Shear Reinforcement	ρ_{H1}	$\sum \frac{A_{vi} \sin \alpha_i}{b_s}$	Applied Load Bearing Size*	Support Reaction Bearing Size*	Maximum Applied Load (kips)	Maximum Shear (kips)	$\frac{V_{max}}{\sqrt{f'_c b_s d}}$	Behavior at Maximum Applied Load
1	1A	4100	4 legs	#5 @ 11"	0.0031	8 #5 bars	0.0030	0.0043	24" x 36"		1,626	1,141	12.3	Shear Failure
2	1B	4100	4 legs	#5 @ 4"	0.0086	8 #5 bars	0.0030	0.0091	24" x 36"		2050†	1,443	12.4	Flexural Failure
3	2A	4900	2 legs	#7 @ 11"	0.0031	8 #5 bars	0.0030	0.0043	24" x 36"		1,573	1,096	10.9	Initiation of Flexural Yielding
4	2A	4900	2 legs	#7 @ 11"	0.0031	8 #5 bars	0.0030	0.0043	8" x 36"		1,510	1,052	10.4	Shear Failure
5	2B	4900	2 legs	#7 @ 5 1/2"	0.0061	8 #5 bars	0.0030	0.0068	24" x 36"	16" x 36"	1,628	1,143	11.2	Initiation of Flexural Yielding
6	2B	4900	2 legs	#7 @ 5 1/2"	0.0061	8 #5 bars	0.0030	0.0068	24" x 18"		1,628	1,143	11.3	Initiation of Flexural Yielding
7	2B	4900	2 legs	#7 @ 5 1/2"	0.0061	8 #5 bars	0.0030	0.0068	8" x 36"		1,853	1,303	12.8	Shear Failure
8	3A	2800	4 legs	#4 @ 10"	0.0022	6 #5 bars	0.0022	0.0031	24" x 36"		1,510	1,059	13.8	Shear Failure
9	3B	3000	4 legs	#5 @ 11"	0.0031	8 #5 bars	0.0030	0.0043	8" x 12"		1,262	882	11.1	Shear Failure

*bearing areas are reported as [dimension in direction of span] x [dimension in transverse direction]

†Initiation of flexural yielding at approximately 1,650 kips

As noted in Chapter 3, the specimens were tested in an inverted fashion. As a result, the applied load and the dead weight of the specimens were oriented in opposite directions. Since the beams were loaded asymmetrically, the distributed dead weight of the specimen could not be directly subtracted from the applied force. Therefore, all reported applied loads are simply equal to the upward load exerted by the hydraulic ram. The distributed dead weight of the specimen causes the internal shear to vary slightly at any given point along the specimen. For consistency, all shear values are reported at the midpoint of the shear span, as shown in Figure 4-1. Load verification methods were outlined in Section 3.7.1.

Bearing sizes are reported as [dimension in direction of span] x [dimension in transverse direction], and were always placed along the centerline in the transverse direction. The support reaction bearing size remained constant for all tests. For example, the bearing arrangement for Test 1 is shown in Figure 4-2. Placement of bearing plates is also discussed in section 3.3.

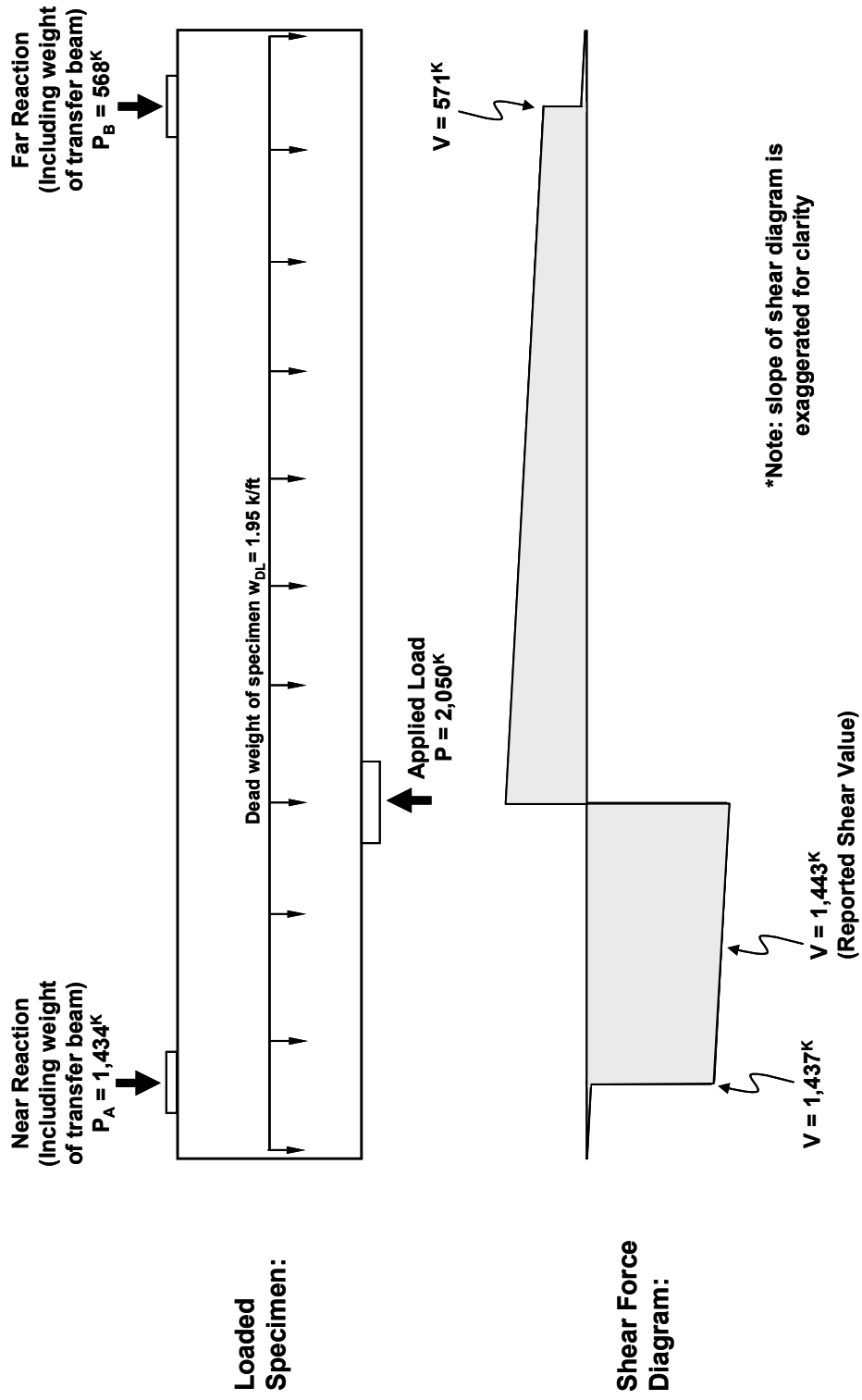


Figure 4-1: Typical specimen shear force diagram at maximum applied load

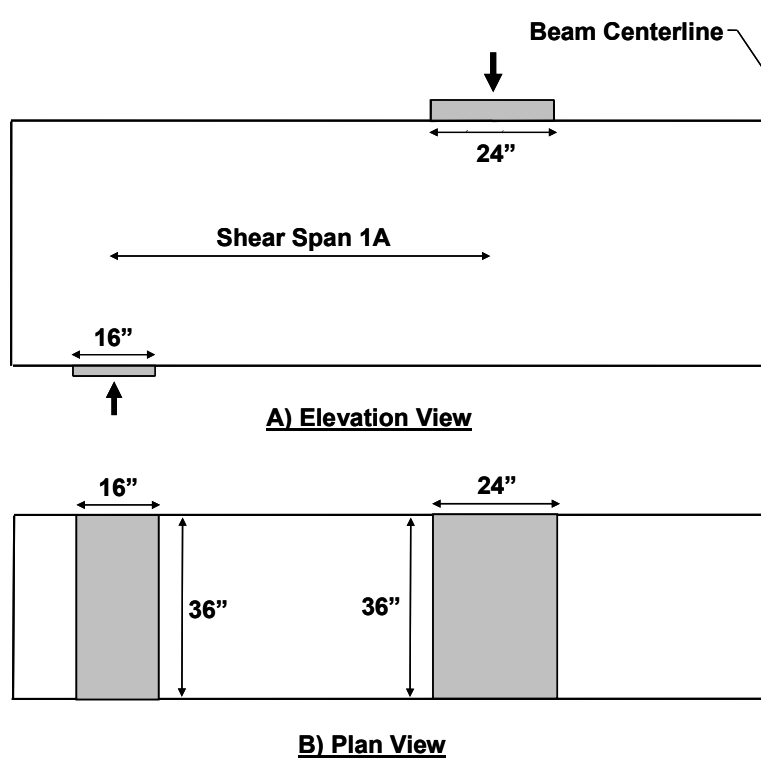


Figure 4-2: Test #1 Bearing Geometry

4.3 EXPERIMENTAL RESULTS AND ANALYSIS

The effects of the test variables on both the ultimate strength and serviceability performance of the specimens in the experimental program are discussed within this section. In addition, experimental (measured) capacities are also compared to design capacities estimated using strut-and-tie models.

4.3.1 Ultimate Strength

Although the amount and detailing of transverse reinforcement and bearing plate size were the main test variables, the concrete strength also varied between the three specimens. It was possible to conduct a sufficient number of tests to analyze each variable; the various effects of each test variables was determined through direct comparisons of tests where only one variable was changed from one test to another. To

facilitate such direct comparisons, the results were normalized with respect to compressive strength of concrete.

One way of normalizing the results with respect to concrete strength is to report maximum applied load values in terms of experimentally determined strut efficiencies. Since the shear strength of deep beams is typically proportional to the strength of a direct strut that forms between the load point and reaction point, this method of normalizing the results is appropriate for deep beams. The nodes in the strut-tie-models for the test specimens were assumed to be non-hydrostatic, as shown in Figure 4-3. As a result, the experimentally determined strut efficiency, v_{exp} , is defined as:

$$v_{exp} = \frac{F_{strut}}{f'_c A_{strut,min}} \quad \text{Equation 4-1}$$

$$F_{strut} = \frac{V_{max}}{\sin \theta} \quad \text{Equation 4-2}$$

where:

F_{strut} = force carried by one-panel strut at the maximum applied load, parallel to strut axis (kips)

V_{max} = reported maximum shear in shear span (Figure 4-1) (kips)

θ = angle of strut inclination (Figure 4-3) (deg)

$A_{strut,min}$ = minimum strut area (in²)

f'_c = compressive strength of concrete (ksi)

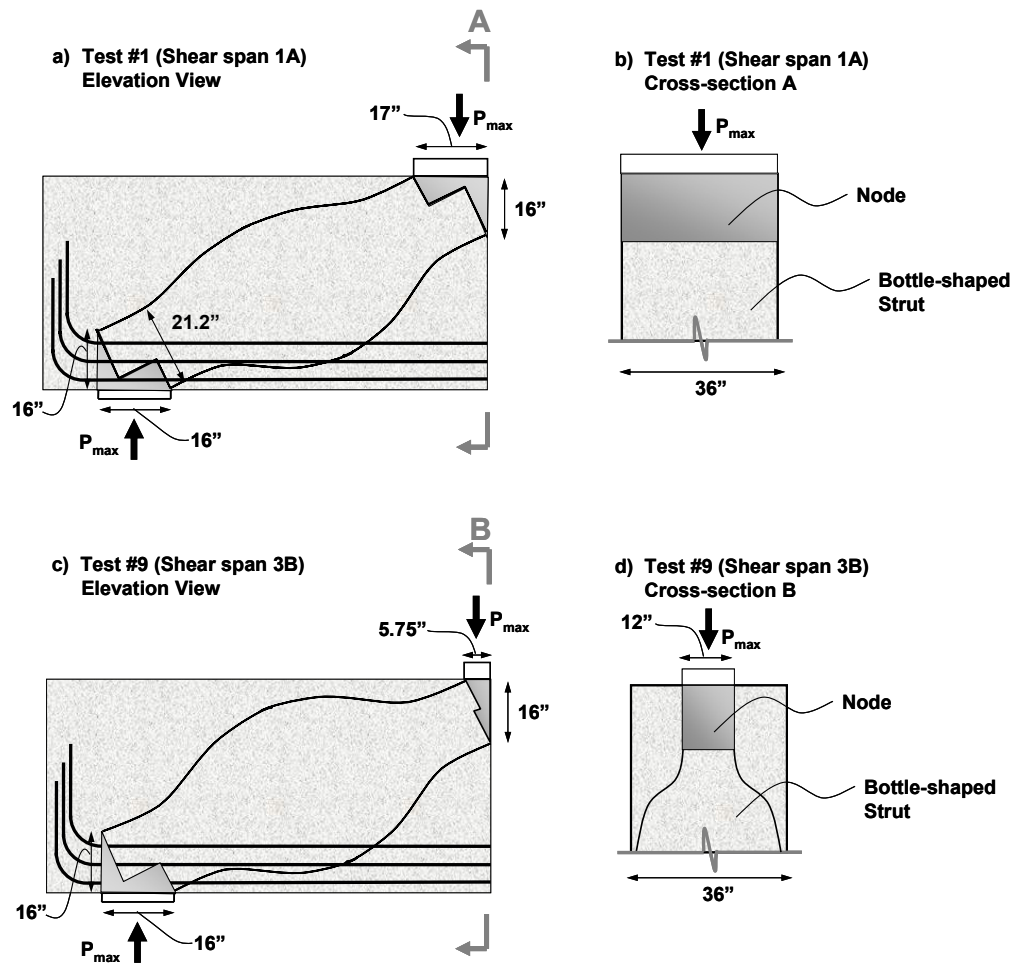


Figure 4-3: Typical node geometry

The minimum strut area occurs at the strut interface with one of the two adjoining nodes. For example, in Test #1 (Figure 4-3a), the minimum strut area occurred at the strut-to-node interface adjacent to the reaction point. The strut efficiency is calculated as:

$$v_{\text{exp}} = \frac{F_{\text{strut}}}{f'_c A_{\text{strut},\text{min}}} = \frac{1,141^K}{4.1\text{ksi}(21.2'')(36'')} \sin 25^\circ = 0.88$$

Modeling of the specimens is discussed in detail in section 4.3.3. The experimental strut efficiency for each of the nine tests is listed in Table 4-3.

Table 4-3: Experimental strut efficiencies

Test Number	Experimental Strut Efficiency, v_{exp}
1	0.88
2	1.12
3	0.71
4	0.80
5	0.74
6	1.45
7	0.99
8	1.20
9	3.27

The shear span in each test exhibited different strength and serviceability behavior. The different modes of failure observed during the tests and the effect of each variable on ultimate strength are discussed individually.

4.3.1.1 Failure Mode

As reported in Table 4-2, the maximum load applied on a specimen was governed by either a shear failure or the initiation of flexural yielding in all but one of the tests. Flexural failure was observed in only one of the tests.

The primary objective of the test program was to study strength and serviceability behavior of deep beams. As part of this primary objective, inducing failure in the compression strut was of interest. This objective was achieved in five of the six shear spans tested during the course of the experimental study. Flexural failure was observed in only in the Test #2 specimen. It is important to note that during several of the tests loading was stopped when the initiation of yielding in the flexural reinforcement was noted. The specimen was unloaded and a smaller applied load bearing plate was used to reload the specimen until the specimen failed in shear (see section 3.3).

4.3.1.1.1 Shear Failure

Five of the nine tests completed resulted in a shear failure. In this section, the shear failure in Test #1 is discussed in detail because it was typical of all shear failures.

A photograph of the shear failure in the shear span of Test #1 is shown in Figure 4-4 (bearing plates are highlighted for clarity). The shear failure initiated with concrete crushing above the applied load bearing plate (this location is highlighted in Figure 4-4), at the strut-to-node interface. The sudden failure of the compression strut was accompanied by a loud crushing sound. After shear failure, the applied load quickly dropped. There was relative displacement of the two concrete “blocks” along the primary crack that formed. Deflection at the load point is shown in Figure 4-5. This behavior was typical of all of the shear failures observed in the experimental program. Failure photos for each of the shear failures observed in the test program are shown in Appendix C.

At failure load both stirrups and the outermost layer of longitudinal reinforcement were at or beyond yielding. Stirrup strains at maximum applied load at various points along the length of the shear span are shown in Figure 4-6. It is interesting to note that while some stirrups yielded at failure, stirrups close to the bearing plates at load and reaction points were strained to a lesser degree. At shear failure, the outermost layer of tensile longitudinal bars began to yield (Figure 4-7). Despite the fact that flexural reinforcement had reached nominal yield, the behavior of the specimen described above indicated a shear failure. The locations of the longitudinal strain gauges are shown in Figure 4-8, and are typical of all tests.

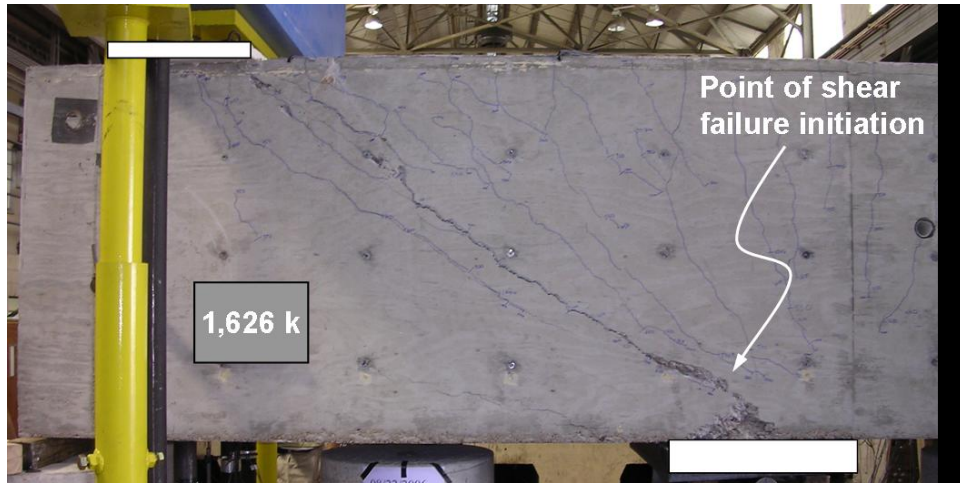


Figure 4-4: Test #1 shear failure

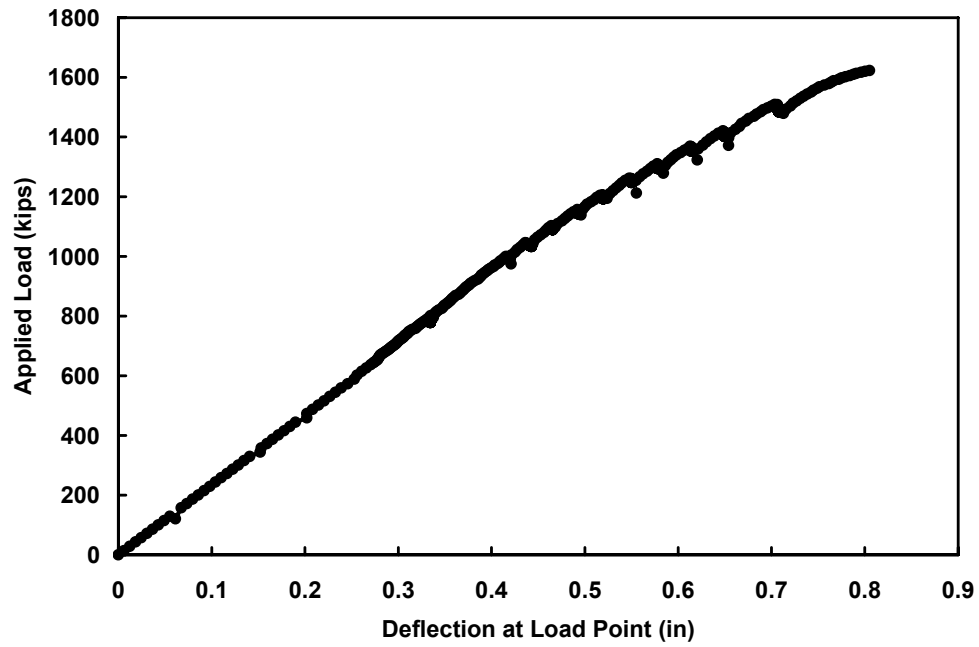


Figure 4-5: Test #1 applied load vs. deflection

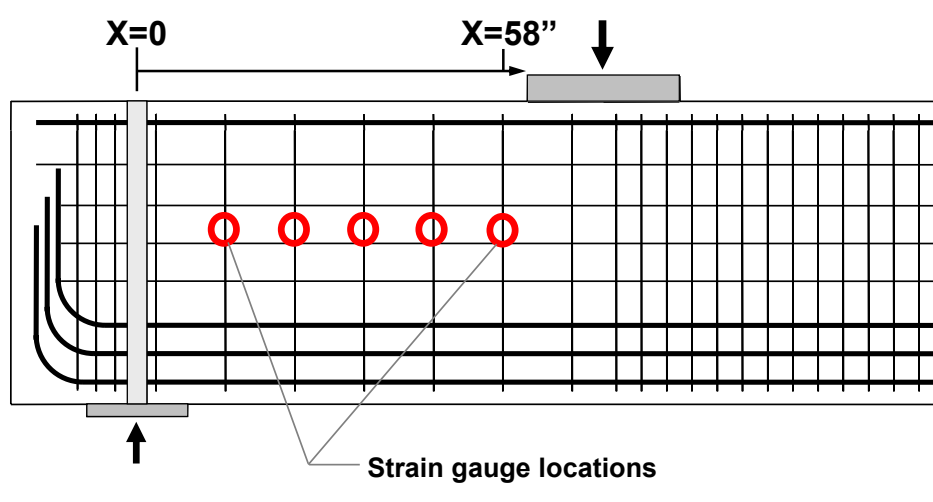
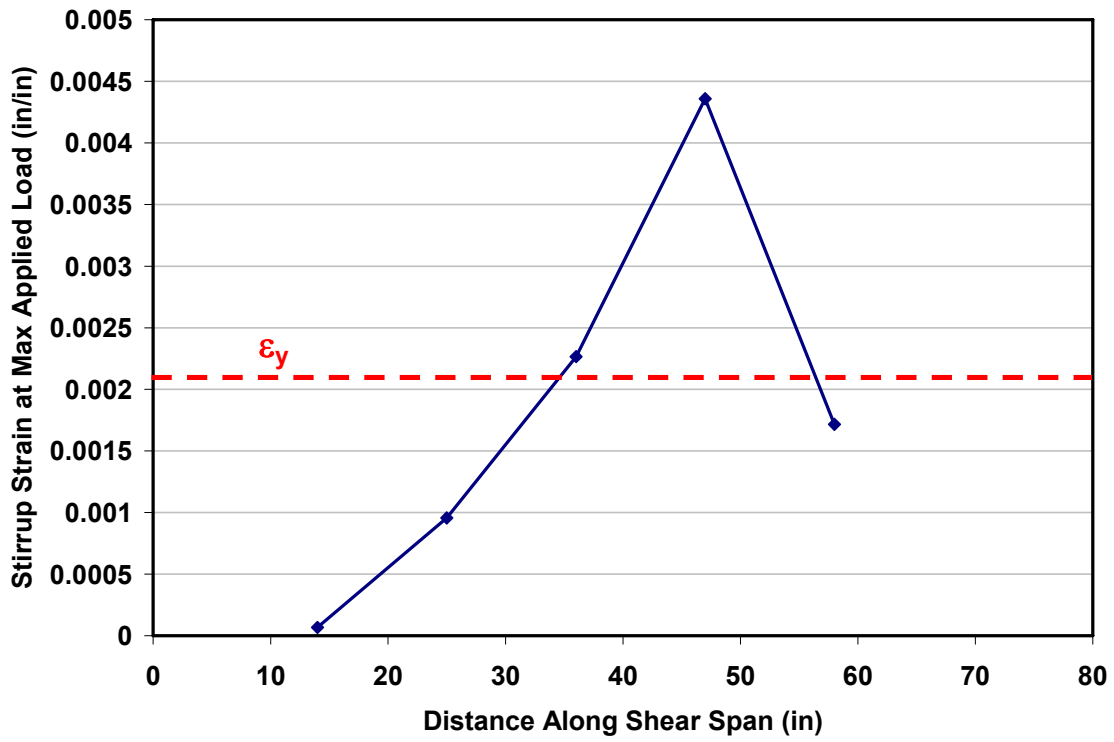


Figure 4-6: Test #1 stirrup strain along shear span at maximum applied load

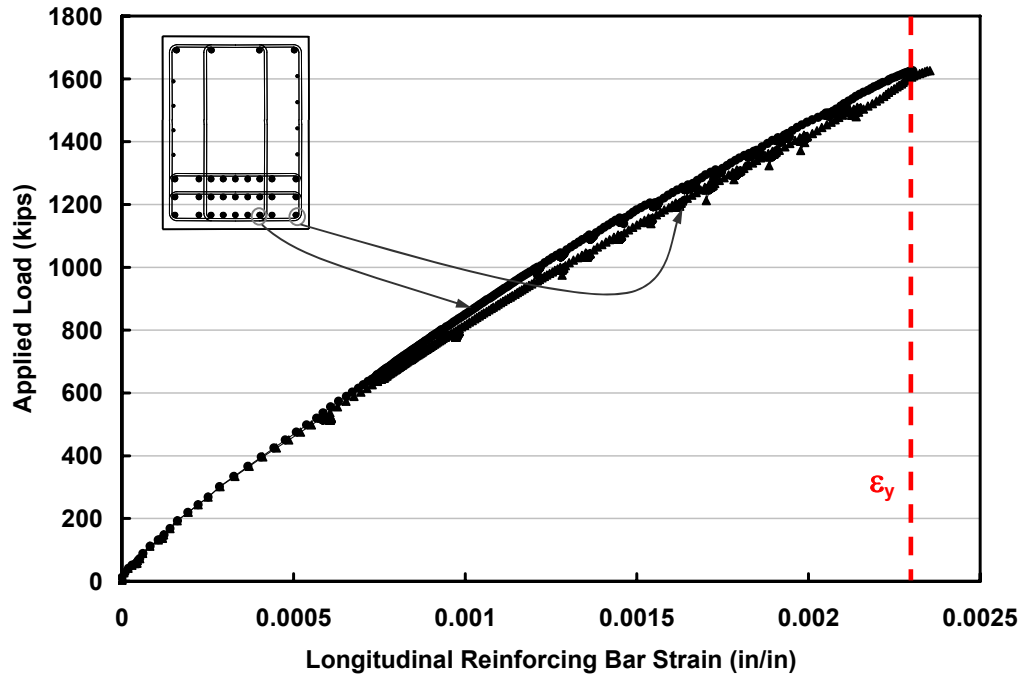


Figure 4-7: Test #1 applied load vs. longitudinal reinforcement strain

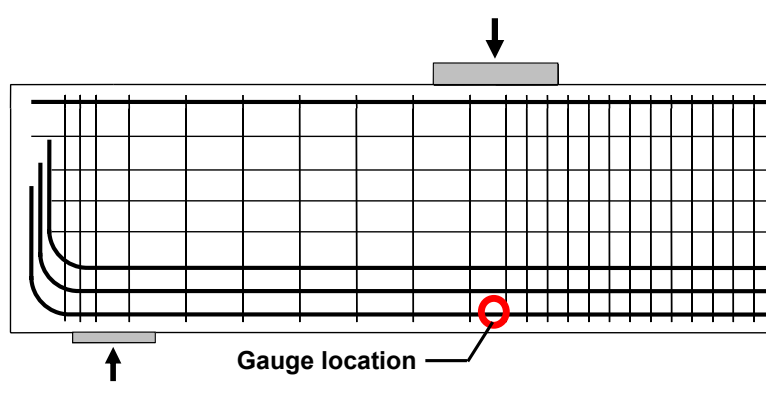


Figure 4-8: Longitudinal strain gauge location

4.3.1.1.2 Flexural Failure

Flexural failure was observed in Test #2. In this test the concrete began to crush and spall off the compression side of the test specimen at approximately 1,650 kips. This

is also approximately the load at which the longitudinal rebar reached nominal yielding in Test #1. This behavior is illustrated in Figure 4-9, Figure 4-10 and Figure 4-11. At an applied load of approximately 2,050 kips the deflection of the specimen increased continuously without an increase in load, and finally failure occurred through crushing of concrete adjacent to the CCC node (Figure 4-10 and Figure 4-11). The flat portion of the load deformation response depicted in Figure 4-9 indicates the yielding of flexural reinforcement prior to failure of the compression region.

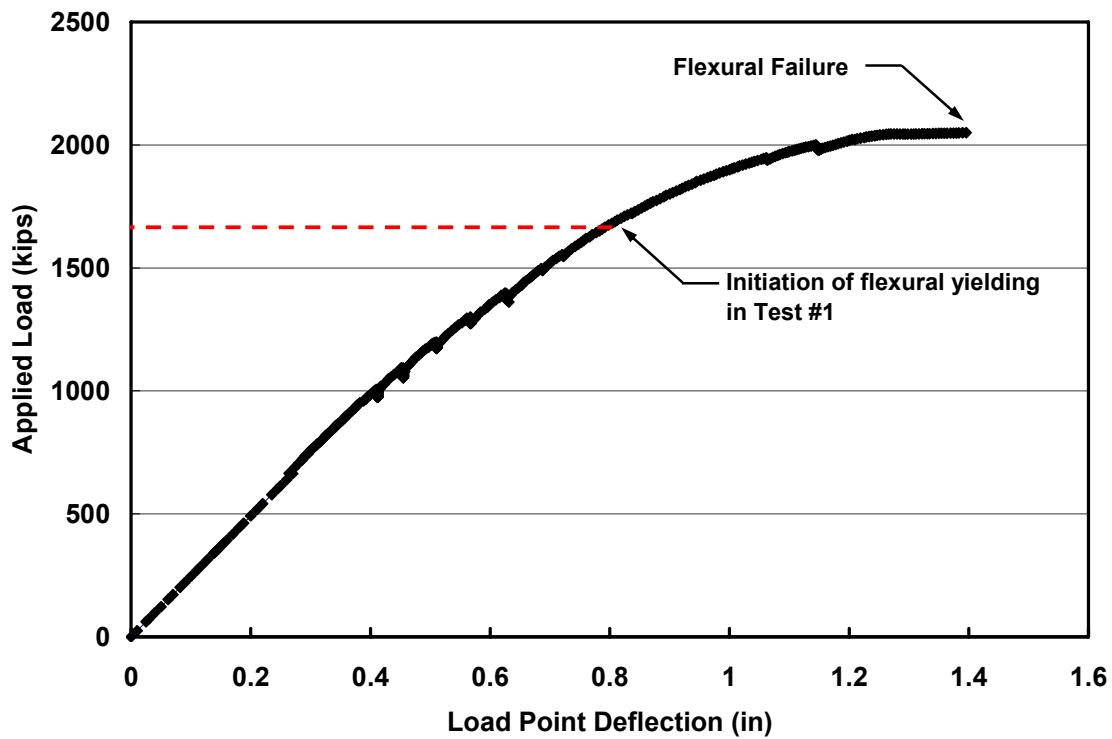


Figure 4-9: Test #2 load vs. deflection

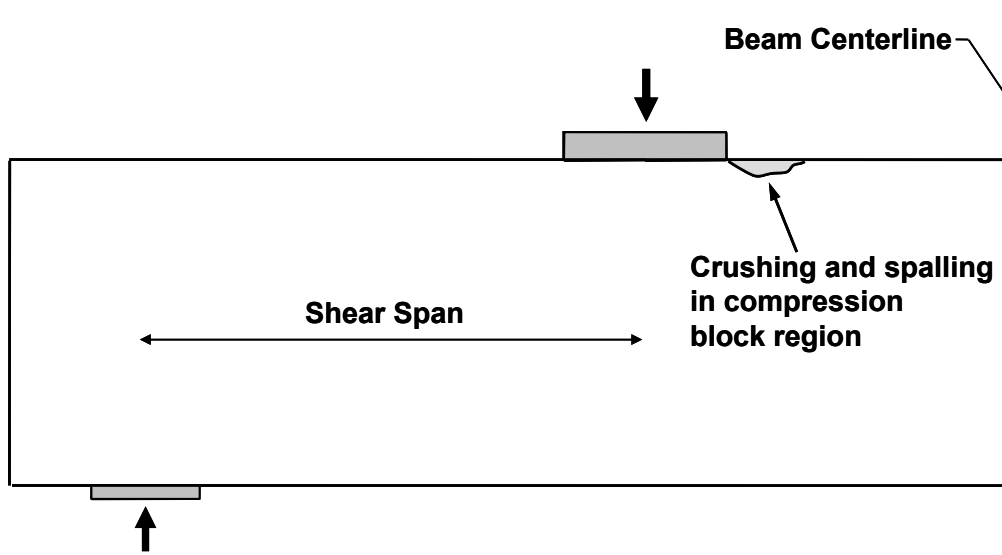


Figure 4-10: Illustration of compression failure



Figure 4-11: Photograph of compression block crushing

4.3.1.1.3 Initiation of Flexural Yielding

The data collected after the initiation of flexural yielding in Test #2 was not valuable to the study of shear performance. Therefore, all subsequent tests were stopped at the point of initial flexural yielding. The applied load vs. longitudinal reinforcement strain plots for two such tests (Test #3 and Test #5) are shown in Figure 4-12 and Figure 4-13.

After the test was stopped, the bearing plate size under the hydraulic ram was reduced and the test was repeated. The goal of repeating the test with a smaller bearing plate size was to induce a shear failure (see section 3.3 and Table 4-1). Stopping a given test at the onset of first flexural yielding also had experimental value, since the load carried by the compression strut up to that point was determined.

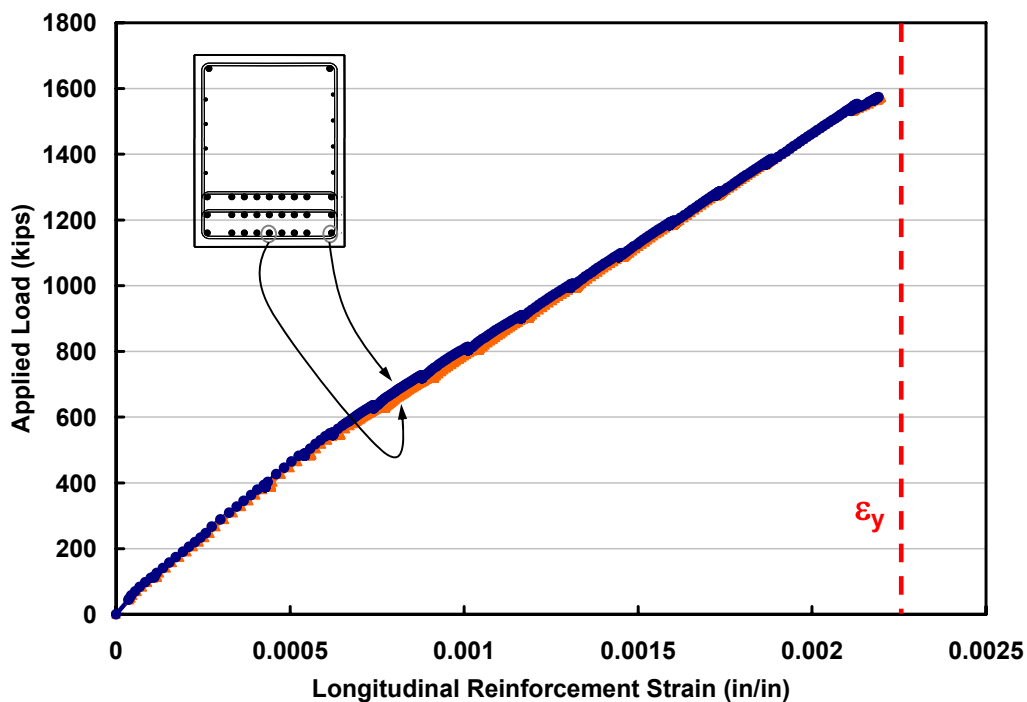


Figure 4-12: Test #3 applied load vs. longitudinal reinforcement strain

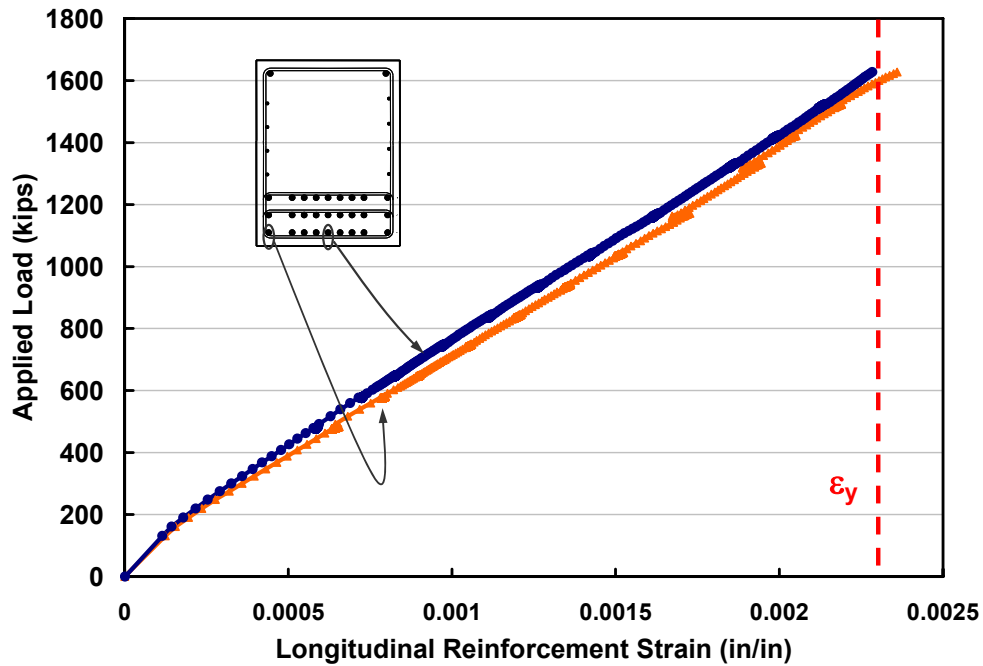


Figure 4-13: Test #5 applied load vs. longitudinal reinforcement strain

4.3.1.2 Examination of Test Variables

A sufficient number of tests were completed to analyze each test variable; the effect of each test variables was determined primarily through direct comparisons of tests where only one variable was changed from one test to another.

4.3.1.2.1 Transverse Reinforcement Ratio

The effect of the amount of transverse reinforcement can be studied by comparing results of the tests in which the amount of reinforcement was the only test variable. The results of tests with four stirrup legs are shown in Table 4-4. Pertinent details of tests on tests with two legs are shown in Table 4-5.

Table 4-4: Comparison of tests with 4-legged stirrups

Test #	Shear Span Tested	f'_c (psi)	$\sum \frac{A_{st}}{bs_i} \sin \alpha_i$	Applied Load Bearing Size	Max Applied Load (kips)	Shear at Max Applied Load (kips)	v_{exp}	Behavior at Max Applied Load
1	1A	4100	0.0043	24" x 36"	1,626	1,141	0.88	Shear Failure
2	1B	4100	0.0091	24" x 36"	1,644	1,443	1.12	Flexural Yielding
8	3A	2800	0.0031	24" x 36"	1,510	1,059	1.20	Shear Failure

Table 4-5: Comparison of tests with 2-legged stirrups

Test #	Shear Span Tested	f'_c (psi)	$\sum \frac{A_{st}}{bs_i} \sin \alpha_i$	Applied Load Bearing Size*	Maximum Applied Load (kips)	Shear at Max Applied Load (kips)	v_{exp}	Behavior at Max Applied Load
4	2A	4900	0.0043	8" x 36"	1,510	1,052	.80	Shear Failure
7	2B	4900	0.0068	8" x 36"	1,853	1,303	.99	Shear Failure

Both Test #1 and Test #8 were conducted in shear spans with 4-legged stirrups and resulted in a shear failure (Table 4-4). The experimentally determined strut efficiency in each the tests does not indicate a correlation between the amount of transverse steel and ultimate shear strength. The shear span in Test #8, which contained the minimum amount of transverse reinforcement required by ACI 318, does not have inferior performance to that of Test #1, which contained minimum transverse reinforcement as required by the more stringent AASHTO LRFD minimum transverse reinforcement requirements. In fact, the shear span with AASHTO minimum transverse reinforcement has inferior performance; this is likely due to the inherent variability of the shear strength of reinforced concrete members.

It should be noted that the shear span in Test #2, which contained significantly more transverse reinforcement than shear spans in Test #1 and #8, had sufficient reinforcement to produce a flexural failure.

The results of tests on shear spans that contained 2-legged stirrups have a different trend than tests with 4-leg stirrups (Table 4-5). In both Test #4 and #7 an 8"x36" applied load bearing plate was used, and each test resulted in a shear failure. It is evident that transverse reinforcement had a marginal positive effect on the strut efficiency at the maximum applied load. However, the strut efficiency was not proportional to the amount of transverse reinforcement. The shear span in Test #7 contained nearly double the vertical transverse reinforcement of the shear span in Test #4, but only had a 23% increase in shear strength.

An examination of the results presented in Table 4-4 and Table 4-5 indicates that there are no clear trends between increased amount of transverse reinforcement and experimental strut efficiency. The slight upward and downward trends are attributed to general experimental data scatter associated with shear data.

The amount of transverse reinforcement required by ACI ($\sum \frac{A_{si}}{bs_i} \sin \alpha_i \geq 0.003$) is similar to amount required in CSA A23.3 ($\rho_{\min} = 0.002$ in each direction, which is equivalent to $\sum \frac{A_{si}}{bs_i} \sin \alpha_i = 0.0028$). AASHTO LRFD is unique in its requirement of $\rho_{\min} = 0.003$ in each direction, which is equivalent to $\sum \frac{A_{si}}{bs_i} \sin \alpha_i = 0.0042$. Based on the test results discussed in this section and from a standpoint of ultimate strength, the minimum transverse reinforcement requirements of ACI are sufficient and the requirements of AASHTO LRFD appear to be overly conservative.

4.3.1.2.2 Quantity of Stirrup Legs

An evaluation of results from Tests #1, #3, and #4 allows a direct comparison of the performance of shear spans with 4-legged stirrup reinforcement and 2-legged stirrup reinforcement. Pertinent information these tests is summarized in Table 4-6.

Table 4-6: Comparison of tests with varying quantity of stirrup legs

Test #	Shear Span Tested	Qty. of Stirrup Legs	f_c (psi)	$\sum \frac{A_{s_i}}{bs_i} \sin \alpha_i$	Applied Load Bearing Size*	Applied Load at Failure (kips)	Shear at Max Applied Load (kips)	V_{exp}	Behavior at Max Applied Load
1	1A	4	4100	0.0043	24" x 36"	1,626	1,141	0.88	Shear Failure
3	2A	2	4900	0.0043	24" x 36"	1,573	1,096	0.71	Initiation of Flexural Yielding
4	2A	2	4900	0.0043	8" x 36"	1,510	1,0452	.80	Shear Failure

The shear spans in Test #1 and Test #4 failed in shear. The quantity of stirrup legs differed between the two tests. In addition, a 24" x 36" applied load bearing plate was used for Test #1, while an 8" x 36" bearing plate was used for Test #4. The strut efficiency for Test #1 was only 11% greater than that observed in Test #4, despite the fact that the bearing area of Test #1 was three times larger than the bearing area for Test #4. If it is assumed that the 8"x36" bearing plate renders the specimen more shear critical than the 24" x 36" bearing plate does, then it can be concluded the shear span where 4-legged stirrups were used (Test #1) had an 11% greater shear capacity *at the most* as compared to the 2-legged shear span. However, given the large difference in bearing area between the two tests, it is reasonable to assume this difference could be less if identical bearing plates were used.

Experimental test results do not indicate a significant difference in strength between the specimen with two stirrup legs and the specimen with four stirrup legs. At the very most, the difference is approximately 10%, though it is likely less. Given the

inherent scatter associated with shear data (Reineck et al., 2003, Brown and Bayrak, 2006), a 10% difference is considered to be negligibly small. As such, it is believed that the difference in ultimate strength between shear spans with two and four stirrup legs is negligible.

The experimental data suggest that the AASHTO limited strut width provision is not well founded from a strength standpoint. As outlined in section 2.2.1.1.2, the provision suggests that the width of a strut adjoining a CTT node in a specimen with 2-legged stirrups can be significantly less than the strut width of a specimen with 4-legged stirrups. However, a significant difference in ultimate strength between tests with 2-legged stirrups and tests with 4-legged stirrups was not observed.

4.3.1.2.3 Bearing Area

The size of the bearing plate used between the hydraulic ram and the test specimen was altered in a pair of tests in the experimental program. Test #1 (shear span 1A) and Test #9 (shear span 3B) were conducted on shear spans that were identical apart from the size of the applied load bearing area. Pertinent data for the two tests in which the applied load bearing area is the only variable are presented in Table 4-7.

Table 4-7: Comparison of tests with varying bearing area

Test #	Shear Span Tested	f'_c (psi)	$\sum \frac{A_{s_i}}{b s_i} \sin \alpha_i$	Applied Load Bearing Size*	Applied Load at Failure (kips)	Shear at Max Applied Load (kips)	V_{exp}	Behavior at Max Applied Load
1	1A	4100	0.0043	24" x 36"	1,626	1,141	0.88	Shear Failure
9	3B	3000	0.0043	8" x 12"	1,262	882	3.28	Shear Failure

A comparison of the results of Tests #1 and #9 indicates that bearing area does not have a significant effect on the ultimate shear strength of a shear span. The shear force carried through shear span 1A (Test #1) was 30% higher than that carried through shear span 3B (Test #9), despite having an applied load bearing area that was

approximately nine times greater. However, the specimen in Test #1 had a concrete compressive strength 36% greater than that of the specimen in Test #9. Therefore, the difference in shear force carried by each of two shear spans can be explained by the differences in the compressive concrete strength between the two specimens. That is, the shear strength of each shear span was proportional to concrete strength rather than bearing area.

The experimental strut efficiency of Test #9 is greater than for Test #1 by nearly a factor of four, as shown in Table 4-7. This is a function of the large difference in bearing areas and minor difference in failure load between the two tests. The test results indicate that the use of smaller bearing plates, which result in correspondingly small CCC-nodes and node-to-strut interface planes, creates correspondingly large strut efficiencies.

The effect of bearing area on strut efficiencies in the context of a strut-and-tie model is discussed further in 4.3.3.1.

4.3.2 Serviceability

The capacity of deep beams designed using strut-and-tie modeling is governed by the lower bound theory of plasticity and as a result the method is inherently conservative. On the other hand, STM does not permit design by serviceability limit states. Therefore, empirical code provisions are used in conjunction with STM to successfully design deep beams. A major focus of this research study is the observation and evaluation of the serviceability performance of deep beam specimens.

The effect of the test variables on the first diagonal cracking load, shear crack widths, and cracking patterns were examined. This investigation was completed, among other reasons, to follow up on the STM design expressions developed as part of TxDOT Project 4371; these provisions were developed based entirely on strength considerations.

As noted in section 3.3, serviceability data could only be reliably collected for six tests: the initial test on each of the six shear spans. The results of those six tests are analyzed in the following sections.

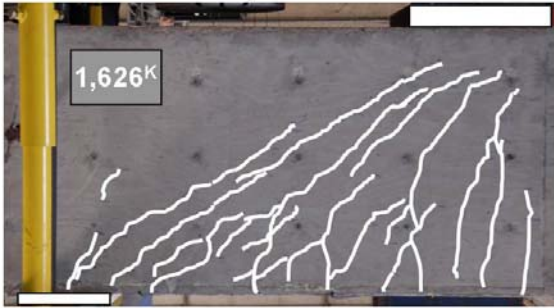
4.3.2.1 Cracking Progression and Pattern

The cracking pattern of a reinforced concrete member is inexorably tied to its behavior. The most important aspect of the serviceability performance of a deep beam is arguably its ability to resist the formation of unacceptably large diagonal shear cracks under service loads. Consultation with TxDOT bridge design engineers revealed the fact that prevention of diagonal cracking is perhaps more desirable than the trying to limit the widths of the diagonal cracks after they form. Diagonal shear cracks are undesirable from both from a safety standpoint and from an aesthetic perspective. Therefore, conservative estimation of the first diagonal cracking load can be of great importance in deep beam design. If this load can be conservatively estimated, diagonal crack formation can be prevented by proportioning bent caps to control shear stresses and/or strut loads under service loads.

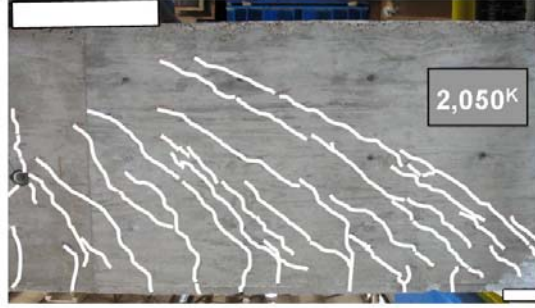
In addition, the formation of parallel shear cracks is important because it can signify an impending shear failure, as evidenced by previous research (Kong et al. 1970, Brown et. al 2006). Finally, the behavior at ultimate capacity is important, and was already outlined in section 4.3.1.

The cracking pattern observed for the initial test on each of the six shear spans was largely the same, regardless of variables such as the amount and detailing of transverse reinforcement, or the applied loading bearing area. The cracking pattern at the maximum applied load for each of six tests is shown in Figure 4-14. The applied load listed in the inset of each photo is the maximum applied load. Maximum shear crack widths were recorded for each of the tests and are discussed in section 4.3.2.2. The progression of cracking for each of the six tests was very similar. The progression of surface cracks for Test #1, which was typical of each of the other five serviceability tests, is presented in Figure 4-15.

Test #1* $\sum \frac{A_{si}}{bs_i} \sin \alpha_i = 0.0043$



Test #2 $\sum \frac{A_{si}}{bs_i} \sin \alpha_i = 0.0091$



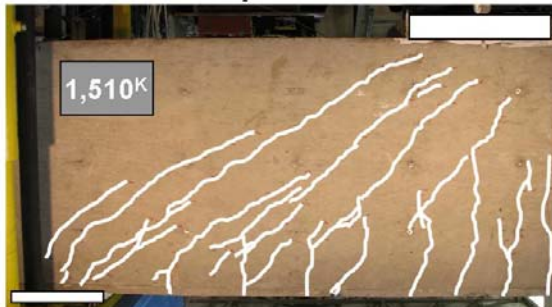
Test #3 $\sum \frac{A_{si}}{bs_i} \sin \alpha_i = 0.0043$



Test #5 $\sum \frac{A_{si}}{bs_i} \sin \alpha_i = 0.0068$



Test #8* $\sum \frac{A_{si}}{bs_i} \sin \alpha_i = 0.0031$



Test #9* $\sum \frac{A_{si}}{bs_i} \sin \alpha_i = 0.0043$



*Test resulted in shear failure

Figure 4-14: Comparison of cracking patterns at maximum applied load

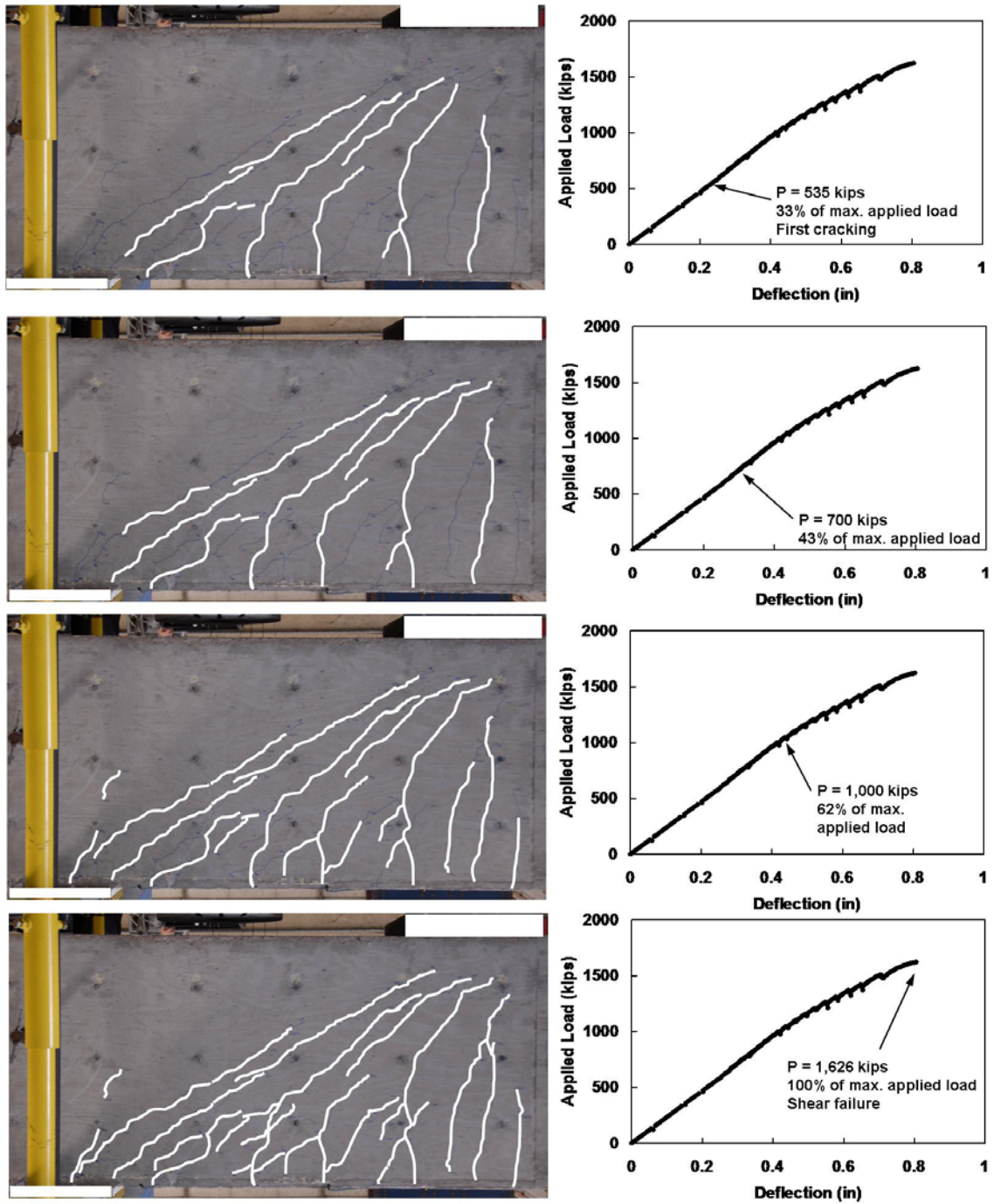


Figure 4-15: Typical progression of cracking

4.3.2.1.1 Diagonal Cracking Load

The most important aspect of serviceability performance in deep beams is arguably the diagonal cracking load. Unlike small flexural cracks in sectional members, which are considered acceptable and necessary for proper structural performance, large shear cracks in deep beams are a sign of poor performance.

The diagonal cracking load was recorded for the first test on each of the three specimens. The second shear span of each specimen underwent cracking as a result of testing on the first side. As a result, the diagonal cracking load could only be measured for the initial test on each specimen, for a total of three tests.

During the early stages of loading, the beam faces were inspected for cracks. When cracking occurred the test was temporarily stopped and the cracks were marked. The first cracks to form in all tests were diagonal shear cracks, rather than flexural cracks. The first cracks were easily spotted and accompanied by a subtle yet noticeable cracking noise.

After each test, strain data on the stirrups was analyzed to verify the load at which first cracking occurred. The point at which the stirrups began to strain in tension is identified as the first cracking load. For example, the strain of a stirrup leg in Test #3 at the time of first cracking is shown in Figure 4-16. From the figure, it appears that first cracking occurred at an applied load of approximately 450 kips; this matches the qualitatively noted first cracking load of 451 kips.

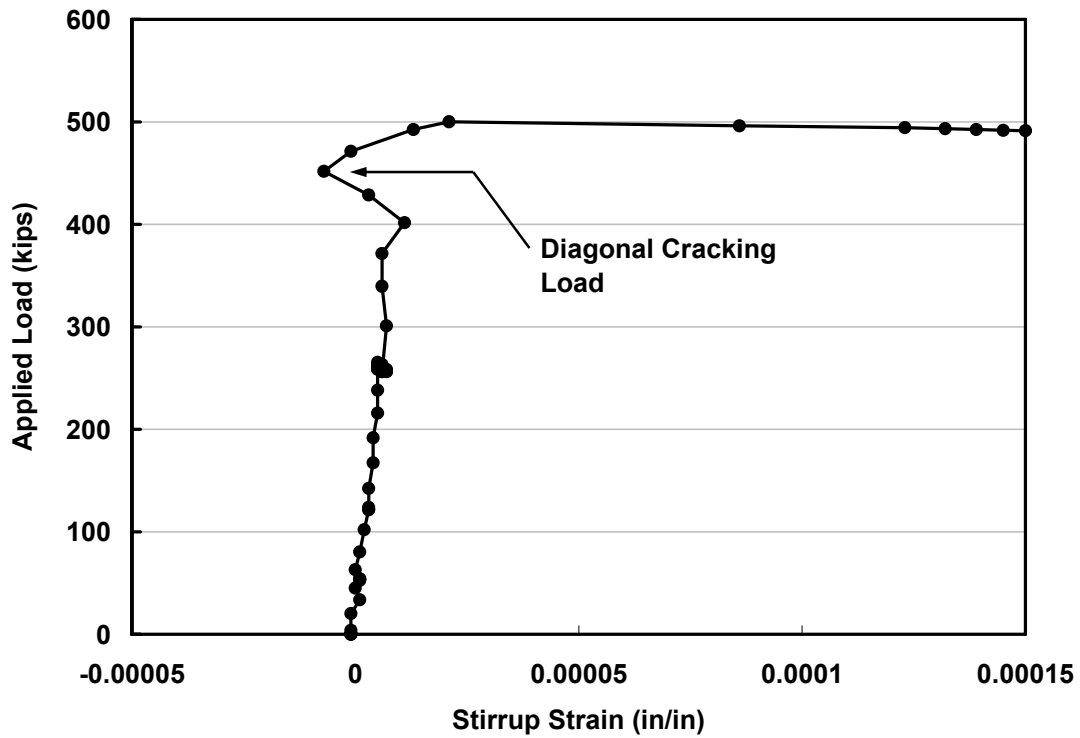


Figure 4-16: Stirrup strain at diagonal cracking load

The diagonal cracking load for the first loading of each specimen is listed in Table 4-8. The ability of a shear span to resist cracking is directly correlated to its ability to restrain dispersion (tensile) forces in the bottle-shaped strut. As a result, the diagonal cracking loads are normalized in terms of $\sqrt{f'_c}$.

Table 4-8: Diagonal cracking loads

Test #	Shear Span Tested	f'_c (psi)	$\sum \frac{A_{s_i}}{b s_i} \sin \alpha_i$	Applied Load Bearing Size*	First Diagonal Cracking Applied Load (kips)	Percentage of Maximum Applied Load (kips)	Shear Force at Diagonal Cracking Load, V_{crack} (kips)	$\frac{V_{CRACK}}{\sqrt{f'_c} b_w d}$
1	1A	4100	0.0043	24" x 36"	535	32.9*	357	3.9
3	2A	4900	0.0043	24" x 36"	451	28.7	297	2.9
8	3A	2800	0.0031	24" x 36"	317	21.0*	202	2.7

*Test resulted in shear failure

Transverse reinforcement did not have a significant effect on the diagonal cracking load. Stirrups did not engage until the point of first cracking; thus, it is expected that first cracking load would be a function of concrete strength only. This observation is consistent with past research that has shown that the amount of transverse reinforcement in a deep beam does not have a significant effect on the first diagonal cracking load (DePaiva and Siess, 1965; Smith Vantsiotis, 1982; Tan et al., 1997; Shin et al., 1999; Oh and Shin, 2001; Brown et al., 2006).

Each specimen's first cracking load is compared to the STM capacity in section 4.3.3.4.

4.3.2.1.2 Formation of parallel shear cracks

Past research has shown that the formation of parallel shear cracks in deep beams can be a strong indicator of impending failure (see section 2.5.14.2). Kong, Robins, and Cole (1970) noted that parallel diagonal shear cracks opened up anywhere from 70 to 90% of the ultimate load, and were a strong indicator of impending failure. Similarly Brown et al. (2006) noted that parallel shear cracks opened up at 65 to 80% of the ultimate load. The conclusions of each study were based test specimens much smaller in scale than those the current experimental program. The effect of parallel cracks on smaller specimens is likely more transparent given the relatively small quantity of diagonal cracks that formed during the duration of a test.

The progression of the parallel diagonal cracks was a strong indicator of imminent failure in the current test program. The diagonal shear cracks typically opened up at mid-depth of the section and propagated toward both the load and reaction points. It was found that the propagation of parallel shear cracks into the area adjacent to reaction point (that is, the CCT node) was nearly always an indication impending failure.

The applied load at which parallel shear cracks propagated into the region adjacent to the reaction bearing plate, and the corresponding percentage of maximum applied load, are shown in Table 4-9. The parallel diagonal cracks that propagated into the CCT node are highlighted for each of the six tests in Figure 4-17.

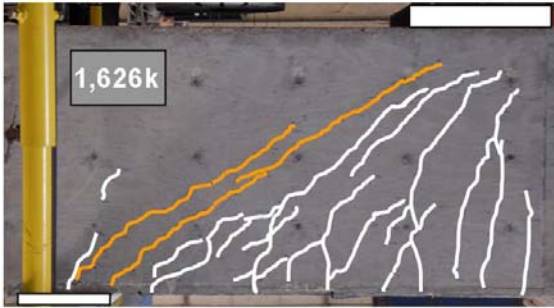
Table 4-9: Propagation of parallel shear diagonal cracks into CCT node

Test Number	Applied Load at Propagation of Parallel Shear Cracks (kips)	Percentage of Maximum Applied Load (kips)
1	1,000	62%*
2	1,301	68%
3	1,098	70%
5	932	57%
8	510	34%*
9	1,096	87%*

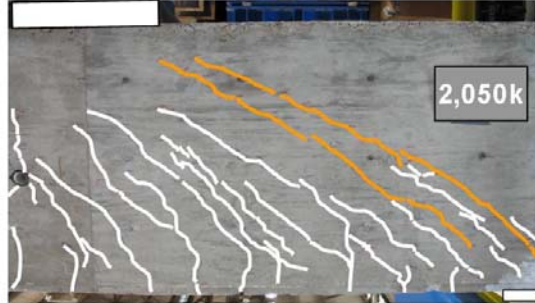
*Test resulted in shear failure

For every test but Test #8, the propagation of parallel cracks into the CCT node occurred between 57 and 87% of the maximum applied load.

Test #1:



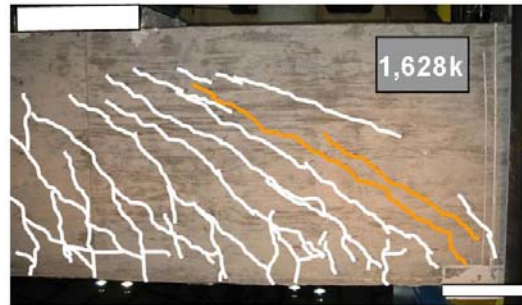
Test #2:



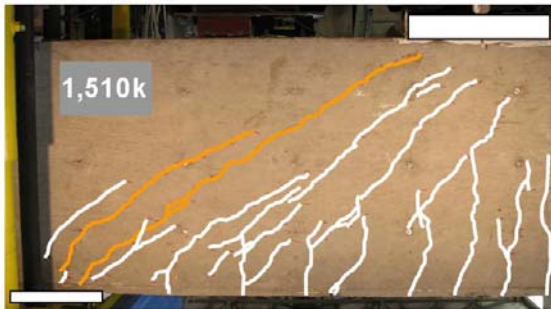
Test #3:



Test #5:



Test #8:



Test #9:

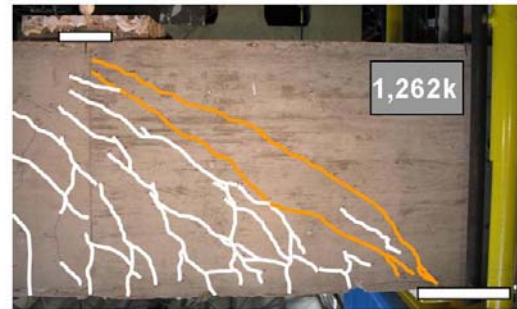


Figure 4-17: Location of parallel diagonal cracks

4.3.2.2 Crack Widths and Reinforcing Bar Strains

The shear span in each of the nine tests was loaded in 100 kip increments (with the exception of Test #1, which was loaded in 50 kip increments). At the conclusion of each loading increment, the test was stopped, cracks were marked on the specimen, and crack widths were measured with a crack comparator. As a matter of safety, crack widths were not measured near the maximum applied load.

The effects of each of the three test variables on crack widths and reinforcement strains are analyzed in this section.

4.3.2.2.1 Transverse Reinforcement Ratio

The transverse reinforcement ratio was found to have an effect on the width of shear cracks in the specimens. Figure 4-18 demonstrates the effect of transverse reinforcement on diagonal crack widths for the three tests on shear spans that both contained 4-legged stirrups and were loaded with a 24"x36" applied load bearing plate. The plot relates the applied load, normalized as percent of maximum applied load, to the maximum diagonal crack width. The percent of maximum applied load is used as the dependent variable in lieu of applied load in order to normalize the data for concrete strength. Due to the finite interval of crack widths on a crack comparator, the plots form "stair-step" lines. A linear trend line was used as a best-fit line for the data set.

It is clear from Figure 4-18 that the amount of transverse reinforcement had an effect on the maximum diagonal crack width. For a given percent of maximum applied load, a greater transverse reinforcement ratio resulted in narrower shear crack widths. However, the amount of transverse reinforcement did not have an effect on the rate at which crack widths grew—the slopes of lines for the three cases are approximately equal. Stated another way, the amount of transverse reinforcement affected the width of the shear cracks initially, but not the rate at which the cracks grew after that point.

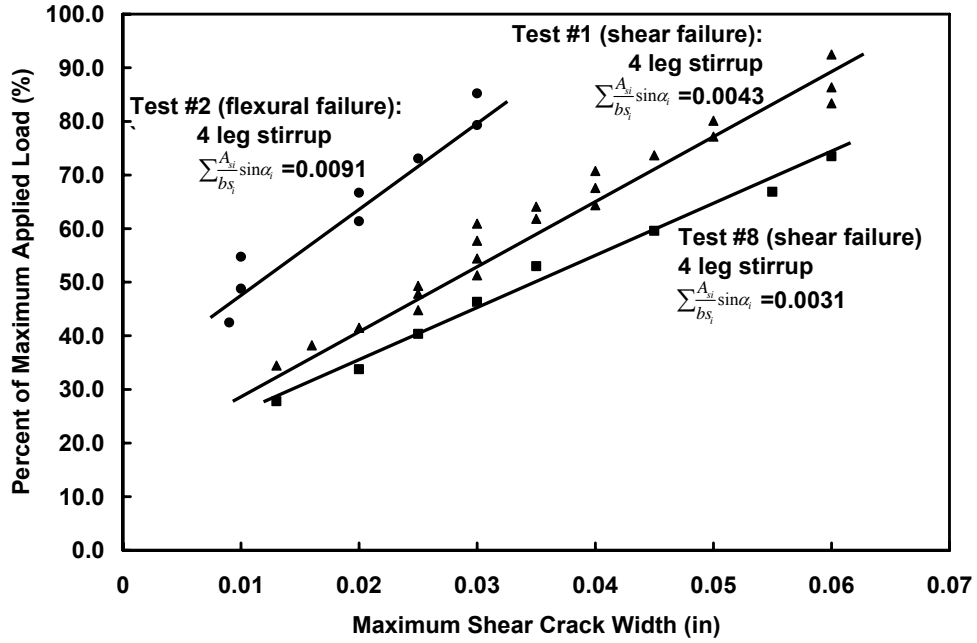


Figure 4-18: Percent of maximum applied load vs. maximum shear crack width

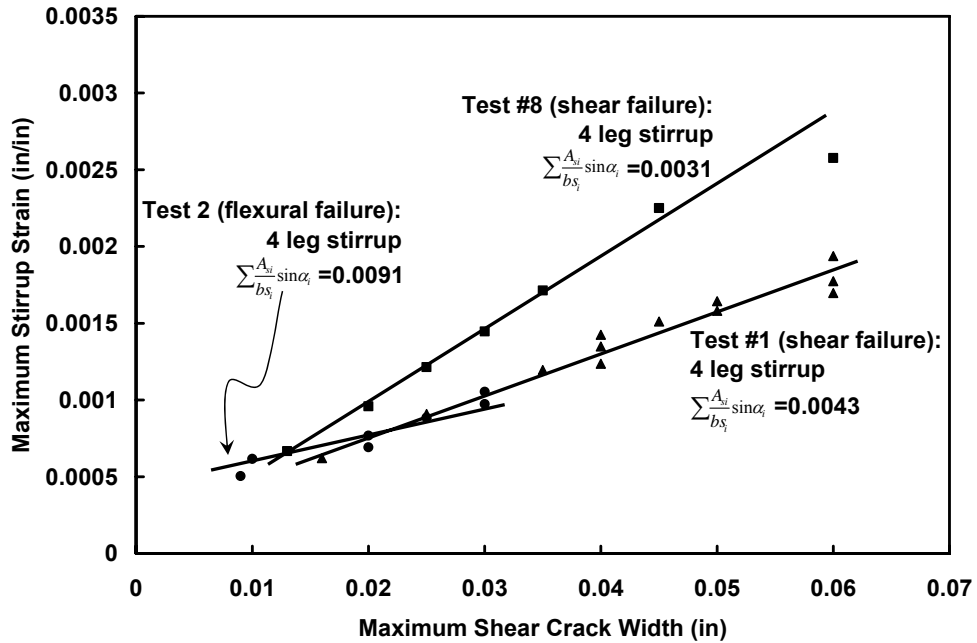


Figure 4-19: Maximum stirrup strain vs. maximum shear crack width

Figure 4-19 shows the maximum stirrup strain as a function of the maximum shear crack widths. The maximum stirrup strain is defined as the maximum strain on any stirrup in the shear span, averaged across all four stirrup legs in that stirrup. The rate at which stirrup strains grow relative to shear cracks widths is inversely proportional to the amount of transverse reinforcement (Figure 4-19). This trend is logical, given that transverse reinforcement strains should grow at a lesser rate when more transverse reinforcement is present. At the first diagonal cracking load, the stirrup strain in each of the specimens is nearly equal.

Similar maximum shear crack width trends were found in tests conducted on shear spans containing 2-legged stirrups. Figure 4-20 shows the effect of transverse reinforcement on diagonal crack widths for the two shear spans that contained 2-legged stirrups and were loaded with a 24"x36" applied load bearing plate (Test #3 and Test #5). The trend in Figure 4-20 is similar to that of Figure 4-18; the crack widths are inversely proportional to the amount of transverse reinforcement in a given shear span. However, there is a slight variation in the rate at which the crack widths grow. Overall, the trends are nearly identical that to those observed in the 4-legged stirrup tests.

It is clear that a greater amount of transverse reinforcement in a given shear span corresponds to smaller shear crack widths throughout the duration of loading. However, the disparity between crack widths in the different shear spans is the smallest at loads corresponding to service loads, shortly after the formation of diagonal cracks. This trend is seen in both Figure 4-18 and Figure 4-20.

Most notably, shortly after the formation of diagonal cracks there is a negligible difference in diagonal crack widths between shear spans that contained minimum transverse reinforcement as per the AASHTO LRFD and ACI 318 (Test #1 and Test #8, respectively) specifications, as shown in Figure 4-18. AASHTO LRFD minimum transverse reinforcement requirements result in the use of 41% additional reinforcement in comparison to ACI 318-05 specifications. The benefit of providing 41% additional reinforcement is marginal, particularly at service loads. Therefore, from a standpoint of

limiting crack widths at service loads, the minimum transverse reinforcement provision of ACI 318 would appear to be sufficient.

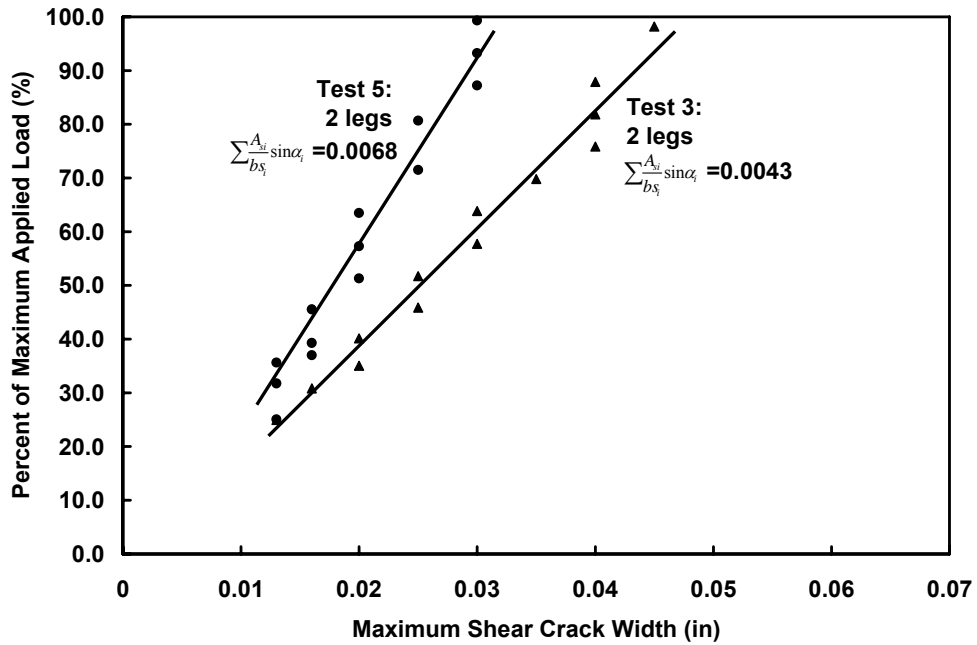


Figure 4-20: Percent of maximum applied load vs. maximum shear crack width

4.3.2.2.2 Quantity of Stirrup Legs

The quantity of stirrups legs had some effect on the maximum shear crack widths of the specimens. Figure 4-21 shows the effect of the quantity of stirrup legs on diagonal crack widths for two tests in which the only variable was the quantity of stirrup legs (Test #1 and Test #3). The plot demonstrates that the rate at which shear cracks grow is lesser for the test with 2-legged stirrups than for the test with 4-legged stirrups. It is also important to observe that immediately after the formation of diagonal cracks, the maximum shear crack width in the shear span containing 2-legged stirrups is comparable to that of the shear span containing 4-legged stirrups. However, at loads near ultimate capacity the shear span containing 2-legged stirrups had narrower shear crack widths than the shear span containing 4-legged stirrups.

Given that the amount of transverse reinforcement in the two shear spans was identical, the shear spans with 2-legged stirrups had more reinforcement near the side faces of the cross-section. Therefore, the 2-legged stirrups were more effective at restraining shear crack widths observed on the side faces. The same trend may not be true for interior crack widths, given that the 2-legged specimens had no stirrup legs in the interior of the beam. However, given that the use of 2-legged stirrups had no discernable negative effects on the maximum shear carried within the shear span, and the widths of the exterior shear cracks were narrower in the specimens with 2-legged stirrups, the widths of the shear cracks in the middle of the section are not a concern.

Past research demonstrated limited variation in crack widths throughout the cross-section of a wide specimen with only 2 stirrup legs (Hsiung, Wayne, and Frantz, 1985). The effect of the quantity of stirrup legs on interior crack widths for current project specimens was not investigated; given the adequate performance of specimens with 2-legged stirrups from a strength perspective and superior performance from a serviceability perspective, consideration of interior crack widths is arguably unnecessary.

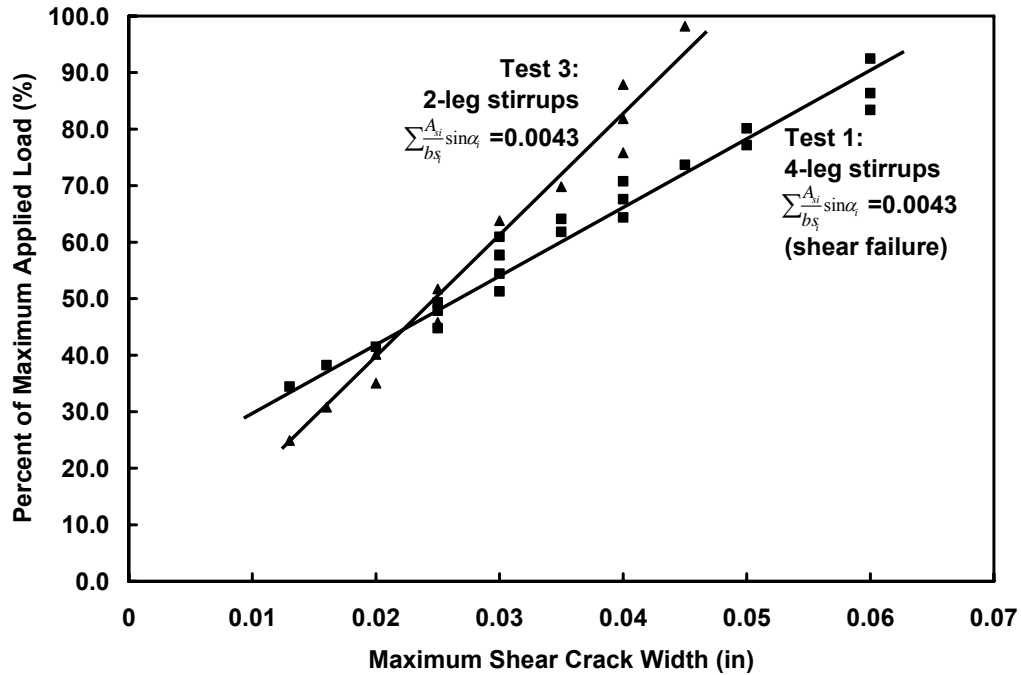


Figure 4-21: Percent of ultimate capacity vs. maximum shear crack width

Hsiung et. al (1985) also noted that specimens with multiple stirrup legs exhibited greater strains in interior stirrups legs than exterior stirrup legs. A similar trend was not evident for specimens in the current experimental program. The difference in strains between interior and exterior stirrup legs varied between shear spans, and between stirrups within a given shear span, with no discernable trend. Figure 4-22 shows the stirrup leg strain for both an interior and exterior stirrup leg, at 50% of the maximum applied load, for each test on a shear span containing 4-legged stirrups. In each case, the stirrup under maximum strain in the given shear span is shown.

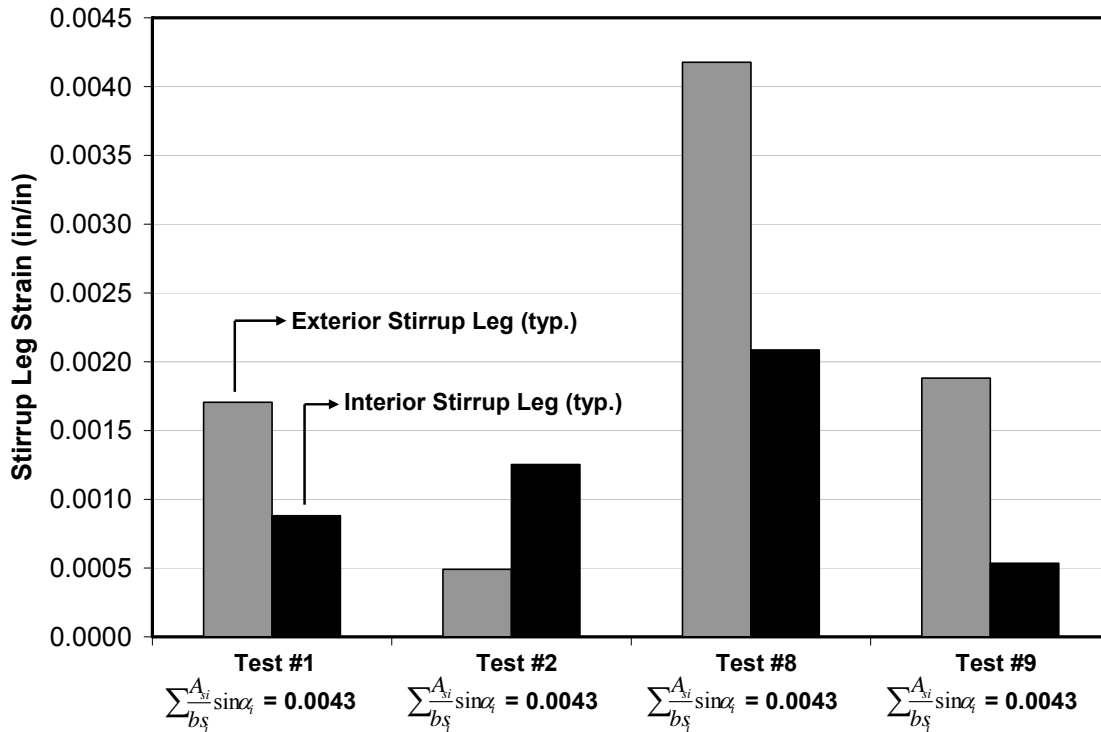


Figure 4-22: Stirrup leg strains at 50% of the maximum applied load

Despite the differences in strains between interior and exterior stirrup legs noted by Hsiung et al. (1985), the researchers found that the quantity of stirrup legs was not related to ultimate shear capacity. In contrast, Anderson and Ramirez (1989) recommended the use of multiple stirrup legs for wide beams. This recommendation was made after finding that specimens with two stirrup legs had diminished ultimate capacities compared to specimens with more than two stirrup legs. However, the maximum difference in ultimate strength between specimens with two legs and specimens with multiple legs that failed in shear was less than 10%, when capacities are normalized relative to concrete strength. Considering the general scatter in shear data (Reineck et al., 2003, Brown and Bayrak, 2006), such a small difference is arguably insignificant.

In addition, Anderson and Ramirez reported that the quantity of stirrup legs had an effect on longitudinal reinforcement strains (See section 2.5.7). The researchers found that increasing the number of stirrup legs decreased stress concentrations near stirrup corners; longitudinal reinforcement placed at the corners of stirrups had a higher magnitude of strain for specimens with fewer stirrup legs.

While the same trend was observed for some of the test specimens in the current experimental program, in other specimens such a trend did not exist. Figure 4-24 through Figure 4-27 shows the results of tests in which longitudinal reinforcement strains were measured for both corner and interior bars at the location illustrated in Figure 4-23. The tests conducted on specimens with 4-legged stirrups, shown in Figure 4-24 and Figure 4-25, demonstrated increased strain of corner longitudinal reinforcement. However, longitudinal reinforcement strains in the specimens that contained 2-legged stirrups did not vary between bars in a given layer, as shown in Figure 4-26 and Figure 4-27. These plots demonstrate that the use of 2-legged stirrups in the specimens did not have an adverse affect on the strains of longitudinal reinforcing bars placed at stirrup corners.

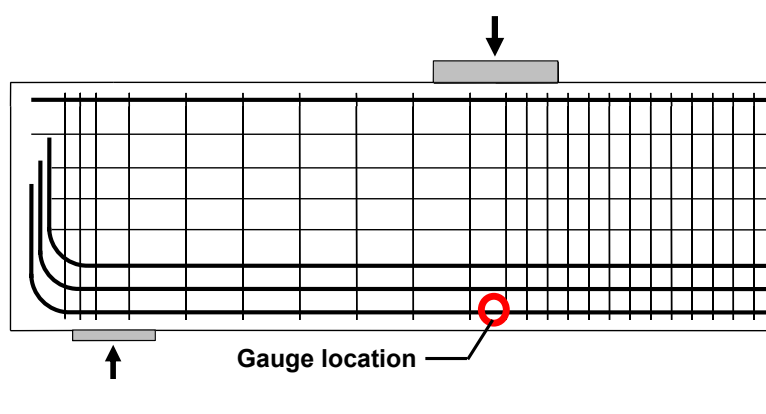


Figure 4-23: Longitudinal reinforcement gauge location

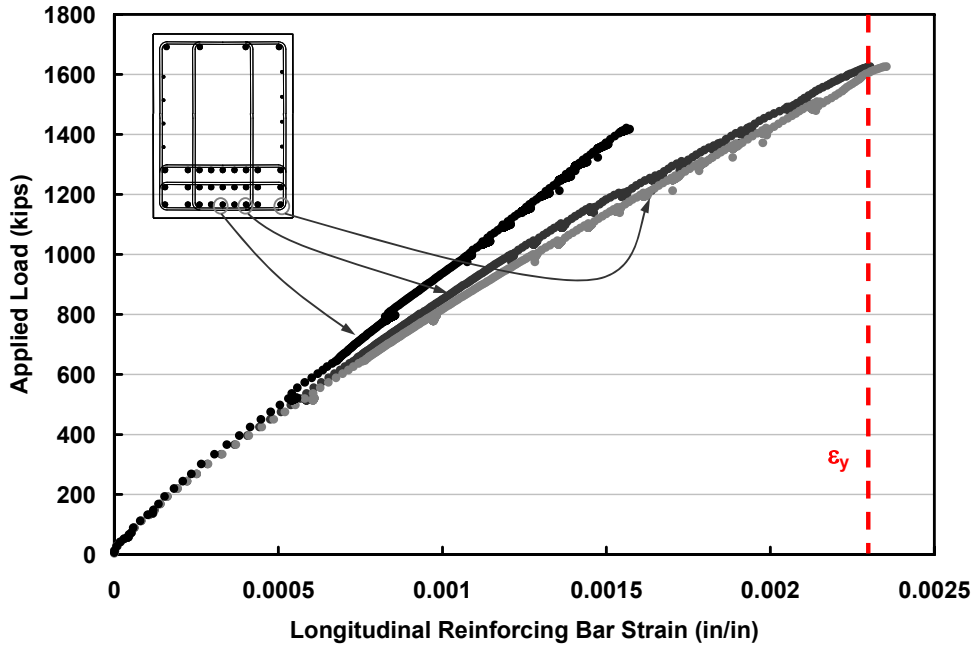


Figure 4-24: Test #1 longitudinal reinforcement strains

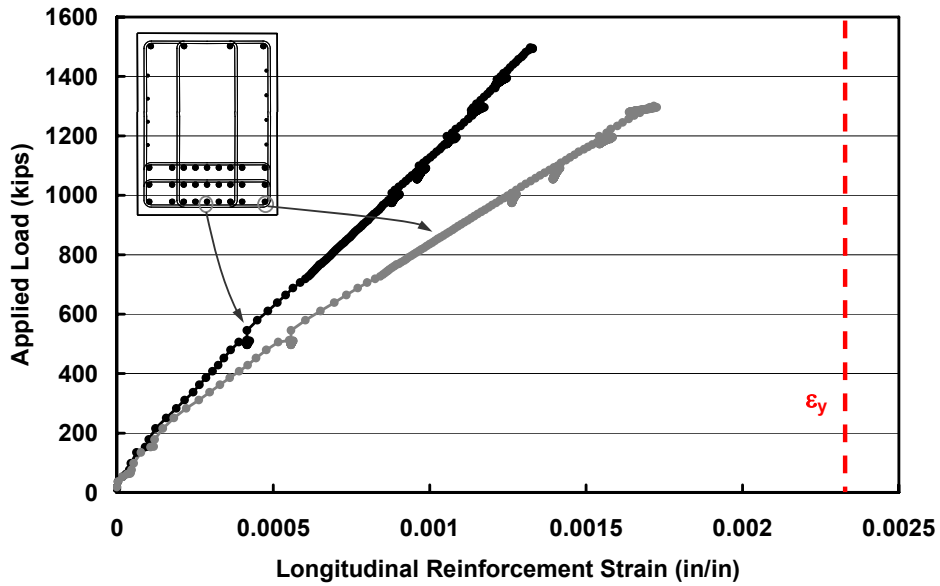


Figure 4-25: Test #2 longitudinal reinforcement strains

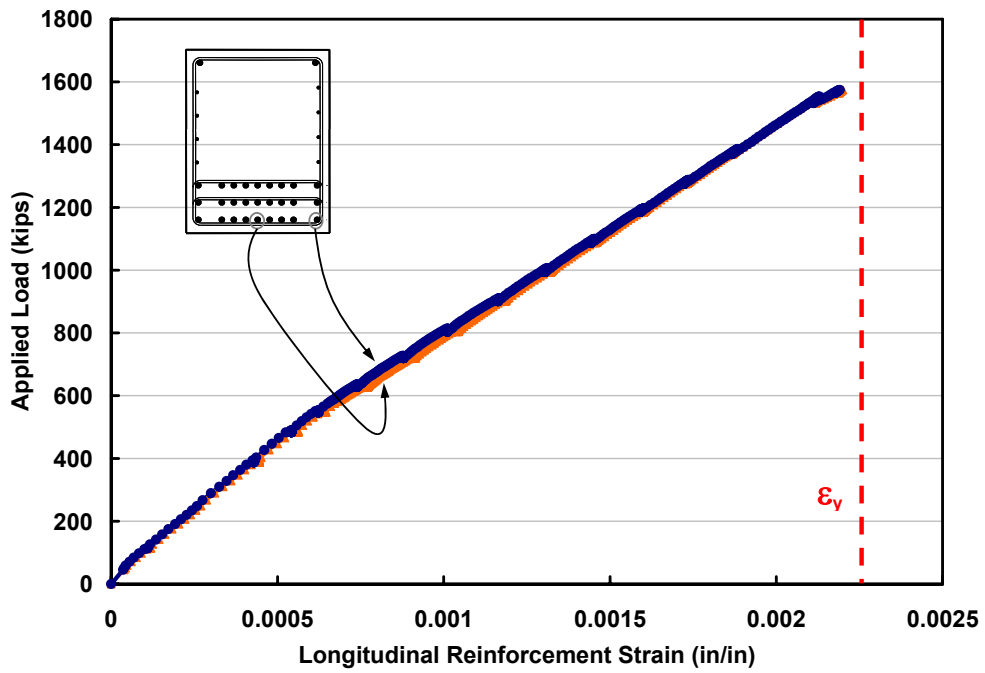


Figure 4-26: Test #3 longitudinal reinforcement strains

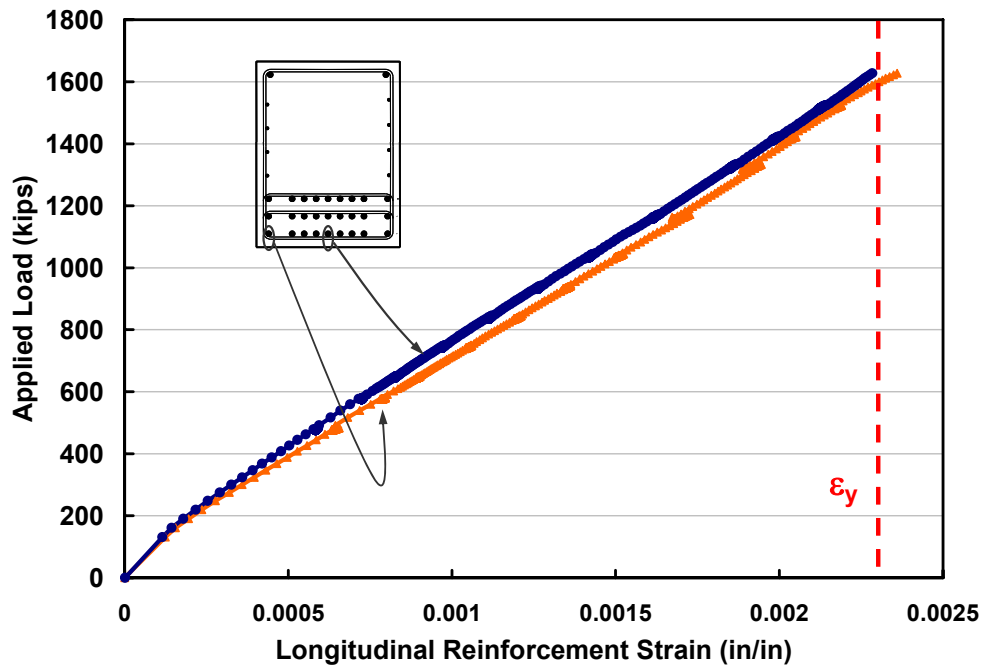


Figure 4-27: Test #5 longitudinal reinforcement strains

It was demonstrated in section 4.3.1.2.2 that the AASHTO LRFD limited strut width provision, and associated use of multiple stirrup legs within a cross-section, was not supported by experimental ultimate strength data. The analysis of the crack widths and strains measured in longitudinal and transverse reinforcement, presented in this section, supports the same conclusion from the aspect of serviceability performance. In fact, specimens with 2-legged stirrups demonstrated improved performance at limiting diagonal crack widths as compared to specimens with 4-legged stirrups.

4.3.2.2.3 Bearing Area

The bearing area did not have a significant effect on the maximum shear crack widths. Figure 4-28 shows the relationship between the percent of maximum applied load and the shear crack width for two tests in which the only variable was the bearing plate size. Relative to Test #1, the shear crack widths for Test #9 are smaller at low applied loads, larger at about 65% of the maximum applied load, and approximately equal near the maximum applied load. Overall, there is not a significant difference between the crack widths for two tests, although at any given point the two may vary slightly.

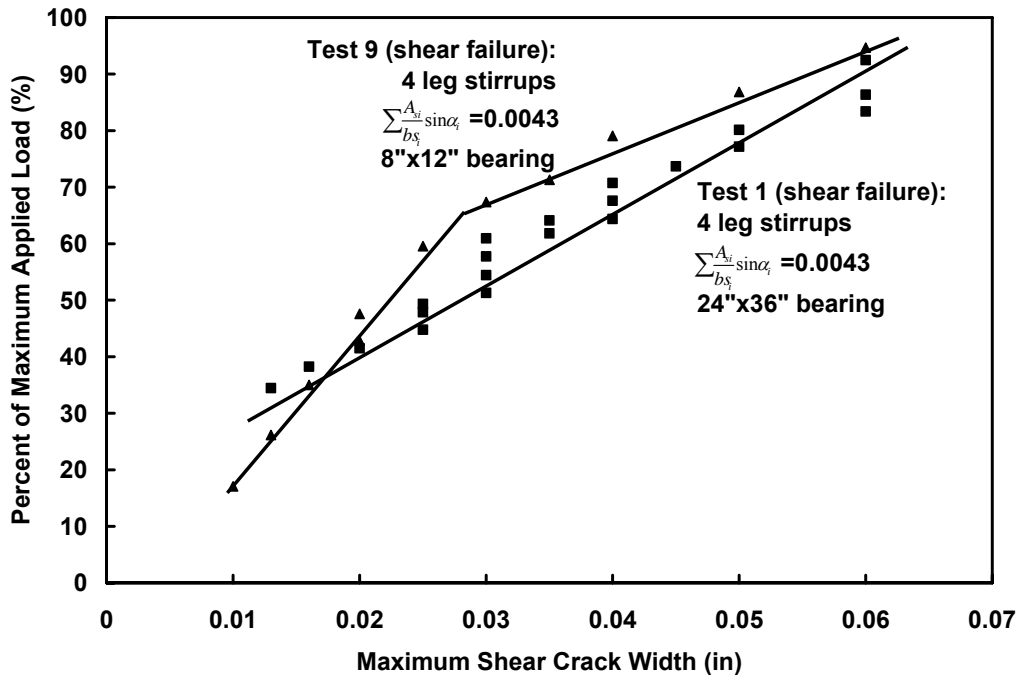


Figure 4-28: Percent of ultimate capacity vs. maximum shear crack width

4.3.2.2.4 Anchorage Zone Longitudinal Rebar Strains

As outlined in section 3.7.3.1, strain gauges were placed along various locations of a corner longitudinal bar in shear span 1A (Test #1) in order to monitor strains near the anchorage zone adjacent to the reaction point. The location of the strain gauges and the strains at the shear failure load in Test #1 are given in Figure 4-29. The plot demonstrates that the longitudinal rebar strain decreases linearly along the location of the reaction bearing plate. This region corresponds to the CCT node when the shear span is designed using strut-and-tie modeling. The longitudinal rebar strain is negligible near the left face of the reaction bearing plate. It should be noted there was no cracking observed in the anchorage zone in any of the tests, indicating adequate development of the longitudinal bars.

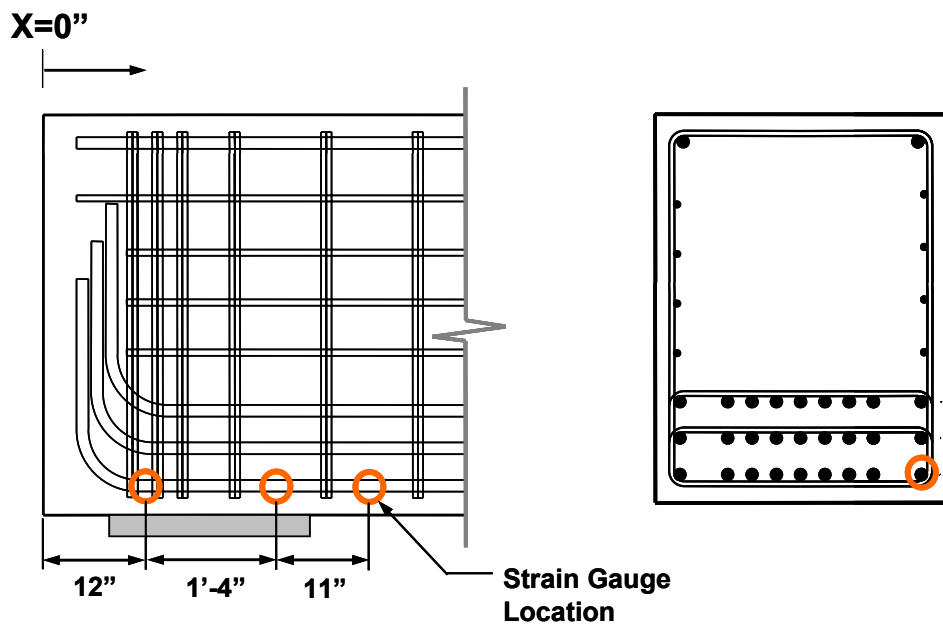
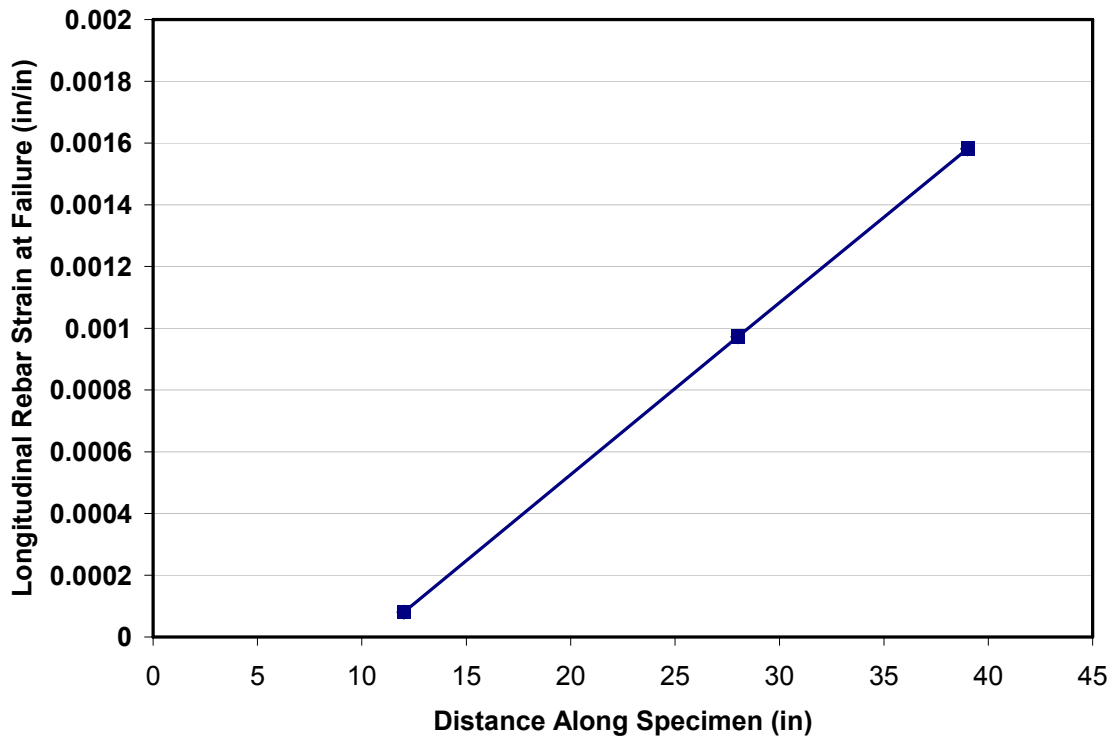


Figure 4-29: Longitudinal rebar strain profile near reaction point

4.3.3 Capacity Estimated by Strut-and-Tie Models

A complete STM analysis of each test would include a strut-and-tie model of the entire specimen. It is convenient to consider each span individually by breaking up the applied load into two loads, each equal to the reaction force at each end of the beam, as shown in Figure 4-30 (Wight and Parra-Montesinos, 2003). The strength of the longer span is dictated by sectional behavior and does not govern the strength of the specimen; therefore, only the short span is considered here.

The conservatism of strut-and-tie modeling (STM) was evident for the specimens in the current experimental program. The measured load was greater than the strength as estimated by STM for each of the nine tests. It should be noted that load factors and resistance factors were neglected in estimating the capacity of a test specimen through the use of STM. Thus the STM capacity reported in the following sections is the unfactored STM capacity.

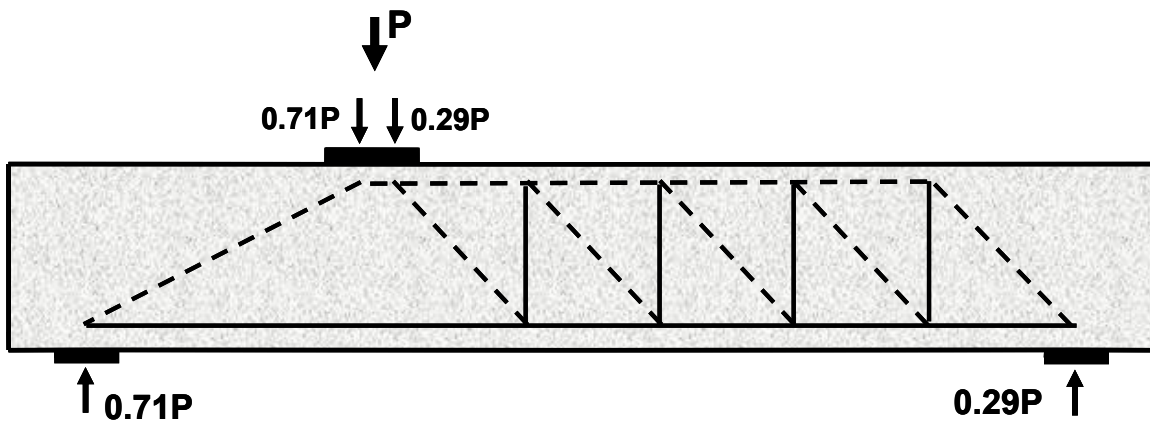


Figure 4-30: Strut-and-tie model of a test specimen

4.3.3.1 One-panel Model

The short shear span of each test can be modeled using a one-panel strut-and-tie model. Other researchers have concluded the behavior of a deep beam loaded with a

single point load is best described by a single strut between the load point and reaction point (Leonhardt & Walther 1966, Brown et al. 2006), provided that the distance between the load and the support is less than or equal to $2d$. A one-panel strut-and-tie model of the shear span in two tests (Test #8 and Test #9) is shown in Figure 4-31.

The geometry of the strut-and-tie elements is governed by the size of the bearing plates and the placement of reinforcement. Non-hydrostatic nodes are utilized in the strut-and-tie models. Hydrostatic nodes for a one-panel model with an a/d ratio near 2.0 are impractical (Figure 2-4). The top dimension of the node at the applied load was assumed to be equal to 71% of the dimension of the bearing plate in the direction of the span. In the case of Test #1 the dimension is 17", corresponding to approximately 71% of the 24" bearing plate dimension (Figure 4-31a)

As suggested in Brown et al. (2006), the depth of this node was assumed to be approximately equal to the depth of the flexural compression block obtained using plane section analysis of the section. The depth of the compression block depends on concrete strength, and therefore varies slightly between specimens. For simplicity of comparisons between the strut-and-tie model of each test, this dimension was assumed to be 16" in all one-panel models. The width (transverse dimension) of the node adjacent to the applied load, and the corresponding strut width at the interface with that node, are simply equal to the transverse bearing plate dimension (for example, 12" in Figure 4-31d).

Bearing plates with widths less than the 36" width of the specimen were used in Tests #6, and #9. Bearing stresses with narrow bearing areas increase due the confining effect of the surrounding concrete, as indicated in ACI section 10.17 and AASHTO section 5.7.5. However, in the interest of keeping the models simple and easily comparable, the benefit of confinement was neglected. The node geometry at the point of the reaction bearing plate was identical for the strut-and-tie model of each of the nine tests.

Detailed calculations for the strut-and-tie model of Test #1, using ACI 318-05, AASHTO LRFD design specifications and TxDOT 4371 modifications are presented in Appendix A.

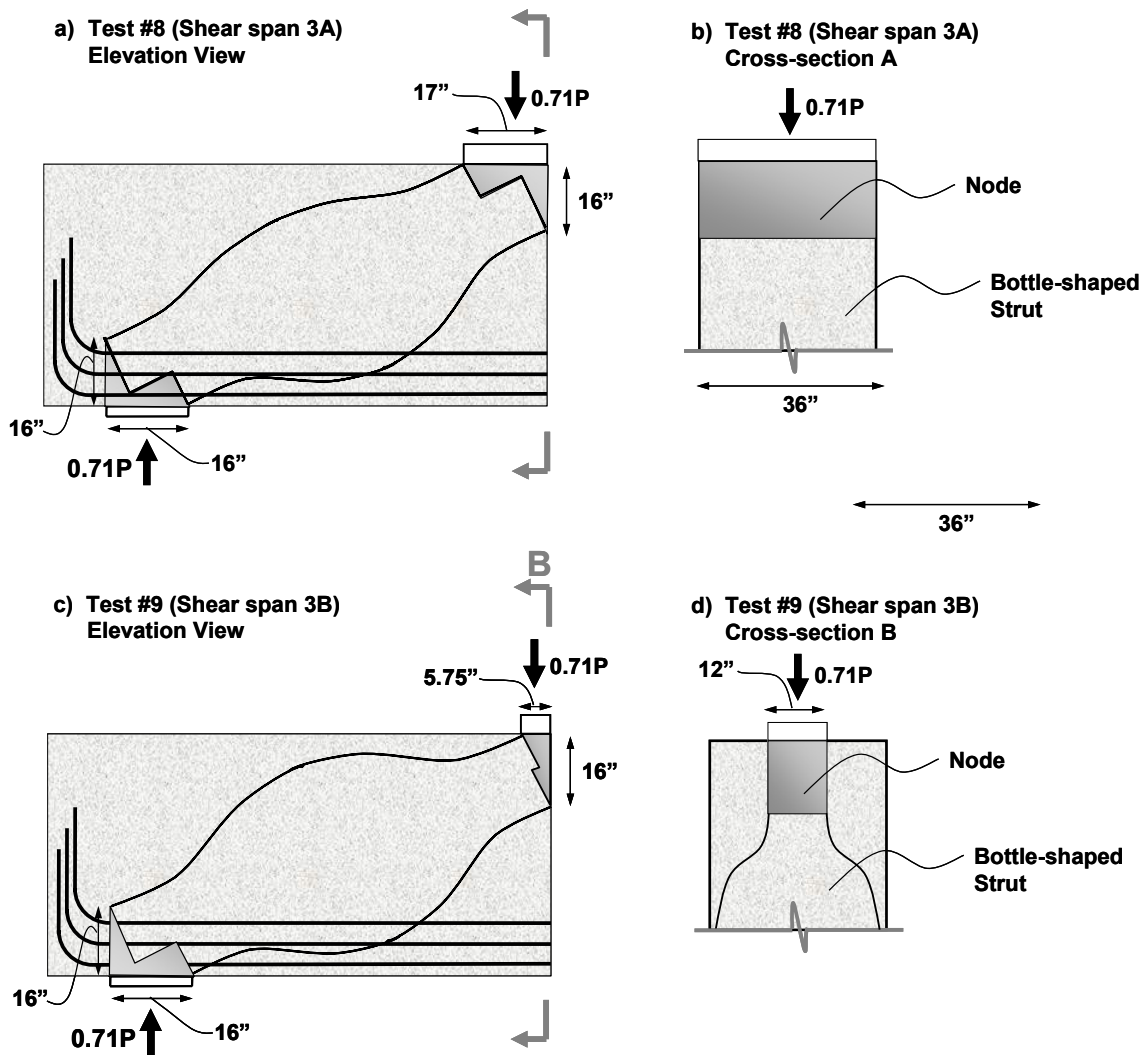


Figure 4-31: Typical strut-and-tie geometry

Figure 4-32 shows a comparison of STM capacities using a one-panel strut-and-tie model and the measured load for each of the nine tests completed. The data on which the Figure 4-32 is based is given in Table 4-10. The governing STM element is also listed.

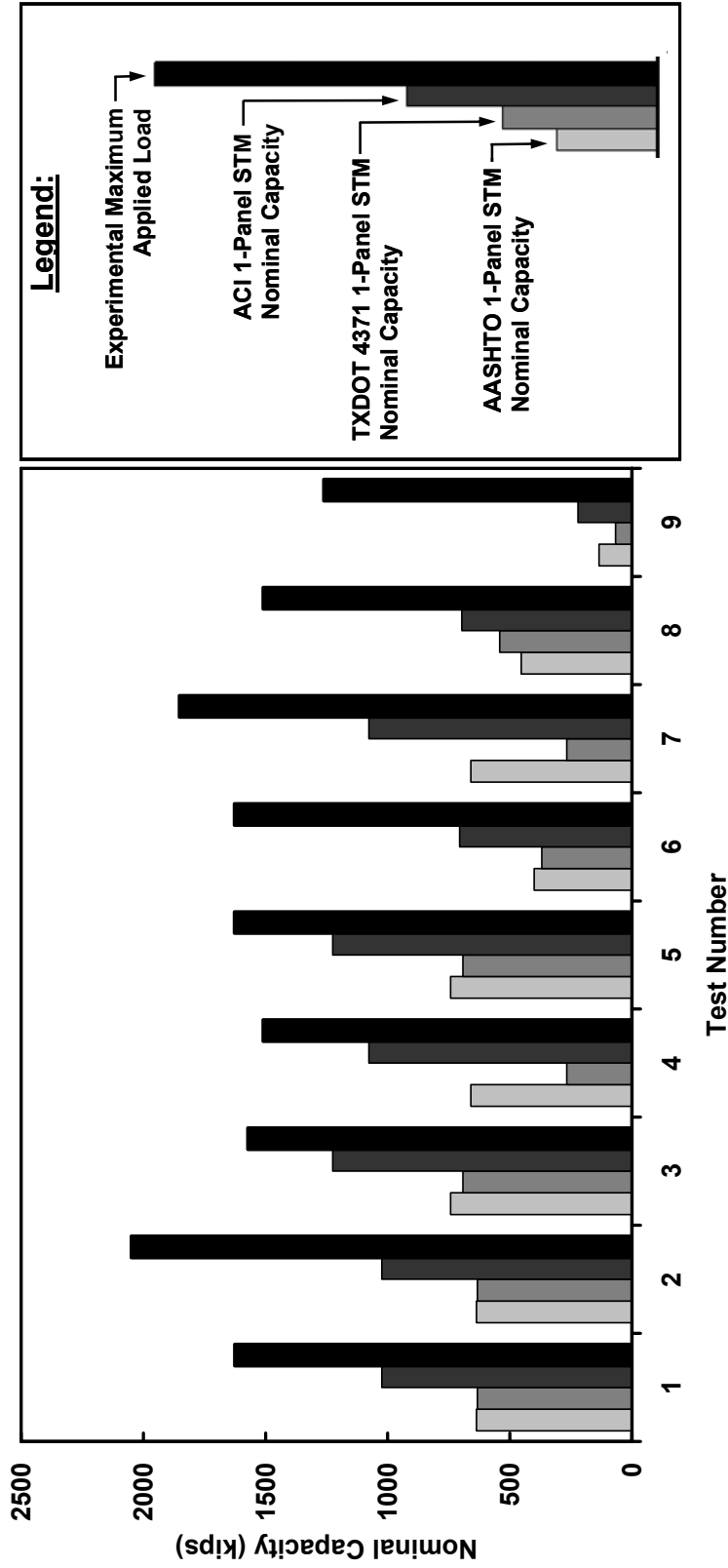


Figure 4-32: STM capacities and maximum applied loads

Table 4-10: STM capacities and maximum applied loads

Test #	Maximum Applied Load, P_{max} (kips)	Shear at Maximum Applied Load, V_{max} (kips)	AASHTO LFRD				TxDOT 4371				ACI 318-05		
			1-Panel Capacity, P_{STM} (kips)	$\frac{P_{MAX}}{P_{STM}}$	Governing Element	1-Panel Capacity, P_{STM} (kips)	$\frac{P_{MAX}}{P_{STM}}$	Governing Element	1-Panel Capacity, P_{STM} (kips)	$\frac{P_{MAX}}{P_{STM}}$	Governing Element		
1	1,626†	1,133	637*	2.6	strut at A	633*	2.6	strut at A	1,024*	1.6	node A		
2	2,050	1,434	637	3.2	strut at A	633	3.2	strut at A	1,024	2.0	node A		
3	1,573	1,095	743	2.1	strut at A	692	2.3	strut at A	1,225	1.3	node A		
4	1,510†	1,050	660	2.3	strut at B	267	5.7	strut at B	1,077	1.4	strut at B		
5	1,628	1,134	743	2.2	strut at A	692	2.4	strut at A	1,225	1.3	node A		
6	1,628	1,134	401	4.1	strut at B	369	4.4	strut at B	706	2.3	strut at B		
7	1,853†	1,294	660	2.8	strut at B	267	6.9	strut at B	1,077	1.7	strut at B		
8	1,510†	1,050	453	3.3	strut at A	541	2.8	strut at A	697	2.2	node A		
9	1,262†	874	135	9.4	strut at B	67	18.7	strut at B	221	5.7	strut at B		

*STM calculations for this test are given in Appendix A

†Test resulted in shear failure

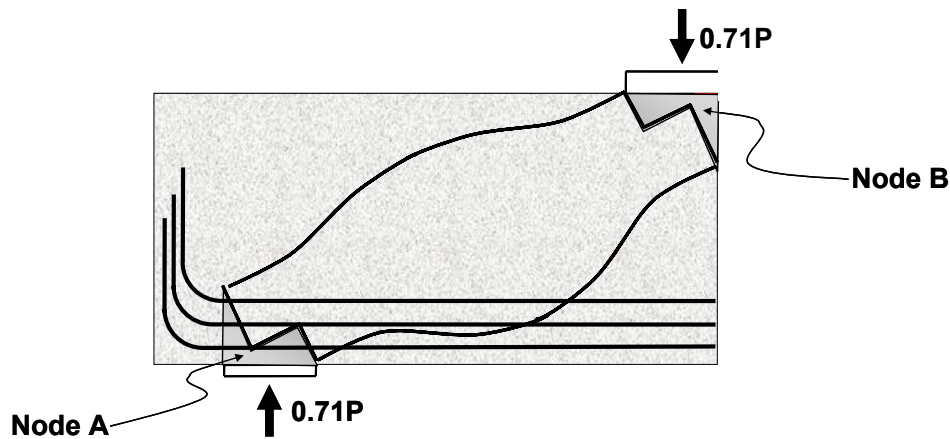


Figure 4-33: STM element naming scheme

It is clear that all three STM design methods provide conservative estimates of strength. Beyond this, several notable trends are evident. First, the use of ACI 318 STM provisions results in the least conservative STM capacities. In addition, the use of TxDOT 4371 STM provisions provides very conservative STM capacities when a bearing plate with small dimension in the direction of the span is utilized. Finally, the tests that utilized the smallest applied load bearing areas (Tests #4, #6, #7, and #9) demonstrate the largest discrepancy between the experimental maximum applied load and the STM capacity.

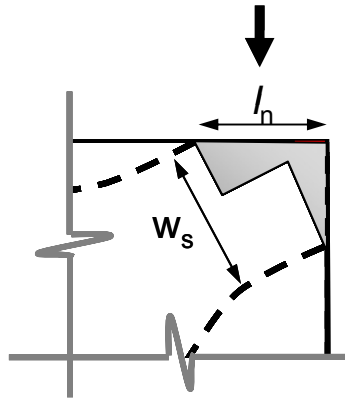
The use of ACI 318-05 Appendix A provisions results in the least conservative STM capacity, because the determination of strut efficiency in ACI is not a function of the angle of the strut or the a/d ratio. All tests in the experimental program were carried out with an a/d ratio of 1.85. Despite the fact that the ACI STM provisions neglect a/d in the determination of strut efficiency, these provisions provided conservative estimates of ultimate strength for all the tests conducted during the course of this research study.

Another notable trend in Figure 4-32 is the discrepancy between STM capacities determined using AASHTO LRFD and TxDOT 4371. In tests that utilized a 24"x36" applied load bearing plate, the capacity using these two STM methods is virtually

identical. However, in tests that utilized a bearing plate that is 8” in the direction of the span (Tests #4, #7, #9), the discrepancy is significant. This difference is due to the TxDOT 4371 strut efficiency equation:

$$\nu = \frac{0.85 \tan \theta}{\sqrt{f'_c}} \frac{l_n}{w_s \sin \theta} \quad \text{Equation 4-3}$$

The strut efficiency is a function of l_n/w_s , where l_n is equal to the dimension of the bearing plate in the direction of the span and w_s is equal to the inclined dimension corresponding to the strut-to-node interface (Figure 4-4). If the depth of the node is assumed to remain constant, a reduction in the size of the bearing area will reduce the l_n term to a greater extent than the w_s term. Thus, in instances where the specimen is loaded with a bearing plate that is 8” in the dimension of the span, the corresponding strut efficiency as per TxDOT 4371 is significantly reduced. In contrast, the AASHTO LRFD strut efficiency is not a function of the bearing area.



Equation 4-4: TxDOT 4371 node nomenclature

The tests that utilized the smallest applied load bearing areas (Tests #4, #6, #7, and #9) demonstrated the largest discrepancy between the experimental maximum

applied load and the STM capacity shown in Table 4-10 and Figure 4-34. The plot shows the ratio of the maximum applied load over the STM capacity as a function of applied load bearing area; it is evident that tests with smaller bearing areas have larger differences between the experimental and modeled capacities.

These differences can be explained by that fact that the bearing strength of loaded areas is increased due to the confinement provided by surrounding areas of concrete. When a loaded concrete surface is surrounded by large volumes of concrete, the bearing strength can significantly be increased. This benefit is illustrated in Figure 4-35, which shows the cross-section of a bearing node in a section loaded with a limited bearing width.

The benefit of confinement for loaded areas is acknowledged and discussed in ACI section 10.17 and AASHTO section 5.7.5. However, ACI and AASHTO do not provide explicit guidance on utilizing these provisions in the context of STM. This benefit was not accounted for in the STM capacities presented above.

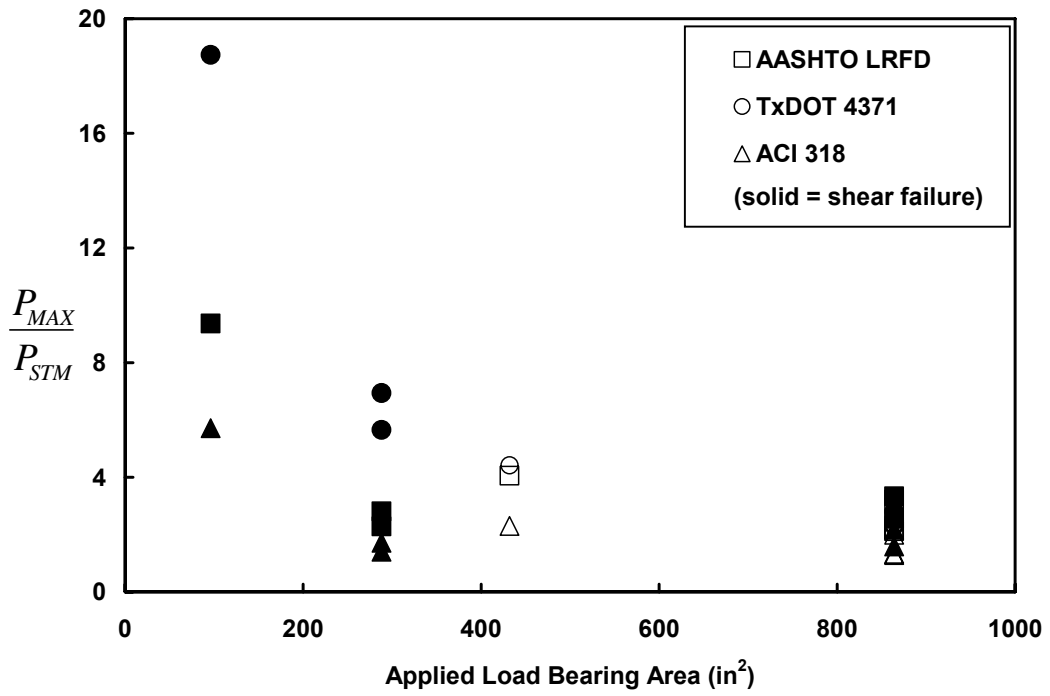


Figure 4-34: $\frac{P_{MAX}}{P_{STM}}$ vs. applied load bearing area

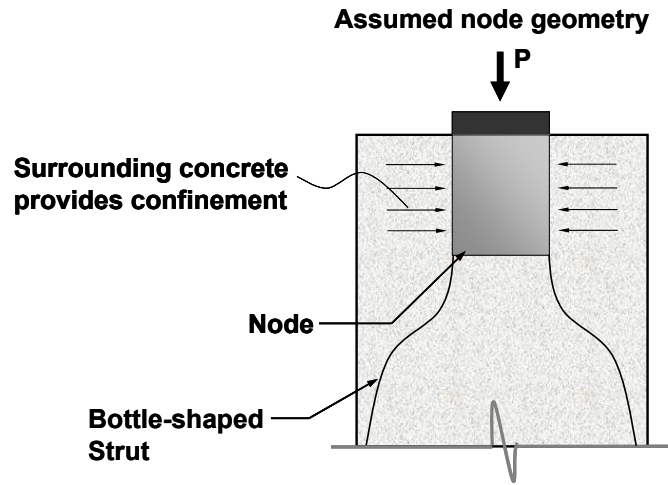


Figure 4-35: Illustration of node confinement

4.3.3.2 Two-panel Model

The short shear span of each specimen can be modeled using a two-panel strut-and-tie model, as shown in Figure 4-36. The use of a two-panel model integrates vertical shear reinforcement, and assumes that stirrups result in a strut-and-tie model similar to that in a B-Region—rather than just serving as crack control reinforcement. A two-panel strut-and-tie model is more difficult to employ than a one-panel strut-and-tie model. The assumptions used in modeling the specimens with a two-panel strut-and-tie model are outlined in the following paragraphs.

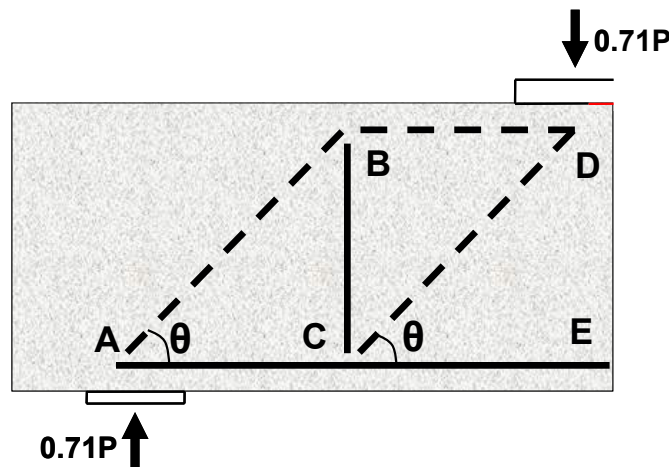


Figure 4-36: Two-panel strut-and-tie model

A primary challenge in modeling a two-panel model is idealizing the vertical tie BC, along with the CCT node at B and the CTT node at C (Figure 4-36). Although the model idealizes tie BC as a single tie at mid-length of the shear span, vertical shear reinforcement is rarely lumped together at one location in a shear span. Instead, stirrups are typically spaced evenly across the shear span. Even so, it is typically assumed that numerous stirrups are engaged as part of tie BC. In AASHTO, the use of a two-panel

model is facilitated by AASHTO 5.6.3, which states that crack control reinforcement may also be utilized as tie reinforcement in a strut-and-tie model. However, ACI 318-05 does not include an equivalent provision.

ACI 318-05 specifies that the minimum angle between a strut and tie is 25 degrees. Therefore it is possible to assume that any stirrup that adjoins to a diagonal strut at an angle of greater than 25 degrees is engaged as part of the vertical tie (Wight and Parra-Montesinos, 2003). This assumption was made for two-panel modeling in the current experimental program, and is illustrated in Figure 4-37, where seven stirrups are considered to be part of Tie BC in shear span 2B.

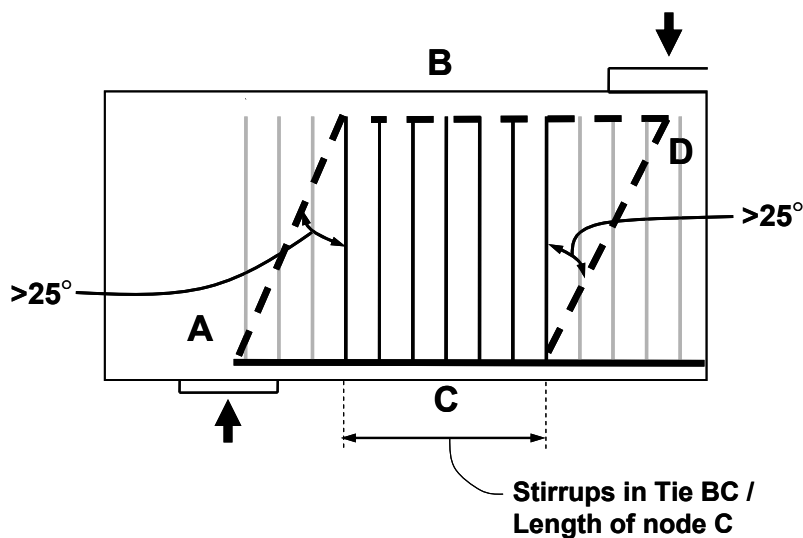


Figure 4-37: Stirrups engaged in tie BC

Unlike the geometry of node A, which is defined by a combination of bearing areas and reinforcement placement, and node D, which is defined by the bearing area and assumed compression block depth, the geometry of nodes B and C are difficult to define. A sketch of the CTT node at C is shown in Figure 4-38. The height of the node, w_{ac} , is defined by the placement of longitudinal reinforcement. However, the horizontal

dimension is ambiguous. It is possible to conservatively assume this dimension is equal to the distance between outermost stirrups included in tie BC (Wight and Parra-Montesinos, 2003).

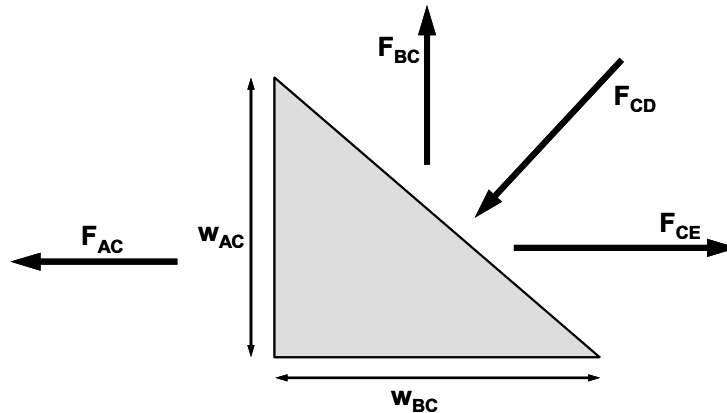


Figure 4-38: Two-panel strut-and-tie model: CTT node

In most cases this horizontal dimension is sufficiently large to prevent the CTT node from governing the strut-and-tie model, despite the low efficiency factor required for CTT nodes. In addition, the CCT node at B (Figure 4-36) typically has similar geometry to node C, but is subject to a higher efficiency factor. Given the ambiguity of the geometry of nodes B and C, it was assumed that these nodes, and the corresponding strut interfaces with these nodes, did not govern the two-panel model. The validity of this assumption is underscored by the fact that deep beams rarely fail at the point of an interior node in experimental tests.

The ambiguity of the CTT node diminishes the significance of the AASHTO limited strut width provision (outlined in section 2.2.1.1.2). The provision applies to struts that are anchored by reinforcement at the point of a node, such as the strut framing into the CTT node (Node C, Figure 4-36), which is anchored by vertical shear reinforcement. As outlined above, the horizontal dimension of the CTT node is ambiguous, but can be assumed sufficiently large to not govern a two-panel model.

Thus, applying a reduction to the strut-to-node interface, as per the AASHTO limited strut width provision, will not cause the strut interface at the CTT to govern the strut-and-tie model. As a result, the AASHTO limited strut width provision was not applied to the struts in the two-panel strut-and-tie model capacities presented in this section.

Consider, for example, the AASHTO limited strut width provision in the context of shear span $2B$, which contained 2-legged stirrups. AASHTO 5.6.3.3.2 limits the width of the strut to 21.8", or 60.6% of the full 36 inch width of the beam, as shown in Figure 4-39. However, the size of the CTT node, and therefore the strut-to-node interface at the node, is ambiguous. Applying an exact reduction to the strut at its interface with a node of ambiguous size is questionable.

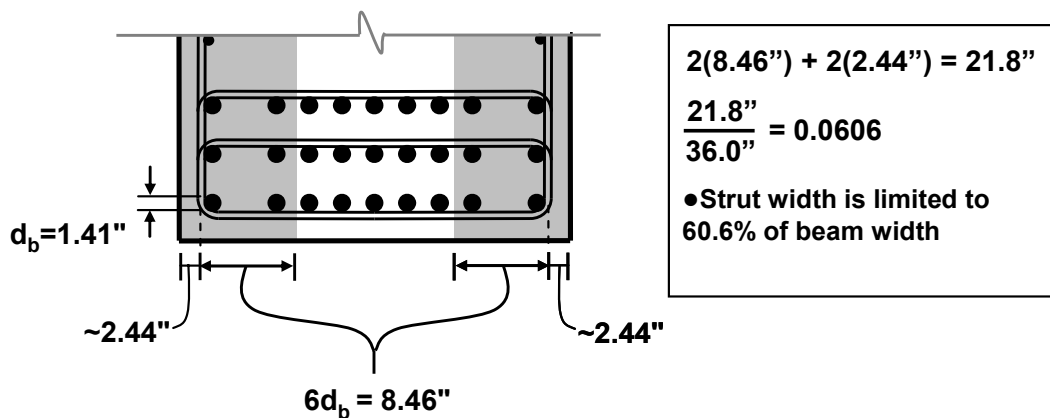


Figure 4-39: Limited strut width for shear span $2B$

The use of the AASHTO limited strut width provision in deep beams is particularly questionable in light of the fact that no such provision exists for sectional shear. A slender member (sectional shear) can be modeled using a strut-and-tie model, as shown in Figure 4-40. The model contains a series of CTT nodes that are subject to the AASHTO limited strut width provision. In this model the anchorage of vertical shear reinforcement is critical to the shear capacity of the member. Despite this fact, the detailing of stirrups in sectional design is not considered to affect the shear capacity of

the member. By the same logic, the detailing of stirrups in a deep beam should not affect the capacity of the member, particularly considering that the shear strength of a deep beam is not strongly correlated to the amount of transverse reinforcement.

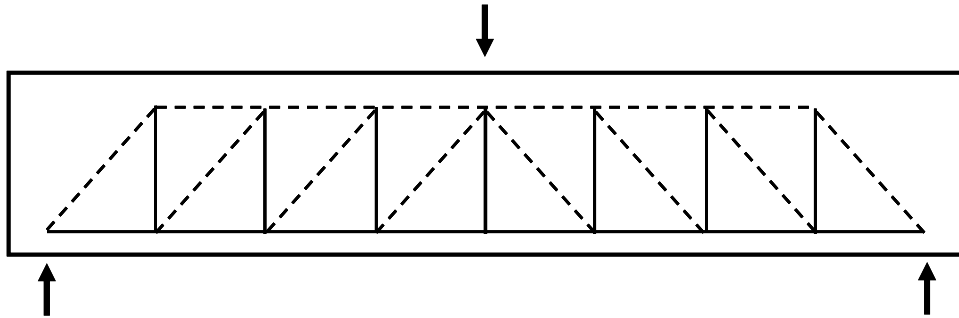


Figure 4-40: Strut-and-tie model of a sectional member

Beyond the interior nodes, an assumption must be made regarding the geometry of the node under the applied load (Node D in Figure 4-36). The assumed geometry of this node is shown in Figure 4-41. The depth of the prismatic strut BD was assumed to be 9", with the lower portion of the node assumed to be 11". The combined depth of the two dimensions (20") is roughly equal to the neutral axis depth, depending on the concrete strength. A reduction in the depth of strut BD would cause it to govern the model; an increase in its dimension would cause unnecessary inclination of strut CD.

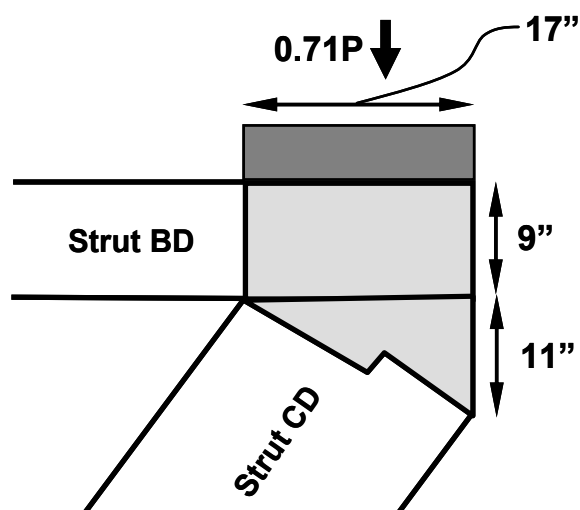


Figure 4-41: CCC node geometry

Capacities estimated by using two-panel strut-and-tie models are compared to experimental maximum applied loads for all nine tests in Table 4-11. The data are plotted in Figure 4-42. A full set of calculations for the two-panel strut-and-tie model of Test #5 is given in Appendix A.

Table 4-11: STM capacities and maximum applied loads

Test #	Maximum Applied Load (kips)	Shear at Maximum Applied Load (kips)	Two-Panel Strut-and-Tie Model					
			AASHTO LRFD		TxDOT 4371		ACI 318-05	
			2-Panel Capacity (kips)	Governing Element	2-Panel Capacity (kips)	Governing Element	2-Panel Capacity (kips)	Governing Element
1	1,626†	1133	314	tie BC	314	tie BC	209	tie BC
2	2,050	1434	942	tie BC	942	tie BC	733	tie BC
3	1,573	1095	304	tie BC	304	tie BC	203	tie BC
4	1,510†	1050	304	tie BC	304	tie BC	203	tie BC
5	1,628	1134	709*	tie BC	709*	tie BC	506*	tie BC
6	1,628	1134	709	tie BC	709	tie BC	506	tie BC
7	1,853†	1294	709	tie BC	709	tie BC	506	tie BC
8	1,510†	1050	270	tie BC	270	tie BC	0	tie BC
9	1,262†	874	300	strut CD at node D	119	strut CD at node D	209	tie BC

*STM calculations for this test are given in Appendix A

†Test resulted in shear failure

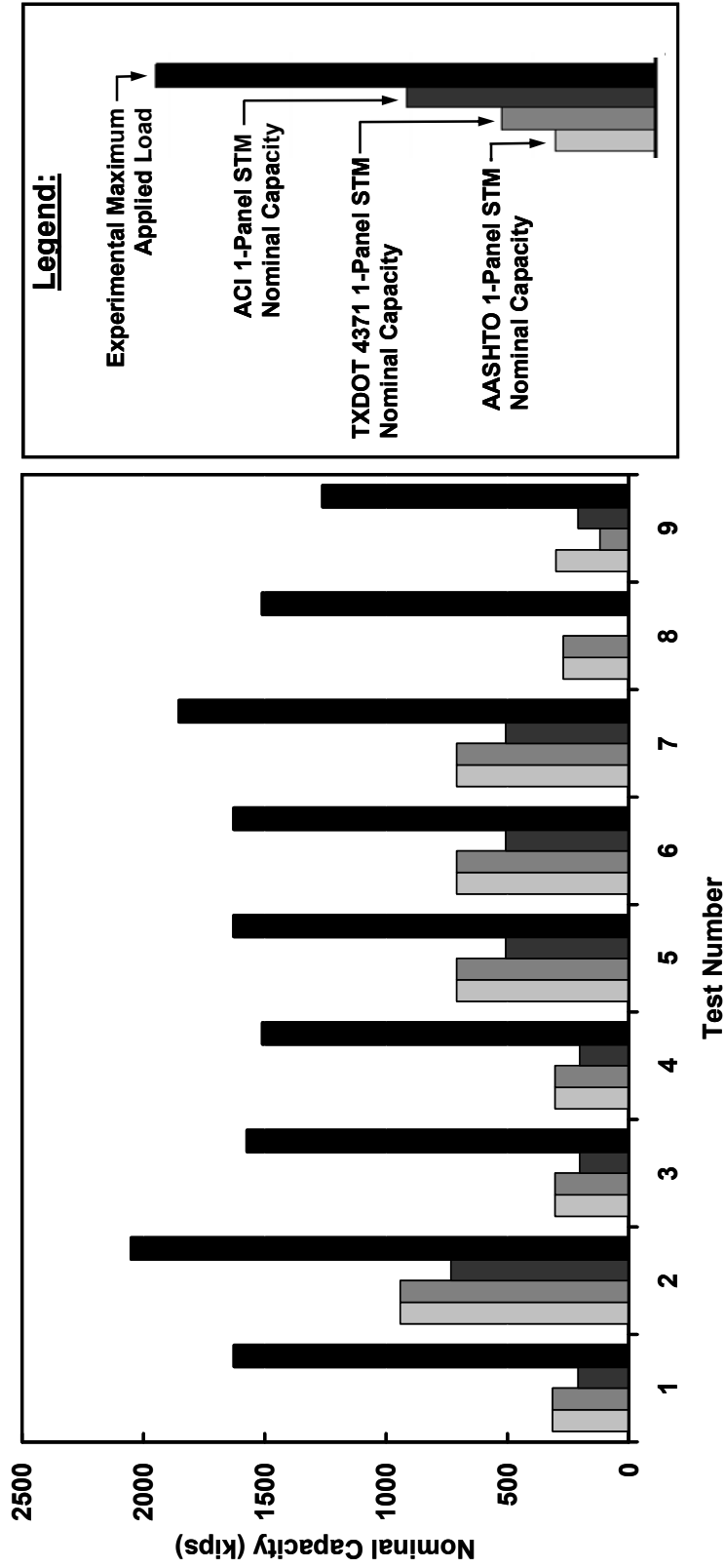


Figure 4-42: Two-panel STM capacities and maximum applied loads

The two-panel STM capacity using AASHTO LRFD and TxDOT 4371 was governed by the vertical tie BC (Figure 4-36) for eight of the nine tests, while the two-panel STM capacity using ACI 318 was governed by the vertical tie BC for all nine tests. Therefore, the conservatism of the two-panel model for a given shear span is directly related to the amount of transverse reinforcement assumed to be part of tie BC. Notably, the vertical tie BC governs the capacity of the strut-and-tie model even in the case of Test #2, where the shear span has nearly three times vertical shear reinforcement required by AASHTO.

AASHTO LRFD specifies that crack control reinforcement may also be utilized as tie reinforcement in a strut-and-tie model. However, Appendix A of ACI 318 does not contain an equivalent provision. As a result, the STM capacity of a two-panel model in ACI is more conservative than either AASHTO LRFD or TxDOT 4371.

Regardless of the strut-and-tie modeling design method used, the efficient use of a two-panel strut-and-tie model requires a tremendous amount of vertical shear reinforcement. The tests with the smallest difference between the maximum applied load and the STM capacity were Test #2 and Tests #5 through #7. These tests were completed on shear spans with vertical reinforcement ratios of 0.0086 and 0.0061, respectively. Therefore, the use of a two-panel strut-and-tie model was inefficient unless an amount of vertical reinforcement at least double AASHTO minimum vertical reinforcement ratio of 0.003 was provided.

4.3.3.3 Model Efficiency

The selection of a strut-and-tie model in a deep beam can be difficult. Examination of concrete surface strains and crack patterns yields valuable insight into the actual load path from the applied loading point to the reaction point.

Concrete strains were measured at mid-length of the bottle-shaped one-panel strut in Test #1, as outlined in section 3.7.3.2 and shown in Figure 4-43. The strain gauges were placed in this manner to obtain a strain profile at mid-length of the bottle-shaped strut, where the extent of dispersion of the strut is the greatest.

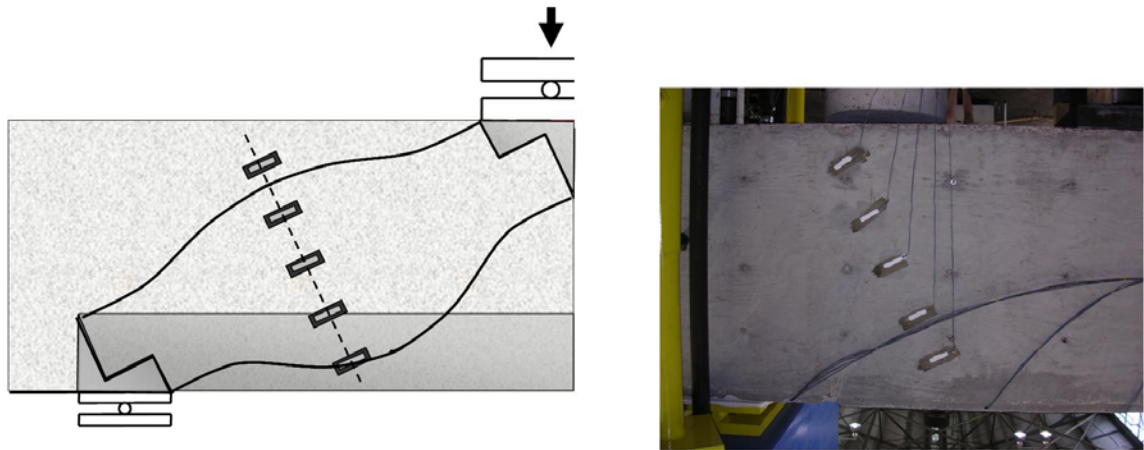


Figure 4-43: Surface strain gauge locations

A plot of concrete strain and stress at the ultimate load vs. distance from the bottle-shaped strut centerline is shown in Figure 4-44. The curve demonstrates that force does indeed flow from the load point to the reaction point in a manner consistent with a bottle-shaped strut, and therefore supports the use of a one-panel strut-and-tie model. The strain profile shown in Figure 4-44 is shown superimposed over the shear span in Figure 4-45, along with an outline of the bottle-shaped strut consistent with the strain measurements.

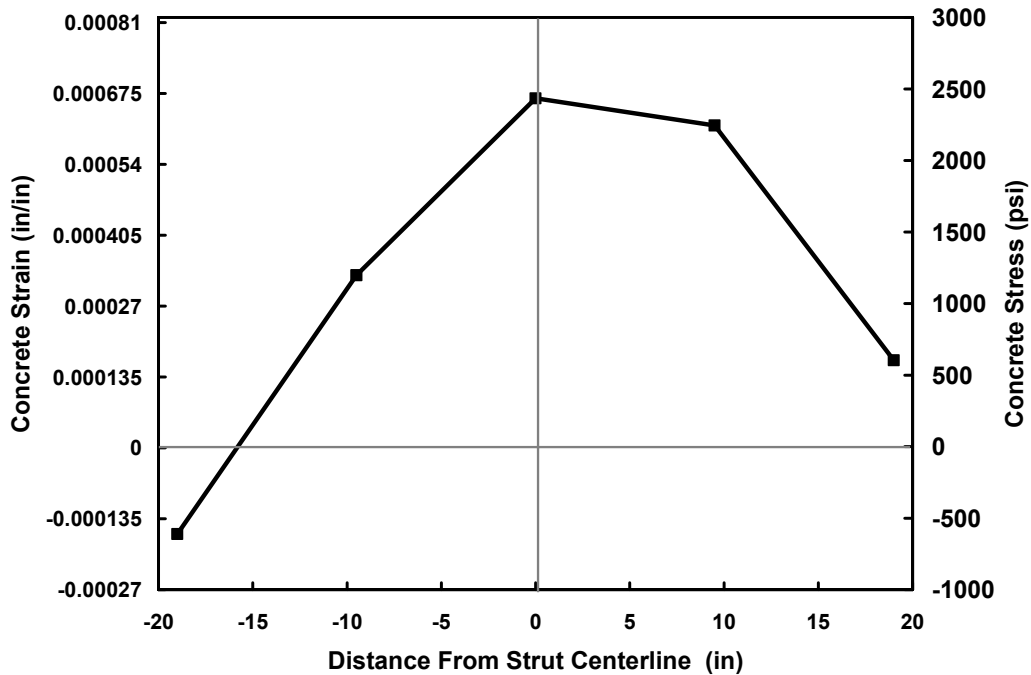


Figure 4-44: Concrete strain and stress vs. distance from strut centerline

The maximum stress inferred from strain measurements in the concrete at the time of failure was 2,430 psi. However, this is the stress at mid-length of the strut; given its bottle shape, the concrete stress is much greater at the strut-to-node interface. Using the above plot, the estimated width of the bottle-shaped strut is approximately 40 inches. Using a one-panel strut-and-tie model, the width of the strut at the node is approximately 21 inches. Assuming that the stress in the strut is proportional to its width, the concrete stress at the node-strut interface is estimated as 4,630 psi. The concrete strength for this specimen was 4,100 psi.

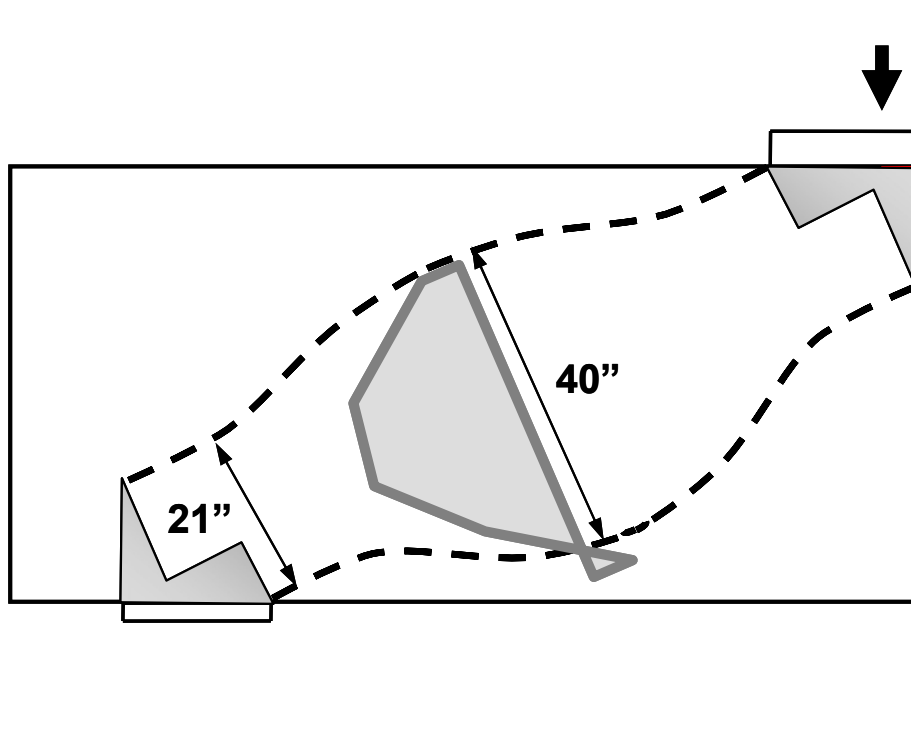


Figure 4-45: Estimation of bottle-shaped strut using concrete strain profile

As noted in the previous section, it was found that two-panel models are inefficient unless a large amount of vertical transverse reinforcement is present. In addition, the use of a two-panel strut-and-tie model is not supported by the cracking pattern of specimens. Figure 4-46 illustrates one and two-panel strut-and-tie models superimposed over the cracking pattern of a typical test specimen. As can be seen in the figure, crack patterns observed in a typical test indicate that the actual load path is a combination of one-panel and two-panel strut-and tie models.

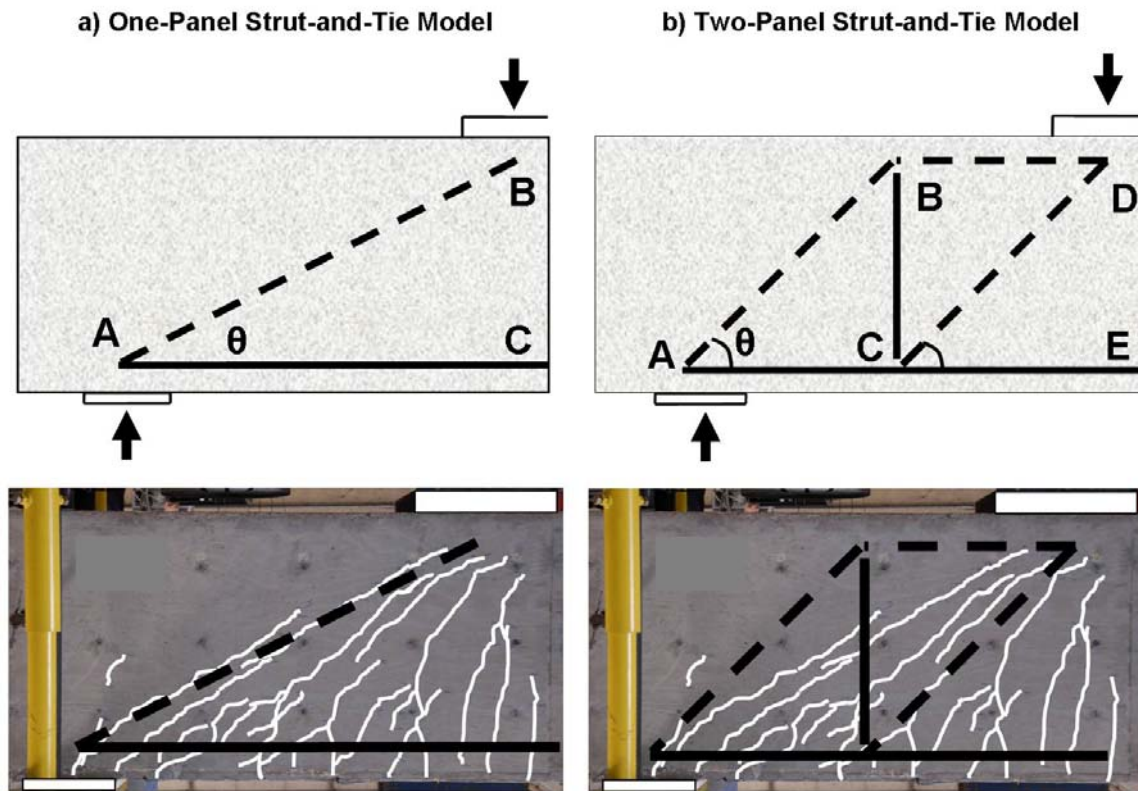


Figure 4-46: Strut-and-tie model comparison to cracking behavior

4.3.3.4 Comparison to First Diagonal Cracking Load

STM does not permit design by serviceability limit states. Even so, the experimentally determined first diagonal cracking load can be compared to the STM capacity for each specimen. The comparison can be used to evaluate the effectiveness of STM from a standpoint of serviceability.

The first diagonal cracking load was recorded for three tests—the original test on each of the three specimens. The first diagonal cracking load and unfactored STM capacity using each of the three STM methods outlined in Chapter 2 is shown in Table 4-12 and Figure 4-47. Since the capacity of a specimen estimated by using a one-panel STM model is a function of the compressive strength of concrete, it was most appropriate

to use. Similarly, the diagonal cracking load is generally considered to be proportional to the square root of the compressive strength.

Table 4-12: Diagonal cracking loads and STM capacities

Test #	Shear Span Tested	f'_c (psi)	$\sum \frac{A_{si}}{b_s} \sin \alpha_i$	AASHTO 1-Panel STM Capacity	TxDOT 1-Panel 4371 STM Capacity	ACI 1-Panel STM Capacity	Diagonal Cracking Applied Load (kips)
1	1A	4100	0.0043	637	633	1024	535
3	2A	4900	0.0043	743	692	1225	451
8	3A	2800	0.0031	453	541	697	317

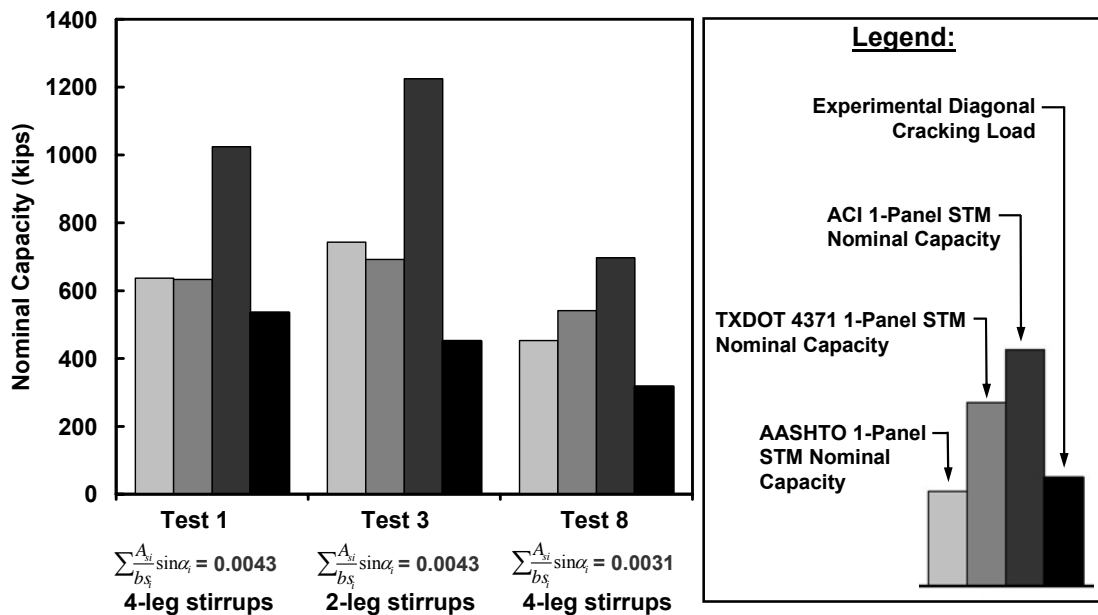


Figure 4-47: Diagonal cracking loads and STM capacities

The data in Table 4-12 and Figure 4-47 indicate that strut capacities estimated through the use of one-panel strut-and-tie models are higher than the diagonal cracking load. Since it is desirable to prevent the formation of diagonal cracks under service loads, the data presented in Table 4-12 and Figure 4-47 are further analyzed.

The load and resistance factors of both AASHTO LRFD and ACI 318 are listed in Table 4-13. The factors used by TxDOT 4371 guidelines are identical to that of AASHTO LRFD. The load factors listed are those for the load combination that includes only dead and live loads. ACI stipulates a single strength reduction factor for all STM elements, while AASHTO LRFD stipulates a single resistance factor for STM elements in compression. A one-panel strut-and-tie model is composed entirely of components in compression, and therefore each component is subject to the ϕ factor shown below.

Table 4-13: Load and resistance factors

Structural Design Code	Load Factor: DL	Load Factor: LL	STM Resistance Factor or Strength Reduction Factor, ϕ
AASHTO LRFD	1.25	1.75	0.70*
ACI 318-05	1.2	1.6	0.75

*For compression members in a strut-and-tie model

The first diagonal cracking load can be expressed as a fraction of the STM capacity (Table 4-14). This value can be compared to the ratio of factored STM capacity to unfactored STM capacity. This ratio depends on the assumed proportion of dead and live load being applied to the specimen. It is possible to solve for the minimum fraction of assumed live load on a specimen such that the factored STM capacity is less than the first diagonal cracking load.

Table 4-14: Cracking load fraction of STM capacity

Test #	AASHTO 1-Panel STM Capacity	TxDOT 1-Panel 4371 STM Capacity	ACI 1-Panel STM Capacity	Applied Load at Diagonal Cracking (kips)	Cracking Load Fraction of AASHTO STM Capacity	Cracking Load Fraction of TxDOT 4371 STM Capacity	Cracking Load Fraction of ACI 318-05 STM Capacity
1	637	633	1024	535	0.84	0.85	0.52
3	743	692	1225	451	0.61	0.65	0.37
8	453	541	697	317	0.70	0.59	0.45

For example, the lowest ratio of the first diagonal cracking load to AASHTO STM capacity is 0.61 (Table 4-14). In a typical strut-and-tie model design load and resistance factors are used. In other words, the factored strut capacity (ϕF_n) is kept greater than the factored load in the strut (F_u). This implies an apparent factor of safety that is roughly equal to an effective load factor divided by the ϕ factor, where the effective load factor can be viewed as the average load factor applied to the dead load and live load. Although unrealistic, the smallest apparent factor of safety can be calculated as the dead load factor divided by the ϕ factor, since the dead load factor is smaller than the live load factor in ACI 318-05 and AASHTO LRFD.

Using AASHTO LRFD Bridge Design Specifications and assuming conservatively that the corresponding specimen is loaded entirely with dead load, the unfactored strut capacity is multiplied by a factor of $\phi/1.25$ to calculate the maximum load that can be permitted on that strut in a typical design environment:

$$\frac{\phi}{LOAD FACTOR} = \frac{\phi}{1.25} = \frac{0.70}{1.25} = 0.56$$

The above calculation implies that the unfactored or service loads on that diagonal strut are separated from the factored loads by a factor of 1.8 (apparent factor of safety).

Conversely the largest load that can be permitted on a strut is equal to $(1/1.8 = 0.56)$ 56% of its STM capacity:

$$\frac{\text{Factored Strut Capacity}}{\text{Unfactored Strut Capacity}} = 0.56 < 0.61 = \frac{\text{First Diagonal Cracking Load}}{\text{Unfactored Strut Capacity}}$$

Therefore, for each specimen the factored STM capacity using AASHTO is less than the load corresponding to the first diagonal cracking load. That is, an equivalent structure in the field designed using STM would not undergo diagonal cracking, irrelevant of the fraction of DL and LL on the structure. As the ratio of LL to DL increases the effective load factor will increase and the ratio of the ϕ factor to effective load factor will decrease.

The same is true of the STM capacity calculated using TxDOT 4371 provisions. The lowest fraction of first diagonal cracking load to TxDOT 4371 STM strut capacity is 0.59. Therefore in the worst case, the factored strut capacity using TxDOT 4371 provisions is less than first diagonal cracking load:

$$\frac{\text{Factored Strut Capacity}}{\text{Unfactored Strut Capacity}} = 0.56 < 0.59 = \frac{\text{First Diagonal Cracking Load}}{\text{Unfactored Strut Capacity}}$$

The same observation is not true of specimen STM capacities determined using ACI. The lowest fraction of first diagonal cracking load to ACI STM strut capacity is 0.37. Assuming that the corresponding specimen is loaded entirely with live load (the least conservative assumption), the unfactored strut capacity is multiplied by a factor of $\phi/1.60$ to account for load and resistance factors:

$$\frac{\phi}{\text{LOAD FACTOR}} = \frac{\phi}{1.25} = \frac{0.75}{1.60} = 0.47$$

$$\frac{\text{Factored Strut Capacity}}{\text{Unfactored Strut Capacity}} = 0.47 > 0.37 = \frac{\text{First Diagonal Cracking Load}}{\text{Unfactored Strut Capacity}}$$

Therefore the factored strut capacity using ACI 318 is greater than the first diagonal cracking load, regardless of the assumed type of loading on the structure.

The above analyses indicate that a deep beam with an a/d ratio near 2.0 designed using a factored one-panel strut-and-tie model with either the AASHTO LRFD or TxDOT 4371 provisions is unlikely to undergo diagonal cracking. Conversely, a deep beam with an a/d ratio near 2.0 designed using a factored one-panel strut-and-tie model with the ACI STM provisions will likely undergo diagonal cracking.

It is important to recognize that these observations are based on results from three tests. These tests were conducted on full-scale specimens that were the largest specimens with shear reinforcement tested in the history of shear research (see section 2.4). In future tests somewhat lower diagonal cracking loads may be observed. However, this possibility does not change the general trends discussed above.

In addition, the applicability of these results is underscored by the fact that the project specimens were designed to be more shear critical than typical TxDOT deep beams. Typical field members will have less of a propensity to undergo diagonal cracking.

4.4 MINIMUM HORIZONTAL AND VERTICAL TRANSVERSE REINFORCEMENT RATIOS

The research reviewed in Chapter 2 of this document indicated that the effectiveness of horizontal or vertical transverse reinforcement in a deep beam is largely dependent on the a/d ratio. For example, Kong et al. (1970) found that horizontal skin reinforcement was most effective in specimens tested with very low a/d ratios. By the same token, a host of research studies have found that vertical reinforcement is most effective in specimens loaded such that a/d is near 2.0 (see section 2.5.14).

An analysis of forces in a bottle-shaped strut supports these experimental results. In a deep beam, the dispersion of compression in a bottle-shaped strut will cause tensile

forces along the strut in a direction perpendicular to the strut axis (Figure 4-48a). Reinforcement is most efficiently placed perpendicular to the axis of a bottle-shaped strut. However, in practice reinforcement is typically placed orthogonally. Therefore, in deep beams loaded such that a/d is near 2.0 (with a correspondingly small angle of strut inclination) the tensile dispersion forces are nearly vertical and are therefore effectively resisted by vertical reinforcement (Figure 4-48b). Conversely, the tensile forces in deep beams loaded such that a/d is just above zero (with a correspondingly large angle of strut inclination) will be most effectively resisted by horizontal reinforcement (Figure 4-48c). In short, the effectiveness of horizontal or vertical shear reinforcement depends largely on the strut angle of inclination.

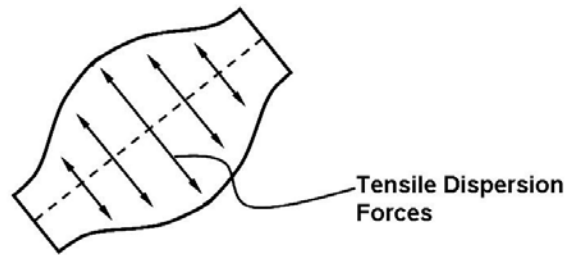
This concept is not directly accounted for in the STM design provisions of both of the structural design codes considered in this document. Only AASHTO LRFD explicitly requires that both horizontal and vertical transverse reinforcement must be present in a deep beam. The code specifies an amount of transverse reinforcement equal to at least 0.003 times the gross cross-sectional area in each orthogonal direction.

Conversely, ACI requires that the combination of horizontal and vertical reinforcement must be greater than a specified minimum. As outlined in Chapter 2, ACI A.3.3 specifies that horizontal and vertical reinforcement crossing a bottle-shaped strut must satisfy:

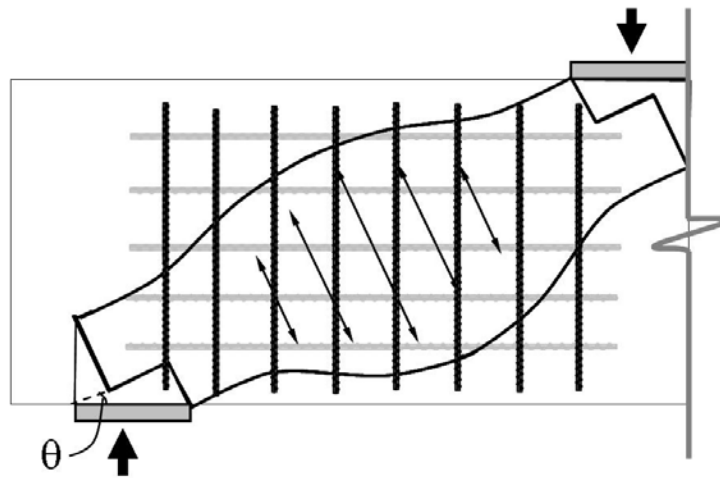
$$\sum \frac{A_{s_i}}{bs_i} \sin \alpha_i \geq 0.003$$

Equation 4-5

a) Illustration of bottle-shaped strut dispersion forces



**b) Small angle of strut inclination;
Vertical reinforcement effectively restrains dispersion forces**



**c) Large angle of strut inclination;
Horizontal reinforcement effectively restrains dispersion forces**

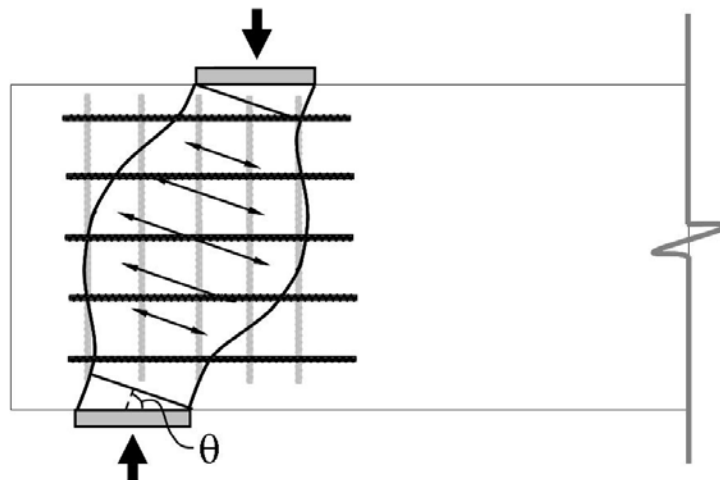


Figure 4-48: Effect of strut inclination on effectiveness of reinforcement

In addition, ACI specifies that if transverse reinforcement is placed in only one direction, the angle between the strut axis and the reinforcement axis (α) must not be less than 40 degrees. Even so, it is possible to satisfy the minimum requirement of ACI 318 by placing transverse reinforcement in an inefficient manner.

It is important to note that the forces in a bottle-shaped strut, analyzed using Mohr's Circle for stress, would indicate that the trigonometric term in the ACI equation should be squared. When this equation was introduced in 2002 by ACI the trigonometric term was not squared, resulting in an equation that is both simple and conservative.

In lieu of using ACI A.3.3, ACI 11.8 allows placement of transverse reinforcement in a deep beam such that the minimum horizontal reinforcement ratio is 0.0015 and the minimum vertical transverse reinforcement ratio is 0.0025. This provision has undergone changes in recent years. ACI 318-99 and earlier versions of the code required a minimum of 0.0015 times the gross cross-sectional area in the vertical direction, and 0.0025 times the gross cross-sectional area in the horizontal direction. In 2002, the minimum reinforcement ratio required in each direction was interchanged; the ACI 318-05 commentary states the change was made to because past research indicated that vertical shear reinforcement is more effective than horizontal shear reinforcement. Among the research cited is the study by Rogowski, MacGregor, and Ong (1986) that was summarized in Chapter 2.

Similarly to the ACI Appendix A provisions, TxDOT 4371 guidelines specify that the combination of horizontal and vertical transverse reinforcement must be greater than a specified minimum:

$$\rho_{\perp} = \sqrt{\left(\frac{A_{sH}}{b s_H}\right)^2 + \left(\frac{A_{sV}}{b s_V}\right)^2} > \rho_{\perp, \min} \quad \text{Equation 4-6}$$

Using either ACI 318 Appendix A provisions or TxDOT 4371 guidelines, it is possible to satisfy minimum transverse reinforcement requirements by placing horizontal or vertical shear reinforcement without regard for a/d ratio and angle of strut inclination.

Given that the effectiveness of a given direction of transverse reinforcement is dependent on the a/d ratio (and corresponding angle of strut inclination), the omission of reinforcement in an orthogonal direction could be detrimental to the serviceability performance of the beam. For example, placing little or no vertical reinforcement in a deep beam loaded such that $a/d = 2.0$ is a very inefficient placement of reinforcement.

As a result, it is suggested that a minimum amount of transverse reinforcement in each orthogonal direction be included. The minimum amount of horizontal and vertical reinforcement should be a function of the angle of inclination. Proposed minimum horizontal and vertical reinforcement ratios are shown in Figure 4-49.

The basis for the suggested minimum transverse reinforcement ratios (0.0025 and 0.0015) is ACI 11.8. ACI suggests that vertical shear reinforcement is more effective in deep beams, and stipulates a minimum vertical reinforcement ratio of 0.0025. Horizontal shear reinforcement was deemed less effective, and minimum horizontal reinforcement ratio of 0.0015 is stipulated.

The minimum values in Figure 4-49 relate these minimum reinforcement ratios to the angle of strut inclination. As discussed above, the effectiveness of transverse reinforcement depends on the angle of the strut inclination. When a member is loaded such that a/d is near 2.0 (and the angle of inclination is less than 25 degrees), the minimum vertical reinforcement ratio is 0.0025, and the minimum horizontal reinforcement ratio is 0.0015. Conversely when a member is loaded such that a/d is near zero (and the angle of inclination is above 65 degrees), the specified minimum reinforcement ratios are interchanged.

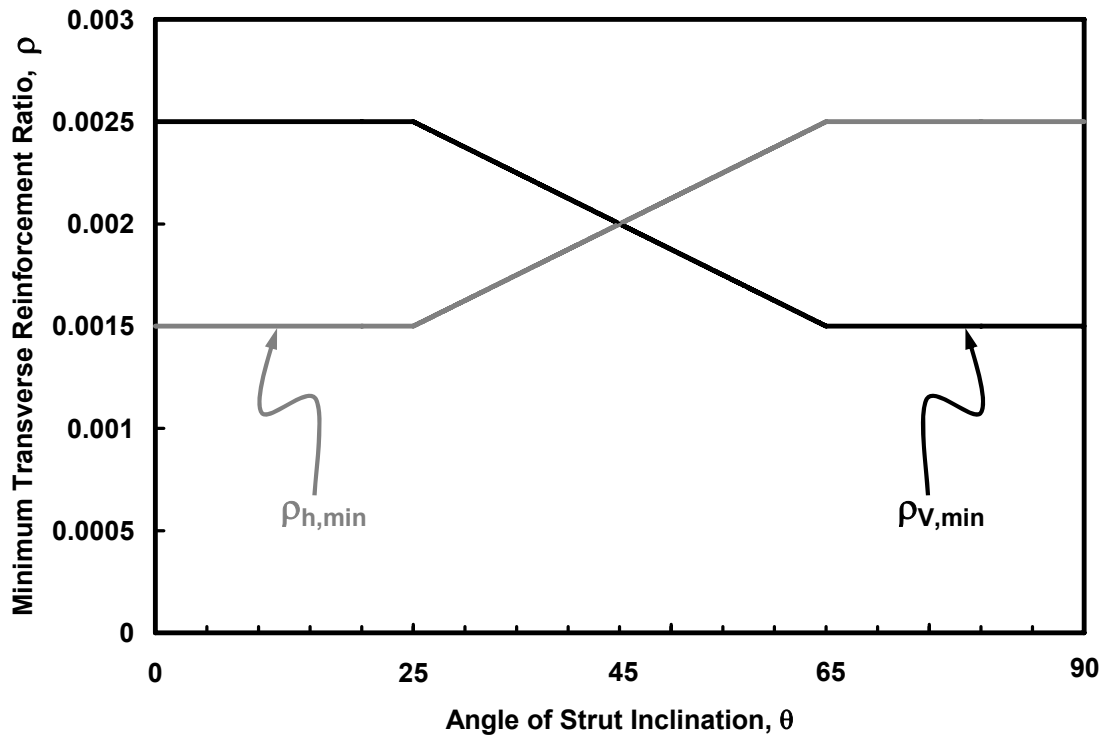


Figure 4-49: Suggested minimum transverse reinforcement ratio

The suggested minimum reinforcement ratios of the above figure are to be used in addition to the existing minimum transverse reinforcement requirements of both ACI 318-05 provisions and TxDOT 4371 guidelines. It is important to note that this modification is suggested on the basis of past research and simple analysis of forces in a bottle-shaped strut.

4.5 SUMMARY

Nine tests were performed on three specimens, as outlined in Table 4-1. The variables in the tests were the amount and detailing of horizontal and vertical shear reinforcement, and the applied load bearing area. Concrete strength also varied between the three specimens. From these tests a number of observations were made and conclusions were reached regarding the effect of the test variables on the strength and

serviceability performance of the deep beams. Additional conclusions were drawn regarding the effectiveness of using strut-and-tie modeling to estimate the capacity of the specimens.

4.5.1 Transverse Reinforcement Ratio

The transverse reinforcement ratio had a marginal effect on the ultimate shear capacity of the specimens. In tests of shear spans with 4-legged stirrups, there was no trend relating ultimate shear capacity to the amount of transverse reinforcement. However, the test on the specimen with nearly triple the minimum AASHTO requirement for vertical reinforcement (Test #2, $\rho_v = 0.0086$) contained sufficient reinforcement to initiate a flexural failure rather than a shear failure. In tests of specimens with 2-legged stirrups, the effect of doubling the amount of vertical reinforcement was a 23% increase in the shear strength of the specimen. Considering the general scatter in shear data (Reineck et al., 2003, Brown and Bayrak, 2006), such a small difference is deemed insignificant.

There was not a significant difference in ultimate shear strength between the shear spans with minimum transverse reinforcement required by AASHTO LRFD and ACI 318, respectively. Thus, the minimum amount of transverse reinforcement as required by ACI is adequate from an ultimate strength perspective. Additional reinforcement produces only marginal increases in ultimate capacity. It is notable that this conclusion matches that made by Brown et al. (2006) based on smaller-scale test specimens. The conservative minimum transverse reinforcement requirement of the AASHTO LRFD code (that is, an amount of transverse reinforcement equal to 0.003 times the gross concrete area in each direction) is unwarranted from a standpoint of ultimate strength performance.

The amount of transverse reinforcement did not appreciably affect the applied load at which first shear cracking occurred. Transverse reinforcement did not engage until the first shear cracks opened.

The transverse reinforcement ratio had an effect on shear crack widths. Transverse reinforcement was effective at reducing crack widths throughout the duration of loading. However, the amount of transverse reinforcement did not affect the rate of growth of the shear cracks. Shortly after the formation of diagonal cracks, the widths of the cracks were comparable in specimens that met the AASHTO minimum and ACI 318 minimum reinforcement requirements. AASHTO LRFD minimum transverse reinforcement requirements result in the use of 41% additional reinforcement in comparison to ACI 318-05 specifications. The benefit of providing 41% additional reinforcement is marginal, particularly at service loads.

The minimum transverse reinforcement requirements of ACI 318 and TxDOT 4371 allow the placement of transverse reinforcement in a deep beam without consideration of the angle of strut inclination. A minimum amount of transverse reinforcement that is dependent on the strut angle of inclination should be required in each orthogonal direction. Such a minimum requirement was proposed in Figure 4-49, and is meant to be used in addition to the existing STM provisions of ACI 318 and TxDOT 4371.

4.5.2 Quantity of Stirrup Legs at a Section

The quantity of stirrup legs did not have a significant effect on the ultimate shear capacity of the specimens. The difference in shear strength between tests on shear spans with identical amounts of transverse reinforcement but a different number of stirrup legs (4-legged stirrups and 2-legged stirrups) was approximately 10% in the worst case. Considering the general scatter in shear data (Reineck et al., 2003, Brown and Bayrak, 2006), such a small difference is deemed insignificant.

The marginal difference in ultimate strength between specimens with multiple stirrups and those with 2 stirrup legs is consistent with past research. Hsiung and Frantz (1985) found that the quantity of stirrup legs in a beam had no effect on ultimate shear capacity. Anderson and Ramirez (1989) found that specimens with multiple stirrup legs had higher ultimate capacities than those two stirrups legs; however, when normalized

relative to concrete strength, the maximum difference between the ultimate capacities of specimens that failed in shear was less than 10%.

The quantity of stirrup legs had a minor effect on exterior crack widths. Specimens transversely reinforced with 2-legged stirrups were more effective at restraining shear crack widths at loads near ultimate than those with 4-legged stirrups. This observation is logical given that in the specimen with 2-legged stirrups, the reinforcement was concentrated along side faces.

The effect of the quantity of stirrup legs on interior cracks widths is unknown. However, given the adequate performance of specimens with 2-leg stirrup from both a strength and serviceability standpoint, consideration of interior crack widths is unnecessary. In addition, past research has demonstrated limited variation in crack widths throughout the cross-section of a wide specimen with only 2 stirrup legs (Hsiung and Frantz, 1985).

4.5.3 Bearing Area

The size of the bearing area had a minimal effect on the ultimate shear strength. Large differences in applied load bearing area did not translate to large differences in shear strength. The capacity of shear spans loaded with different bearing plate sizes was proportional to the compressive concrete strength rather than bearing area. Beneficial effects of confinement present for smaller bearing areas at the applied load point appeared to have offset the increased CCC node stress associated with smaller bearing plates.

Bearing area did not appreciably affect maximum shear crack widths. The maximum shear crack width grew linearly with increasing loads for tests with a 24"x36" applied load bearing area. Conversely, crack widths in the test with an 8"x12" bearing area, crack widths did not grow linearly with increasing loads. Even so, at any given fraction of ultimate capacity the crack widths were approximately equal, regardless of the applied load bearing size.

4.5.4 Strut-and-Tie Modeling

The strut-and-tie modeling provisions of AASHTO LRFD and the design guidelines included in TxDOT 4371 are adequate from a standpoint of serviceability. If the specimens tested in this study were designed using AASHTO LRFD provisions or TxDOT 4371 provisions, diagonal cracks under service loads would not have occurred regardless of the assumed ratio of dead load to live load. Conversely, the strut-and-tie modeling provisions of ACI 318 Appendix A are not adequate from a standpoint of serviceability, if the formation of diagonal cracks under service loads is not desired.

Strut-and-tie modeling provided conservative estimates of ultimate strength for all the tests conducted in the experimental program. The ACI 318 STM provisions provided the greatest strut efficiency and corresponding least conservative STM capacity for each test. The specimens were tested such that $a/d = 1.85$, and therefore required a shallow angle of strut inclination when modeled with a one-panel strut-and-tie model. However, ACI 318 utilizes constant strut efficiencies irrelevant of the strut inclination. On one hand it could be argued that from a strength standpoint the strut efficiency factors of ACI 318-05 eliminate unnecessary conservatism that was seen in applying AASHTO LRFD provisions and TxDOT 4371 guidelines to the specimens tested in this study. On the other hand, it must be remembered that the high efficiency factors of ACI 318-05 Appendix A provisions would have all but guaranteed shear cracks under service loads for all of the specimens tested in this study.

The STM capacity of shear spans loaded with limited bearing widths is exceedingly conservative. Accounting for the effect of confinement, as per ACI 10.17 or AASHTO 5.7.5, may ease the excessive conservatism of strut-and-tie models for limited bearing widths.

Concrete surface gauges placed on the side face of a shear span demonstrated that the load travels from the point of application of a concentrated load to the point of reaction by a single bottle-shaped strut. This behavior is consistent with the behavior assumed to occur in a one-panel strut-and-tie model. A two-panel strut-and-tie model is

not efficient unless a given shear span contains an amount of transverse reinforcement well in excess of the minimum transverse reinforcement requirement of ACI 318 or AASHTO LRFD.

As evidenced by strength and serviceability test data, the use of the AASHTO limited strut width provision (AASHTO 5.6.3.3.2) is not warranted for deep beams. Most importantly, the use of multiple stirrup legs did not significantly improve the ultimate strength or serviceability performance of specimens. In addition, the provision is not warranted for strut-and-tie modeling. The provision applies to the strut-to-CTT node interface of a two-panel (or multiple-panel) strut-and-tie models. The size of this CTT node is ambiguous, but can be considered sufficiently large to prevent the node from governing the strut-and-tie model. Limiting the width of a strut based on an ambiguous CTT nodal geometry is not justified. The use of full strut widths in two-panel STM models for the specimens tested in this study resulted in conservative estimates of STM capacities.

CHAPTER 5

Summary, Conclusions, and Recommendations

5.1 SUMMARY OF RESEARCH STUDY

A research study was conducted at the Ferguson Structural Engineering Laboratory (FSEL) at the University of Texas at Austin to investigate the effect of the amount and detailing of transverse reinforcement and the applied load bearing area on the ultimate shear strength and serviceability performance of large-scale reinforced concrete deep beams. The research was partially motivated by the poor serviceability performance of a number of large-scale TxDOT bent caps. In addition, the project was undertaken to follow up on the strut-and-tie modeling provisions developed as part of TxDOT Research Project 4371, which were based entirely on strength considerations.

In order to accommodate the high loads required to fail large-scale deep beams, a new test setup was designed and constructed in Ferguson Structural Engineering Laboratory (FSEL). As used in the current experimental program, the setup could safely resist an asymmetrically applied point load of 2,500 kips. The test setup can be reconfigured to safely resist a point load of 6,000 kips.

The experimental program for the current research project consisted of nine tests conducted on three large-scale reinforced concrete deep beams. The deep beams may be the largest specimens with shear reinforcement in the history of shear research. At least two tests were performed on each test specimen. The beams had sufficient length (L/d ratio of 6.4) to obtain two independent shear tests, one on each end of the specimen, for a total of six shear spans tested. In each case the a/d ratio was 1.85. In several tests it was necessary to stop loading

at the initiation of flexural yielding and retest with a smaller, more shear-critical applied load bearing plate in order to successfully attain a shear failure.

In addition to gathering ultimate strength data, the serviceability performance of the specimens was extensively evaluated. Each test was carried out in loading increments of 100 kips with the exception of Test #1, which was loaded in 50 kip increments. At the conclusion of each loading increment cracks were marked and crack widths were measured. The first diagonal cracking load, cracking pattern, formation of parallel diagonal shear cracks, maximum shear crack widths, and deflection was measured or observed for each of the tests.

The measured ultimate capacity and first diagonal cracking load for each of the tests were compared to the design capacity estimated by using strut-and-tie modeling. The strut-and-tie modeling capacity was calculated using two different U.S. strut-and-tie modeling provisions (AAHSTO LRFD 4th edition, and ACI 318-05 Appendix A) and the TxDOT 4371 STM provisions.

5.2 CONCLUSIONS

The effect of the amount and detailing of transverse reinforcement and bearing area on the ultimate shear strength and serviceability performance of deep beams was evaluated in the current study. In addition, the experimental capacity and first cracking load in each test was compared to the design capacity estimated by using strut-and-tie modeling. The conclusions of the study are presented in this section. Unless otherwise noted, the conclusions drawn are based on the data obtained within the experimental study.

5.2.1 Transverse Reinforcement Ratio

- **An amount of transverse reinforcement beyond the minimum requirement of ACI 318-05 is unwarranted from standpoint of ultimate strength in deep beams.** Additional reinforcement produces marginal, if any, increases in ultimate capacity. In specimens with 4-legged stirrups, there was no trend relating ultimate shear capacity to the amount of transverse reinforcement. The specimen containing minimum transverse reinforcement required by ACI 318 did not have inferior performance to the specimen containing the minimum amount of transverse reinforcement required by AASTHO LRFD. However, one specimen contained sufficient reinforcement ($\rho_v = 0.0086$) to initiate a flexural failure rather than a shear failure. In specimens with 2-legged stirrups, the effect of doubling the amount of vertical reinforcement resulted in a 23% increase in the shear strength of the specimen. Considering the general scatter in shear data, such a small difference was deemed insignificant.
- **The load at which first diagonal crack occurs is unaffected by the amount of transverse reinforcement.** The amount of reinforcement did not affect the load at which first diagonal cracking occurred. Transverse reinforcement did not engage until the first shear cracks opened.
- **The amount of transverse reinforcement affects shear crack widths.** Transverse reinforcement was effective at reducing crack widths throughout the duration of loading, particularly at loads near ultimate. However, the benefit of providing the minimum transverse reinforcement amount required by AASHTO, which corresponds to a 41% increase over ACI minimum requirement, is marginal at service loads.

- **A minimum reinforcement ratio in each orthogonal direction is recommended.** Past research has indicated that the effectiveness of shear reinforcement in a deep beam is strongly related to the angle of strut inclination. The minimum transverse reinforcement requirements of ACI 318 and TxDOT 4371 allow the placement of transverse reinforcement in a deep beam without consideration of the angle of strut inclination. A minimum amount of transverse reinforcement that is dependent on the strut angle of inclination should be required in each orthogonal direction.

5.2.2 Quantity of Stirrup Legs

- **The quantity of stirrup legs did not have a significant effect on the ultimate shear capacity of the specimens.** The difference in shear strength between shear spans with identical amounts of transverse reinforcement but differing quantity of stirrup legs (4-legged stirrups and 2-legged stirrups) was approximately 10% in the worst case. Considering the general scatter associated with shear data, such a small difference is deemed insignificant. The marginal difference in ultimate strength between beams with multiple stirrups and those with 2 stirrup legs is consistent with past research (Hsiung and Frantz, 1985, Anderson and Ramirez, 1989).

- **Specimens with two stirrup legs were more effective at restraining shear cracks than specimens with multiple stirrup legs.** The quantity of stirrups legs had a negligible effect on exterior crack widths at loads near service level. At loads near ultimate, specimens transversely reinforced with 2-legged stirrups were more effective at restraining exterior shear crack widths at loads near ultimate than those with 4-legged stirrups. This observation is logical given that the specimen with 2-legged

stirrups contained a greater amount of reinforcement along side faces. Given the adequate strength performance and superior serviceability performance of specimens containing 2-legged stirrups, consideration of interior crack widths is arguably unnecessary. In addition, past research has demonstrated limited variation in crack widths throughout the cross-section of a wide specimen with only 2 stirrup legs (Hsiung and Frantz, 1985)

5.2.3 Bearing Area

- **The applied load bearing area had a marginal effect on the ultimate shear strength.** The capacity of shear spans loaded with different bearing plate sizes was proportional to the compressive concrete strength rather than bearing area. Beneficial effects of confinement present for smaller bearing areas appeared to have offset the increased CCC node stress associated with smaller bearing plates.

- **The applied load bearing area did not appreciably affect shear crack widths.** The maximum shear crack width grew linearly with increasing loads for tests with a 24"x36" applied load bearing size. Conversely, crack widths in the test with an 8"x12" applied load bearing size did not grow linearly with increasing loads. Even so, at any given fraction of ultimate capacity the crack widths were approximately equal, irrelevant of the applied load bearing size.

5.2.4 Strut-and-Tie Modeling

- **Strut-and-tie modeling provided conservative estimates of ultimate strength for all the tests conducted in the experimental program.** The capacity of the shear span in each test, as predicted by the strut-and-tie

modeling provisions of AASHTO LRFD, ACI 318, and TxDOT 4371 was less than the experimental capacity.

- **The strut-and-tie modeling provisions of AASHTO LRFD and TxDOT 4371 are adequate from a standpoint of serviceability.** If the specimens tested in this study were designed using AASHTO LRFD provisions or TxDOT 4371 provisions, diagonal cracks under service loads would not have occurred regardless of the assumed ratio of dead load to live load.

- **The strut-and-tie modeling provisions of ACI 318 Appendix A are not adequate from a standpoint of serviceability, if diagonal cracks at service loads are not desired.** If specimens tested in the current study were designed using ACI 318-05 STM provisions, the formation of diagonal cracks under service loads would likely have occurred irrelevant of the ratio of dead to live load. The strut efficiency required by ACI 318 STM provisions is not a function of the angle of strut inclination, and was therefore higher than the strut efficiency estimated by AASHTO LRFD in each of the tests. The ACI provisions should arguably be used with caution when modeling struts with angles of inclination near 25 degrees, such as in shear spans in the current study.

- **The STM capacity of shear spans loaded with limited bearing widths is exceedingly conservative.** However, accounting for the effect of confinement, as per ACI 10.17 or AASHTO 5.7.5, may ease the excessive conservatism of strut-and-tie models for limited bearing widths.

- **A considerable percentage of the load flows from the applied load point to the closest reaction point through a single, bottle-shaped strut.** Concrete surface strain data indicated that the load travels through

the shear span in a manner consistent with the assumed flow of forces in a one-panel strut-and-tie model.

- **A two-panel strut-and-tie model is not efficient unless a given shear span contains an amount of transverse reinforcement well in excess of the minimum transverse reinforcement requirement of ACI 318 or AASHTO LRFD.** The STM capacity of shear spans containing amounts transverse reinforcement consistent with code minima were found to be exceedingly conservative when modeled with a two-panel model.

- **The use of the AASHTO limited strut width provision (AASHTO 5.6.3.3.2) is not warranted for deep beams.** The use of multiple stirrup legs did not significantly improve the ultimate strength or serviceability performance of the specimens. In addition, the provision is not warranted from a modeling standpoint. The provision applies to struts that are anchored by reinforcement at the point of an ambiguous CTT node. Limiting the width of a strut based on an ambiguous CTT nodal geometry is not justified. The use of full strut widths in two-panel STM models for the specimens tested in this study resulted in conservative estimates of STM capacities.

5.3 RECOMMENDATIONS FOR FUTURE RESEARCH

- **How many reinforcing bars compromise a tie?** The capacity of a two-panel strut-and-tie model is significantly influenced by the quantity of stirrups considered to be part the vertical tie element.

- **What is the effect of reducing the size of the bearing area at the CCT node?** In the current study only the size of the applied load bearing area, and therefore the adjacent CCC node, was altered. Changing the size

of the bearing plate at the reaction point may yield different strength and serviceability behavior.

APPENDIX A

Strut-and-Tie Models

Appendix A includes the following sets of detailed strut-and-tie model calculations:

- One-panel strut-and-tie model of Test #1 using AASHTO LRFD provisions
- One-panel strut-and-tie model of Test #1 using TxDOT 4371 provisions
- One-panel strut-and-tie model of Test #1 using ACI 318 Appendix A provisions
- Two-panel strut-and-tie model of Test #5 using AASHTO LRFD provisions
- Two-panel strut-and-tie model of Test #5 using TxDOT 4371 provisions
- Two-panel strut-and-tie model of Test #5 using ACI 318 Appendix A provisions

A.1 ONE-PANEL STRUT-AND-TIE MODEL FOR TEST #1

This section contains a full set of calculations for a one-panel strut-and-tie model of Test #1, using each of the three STM design methods presented in Chapter 2. It is meant to be used in addition to the information and assumptions already provided in section 4.3.3.1. Table A-1 shows pertinent efficiency factors for both the AASHTO LFRD 4th Edition and ACI 318-05. Nodal efficiencies and resistance factors using TxDOT 4371 are identical to those of AASHTO. .

Test #1 was conducted on Shear Span 1A. The geometry and reinforcement configuration of Shear Span 1A is shown in Figure A-1.

Table A-1: Strut and node efficiency factors

Strut or Node Efficiency	ACI 318-05		AASHTO LRFD	
	β_s	Φ	ν	Φ
Strut with uniform cross-section	1.0	0.75	Equation 2-5	0.70
Bottle-shaped strut with reinforcement satisfying A.3.3	0.75	0.75	Equation 2-5	0.70
Bottle-shaped strut without reinforcement satisfying A.3.3	0.60	0.75	Equation 2-5	0.70
Struts in tension members	0.40	0.75	Equation 2-5	0.70
All other cases	0.60	0.75	Equation 2-5	0.70
CCC Node	1.0	0.75	0.85	0.70
CCT Node	0.80	0.75	0.75	0.70
CTT or TTT Node	0.60	0.75	0.65	0.70

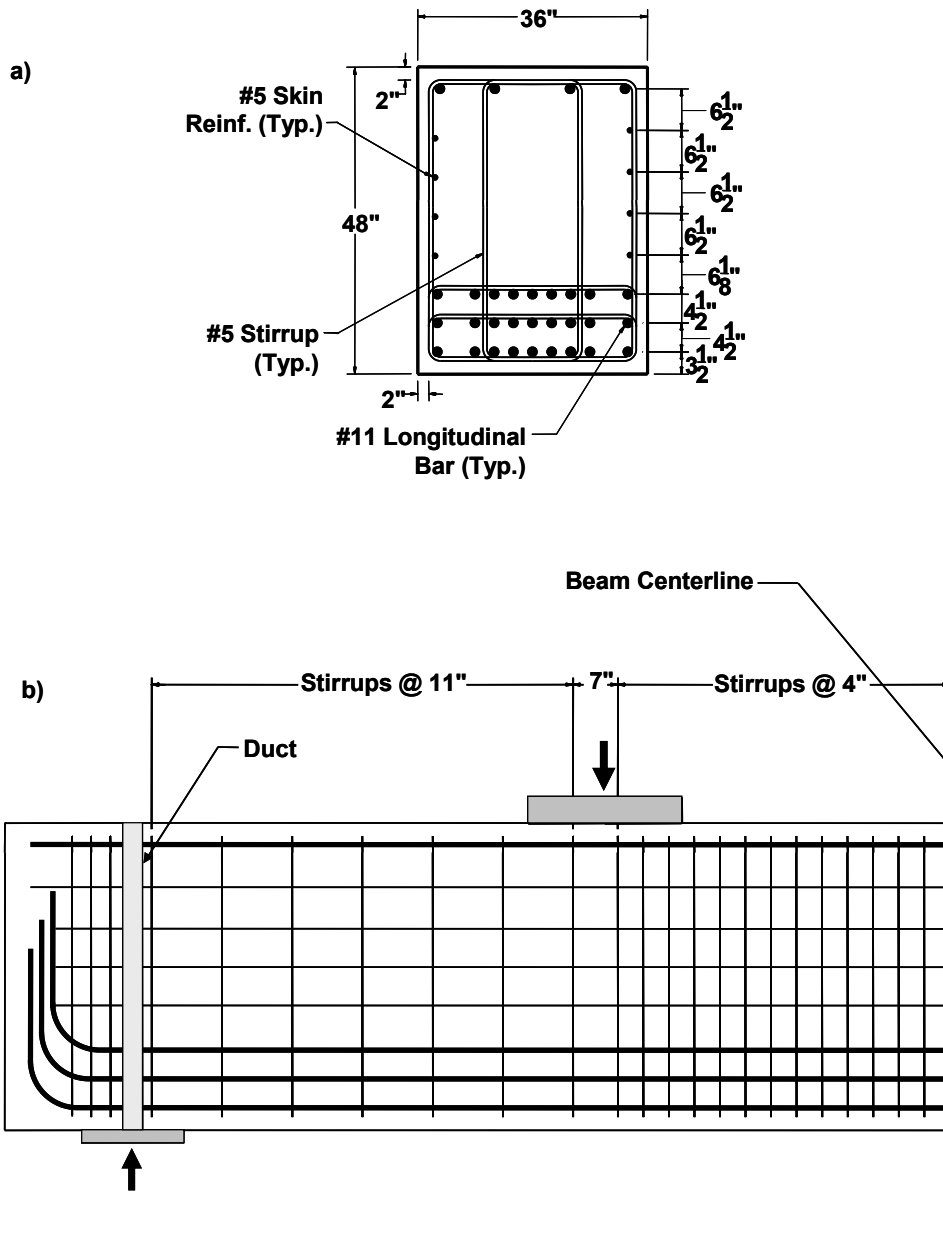


Figure A-1: Shear span 1A a) Cross-section; b) Elevation

In this example the short span is modeled using a one-panel strut-and-tie model. Figure A-3 shows a two-dimensional one-panel model, along with the geometry of the bearing areas.

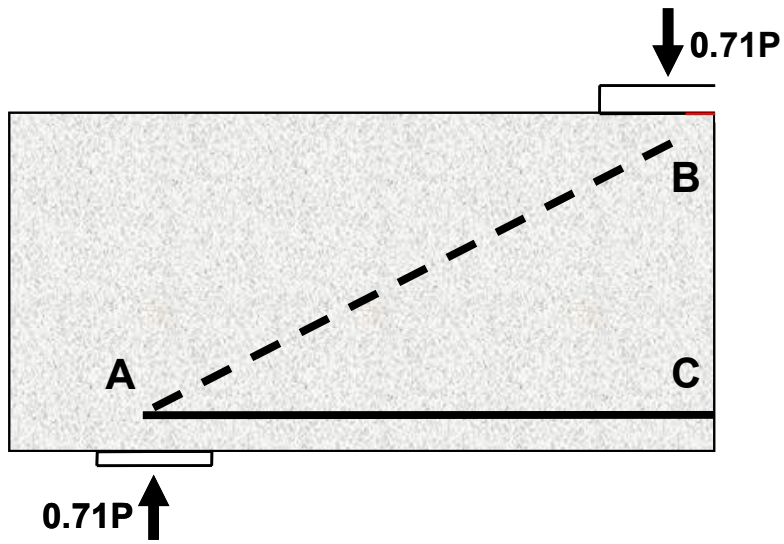


Figure A-2: Test#1 one-panel stick strut-and-tie model

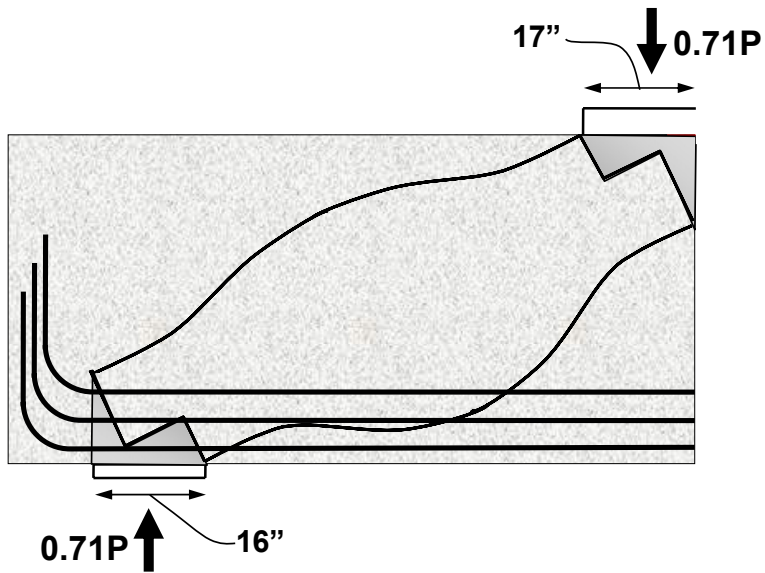


Figure A-3: Test #1 one-panel two-dimensional strut-and-tie model

A.1.1 Design Using AASHTO LRFD

The nominal capacity of the strut-and-tie model for the shear span in Test #1 is 637 kips. The governing element in the model is strength of the strut at its interface with Node A. The nominal capacity of each element in the strut-and-tie model is calculated below.

A.1.1.1 Nodes

The geometry of each node is shown in Figure A-4. Node A is a CCT node and Node B is a CCC node. The depth of node A at its left face, w_t , is equal to the twice the distance from the bottom face of the specimen to the center of Tie AC (16 inches). The length of Node A in the direction of the span is equal to the dimension of the support reaction bearing plate in the direction of the span (16 inches).

The depth of the CCC node (Node B) is typically assumed to be approximately equal to the depth of the flexural compression block at the nominal flexural capacity of the section. Using this assumption, the depth w_t would be equal to approximately 20 inches, depending on the concrete strength. A depth of 16 inches was selected so that the angle of inclination of Strut AB would remain approximately 25 degrees—the minimum angle between a strut and adjoining tie allowed by ACI 318-05.

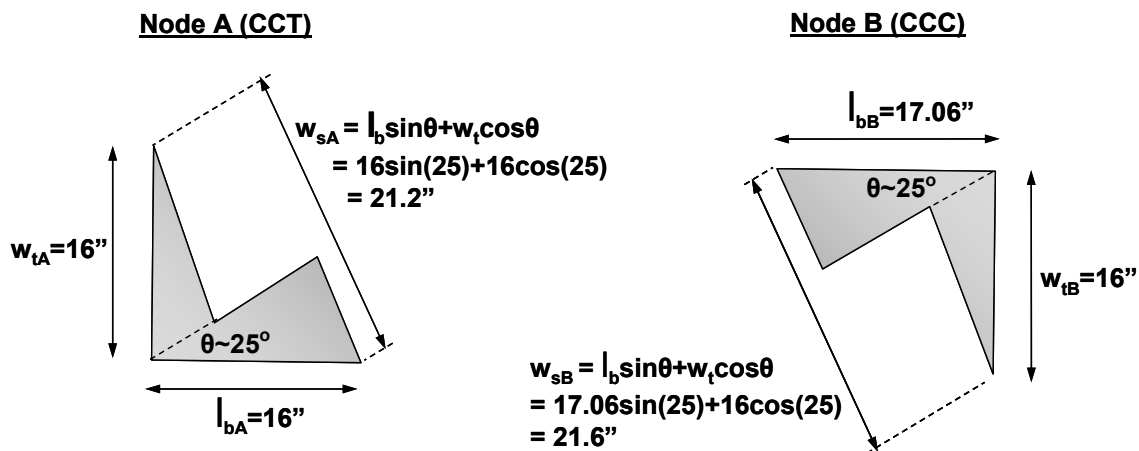


Figure A-4: Node A and Node B geometry

The nominal capacity of a node in AASHTO is:

$$P_{nA} = \nu f'_c A_n$$

ν is equal to 0.85 for a CCC node and 0.75 for CCT node.

The load on each face of the nodes at the nominal applied load capacity of 633 kips is shown in Figure A-5.

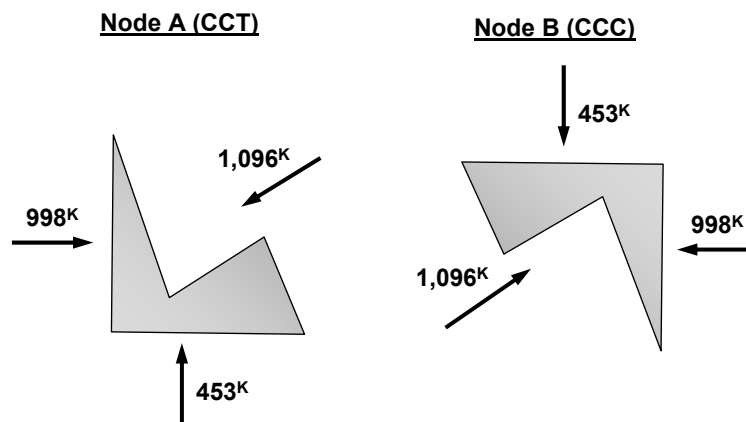


Figure A-5: Nodal forces

The nominal capacity of the Node A bottom face:

$$P_{nA} = \nu f'_c A_n = 0.75(4.1ksi)(16'')(36'') = 1,771^k > 453^k$$

Nominal capacity of the Node A left face:

$$P_{nA} = \nu f'_c A_n = 0.75(4.1ksi)(16'')(36'') = 1,771^k > 998^k$$

Nominal capacity of the Node A inclined face:

$$P_{nA} = \nu f'_c A_n = 0.75(4.1ksi)(21.2'')(36'') = 2,344^k > 1096^k$$

The nominal capacity of the Node B top face:

$$P_{nA} = \nu f'_c A_n = 0.85(4.1ksi)(17'')(36'') = 2,141^k > 453^k$$

Nominal capacity of the Node B right face:

$$P_{nA} = \nu f'_c A_n = 0.85(4.1ksi)(16")(36") = 2,007^k > 998^k$$

Nominal capacity of the Node B inclined face:

$$P_{nA} = \nu f'_c A_n = 0.85(4.1ksi)(21.2")(36") = 2,72^k > 1096^k$$

A.1.1.2 Struts

The force in the strut at the nominal design capacity using strut-and-tie modeling is 1,096^k. The angle of the one-panel strut is approximately 25 degrees, as shown above. The strut capacity is governed by the strut-to-node interface at one of the two nodes. As outlined in Chapter 2, the strength of a strut according to AASHTO LFRD is:

$$P_n = f_{cu} A_{cs}$$

$$f_{cu} = \frac{f'_c}{0.8 + 170\varepsilon_1} \leq 0.85f'_c$$

$$\varepsilon_1 = \varepsilon_s + (\varepsilon_s + 0.002) \cot^2 \alpha_s$$

In calculating the strain, ε_s is assumed to be the concrete strain at the center of the node in the direction of the adjoining tie. The strain at the vertical face of the node is assumed to be zero, while the strain on the opposite side of the node is equal to the strain in the horizontal tie (Brown et. al., 2006):

$$\frac{998^k}{27 * 1.56in^2 * 60ksi} = 0.000807$$

The strain at the center of the node is therefore the average of this strain value (0.000807) and the strain at the vertical face (zero). The capacity of the strut at Node A is:

$$\varepsilon_s = \frac{0.000807}{2} = 0.000403$$

$$\varepsilon_1 = 0.000403 + (0.000403 + 0.002) \cot^2(25^\circ) = 0.0121$$

$$f_{cu} = \frac{4.1ksi}{0.8 + 170(0.0121)} = 1.44ksi \leq 0.85(4.1ksi) = 3.49ksi$$

$$P_n = f_{cu} A_{cs} = (1.44ksi)[(36")(21.2")] = 1,096^k \text{ (Governs)}$$

Node B is a CCC node, and therefore $\varepsilon_s = 0$ (there is no adjoining tie). The capacity of the strut at Node B is:

$$\varepsilon_s = 0$$

$$\varepsilon_1 = 0 + (0 + 0.002) \cot^2(25^\circ) = 0.0097$$

$$f_{cu} = \frac{4.1ksi}{0.8 + 170(0.0097)} = 1.67ksi \leq 0.85(4.1ksi) = 3.49ksi$$

$$P_n = f_{cu} A_{cs} = 1.67ksi(36")(21.6") = 1302^k > 1096^k$$

A.1.1.3 Ties

The nominal capacity of tie AC is given by:

$$P_n = f_y A_{st} = 60ksi(27)(1.56in^2) = 2527^k > 998^k \text{ (OK)}$$

A.1.2 Design Using TxDOT 4371

The nominal capacity of the strut-and-tie model for the shear span is 637 kips. The governing element in the model is strength of the strut at its interface with Node A. The nominal capacity of each element in the strut-and-tie model is calculated below.

A.1.2.1 Nodes

The calculation of node capacity using the TxDOT 4371 provisions is identical to that of AASHTO LRFD. Since the nominal capacity of the strut-and-tie model using

AASHTO (applied load of 633 kips) is nearly identical to that of AASHTO 4371 (637 kips) there is no need to re-check the nodes. Nodal capacities for AASHTO were presented in section A.1.1.1.

A.1.2.2 Struts

The amount of reinforcement within a strut is calculated as:

$$\rho_{\perp} = \sqrt{\left(\frac{A_{sH}}{bs_H}\right)^2 + \left(\frac{A_{sV}}{bs_V}\right)^2}$$

Note that the two terms contained within a set of parenthesis are the horizontal and vertical reinforcement ratio, respectively. The minimum amount of reinforcement required in a strut is given by:

$$\rho_{T,\min} = \frac{P_u}{f_y b \ell m} \geq 0.003$$

If $\rho_T > \rho_{T,\min}$, the strut efficiency is defined as:

$$\nu = \frac{0.85 \tan \theta}{\sqrt{f'_c}} \frac{l_n}{w_s \sin \theta}$$

If $\rho_T < \rho_{T,\min}$, the strut efficiency is defined as:

$$\nu = \frac{0.85 \tan \theta}{3\sqrt{f'_c}} \frac{l_n}{w_s \sin \theta}$$

In the case of Strut AB:

$$\rho_T = \sqrt{(0.003)^2 + (0.0031)^2} = 0.0043$$

$b_{\min} = 21.2''$ (minimum strut width; occurs at interface with node A)

$\ell = 77.5''$ (length of strut)

$$b_{ef} = \frac{\ell}{3} \geq b_{\min} + \frac{\ell}{6} = \frac{77.5''}{3} \geq 21.2 + \frac{77.5''}{6} = 25.8'' \geq 34.1''$$

So, $b_{ef} = 34.1''$

$$m = \frac{2b_{ef}}{b_{ef} - b_{\min}} = \frac{2(34.1'')}{34.1'' - 21.2''} = 5.28$$

$$\rho_{\perp, \min} = \frac{1,089^k}{(60ksi)(36'')(77.5'')(5.28)} = 0.0012 < 0.003$$

So, $\rho_{\perp, \min} = 0.003$

Since $\rho_{\perp} = 0.0043 > \rho_{\perp, \min} = 0.003$, strut efficiency is given by:

$$\nu = \frac{0.85 \tan \theta}{\sqrt{f'_c}} \frac{l_n}{w_s \sin \theta}$$

Strut efficiency at node A:

$$\nu_A = \frac{0.85 \tan \theta}{\sqrt{f'_c}} \frac{l_n}{w_s \sin \theta} = \frac{0.85 \tan(25^\circ)}{\sqrt{4.1ksi}} \frac{16''}{(21.2'') \sin(25^\circ)} = 0.35$$

$$\nu_A \text{ is less than both } 0.85 \frac{l_n}{w_s \sin \theta} = 0.85 \frac{16''}{(21.2'') \sin(25^\circ)} = 1.55 \text{ and } 0.85 \text{ (OK)}$$

Strut efficiency at node B:

$$\nu_B = \frac{0.85 \tan \theta}{\sqrt{f'_c}} \frac{l_n}{w_s \sin \theta} = \frac{0.85 \tan(25^\circ)}{\sqrt{4.1ksi}} \frac{17.06''}{(21.6'') \sin(25^\circ)} = 0.36$$

$$\nu_B \text{ is less than both } 0.85 \frac{l_n}{w_s \sin \theta} = 0.85 \frac{17.06''}{(21.6'') \sin(25^\circ)} = 1.62 \text{ and } 0.85 \text{ (OK)}$$

The capacity of strut at A:

$$P_{nA} = \nu_A f'_c A_{cs} = (0.35)(4.1ksi)[(36'')(21.2'')] = 1089^k \text{ (**Governs**)}$$

The capacity of strut at B:

$$P_{nB} = \nu_B f'_c A_{cs} = (0.36)(4.1ksi)[(36'')(21.6'')] = 1161^k > 1089^k \text{ (OK)}$$

A.1.2.3 Ties

The nominal capacity of tie AC is given by:

$$P_n = f_y A_{st} = 60 \text{ksi}(27)(1.56 \text{in}^2) = 2527^k > 991^k \text{ (OK)}$$

A.1.3 Design Using ACI 318-05

The nominal capacity of the strut-and-tie model for the shear span is reached at an applied load of 1,024 kips. The governing element in the model is Node A. The nominal capacity of each element in the strut-and-tie model is calculated below.

A.1.3.1 Nodes

The geometry of each node was shown in Figure A-4. The node efficiency factors for ACI were shown in Table A-1.

The nominal capacity of a node in ACI is:

$$F_m = f_{cu} A_n$$

$$f_{cu} = 0.85 \beta_n f'_c$$

$$\text{So, } F_m = 0.85 \beta_n f'_c A_n$$

The load on each face of the nodes at the nominal applied load capacity of 1,024 kips is shown in Figure A-6. The node dimensions were given in Figure A-4.

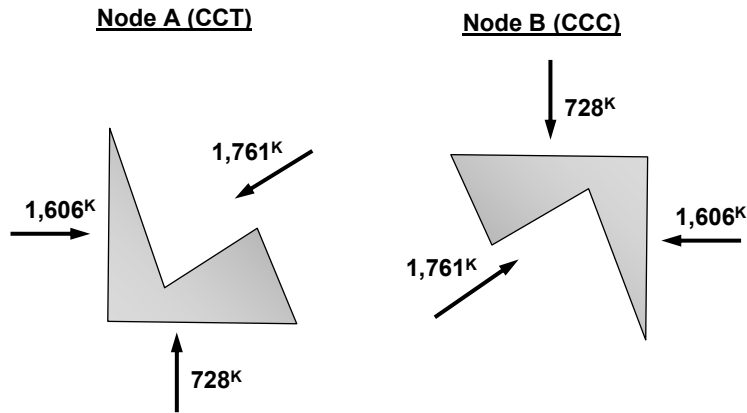


Figure A-6: Nodal forces

β_n is equal to 1.0 for a CCC node and 0.80 for CCT node.

The nominal capacity of the Node A bottom face:

$$F_{nA} = 0.85\beta_n f'_c = 0.85(0.80)(4100 \text{ psi})[(16'')(36'')] = 1,606^k > 728^k$$

Nominal capacity of the Node A left face:

$$F_{nA} = 0.85\beta_n f'_c = 0.85(0.80)(4100 \text{ psi})[(16'')(36'')] = 1,606^k \text{ (**Governs**)}$$

Nominal capacity of the Node A inclined face:

$$F_{nA} = 0.85\beta_n f'_c = 0.85(0.80)(4100 \text{ psi})[(21.2'')(36'')] = 2,126^k > 1,761^k$$

The nominal capacity of the Node B top face:

$$F_{nA} = 0.85\beta_n f'_c = 0.85(1.0)(4100 \text{ psi})[(17'')(36'')] = 2,141^k > 728^k$$

Nominal capacity of the Node B right face:

$$F_{nA} = 0.85\beta_n f'_c = 0.85(1.0)(4100 \text{ psi})[(16'')(36'')] = 2,007^k > 1,606^k$$

Nominal capacity of the Node B inclined face:

$$F_{nA} = 0.85\beta_n f'_c = 0.85(1.0)(4100 \text{ psi})[(21.6'')(36'')] = 2,712^k > 1,761^k$$

A.1.3.2 Struts

The capacity of a strut in ACI is given as

$$F_{ns} = f_{cu} A_c$$

$$f_{cu} = 0.85\beta_s f'_c$$

$$F_{ns} = 0.85\beta_s f'_c A_c$$

Shear span 1A contains AASHTO minimum reinforcement (0.003 times the gross area in each direction) which is well more than is required by ACI A.3.3. $\beta_s = 0.75$ for a bottle shaped strut with reinforcement satisfying A.3.3. $\beta_s = 0.75$ is less than β_n for either node, so β_s governs and should be used in the strut capacity equation, below:

The capacity of strut AB at node A:

$$F_{nsA} = 0.85(0.75)(4100 \text{ psi})[(36")(21.2")] = 1,993^k > 1,761^k$$

The capacity of strut AB at node B:

$$F_{nsA} = 0.85(0.75)(4100 \text{ psi})[(36")(21.6")] = 2,034^k > 1,761^k$$

A.1.3.3 Ties

The nominal capacity of tie AC is given by:

$$P_n = f_y A_{st} = 60 \text{ ksi}(27)(1.56 \text{ in}^2) = 2,527^k > 1,604^k \text{ (OK)}$$

A.2 TWO-PANEL STRUT-AND-TIE MODEL FOR TEST #5

This section contains a full set of calculations for a two-panel strut-and-tie model of Test #5, using each of the three STM design methods presented in Chapter 2. Figure A-7 shows a two-panel strut-and-tie model, along with the geometry of the bearing areas. Table A-1 listed pertinent efficiency factors for both the AASHTO LFRD 4th Edition and

ACI 318-05. Nodal efficiencies and resistance factors using TxDOT 4371 are identical to those of AASHTO.

The assumptions made for two-panel strut-and-tie models in this study were already presented in section 4.3.3.2 of Chapter 4. This section expands on that discussion with detailed calculations.

Test #5 was conducted on Shear Span 2B. The geometry and reinforcement configuration of Shear Span 1A is shown in Figure A-8.

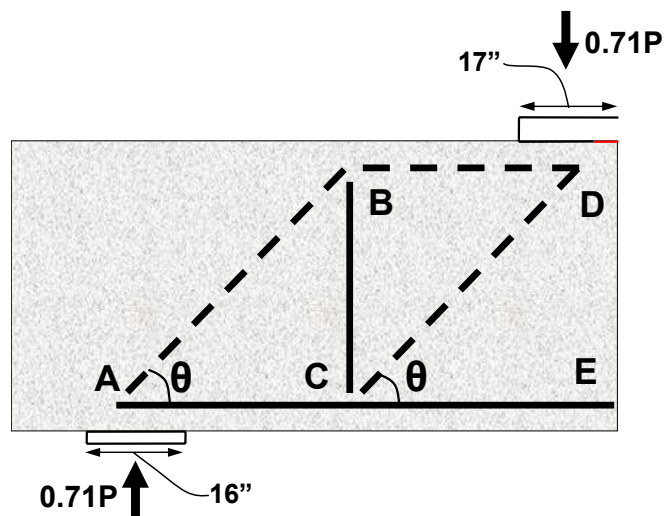


Figure A-7: Two-panel strut-and-tie model

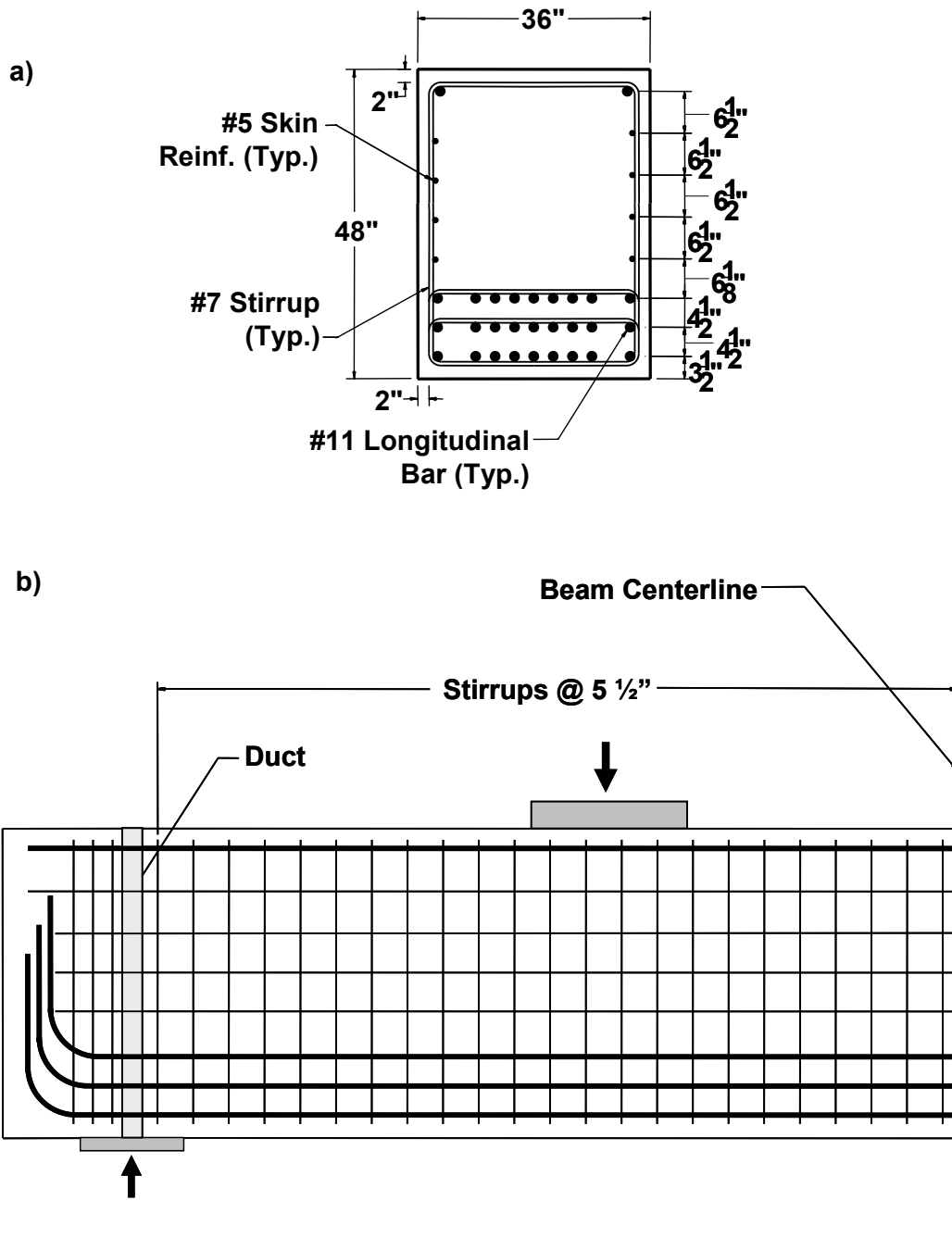


Figure A-8: Shear span 2B a) Cross-section; b) Elevation

A.2.1 Design Using AASHTO LRFD

The nominal capacity of the model is 709 kips. The governing element is tie BC.

A.2.1.1 Nodes

As was outlined in section 4.3.3.2, the interior nodes (B and C) were assumed not to govern. The geometry and forces corresponding to Node A are shown in Figure A-9. The geometry and forces corresponding to Node D are shown in Figure A-10.

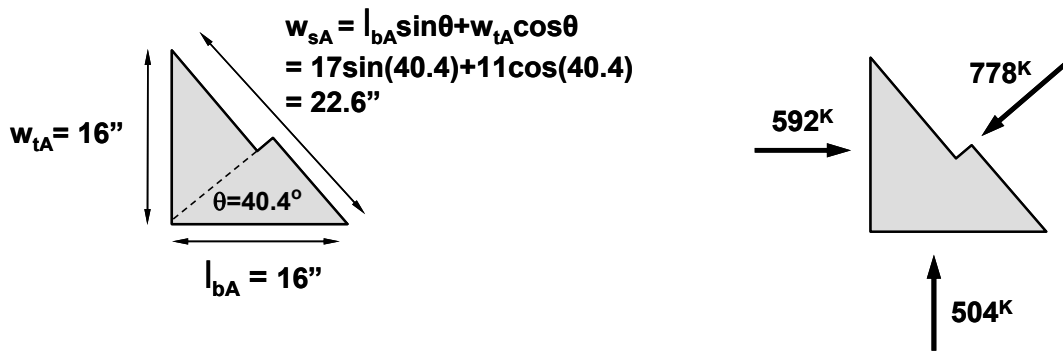


Figure A-9: Node A geometry and forces

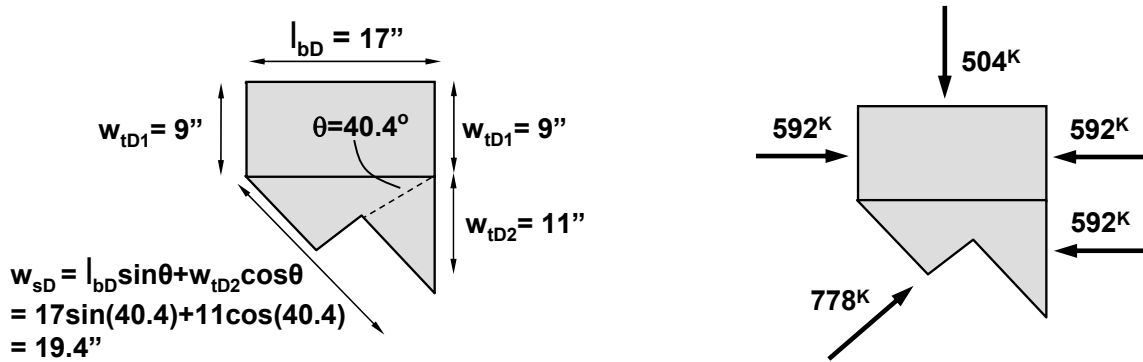


Figure A-10: Node D geometry and forces

The nominal capacity of a node in AASHTO is:

$$P_{nA} = \nu f'_c A_n$$

ν is equal to 0.85 for a CCC node (Node D) and 0.75 for CCT node (Node A).

The nominal capacity of the Node A bottom face:

$$P_{nA} = \nu f'_c A_n = 0.75(4.9ksi)(16")(36") = 2,117^k > 504^k$$

Nominal capacity of the Node A left face:

$$P_{nA} = \nu f'_c A_n = 0.75(4.9ksi)(16")(36") = 2,117^k > 592^k$$

Nominal capacity of the Node A inclined face:

$$P_{nA} = \nu f'_c A_n = 0.75(4.9ksi)(22.6")(36") = 2,983^k > 778^k$$

The nominal capacity of the Node D top face:

$$P_{nA} = \nu f'_c A_n = 0.85(4.9ksi)(17")(36") = 2,558^k > 504^k$$

Nominal capacity of top portion of Node D side faces, w_{tD1} :

$$P_{nA} = \nu f'_c A_n = 0.85(4.9ksi)(9")(36") = 1,349^k > 592^k$$

Nominal capacity of bottom portion of Node D right side face, w_{tD2} :

$$P_{nA} = \nu f'_c A_n = 0.85(4.9ksi)(11")(36") = 1,649^k > 592^k$$

Nominal capacity of the Node D inclined face:

$$P_{nA} = \nu f'_c A_n = 0.85(4.9ksi)(19.4")(36") = 2,913^k > 778^k$$

A.2.1.2 Struts

The force in each inclined strut at the nominal design capacity using strut-and-tie modeling is 778^k . The angle of the one-panel strut is approximately 40.4 degrees, as shown above. The capacity of each inclined strut is governed by the interface with either node A or node D (again, due the ambiguity of Node B and Node C, the strut-to-node

interface was assumed not to govern). As outlined in Chapter 2, the strength of a strut according to AASHTO LFRD is:

$$P_n = f_{cu} A_{cs}$$

$$f_{cu} = \frac{f'_c}{0.8 + 170\varepsilon_1} \leq 0.85 f'_c$$

$$\varepsilon_1 = \varepsilon_s + (\varepsilon_s + 0.002) \cot^2 \alpha_s$$

In calculating the strain, ε_s is assumed to be the concrete strain at the center of the node in the direction of the adjoining tie. The strain at the vertical face of the node is assumed to be zero, while the strain on the opposite side of the node is equal to the strain in the horizontal tie (Brown et al., 2006).

Consider inclined Strut AB (Figure A-7). At Node A, the force in the tie is 592 kips (Figure A-9).

$$\frac{592^k}{27 * 1.56in^2 * 60ksi} = 0.00049$$

The strain at the center of the node is therefore the average of this strain value (0.00049) and the strain at the vertical face (zero). The capacity of the strut at Node A is:

$$\varepsilon_s = \frac{0.00049}{2} = 0.00024$$

$$\varepsilon_1 = 0.00024 + (0.00024 + 0.002) \cot^2(40.4^\circ) = 0.0033$$

$$f_{cu} = \frac{4.9ksi}{0.8 + 170(0.0033)} = 3.58ksi \leq 0.85(4.9ksi) = 4.17ksi$$

$$P_n = f_{cu} A_{cs} = (3.58ksi)[(36")(22.6")] = 2,908^k > 778^k$$

Consider inclined Strut CD. Node D is a CCC node, and therefore $\varepsilon_s = 0$ (there is no adjoining tie). The capacity of the strut at Node D is:

$$\varepsilon_s = 0$$

$$\varepsilon_1 = 0 + (0 + 0.002) \cot^2(40.4^\circ) = 0.00276$$

$$f_{cu} = \frac{4.9ksi}{0.8 + 170(0.00276)} = 3.86ksi \leq 0.85(4.9ksi) = 4.17ksi$$

$$P_n = f_{cu} A_{cs} = 3.86ksi(36")(19.4") = 2,700^k > 778^k$$

Consider prismatic Strut BD. Node D is a CCC node, and therefore $\varepsilon_s = 0$ (there is no adjoining tie). The capacity of the strut at Node D is:

$$\varepsilon_s = 0$$

$$\varepsilon_1 = 0 + (0 + 0.002) \cot^2(40.4^\circ) = 0.00276$$

$$f_{cu} = \frac{4.9ksi}{0.8 + 170(0.00276)} = 3.86ksi \leq 0.85(4.9ksi) = 4.17ksi$$

$$P_n = f_{cu} A_{cs} = 3.86ksi(36")(9") = 1,250^k > 592^k$$

A.2.1.3 Ties

The nominal capacity of tie AC is given by:

$$P_n = f_y A_{st} = 60ksi(27)(1.56in^2) = 2527^k > 592^k \text{ (OK)}$$

The nominal capacity of tie CE is given by:

$$P_n = f_y A_{st} = 60ksi(27)(1.56in^2) = 2527^k > 592^k(2) = 1185^k \text{ (OK)}$$

Tie BC is assumed to contain seven stirrups. It was assumed that any stirrup that adjoins to a diagonal strut at an angle of greater than 25 degrees is engaged as part of the vertical tie (Wight and Parra-Montesinos, 2003). The nominal capacity of tie BC is given by:

$$P_n = f_y A_{st} = 60ksi(7stirrups)(2legs)(0.60in^2) = 504^k \text{ (Governs)}$$

A.2.2 Design Using TxDOT 4371

The nominal capacity of the model is 709 kips. The governing element is tie BC. The model geometry and forces are identical to those presented in section A.2.1.

A.2.2.1 Nodes

The calculation of node capacity using the TxDOT 4371 provisions is identical to that of AASHTO LRFD. See section A.2.1.1.

A.2.2.2 Struts

The amount of reinforcement within a strut is calculated as:

$$\rho_{\perp} = \sqrt{\left(\frac{A_{sH}}{bs_H}\right)^2 + \left(\frac{A_{sV}}{bs_V}\right)^2}$$

Note that the two terms contained within a set of parenthesis are the horizontal and vertical reinforcement ratio, respectively. The minimum amount of reinforcement required in a strut is given by:

$$\rho_{T,\min} = \frac{P_u}{f_y b l m} \geq 0.003$$

If $\rho_T > \rho_{T,\min}$, the strut efficiency is defined as:

$$v = \frac{0.85 \tan \theta}{\sqrt{f'_c}} \frac{l_n}{w_s \sin \theta}$$

If $\rho_T < \rho_{T,\min}$, the strut efficiency is defined as:

$$v = \frac{0.85 \tan \theta}{3\sqrt{f'_c}} \frac{l_n}{w_s \sin \theta}$$

Consider inclined Strut AB:

$$\rho_T = \sqrt{(0.003)^2 + (0.0061)^2} = 0.0068$$

$b_{\min} = 22.6''$ (minimum strut width; occurs at interface with node A)

$\ell = 44.4''$ (length of strut)

$$b_{ef} = \frac{\ell}{3} \geq b_{\min} + \frac{\ell}{6} = \frac{44.4''}{3} \geq 22.6 + \frac{44.4''}{6} = 14.8'' \geq 30.0''$$

So, $b_{ef} = 30.0''$

$$m = \frac{2b_{ef}}{b_{ef} - b_{\min}} = \frac{2(30.0'')}{30.0'' - 22.6''} = 8.10$$

$$\rho_{\perp, \min} = \frac{778^k}{(60ksi)(36'')(77.5'')(8.10)} = 0.001 < 0.003$$

So, $\rho_{\perp, \min} = 0.003$

Since $\rho_{\perp} = 0.0068 > \rho_{\perp, \min} = 0.003$, strut efficiency is given by:

$$\nu = \frac{0.85 \tan \theta}{\sqrt{f'_c}} \frac{l_n}{w_s \sin \theta}$$

Strut efficiency at node A:

$$\nu_A = \frac{0.85 \tan \theta}{\sqrt{f'_c}} \frac{l_n}{w_s \sin \theta} = \frac{0.85 \tan(40.4^\circ)}{\sqrt{4.9ksi}} \frac{16''}{(22.6'') \sin(40.4^\circ)} = 0.36$$

$$\nu_A \text{ is less than both } 0.85 \frac{l_n}{w_s \sin \theta} = 0.85 \frac{16''}{(22.6'' \sin(40.4^\circ))} = 0.931 \text{ and } 0.85 \text{ (OK)}$$

The capacity of strut at A:

$$P_{nA} = \nu_A f'_c A_{cs} = (0.36)(4.9ksi)[(36'')(22.6'')] = 1,423^k > 778^k$$

Consider inclined Strut CD:

(nearly identical geometry to Strut AB, so $\rho_{\perp, \min} = 0.003$)

Since $\rho_{\perp} = 0.0068 > \rho_{\perp, \min} = 0.003$, strut efficiency is given by:

$$\nu = \frac{0.85 \tan \theta}{\sqrt{f'_c}} \frac{l_n}{w_s \sin \theta}$$

Strut efficiency at node D:

$$\nu_A = \frac{0.85 \tan \theta}{\sqrt{f'_c}} \frac{l_n}{w_s \sin \theta} = \frac{0.85 \tan(40.4^\circ)}{\sqrt{4.9 \text{ksi}}} \frac{17''}{(19.4'') \sin(40.4^\circ)} = 0.44$$

$$\nu_A \text{ is less than both } 0.85 \frac{l_n}{w_s \sin \theta} = 0.85 \frac{17''}{(19.4'' \sin(40.4^\circ))} = 1.15 \text{ and } 0.85 \text{ (OK)}$$

The capacity of strut at D:

$$P_{nA} = \nu_A f'_c A_{cs} = (0.44)(4.9 \text{ksi})[(36'')(19.4'')] = 1,517^k > 778^k$$

Consider prismatic strut BD. Since strut angle of inclination is equal to zero, $\nu = 0.85$.

The capacity of strut at D:

$$P_{nA} = \nu_A f'_c A_{cs} = (0.85)(4.9 \text{ksi})[(36'')(9'')] = 1,349^k > 592^k$$

A.2.2.3 Ties

The nominal capacity of tie AC is given by:

$$P_n = f_y A_{st} = 60ksi(27)(1.56in^2) = 2527^k > 592^k \text{ (OK)}$$

The nominal capacity of tie CE is given by:

$$P_n = f_y A_{st} = 60ksi(27)(1.56in^2) = 2527^k > 592^k(2) = 1185^k \text{ (OK)}$$

Tie BC is assumed to contain seven stirrups. It was assumed that any stirrup that adjoins to a diagonal strut at an angle of greater than 25 degrees is engages as part of the vertical tie (Wight and Parra-Montesinos, 2003). The nominal capacity of tie BC is given by:

$$P_n = f_y A_{st} = 60ksi(7stirrups)(2legs)(0.60in^2) = 504^k \text{ (Governs)}$$

A.2.3 Design Using ACI 318-05

The nominal capacity of the model is 709 kips. The governing element is tie BC. The model geometry and forces are identical to those presented in section A.2.1.

A.2.3.1 Nodes

The geometry of each node was shown in Figure A-9 and Figure A-10. The node efficiency factors for ACI were shown in Table A-1.

The nominal capacity of a node in ACI is:

$$F_m = f_{cu} A_n$$

$$f_{cu} = 0.85\beta_n f'_c$$

$$\text{So, } F_m = 0.85\beta_n f'_c A_n$$

β_n is equal to 1.0 for a CCC node and 0.80 for CCT node (Table A-1)

The nominal capacity of the Node A bottom face:

$$F_{nA} = 0.85\beta_n f'_c = 0.85(0.80)(4900 \text{ psi})[(16'')(36'')] = 1,919^k > 504^k$$

Nominal capacity of the Node A left face:

$$F_{nA} = 0.85\beta_n f'_c = 0.85(0.80)(4900 \text{ psi})[(16'')(36'')] = 1,919^k > 592^k$$

Nominal capacity of the Node A inclined face:

$$F_{nA} = 0.85\beta_n f'_c = 0.85(0.80)(4900 \text{ psi})[(22.6'')(36'')] = 2,705^k > 778^k$$

The nominal capacity of the Node D top face:

$$F_{nA} = 0.85\beta_n f'_c = 0.85(1.0)(4900 \text{ psi})[(17'')(36'')] = 2,558^k > 504^k$$

Nominal capacity of top portion of Node D side faces, w_{tD1} :

$$F_{nA} = 0.85\beta_n f'_c = 0.85(1.0)(4900 \text{ psi})[(9'')(36'')] = 1,349^k > 592^k$$

Nominal capacity of bottom portion of Node D right side face, w_{tD2} :

$$F_{nA} = 0.85\beta_n f'_c = 0.85(1.0)(4900 \text{ psi})[(11'')(36'')] = 1,649^k > 592^k$$

Nominal capacity of the Node D inclined face:

$$F_{nA} = 0.85\beta_n f'_c = 0.85(1.0)(4900 \text{ psi})[(19.4'')(36'')] = 2,914^k > 778^k$$

A.2.3.2 Struts

The capacity of a strut in ACI is given as

$$F_{ns} = f_{cu} A_c$$

$$f_{cu} = 0.85\beta_s f'_c$$

$$F_{ns} = 0.85\beta_s f'_c A_c$$

Shear span 1A contains AASHTO minimum reinforcement (0.003 times the gross area in each direction) which is well more than the amount required by ACI A.3.3. $\beta_s = 0.75$ for a bottle shaped strut with reinforcement satisfying A.3.3. $\beta_s = 0.75$ is less than β_n for both Node A and Node D, so β_s governs and should be used in the strut capacity equation for inclined struts, below:

The capacity of inclined strut AB at node A:

$$F_{nsA} = 0.85(0.75)(4900\text{ psi})[(36")(22.6")] = 2,536^k > 778^k$$

The capacity of inclined strut CD at node D:

$$F_{nsA} = 0.85(0.75)(4900\text{ psi})[(36")(19.4")] = 2,185^k > 778^k$$

The capacity of prismatic strut BD at node D (Note that $\beta_s = \beta_n = 1.0$ for a prismatic strut at the interface with a CCC node):

$$F_{nsA} = 0.85(1.0)(4900\text{ psi})[(36")(9")] = 1,349^k > 592^k$$

A.2.3.3 Ties

The nominal capacity of tie AC is given by:

$$P_n = f_y A_{st} = 60\text{ksi}(27)(1.56\text{in}^2) = 2527^k > 592^k \text{ (OK)}$$

The nominal capacity of tie CE is given by:

$$P_n = f_y A_{st} = 60\text{ksi}(27)(1.56\text{in}^2) = 2527^k > 592^k (2) = 1185^k \text{ (OK)}$$

Tie BC is assumed to contain seven stirrups. It was assumed that any stirrup that adjoins to a diagonal strut at an angle of greater than 25 degrees is engages as part of the vertical tie (Wight and Parra-Montesinos, 2003). The nominal capacity of tie BC is given by:

$$P_n = f_y A_{st} = 60\text{ksi}(7\text{ stirrups})(2\text{ legs})(0.60\text{in}^2) = 504^k \text{ (Governs)}$$

APPENDIX B

Specimen Anchorage Detail

Appendix B includes drawings of the anchorage detail used in each of the specimens.

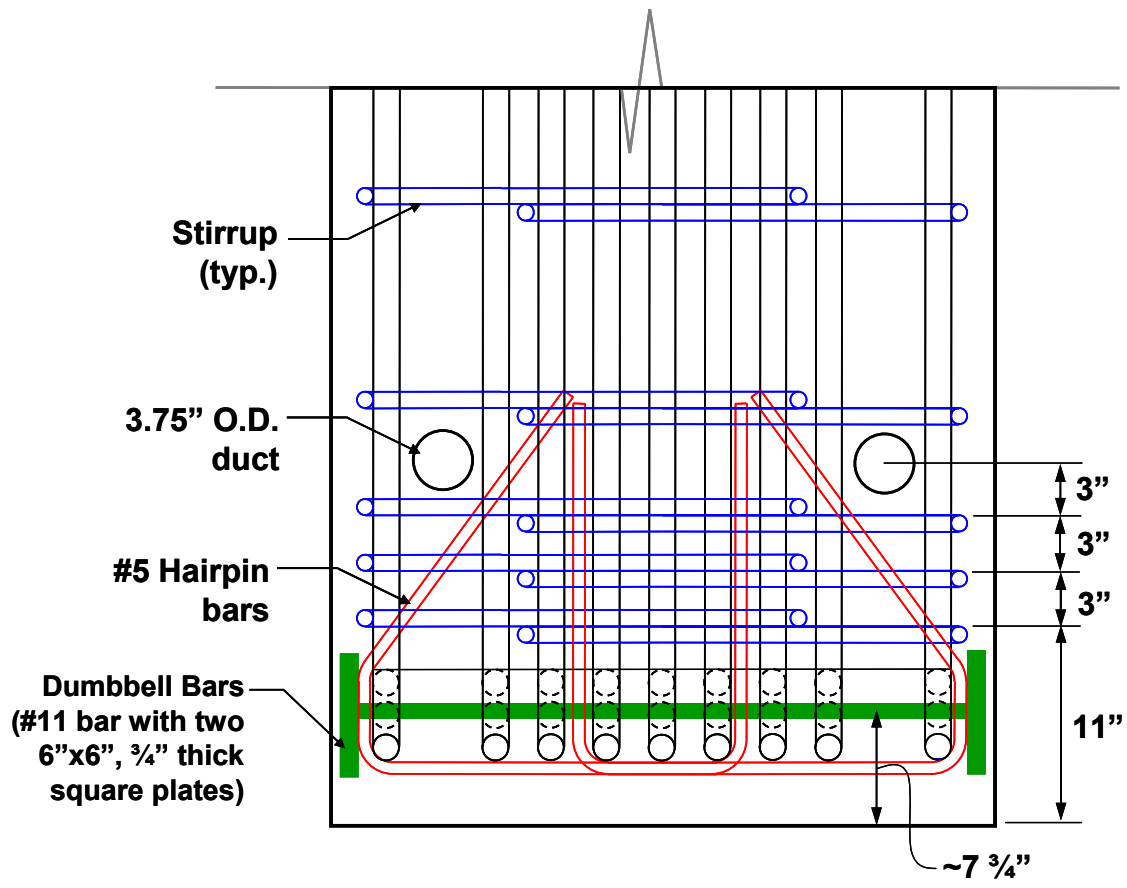


Figure B-1: Anchorage detail, plan view

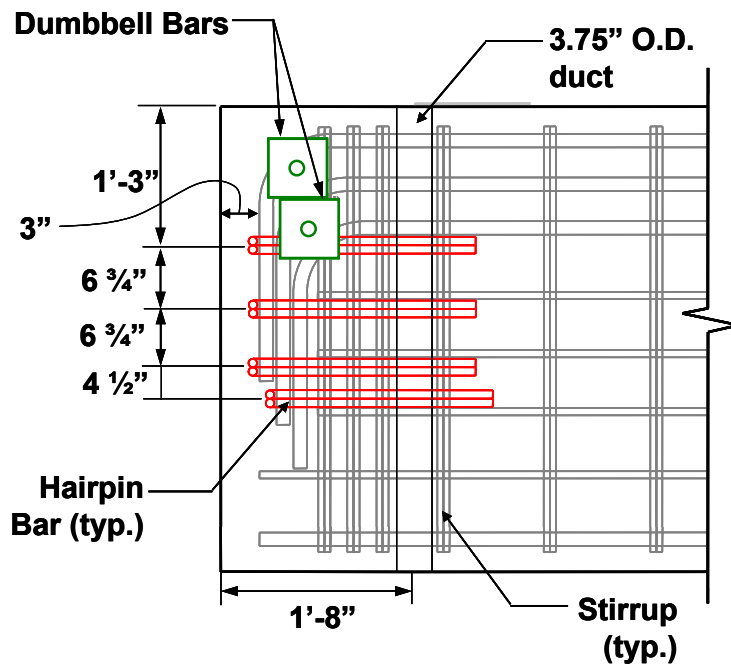


Figure B-2: Anchorage detail, elevation view



Figure B-3: Anchorage detail photo

APPENDIX C

Failure Photos

Appendix C includes a photograph of each of the five shear failures observed during the experimental program.

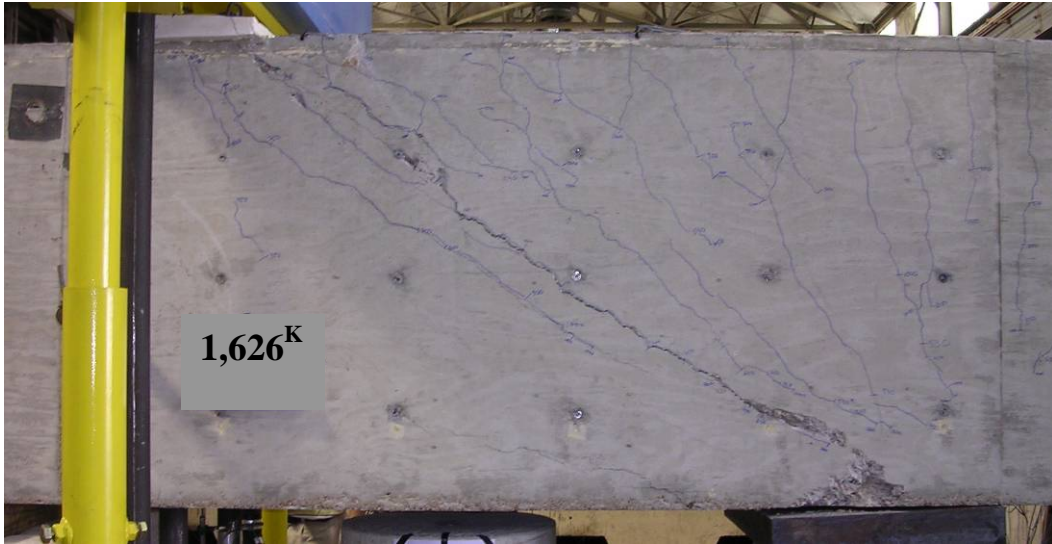


Figure C-1: Test #1 shear failure

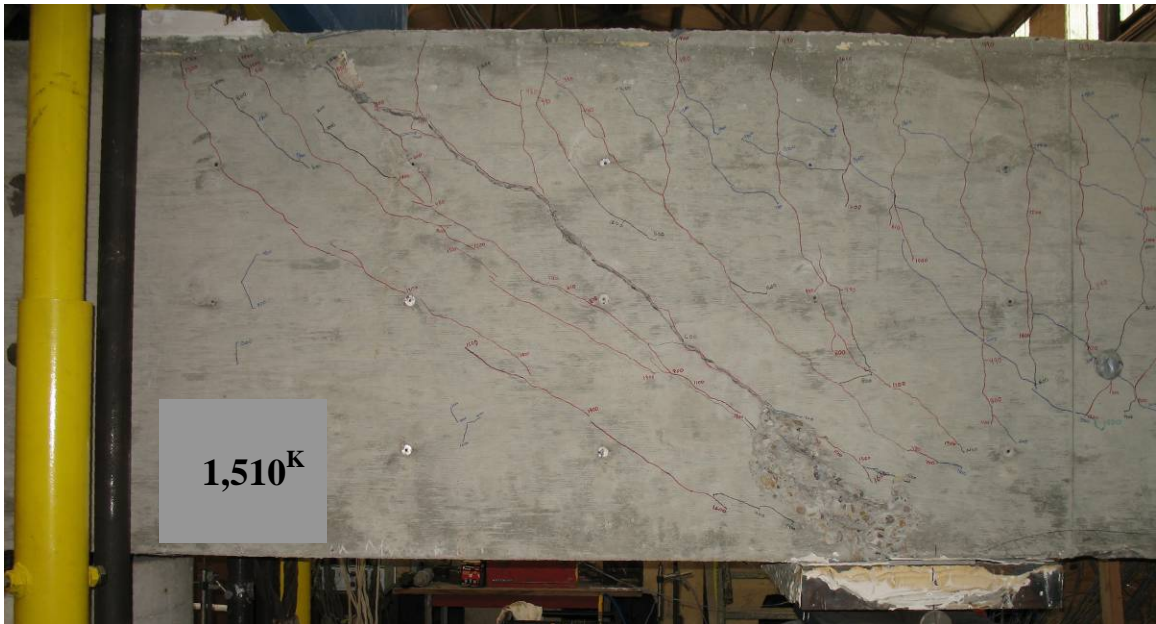


Figure C-2: Test #4 shear failure

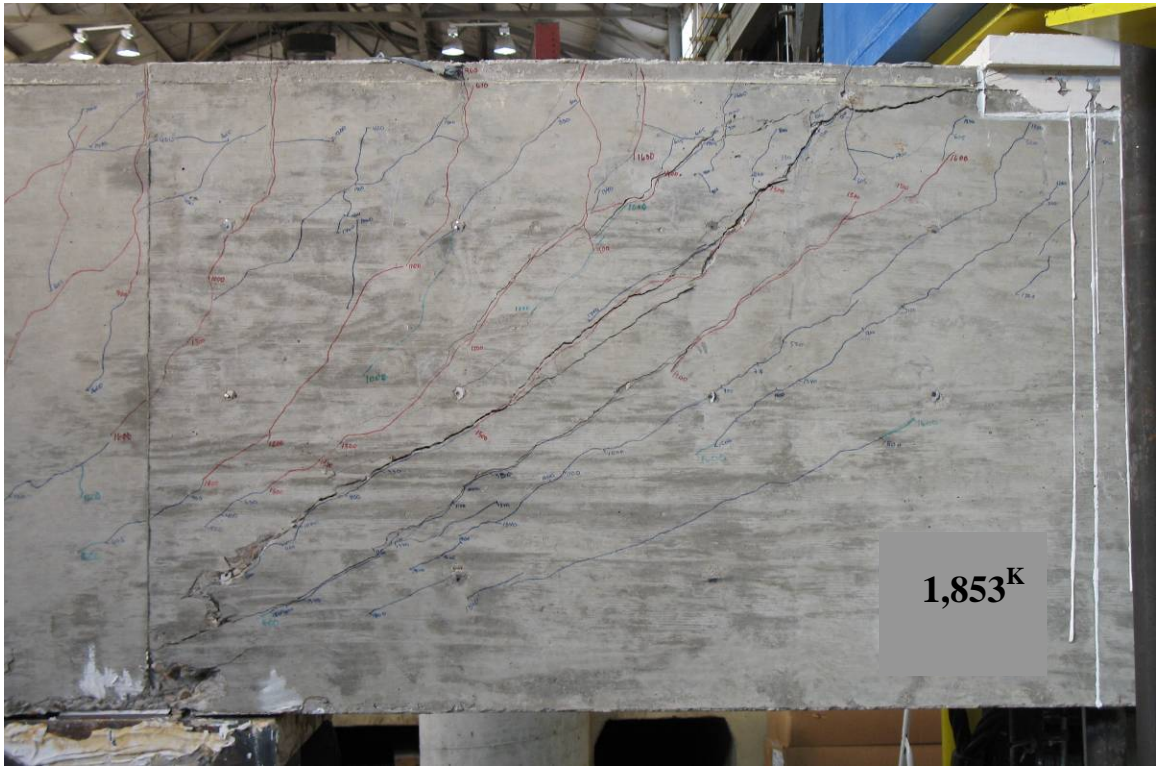


Figure C-3: Test #7 shear failure

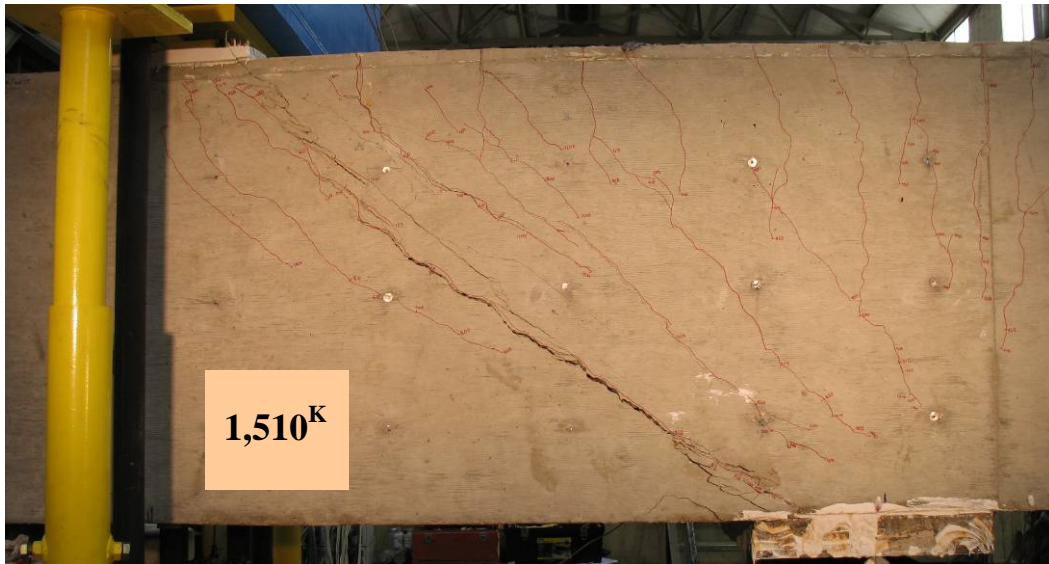


Figure C-4: Test #8 shear failure



Figure C-5: Test #9 shear failure

BIBLIOGRAPHY

1. AASHTO, *LRFD Bridge Design Specifications*, 4th Edition, American Association of State Highway and Transportation Officials, Washington, D.C., 2007.
2. ACI Committee 318, *Building Code Requirements for Reinforced Concrete (ACI 318-99)*, American Concrete Institute, Farmington Hills, MI, 1999.
3. ACI Committee 318, *Building Code Requirements for Reinforced Concrete (ACI 318-02)*, American Concrete Institute, Farmington Hills, MI, 2002.
4. ACI Committee 318, *Building Code Requirements for Reinforced Concrete (ACI 318-05)*, American Concrete Institute, Farmington Hills, MI, 2005.
5. ASCE-ACI Committee 445, 1998, "Recent Approaches to Shear Design of Structural Concrete," American Concrete Institute, Farmington Hills, MI, 42 pp.
6. ASTM C39/C39M-99, 1999, "Standard Test Method for Compressive Strength of Cylindrical Concrete Specimens," American Society for Testing and Materials, West Conshohocken, Pennsylvania.
7. Anderson, N.S., and Ramirez, J.A., 1989, "Detailing of Stirrup Reinforcement," *ACI Structural Journal*, Vol. 86, No. 5, pp. 507-515.
8. Bergmeister, K., Breen, J.E., Jirsa, J.O., and Kreger, M.E., 1993, "Detailing for Structural Concrete," Center for Transportation Research Report CTR 0-1127-3F, Austin, Texas.
9. Brown, M.D., and Bayrak, O., 2006, "Minimum Transverse Reinforcement for Bottle-Shaped Struts," *ACI Structural Journal*, Vol. 103, No. 6, pp. 813-821.
10. Brown, M. D.; Sankovich, C. L.; Bayrak, O.; Jirsa, J. O.; Breen, J. E.; and Wood, S. L., "Design for Shear in Reinforced Concrete Using Strut-and-Tie Models," *Report No. 0-4371-2*, Center for Transportation Research, University of Texas at Austin, Austin, Tex., Apr. 2006.
11. de Paiva, H. A. R., and Siess, C. P., 1965, "Strength and Behavior of Deep Beams," *ASCE Structural Journal*, V. 91, No. 10, pp. 19-41.

12. Hsiung, W., and Frantz, G. C., 1985, "Transverse Stirrup Spacing in R/C Beams," *ASCE Structural Journal*, V. 111, No. 2, pp. 353-363.
13. Kong, F. K., Robins, P. J., and Cole, D. F., 1970, "Web Reinforcement Effects on Deep Beams," *ACI Journal*, V. 67, No. 12, pp. 1010-1016.
14. Leonhardt, F. and Walther, R.; "Wandartige Trager"- Bulletin No. 178, Wilhelm Ernst und Sohn, Berlin, 1966, 159pp.
15. MacGregor, J.G. and Wight, J.K., 2005, "Reinforced Concrete: Mechanics and Design (4th Edition)," Prentice Hall, Upper Saddle River, New Jersey.
16. Oh, J. K., and Shin, S. W., 2001, "Shear Strength of Reinforced High-Strength Concrete Deep Beams," *ACI Structural Journal*, V. 98, No. 2, pp. 164-173.
17. Powanusorn, S., and Bracci, J. M., 2006, "Behavior of Reinforced Concrete Members Prone to Shear Deformations: Part I—Effect of Confinement," *ACI Structural Journal*, V. 103, No. 5, pp. 736-746.
18. Reineck, K.H., Kuchma, D.A., Kim, K.S., and Marx, S., 2003, "Shear Database for Reinforced Concrete Members without Shear Reinforcement," *ACI Structural Journal*, V. 103, No. 2, pp. 240-249.
19. Rigotti, M., 2002, "*Diagonal Cracking in Reinforced Concrete Deep Beams – An Experimental Investigation*," Master's Thesis, Concordia University, 220 pp.
20. Rogowsky, D. M., MacGregor, J. M., and Ong, S. Y., 1986, "Tests of Reinforced Concrete Deep Beams," *ACI Journal*, V. 83, No. 4, pp. 614-623.
21. Schlaich, J., Schäfer, K., and Jennewein, M., 1987, "Towards a Consistent Design of Structural Concrete," *PCI Journal*, Vol. 32, No. 3, pg. 74-150, Chicago, Illinois.
22. Shin, S., Lee, K., Moon, J., and Ghosh, S. K., 1999, "Shear Strength of Reinforced High-Strength Concrete Beams with Shear Span-to-Depth Ratios between 1.5 and 2.5," *ACI Structural Journal*, V. 96, No. 4, pp. 549-556.
23. Shioya, T., 1989, "Shear Properties of Large Reinforced Concrete Members," *Special Report*, Institute of Technology, Shimizu Corp., No. 25, 198 pp. (In Japanese).
24. Smith, K. N., and Vantsiotis, A. S., 1982, "Shear Strength of Deep Beams," *ACI Journal*, V. 79, No. 3, pp. 201-213.

25. Tan, K., Kong, F., Teng, S., and Weng, L., 1997, "Effect of Web Reinforcement on High-Strength Concrete Deep Beams," *ACI Structural Journal*, V. 94, No. 5, pp. 572-582.
26. Texas Department of Transportation, www.dot.state.tx.us, Bridge Division Standard Drawings, 2007.
27. Van Landuyt, D., Telephone Conversation, November 2006.
28. Wight, J.K., and Parra-Montesinos, G., 2003, "Use of Strut-and-Tie Model for Deep Beam Design as per ACI 318 Code," *ACI Concrete International*, Vol. 25, No. 5, pp. 63-70.
29. Young, B.S., Bracci, J.M., Keating, P.B., and Hueste, M.B.D., 2002, "Cracking in Reinforced Concrete Bent Caps," *ACI Structural Journal*, V. 99, No. 4, pp. 488-498.

VITA

Matthew Ryan Huizinga was born in Grand Rapids, Michigan, on August 9, 1982, the son of Dorothy Huizinga and Donald Huizinga. After graduating from Grand Rapids Christian High School in Grand Rapids, MI, he attended the University of Michigan in Ann Arbor, MI and received his Bachelor of Science in Civil Engineering in May of 2005. In August of 2005, he began his study in the Graduate School at the University of Texas at Austin, working as a research assistant at the Phil M. Ferguson Structural Engineering Laboratory.

Permanent address: 13920 Rolling Creek Dr.
Lowell, MI 49331

This thesis was typed by the author.